the Energy to Lead

gti

REPORT

Final Report

Project: Advanced Oxy-Combustion Technology Development and Scale Up for New and Existing Coal-Fired Power Plants (Phase II)

Reporting period start date: 10/1/2012

Reporting period end date: 12/31/2018

Authors: Mark Fitzsimmons, Doug M. Heim, William W. Follett IV (GTI),

Stevan Jovanovic, Makini Byron (Linde),

Robin W. Hughes, David J. McCalden, S. Champagne (CanmetENERGY)

Report Issued: March 29, 2019

DOE Award number: DE-FE0009448

Submitting Organization: GTI

GTI Contact:
William W. Follett
Program Manager
818-405-9546
bfollett@GTI.energy

GTI
1700 S. Mount Prospect Rd.
Des Plaines, Illinois 60018

Linde LLC
575 Mountain Ave.
Murray Hill, NJ 07974-2097

CanmetENERGY
1 Haanel Dr.
Ontario K1A 1M1

Disclaimer

Abstract

The objective of this project was to develop an advanced Oxy-Combustion Pressurized Fluidized Bed Combustor (Oxy-PFBC) technology and mature it to TRL 6 through pilot testing. Performance goals included demonstrating capture of 90% or greater of the produced carbon dioxide, with no more than a 35% increase in the cost of electricity. A 1 MWth pilot scale plant was designed, built and operated at CanmetENERGY in Ottawa. Extensive support work was carried out on component testing, analysis and commercial planning.

The team members included GTI, Linde, Natural Resources Canada (CanmetENERGY), Pennsylvania State University, Electric Power Research Institute (EPRI), and General Electric. Additional research was provided by the University of Ottawa. Funding was provided by the US Department of Energy, Alberta Innovates and each of the team members. The total funding for Phase II was $18.537M with $12.058M. The period of performance for Phase II was from July 1, 2014 through December 31, 2018.

Component testing conducted in preparation for pilot testing included cold flow testing at atmospheric and pressurized conditions, and coal and limestone reactivity tests at elevated temperatures and pressures. These tests validated in-bed heat exchanger heat transfer capability, bed stability, and coal particle residence time predictions. They also quantified coal and limestone reactivity at the expected combustor temperatures and pressures.

The 1 MWth pilot testing achieved all performance goals with the exception of carbon conversion. The combustor achieved oxy-combustion at the full target pressure of 8 bar. Two key combustor performance goals that were achieved include exceeding the target sulfur capture in the combustor as well as exceeding the acid dewpoint target at full operating pressure. This validates assumptions about the pressures that can be achieved without acid gas condensation and the associated corrosion risks. The ability to achieve target operating pressures supports combustor cost assumptions. In addition, the CO_2 processing unit (CPU), demonstrated a new technology, the deoxidation (DeOxo) reactor. The CPU achieved all of its performance targets, while the DeOxo reactor demonstrated the ability to achieve 100 ppm or less of oxygen in the flue gas stream to meet CO_2 pipeline specs.

The pilot combustor was damaged during testing and an incident investigation was conducted. The primary cause of the hardware damage was due to anomalous temperature readings, caused by sensors buried and insulated in bed particles trapped by heat exchanger tubes near the wall. This led to higher gas velocities than intended, which then caused lower fuel residence time, lower carbon conversion, freeboard burning, and undetected excess temperatures in the combustor. As a result, the TRL 6 goal was not achieved.

Updated technoeconomic analysis predicts that the Oxy-PFBC can achieve the goal of <35% increase in COE with 90% CO2 capture if the carbon conversion performance target can be demonstrated in future testing.

Contents

Executive Summary

The Oxy-fired Pressurized Fluidized Bed Combustor (Oxy-PFBC) is an innovative, highly integrated, innovative system designed to lower the capital and operating cost of clean power production as a competitive alternative to natural gas powered generation. Pressurized combustion in oxygen and recycled carbon dioxide gas eliminates the presence of nitrogen and other constituents of air, minimizing the generation of pollutants and enabling the economic capture of byproduct carbon dioxide gas. Oxy-PFBC is fuel-flexible, suitable for converting coal, petcoke, biomass or coal biomass blends into clean power. The technology basis has been proven at commercial scale for pressurized air-blown systems, but it has not been demonstrated for oxy-combustion at pressure.

This project Advanced Oxy-Combustion Technology Development and Scale Up for New and Existing Coal-Fired Power Plants (Phase II) builds on previous US Department of Energy-funded Phase 1 work completed by the GTI team, including CanmetENERGY, with the specific goal to develop technologies for coal-fired power to capture >90% of the produced carbon dioxide, with no more than a 35% increase in the cost of electricity. The objective of the project is to conduct the testing required to mature the Oxy-PFBC concept to Technology Readiness Level (TRL) 6, and plan a First-of-a-Kind [FOAK] commercial, scaled up field demonstration of the Oxy-PFBC concept.

The Oxy-PFBC Phase II program involved testing US coals and execution of a complimentary Enabling Technologies for Oxy-PFBC project that tested both Canadian and US coals. A 1 MWth pilot scale plant was designed, built and operated at CanmetENERGY in Ottawa. Extensive support work was carried out on component testing, analysis and commercial planning.

The team members included GTI, Linde, Natural Resources Canada (CanmetENERGY), Pennsylvania State University, Electric Power Research Institute (EPRI), and General Electric. Additional research was provided by the University of Ottawa. Funding was provided by the US Department of Energy, Alberta Innovates and each of the team members. The total funding for Phase II was $18.537M with $12.058M. The period of performance for Phase II was from July 1, 2014 through December 31, 2018.

To enable a successful pilot scale demonstration, several components of the Oxy-PFBC concept needed to be tested and validated. The key component achievements from the project included:

- Cold flow fluidized bed tests validated in-bed heat exchanger capability and bed stability for atmospheric pressure conditions;
- Pressurized elutriation testing validated coal particle residence time and heat transfer for in-bed heat exchanger tubes at elevated pressure;
- Coal and limestone characterization tests quantified reactivity of coal and limestone at elevated pressure and CO_2 levels as expected in pilot operation. Test results validated sufficient residence time for coal particles, but indicated that limestone/dolomite would not have sufficient residence time. As a result, limestone particle size distribution specification was revised so that calcium would be retained in the bed for sufficient residence time for sulfur capture; and
- An agglomeration model was developed and validated, and simulations predicted that there is low likelihood of agglomeration if the bed temperatures are held near or below the planned operating temperatures of 850-900C and there is sufficient dolomite in the bed to increase ash melting temperatures.

The 1 MWth pilot was designed and fabricated at the pilot plant test facility in Ottawa, Canada at the CanmetENERGY facility. It was commissioned and tested as follows:

- Commissioning tests were completed in April 2017 - Demonstrated robust and repeatable ignition of coal, and the ability to sustain combustion with air.
- Three performance tests were completed in May, July and October 2017
    - May 2017 – Demonstrated the ability to ignite and sustain combustion with oxygen, including at elevated pressure. All Linde CO_2 Purification Unit (CPU) modules demonstrated to be functional. De-Oxo unit achieved performance goals with synthetic flue gas. A pilot operational issue was experienced and resolved with coal eroding through the feed line.
    - July 2017 – Demonstrated oxy-combustion at full operating pressure (8 bara), and demonstrated the ability of the combustor to capture greater than 99% of the fuel sulfur upstream of the Linde CPU, exceeding the goal of 90%. Identified issues with lower bed density and lower carbon conversion than expected. Dolomite-based agglomerates formed in the bed.
    - October 2017 – Continued to demonstrate oxy-combustion at pressure, but experienced issues with significant temperature gradients in the bed, low bed density, agglomeration and burning above the bed in the freeboard area. This led to slagging in the combustor and damage to internal hardware prior to auto shutdown.

Root cause analysis after completion of testing determined that anomalous temperature readings, caused by sensors buried and insulated in bed particles trapped by heat exchanger tubes near the wall, was the primary factor in the low bed density, low carbon conversion, slagging and combustor damage. The insulated sensors led to low average combustor temperature readings, which led to significantly higher than expected gas velocities, which led to lower bed density, lower fuel residence time and carbon conversion, freeboard burning, and undetected excess temperatures in the combustor.

Prior to experiencing bed agglomeration, encouraging results were obtained which support the overall potential of the Oxy-PFBC technology. A summary of the component and system performance targets and actual performances achieved are shown below in Table ES-1.

Table ES-1. Performance metrics: Oxy-PFBC testing met or exceeded all performance targets with the exception of carbon conversion.

Performance of components at Small Pilot scale	Achieved	Target
Carbon Conversion	87%	99%
Sulfur Capture in-bed	95%	95%
Sulfur Capture after filter	99%	97%
Sulfur Capture after Direct Contact Cooler	99.8%	99%
Bed Temperature	850C	850C

NOx lb/MWh gross after Direct Contact Cooler	10e-8	<0.7
Acid dewpoint	190C	<230C
Water pH achieved in condensed flue gas effluent	7.0	7.0
O_2 level achieved with low cost catalytic system (ppm)*	100	<100
% of heat captured at high temp to achieve target efficiency (requires larger scale to validate stages)	33%	17%

- The carbon conversion goal was the only performance goal that was not met and is a result of anomalous temperature readings.
- The in-situ sulfur capture performance goals were exceeded. Sulfur capture targets are important to prevent corrosion in downstream components through sulfuric acid condensation, and overall required to meet air quality standards while avoiding the expense of a downstream flue gas desulfurization system.
- All CO_2 purification unit goals were achieved with simulated flue gas including removal of NO_x, SO_x and O_2. The NO_x target is upstream of the LICONOX unit and insures that it can remove sufficient remaining NO_x to meet CO_2 pipeline purity specs. The O_2 target is also based on meeting CO_2 pipeline purity specifications.

- The 17% target for percent of heat captured at high temperature for a single stage (51% for all three stages) was achieved. This drives cycle efficiency by determining how much high quality heat can be extracted in the in-bed heat exchanger versus the lower quality heat from the convective heat exchanger (CHX). This balance between high quality and lower quality heat extraction for a given power level is driven primarily by the mass flow of the flue gas, which in turn is driven by oxygen partial pressure. Higher oxygen levels were achieved by reducing the recycle CO_2 flow, resulting in a corresponding reduction in flue gas flow that was cooled by the CHX, and reduced low quality heat extraction by the CHX for a given power output.

The Oxy-PFBC technology was built and operated at pilot scale and fell short of demonstrating TRL 6. To achieve TRL 6 all equipment must be operated at pilot scale in an integrated manner. All of the components were operated at this scale, however, a portion of the gas cleanup equipment, specifically the Linde LICONOX and DeOxo modules (to remove NO_X/SO_X and O_2, respectively), were not operated in an integrated manner with the PFBC to achieve the full TRL 6 designation. This was primarily due to intermittent operation of the fuel feed and bed ash drain systems. Although neither of these are new technologies being demonstrated, they still prevented achievement of the continuous run times necessary to characterize flue gas composition prior to starting up the full gas cleanup system. The LICONOX and DeOxo modules were demonstrated in standalone mode through the use of simulated flue gas. Based on test results, the technology is assessed at TRL 4-5.

The team still has outstanding issues at this time. Although the Oxy-PFBC completed all three planned tests, during the last test the hardware significantly exceeded allowable temperatures resulting in hardware damage and agglomeration of the combustor. An incident investigation was completed with a review board of outside experts. The review board concluded that the basic technology is sound with no

showstoppers, and worked with GTI to develop mitigation actions to resolve the operational issues encountered.

In addition to pilot testing, the subject project also developed scaled up Oxy-PFBC design concepts, evaluated the performance and levelized costs of commercial plants, and developed a roadmap for technology commercialization.

Scale up and commercialization accomplishments were:

- Conceptual level demonstration plant designs were developed for 5 and 20 MWe (15 and 60 MWth) plants
- Technoeconomic analysis updated in October 2017 and early in the project in June 2013, both confirmed that the cost of electricity (COE) projections were attractive as compared to alternate coal-fired power generation options with carbon capture.
- Alternate proprietary system architectures were developed that have the potential to provide additional significant reductions in projected COE relative to the steam Rankine cycle
- Significant commercial interest was shown in the technology, with commitments from commercialization partners and next stage funders to support a response to the Funding Opportunity Announcement DE-FOA-0001459, “Pre-Project Planning for Advanced Combustion Pilot Plants”, in October 2017. Five (5) host sites in three (3) countries committed to participate in a follow-on small scale demonstration project of Oxy-PFBC.

This final report is organized based on the project tasks, with a section providing an overview of each. The tasks are: Component Testing, Design, Analysis, Pilot Testing and Commercialization Plan.

1.0 Introduction

1.1 Project Background and Rationale

In support of the U.S. Department of Energy National Energy Technology Laboratory's (DOE/NETL) objectives for reduction of greenhouse gases emitted by coal fired plants, this project sought to validate a novel pressurized oxy-combustion process in a fluidized bed reactor for efficient, clean, coal-based power generation with carbon capture and sequestration (CCS). The pressurized oxy-combustion process burns solid fuels (Coal, biomass, petcoke) in oxygen with recycled carbon dioxide-rich flue gas to eliminate the presence of nitrogen and other constituents of air, minimizing the generation of pollutants and producing a concentrated CO_2 stream enabling the economic capture of the carbon dioxide gas.

The technology key benefits include production of electricity from coal with near zero emissions, while captured CO_2 may be utilized for enhanced oil recovery or sequestered in suitable geological repositories. The Phase II program utilized pilot plant testing to advance the technology and validate performance and economics predictions for new coal plants and the retrofit of existing coal plants.

The project funding for the Oxy-PFBC Phase II effort, described here in this report, was $18.4M with a period of performance from July 1, 2014 through October 31, 2017. The end date of the project was extended to 2019. The US DOE provided $11.9M of funding, while Alberta Innovates provided CDN$1.6M. The remainder ($4.9M) was provided by team members.

1.2 Project Goals and Objectives

The specific goal of this project was to develop technologies for coal-fired power to capture >90% of the produced carbon dioxide, with no more than a 35% increase in cost of electricity.

The objective of the project was to conduct the testing required to mature the Oxy-PFBC concept to Technology Readiness Level (TRL) 6, and plan a commercial, scaled up field demonstration of the Oxy-PFBC concept. The primary objective for the first budget period of Phase II, Budget Period 2, was to complete detailed design of the pilot and secure funding from Alberta Innovates or other partners so that a GO/NO GO decision can be made about proceeding with the remainder of Phase II. In addition, a GO/NO GO decision point was defined during Budget Period 2 based on the ability to identify a viable testing site for the pilot facility. The primary objective for the second budget period of Phase II, Budget Period 3, was to complete the pilot facility fabrication and commission the facility. The primary objectives for the third and final budget period of Phase II, Budget Period 4, were to complete pilot testing necessary to achieve TRL 6, and to complete the commercialization plan activities.

The team members included GTI, Linde, Natural Resources Canada (CanmetENERGY), Pennsylvania State University, Electric Power Research Institute (EPRI), and General Electric. Additional research was provided by the University of Ottawa. Funding was provided by the US Department of Energy, Alberta Innovates, and each of the team members.

1.3 Technology Overview

The commercial scale Oxy-PFBC power plant system (Figure 1-1) is an indirect cycle that utilizes a high aspect ratio bubbling fluidized bed. An indirect cycle generates power by heating a working fluid, rather

than generating power directly from the hot flue gas as has been done in air-fired PFBCs. One advantage of an indirect cycle is that it eliminates reliability issues associated with high temperature flue gas filters and gas turbine erosion.

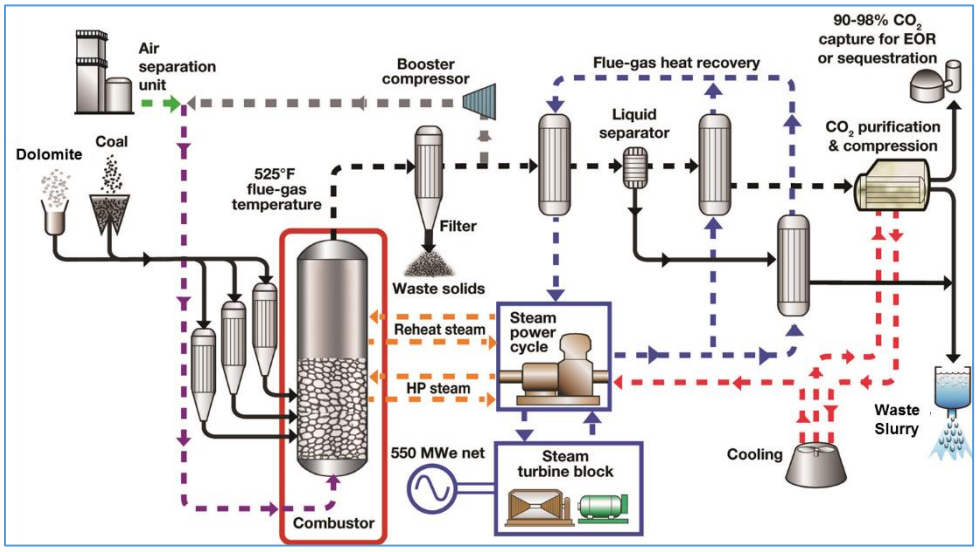

Figure 1-1. The architecture for a commercial scale Oxy-PFBC with a steam Rankine cycle.

The Oxy-PFBC includes two classes of particles: larger particles that make up the fluidized bed, and smaller pulverized coal and dolomite particles that are elutriated, or carried up, through the bed by the gas flow that fluidizes the bed particles. The fluidizing gas is composed of oxygen mixed with recycled flue gas. The air separation unit (ASU), which supplies oxygen from air, is thermally integrated so that waste heat is utilized to improve plant efficiency. In-bed and convective heat exchangers remove heat from the PFBC and are used to drive a supercritical steam power generation cycle (or an optional supercritical CO_2 Brayton cycle.) Sulfur capture is largely achieved by the large dolomite particles in the bed and the smaller ones elutriated through the bed. As a result, the flue gas desulfurization unit can be eliminated, thus reducing cost. The remaining gas cleanup system utilizes candle filters for ash and dolomite removal, and a CO_2 purification unit that consists of a direct contact cooler (DCC) for water separation, and Linde LICONOX® and DEOXO systems for NOx/SOx polishing and oxygen removal, respectively.

Pilot description

The 1 MWth pilot plant is similar to the commercial scale system shown in Figure 1-1 with some exceptions. First, the oxygen is provided by tanks on site, rather than utilizing an ASU. Second, no steam or power is generated. The combustor cooling is provided by thermal fluid (Therminol®) and air rather than steam. The air heat exchangers can be toggled on and off during operation to enable the heat removal to track heat generation in real time. Next, fuel injection occurs in one or two stages, rather than three stages at commercial scale. Finally, the CO_2 is purified, but does not undergo additional compression for sequestration as it would in a commercial plant.

2.0 Component Testing

Three component test activities were planned for this program. These included Cold Flow Tests (atmospheric pressure fluidized bed tests conducted at GTI), Coal and Limestone Characterization Tests (high pressure reactivity tests of coal and limestone particles), and Pulverizing and Drying Tests (quantify energy and methods required to pulverize and dry coal prior to injection into combustor – tests were not conducted). The Pulverizing and Drying Tests were eliminated, but another test activity for Pressurized Elutriation Testing was added after the program started to reduce uncertainties regarding the effect of pressurization on particle residence times and heat transfer to the in-bed heat exchangers.

The goal of the Cold Flow Tests was to quantify in-bed heat exchanger heat transfer coefficients, which are critical to creating a smaller low cost combustor, determining bed stability, and quantifying coal/dolomite particle residence times. The Coal and Limestone Characterization Tests were used to quantify coal and limestone/dolomite reactivity in a simulated Oxy-PFBC environment at appropriate pressures, temperatures and O_2 and CO_2 concentrations. This was important for determining particle residence time requirements for coal combustion and dolomite sulfur absorption. The pressurized elutriation tests measured the effect of elevated pressure on simulated coal particle elutriation rates and heat transfer to the heat exchanger tubes, since the earlier Cold Flow Tests could only be run at atmospheric pressure.

This section provides a high level summary of the test activities. For further information, see the full reports which are included as Attachments for the Cold Flow Tests (Appendix A) and Coal and Limestone Characterization Tests (Appendices B and C).

2.1 Cold Flow Tests

The Oxy-PFBC is a transformational technology that can potentially lead to significantly lower cost electricity with CO_2 capture. The most important driver for lower cost of electricity is the CapEx of the equipment which is projected to be significantly less expensive than traditional boilers with post combustion capture. The cold flow test is focused on items that drive combustor cost. The GTI Oxy-PFBC combustor at commercial scale is projected to be one third the size and half the cost of a traditional atmospheric pressure pulverized coal boiler. This more compact size is enabled in part by the elevated operating pressure, which reduces gas volume and the required size of the reactor. The other important feature is the in-bed heat exchanger, which is submerged in the fluidized bed particles. This results in five times the heat transfer of a traditional convective heat exchanger, thus enabling it to fit into the much smaller combustor. The result is a compact, low cost combustor.

The goals of the Cold Flow Test were to reduce uncertainty in three key areas that drive combustor design and cost: 1) Heat transfer for in-bed heat exchangers, 2) Particle residence time for fine coal and dolomite particles, and 3) Verifying that stable bed behavior can be achieved at full pilot scale.

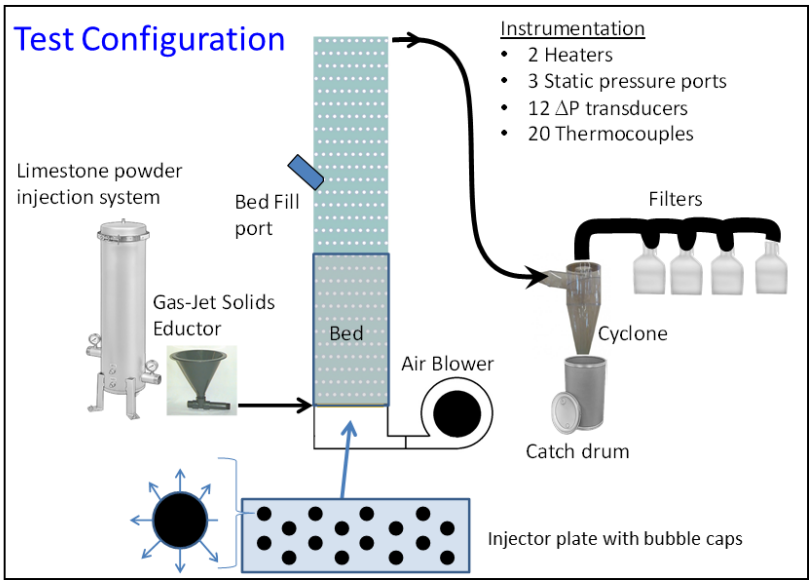

Figure 2-1. Cold Flow Test Configuration was used to test heat transfer, particle residence time and bed stability.

The Cold Flow Test utilized a test rig with a cross section that measured 12" x 20.5" and was 23' high (see figure 2-1). It was tested at facilities in Simi Valley, California. For comparison, the pilot scale rig at CanmetENERGY has a cross section of 9" x 14.5" and is of similar height to the test rig. The bed particles were 1 mm diameter glass beads, similar material to dolomite which is used for bed material in the pilot plant.

Several bed heat exchanger configurations were tested, including horizontal and vertical tubes. Although heat exchanger tubes were not active, some tubes were instrumented and had heaters inside to allow measurement of heat transfer for cases where the tubes were in or out of the fluidized bed. Elutriation tests were conducted using silicon carbide to simulate fine coal/dolomite particles, which have a similar density.

The heat transfer test results validated heat transfer assumptions used during the design of the pilot and commercial scale combustors using the Molerus and Yang correlation (see Figure 2-2). The figure shows heat transfer data for two different heat exchanger tubes with embedded heaters. The vertical axis of the figure is heat transfer coefficient, while the horizontal axis is the gas velocity nondimensionalized by the minimum fluidization velocity (Umf). The lower heater (maroon squares) is always immersed in the bed. As U/Umf is increased, the heat transfer coefficient jumps suddenly for U/Umf a little greater than one as the bed becomes fluidized. The heat transfer coefficient shows better performance than predicted by the Molerus and Yang correlation. The upper heater (purple crosses) does not get submerged by the fluidized bed until U/Umf of ~3.5. It also shows excellent heat

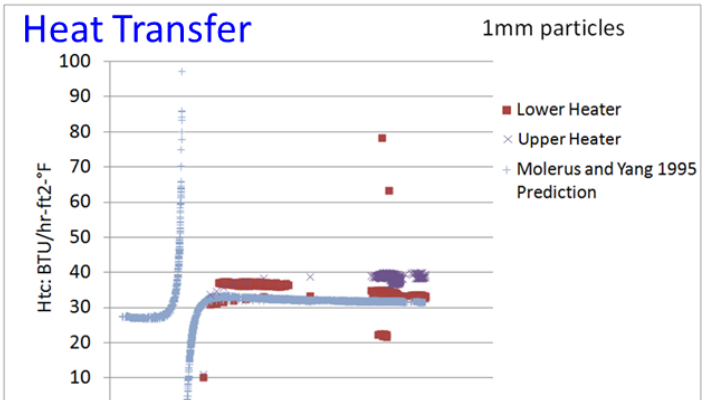

Figure 2-2. Measured heat transfer coefficient exceeds predictions, providing confidence in Oxy-PFBC heat removal capability.

transfer performance that is better than the correlation. These results validated the high heat transfer coefficients that were predicted for the in-bed heat exchanger.

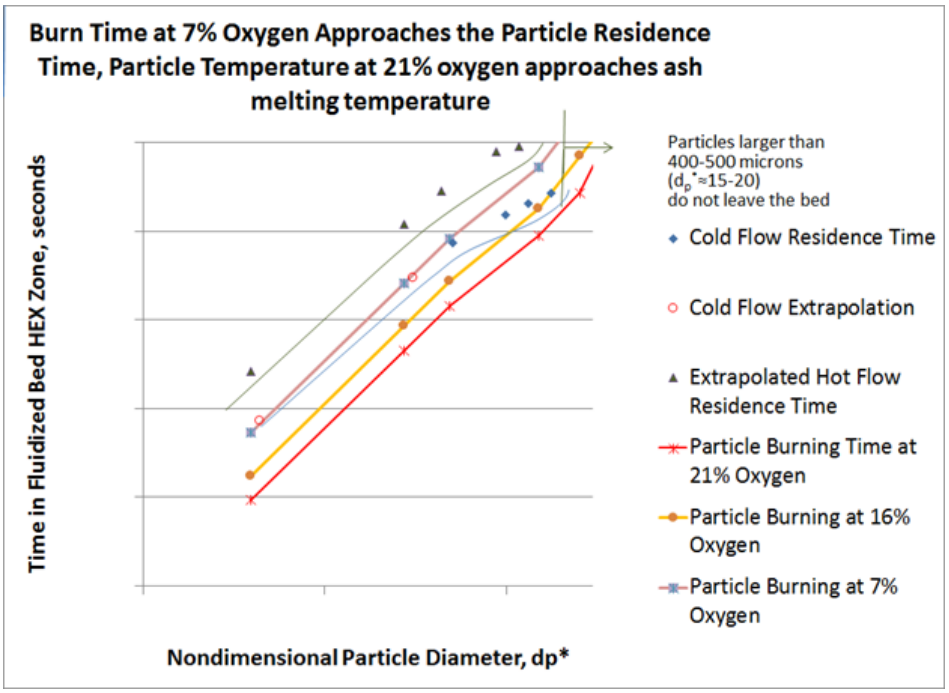

Figure 2-3. Particle residence time in hot flow exceeds particle burning time.

The particle elutriation test results, when combined with the coal reactivity test results, validated that particle residence time exceeds coal reaction time requirements (see Figure 2-3), however limitations of atmospheric testing indicated need for additional testing at elevated pressure, which is discussed later in this report. The figure shows particle residence time as a function of nondimensional particle diameter based on test data results (solid blue diamonds) and extrapolates those results to smaller particle diameters (red circle outlines). Analysis was used to determine residence time in a hot flow combustor environment. These are shown as black triangles near the top of the graph. In addition, lines are shown for particle burning time at several different oxygen concentrations (7%, 16% and 21%). The test results indicate that the particles have sufficient residence time with margin at all of these oxygen concentrations. However, most elutriation correlations break down for pressurized conditions, reducing confidence in the ability to extrapolate results to Oxy-PFBC operating conditions (see Figure 2-4.) The residence time should increase with particle size, but at elevated pressure, most of the models did not show this trend. As a result, a need for pressurized elutriation testing was identified and was conducted at the University of Ottawa as discussed elsewhere in this report.

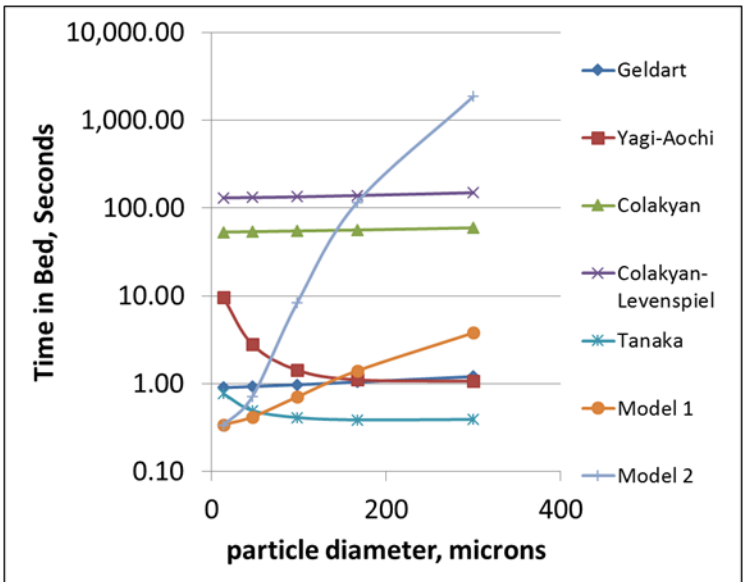

Figure 2-4. Most elutriation models evaluated did not predict proper trends for elevated pressure cases.

Test results also validate the ability to achieve stable bed operation at scales similar to the pilot rig (see Figure 2-5). The first configuration exhibited pressure oscillations as shown in the blue pressure trace on the left. This pressure, labeled Pin, was measured at the fuel injection port at the bottom of the combustor. The combustor operating conditions and physical configuration were altered so that the final configuration pressure oscillations were reduced by more than an order of magnitude compared to the first configuration.

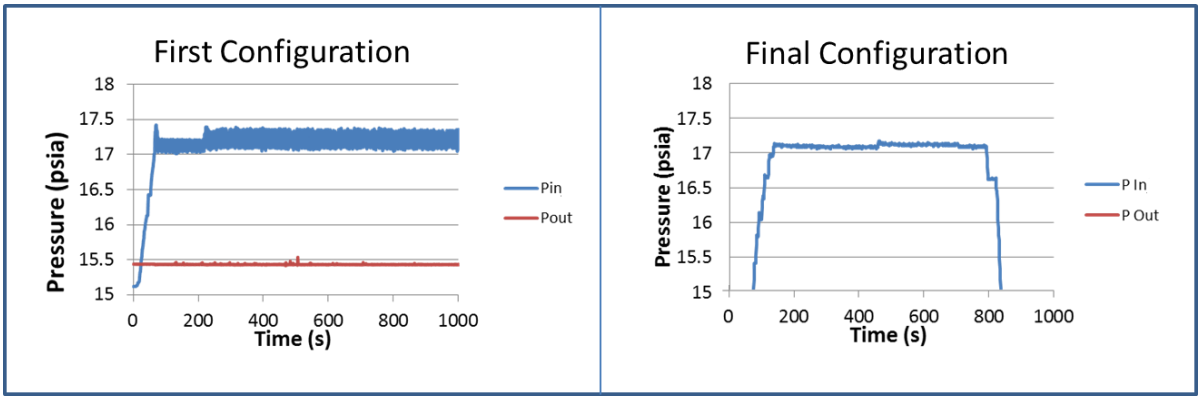

Figure 2-5. Cold flow testing demonstrated ability to achieve bed stability during operation.

2.2 Coal and Limestone Characterization Tests

The goals of the Coal and Limestone Characterization Tests were to characterize coal and limestone/dolomite reaction rates to determine if: 1) Full combustion can be achieved in the combustor based on residence times determined in the Cold Flow Test, and 2) Sufficient sulfur capture can be achieved within available residence times.

2.2.1 Coal Testing

To achieve the cost benefits of the Oxy-PFBC's compact combustor, fast reaction rates are required to insure full combustion within the reduced volume reactor. This is achieved by utilizing smaller coal particles than are typically used in conventional fluid bed combustors and by adjusting oxygen concentration levels. The smaller particles get carried out of the combustor with the fluidization gas and consequently have a reduced residence time compared to traditional fluidized beds that utilize larger particles which remain in the bed. The coal kinetics tests were used to quantify the reaction rates and support analysis on residence time requirements as discussed in the Cold Flow Tests section.

This is a summary of the testing effort. A more complete report is included in Appendix B, Coal Reactivity Report.

2.2.2 Coal Kinetics Test Objectives

The objective of the Coal Kinetics Testing was to measure the coal kinetic reaction rates of coal oxidation in a pressurized CO_2/O_2/steam environment to determine particle residence time requirements in the pilot and commercial scale combustors. The results of the testing were used to calibrate and validate the coal kinetics model in the GTI 1-D PFBC Kinetic Performance Code.

2.2.3 Coal Kinetics Testing Approach

Experiments were conducted using Illinois #6 bituminous coal in a laboratory scale oxy-fired pressurized fluidized bed combustor (PFBC) at Penn State University (PSU). Independent parameters that were varied include pressure, temperature, O_2/CO_2 concentration and coal particle size. The laboratory scale PFBC has a cross-sectional flow area of about 20 cm^2 contained within an electrically heated furnace. The PFBC was operated at a pressure from atmospheric to approximately 7.89 atm. Furnace wall temperatures were set between 800 and 875^o C. The oxy-fluidization gas composition contained between 5.3 and 16.0 vol% oxygen (O_2) with the balance being carbon dioxide (CO_2) gas. The fluidization gas flow rate to the PFBC was 3.0 to 6.3 standard liters per minute (slpm) with superficial gas velocities on the order of 1.4 cm/s. The Illinois #6 bituminous particle sizes for the initial runs were nominally 74 microns but increased to approximately 177 microns for the later experiments.

The laboratory scale PFBC reactor configuration is shown in Figure 2-6. The reactor is a batch fed reactor and is electrically heated until the reactor desired operating temperature was achieved. Gases were fed from compressed gas cylinders. The mass flow meters were adjusted to obtain the required flow of oxygen and carbon dioxide. These individual gas streams were fed to a mixing tank. Water was fed into a steam generator (stainless steel coil wound in a horizontal furnace) using a high pressure liquid chromatography pump. The gases from the mixing tank and the steam from the steam generator were mixed on their way into the annular section of the reactor where the gases are preheated and pass through the metallic frit to fluidize the feed particles. A thermocouple was placed just above the bed to monitor the temperature of the bed. Approximately five grams of Illinois coal was fed into the reactor through a lock hopper placed above the reactor. High-pressure carbon dioxide pulse was given to feed the coal into the reactor. The product gases from the reactor flowed through a heat exchanger and a pair of particle filters. The gases then flowed through a back- pressure regulator to a condenser where the moisture from the products was condensed. The back pressure regulator was adjusted to maintain the pressure inside the reactor. The dry products of combustion then flowed to a bank of gas analyzers, which monitored oxygen, carbon dioxide, carbon monoxide concentrations. The bank also had analyzers to measure sulfur dioxide and nitrogen oxides. In these tests the combustion gases were diluted with a known amount of argon after the condenser to bring the concentrations down to match with the ranges of the analyzers.

The reactivity of coal was measured by the concentrations of carbon dioxide and carbon monoxide flowing in the products of combustion. The type of data collected from each test is shown in Figure 2-7. The exiting concentrations of oxygen and carbon dioxide gas (in vol%) was continually measured along with the exiting carbon monoxide and sulfur oxide gas (in parts per million, ppm). These concentrations were subsequently used together with the measured fluidizing gas flow rate to determine the coal's moisture-ash-free (maf) weight loss history from a PSU data reduction analysis. These maf weight loss histories were then divided by the initial maf mass of bituminous coal placed into the reactor to provide the coal's maf mass conversion history.

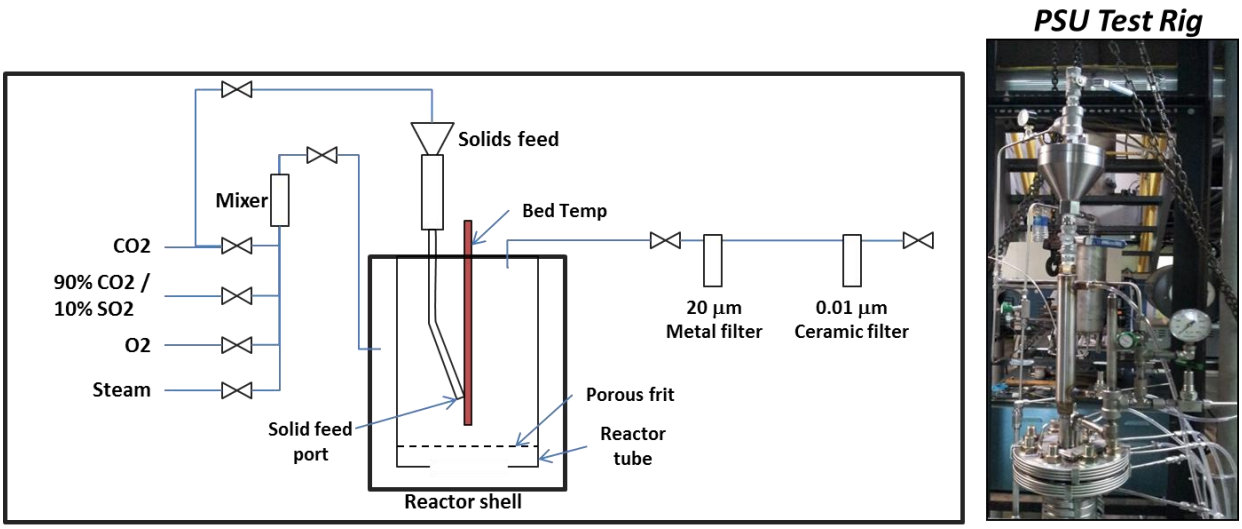

Figure 2-6. PSU oxy-fired PFBC test rig used to characterize coal kinetic rates

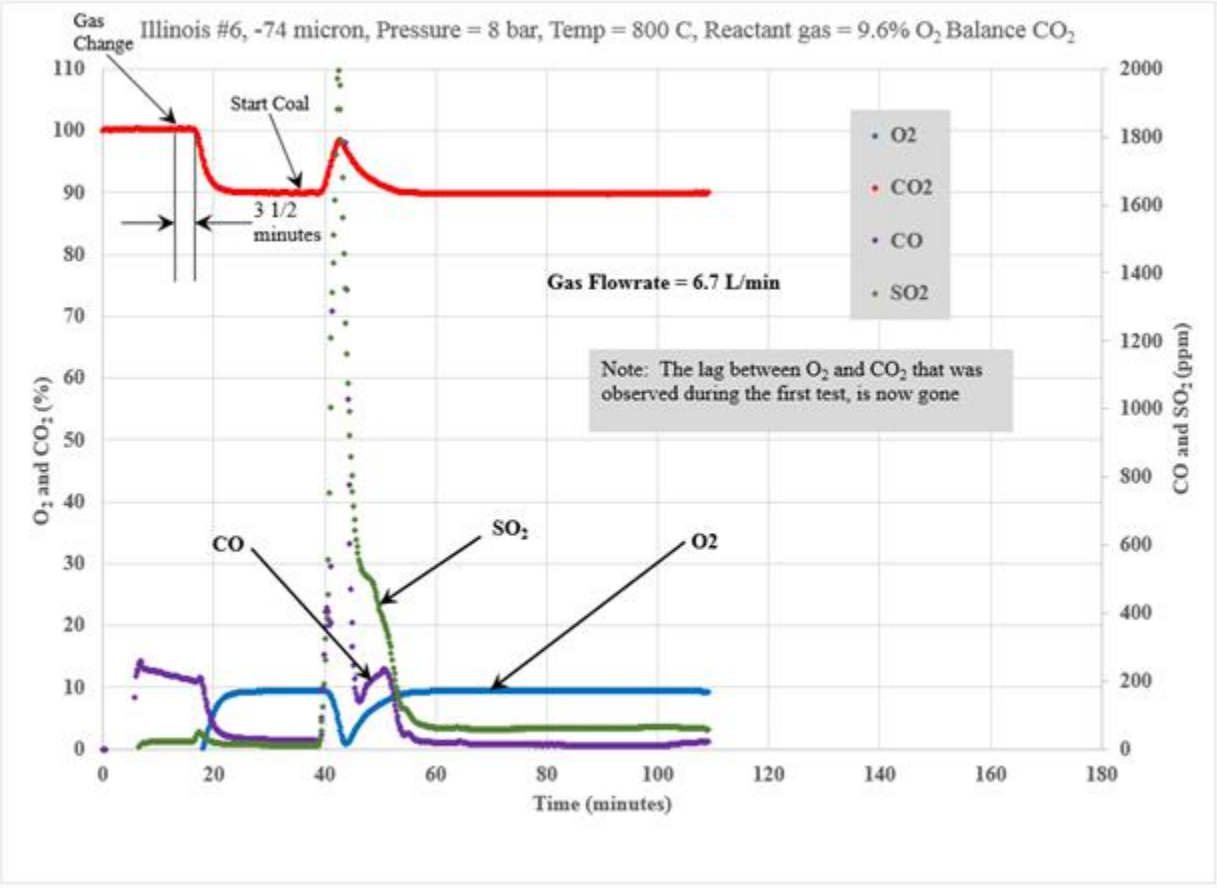

Figure 2-7. Typical raw data from a PSU coal reactivity test.

The GTI transient coal reactivity kinetic model used for PSU test data correlation assumed: (1) the gas flow through the PFBC is one-dimensional uniform plug flow (PF), and (2) the thin layer of coal or char mass within the fluidized bed recirculates under well-stirred-reactor (WSR) conditions. This PF/WSR kinetic model was shown to reasonably correlate the experimental test data by the adjustment of only one model parameter, the radiation heat transfer rate from the upper freeboard furnace section into the lower 0.25-cm thick fluidized bed layer. The radiation heat transfer rate into the bed was found to be on the order of 200 Watts. All other model parameters were taken from American Society for Testing and Materials (ASTM) ultimate/calorific analyses and historical kinetic parameters for bituminous coal devolatization and heterogeneous char-O_2 oxidation as used by GTI since the 1980's whose origins are from the laboratory work conducted at the Massachusetts Institute of Technology and West Virginia University -- among other institutions.

The GTI transient coal reactivity model, which was used in the 1-D PFBC Kinetic Performance Code, was modified to appropriately model the coal burning in the PSU test rig. The modification was required because the PSU test rig utilized larger coal particles (up to 177 microns) compared to the GTI Oxy-PFBC. This was addressed by adding a "shrinking core" char-O_2 model to better model gas diffusion through the larger particles.

2.2.4 Coal Kinetics Testing Results

The GTI model showed reasonable data correlation for the twelve bituminous coal reactivity tests conducted when looking at carbon burnout rates (i.e. time to achieve 98% carbon conversion). Twelve cases were run by PSU and all were modeled by GTI. Plots of all cases are included in the Appendix, but three samples are included here in Figure 2-8.

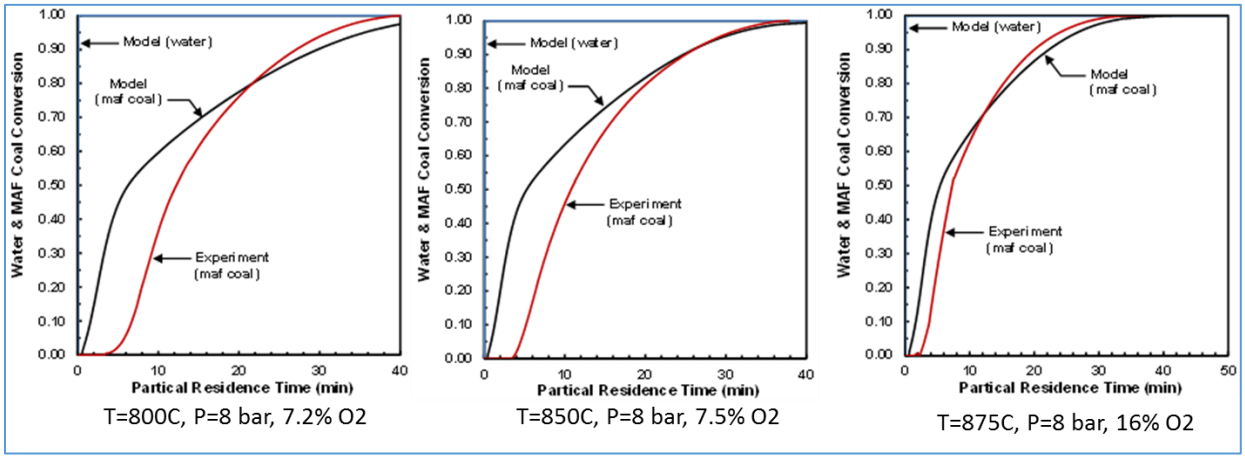

Figure 2-8. Burnout (time to >98% carbon conversion) is reasonably predicted by the GTI model

The slow carbon burnout times in the PSU rig are not indicative of residence time in the GTI Oxy-PFBC. Although the fluidizing/oxidizing gas entering the bottom of the reactor's fluidized bed was already pre-heated to the furnace temperature, the gas was quickly cooled by the lower temperature coal particles so that this gas actually exited the bed at the coal particle temperature. Even as the coal particles heated up to the furnace temperature the fluidizing/oxidizing gas flow rate was so low that the gas always exited the fluidized bed within a few degrees of the particle's temperature. The fluidizing/oxidizing gas flow rate through the fluidized bed was required to be

very low due to the small size of the coal particles (which had very low terminal velocities thus requiring very low gas superficial velocities) when compared to a usual fluidized bed coal particle size at a few millimeters in diameter.

Combining the results of this testing with the Cold Flow Test results indicate that coal particles in the Oxy-PFBC should have sufficient residence time for complete combustion.

2.2.5 Limestone Tests

The GTI Oxy-PFBC utilizes direct injection of limestone or dolomite into the combustor as the system's primary SOx removal process. This is expected to lower the cost of sulfur removal by eliminating the flue gas desulfurization (FGD) unit and its associated capital costs. The limestone kinetics tests are used to quantify the reaction rates and support analysis on residence time requirements for limestone. Results of the testing indicated that dolomite particles are the most reactive, and at least some of the dolomite particles need to be large enough to stay in the bed to provide sufficient residence time for sulfur capture. The testing results reduced the risk associated with inadequate sulfur capture in the bed. Later testing in the pilot plant indicated that the Oxy-PFBC exceeded the sulfur capture goal of 90% by capturing 99%+ of the sulfur within the combustor and filter.

2.2.6 Limestone Kinetics Test Objectives

The test objectives were to evaluate limestone sulfation reaction rates in pressurized combustion conditions for a variety of limestone and dolomite materials so that particle residence time requirements could be determined. The test data was also used to validate GTI's sulfation kinetic model.

This is a summary of the testing effort. A more complete report is included in Appendix C, Dolomite Reactivity Report.

2.2.7 Limestone Kinetics Approach

The experiments, conducted by Pennsylvania State University (PSU), utilized an experimental apparatus that was a small pressurized fluidized bed reactor (PFBR) maintained at constant temperatures in an electrically heated furnace. The PFBR operated at a pressure of approximately 7.89 atm and at temperatures between 825 and 875ºC. The fluidization gas composition was nominally 92 vol% carbon dioxide (CO_2), 7 vol% oxygen (O_2) and 2,400 parts per million dry (ppm-dry) or 0.24 vol% sulfur dioxide (SO_2). The fluidization gas flow rate to the PFBR was approximately 5 standard liters per minute (slm) and its superficial gas velocity within the PFBR was on the order of 1.4 cm/s. Four granular limestones were tested – identified as Graymont, Michigan, Dolomite-A, and Dolomite-B – which had been pulverized to a particle size of minus 200 mesh (or minus 74-micron). The limestone mass charge into the PFBR was approximately 5 grams. During the run, the instantaneous exit SOx mole fraction, was continuously measured.

The GTI sulfation kinetic model used for test data correlation assumed: (1) the gas flow through the PFBR is one-dimensional uniform plug flow (PF), and (2) the thin layer of limestone mass within the fluidized bed recirculates under well-stirred-reactor (WSR) conditions. This PF/WSR kinetic model was shown to reasonably correlate the experimental test data. The activation energy of the sulfation's rate limiting reaction step was found to be 24.1 kcal/mol with pre-exponential velocities ranging from 4.6 cm/s (for Dolomite-B) to 746 cm/s (for Dolomite-A).

2.2.8 Limestone Kinetics Results

The effective reaction rate was determined for each limestone/dolomite sample as a function of time during the test (as shown in Figure 2-9). The results for each limestone and dolomite are provided for three different test temperatures: 825, 850 and 875C.

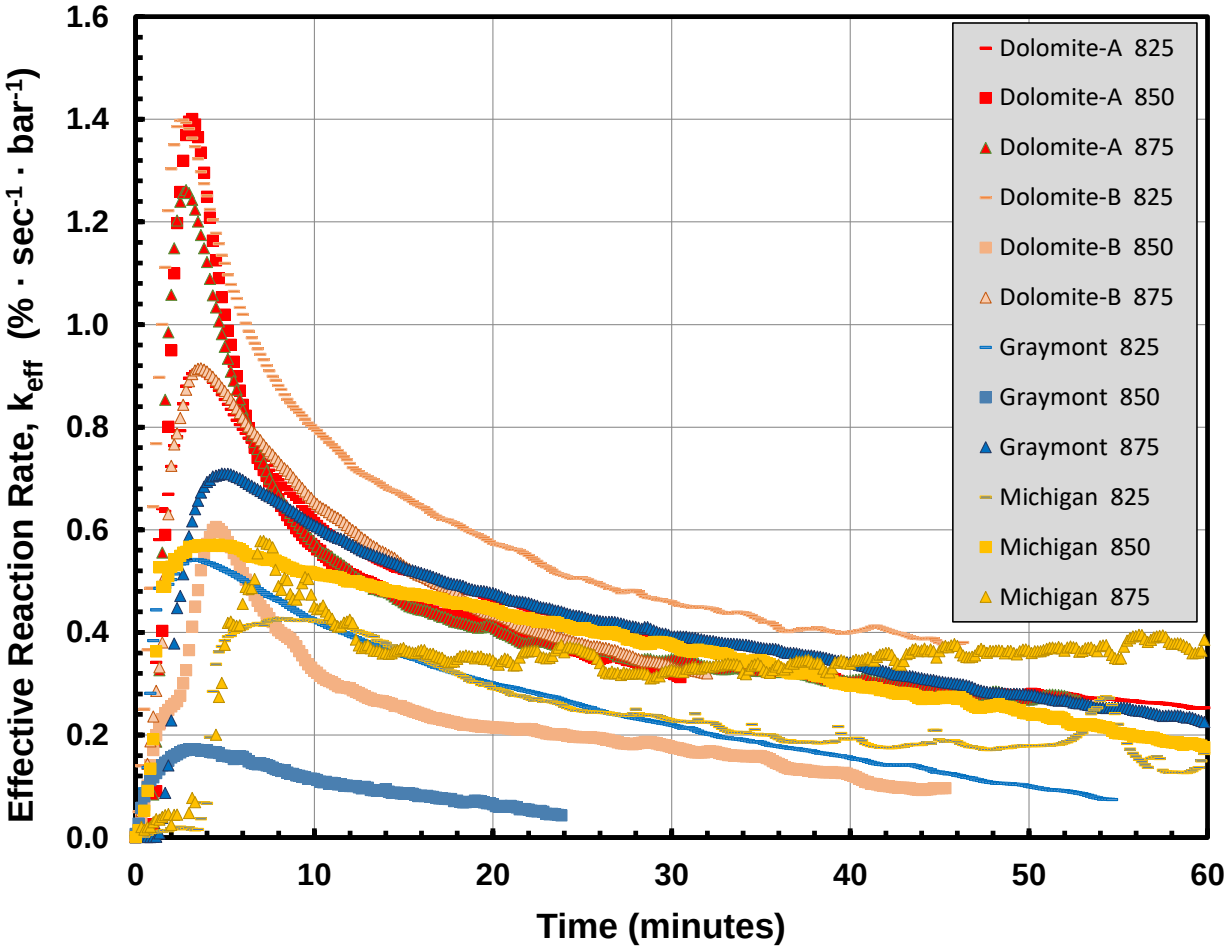

Figure 2-9. Limestone and Dolomite Reaction Rate Histories

2.3 Pressurized Elutriation Testing

2.3.1 Pressurized Elutriation Test Objectives

The objectives of the Pressurized Elutriation Test were to quantify the elutriation rates for coal and limestone particles at elevated pressures and quantify the impact of elevated pressure on heat transfer to the in-bed heat exchanger tubes in the fluidized bed at high pressure. Both elutriated particle

residence times and heat transfer coefficients are important since these support the efforts of GTI to shrink the combustor and its capital cost, as well as lower the overall cost of electricity.

2.3.2 Pressurized Elutriation and Heat Transfer Test Approach

The work presented here involved cold flow testing at non-reactive conditions in a pressurized fluidized bed. Large glass beads (mean particle diameter 1.0 mm) were used to simulate the combustor large bed material and smaller glass beads (fines; 0.040-0.180 mm in diameter) as the coal surrogate. The experimental apparatus (Figure 2-10) consisted of a stainless steel cylindrical fluidization column with a total height of 3 m. A feeder with a 0.019 m (3/4 inch) auger was placed inside a pressure vessel and used for the continuous feeding of fines. The feeder discharge (via the auger) was connected to the fluidization column via a 6.35 mm (1/4 inch) stainless steel tube pneumatic convey line. The injector was located 0.15 m above the distributor plate. The injector outlet was at the center of the fluidized bed. A tube bundle, consisting of five rows of tubes (Figure 2-10, left), was placed above the injector to simulate the in-bed heat exchanger tubes in the Oxy-PFBC pilot plant. To simulate a coal combustor, experiments were conducted in a continuous mode where fines particles were continuously fed to the fluidized bed at a rate of 5.9 kg/h. Downstream, entrained particles were continuously captured via two parallel filters outfitted at the column outlet. Each filter contained a filter bag used to determine the fines residence time at steady-state.

For the study of tube-to-bed heat transfer in this system, the center tube in the second row of the tube bank was replaced with a heating cartridge in a copper tube (Figure 2-11). Thermocouples were soldered to the copper tube surface at 5 points spaced by 45° from the bottom to the top to allow for local heat transfer coefficients to be

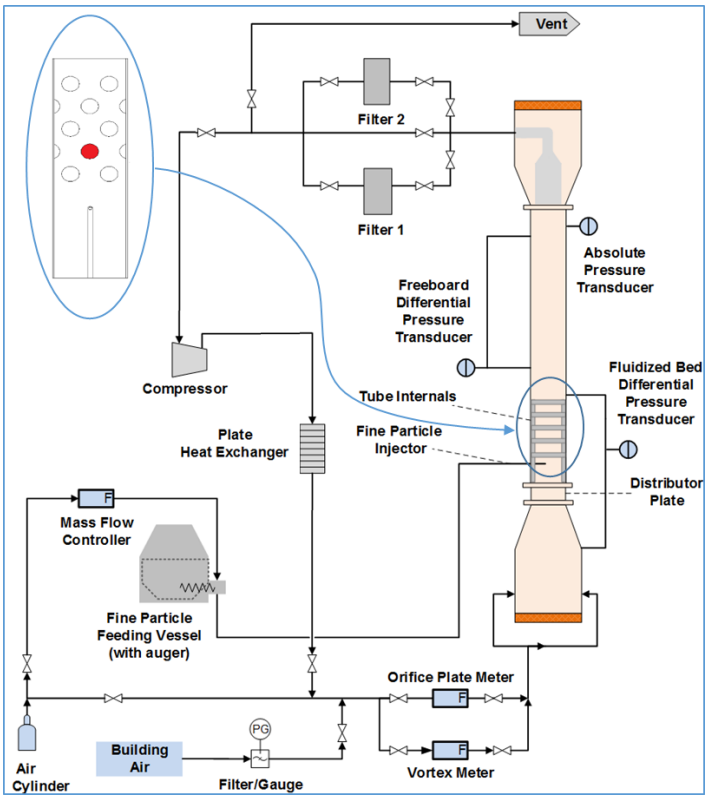

Figure 2-10. High-pressure fluidization system at University of Ottawa (Canada); Tube bank (circled) with heated tube highlighted in red.

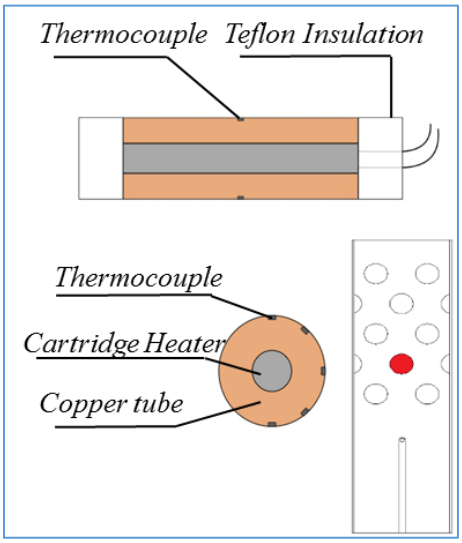

Figure 2-11. Cross-sectional views of the heated tube (shown in red) indicating thermocouple locations.

measured. The heater cartridge was supplied DC power, depending on operating conditions. Experiments were performed at 101 and 1200 kPaa, with the same bed material as above, and with or without fines (mean particle diameter of 0.06 mm) at a feed rate of 9.5 kg/h.

2.3.3 Pressurized Elutriation and Heat Transfer Test Results

The effects of operating pressure and presence of a tube bank within the bed of large particles on the average bubble size and fines (fuel) residence time within the bed are presented in Figure 2-12. Raising the pressure from 101 to 1200 kPaa at a constant excess gas velocity (U-Umf) of 0.51 m/s increased the fines average residence time. This is likely due to a lower superficial gas velocity and hence drag force on the fines as well as a reduced bubble size, which decreases the momentum of particles ejected into the freeboard. The combined effects of pressure and tube bank decreased the bubble size such to transition from the slugging to bubbling flow regime.

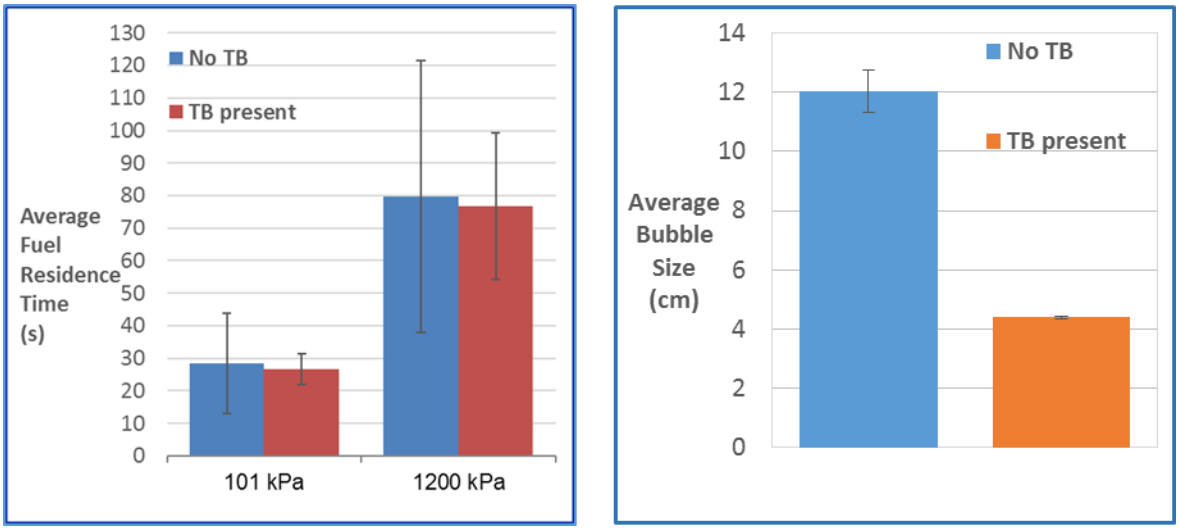

Figure 2-12. Effect of pressure and presence of tube bank (TB) at an excess gas velocity (U-Umf =0.51 m/s) on fines average residence time within the bed (left); and average bubble size (right).

The heat transfer results are presented in Figure 2-13, which shows the effect of operating pressure as well as the injection of fines into the fluidized bed. For an excess gas velocity of 0.51 m/s, increasing the pressure from 105 to 1200 kPaa nearly doubled the heat transfer coefficient (h). This corresponds to the average gas bubble size decreasing with pressure allowing better contact between the bed material and tubes. Results were in good agreement with the model prediction by Molerus et al. Injecting 9.5 kg/hr of fines at both pressures consistently reduced the average heat transfer coefficient by approximately 5%. Further experiments will be performed to determine the

Figure 2-13. Average heat transfer coefficient across the heated tube in a fluidized bed with and without the addition of fines (9.5 kg/h) at pressures of 105 and 1200 kPa. Predicted values from Molerus et. al. correspond to results without fines.

mechanism by which the fine particles impact heat transfer. The increase in heat transfer by a factor of >1.9 due to increasing pressure (as shown in Figure 2-13) exceeds the factor of 1.7 used for design, providing further support for the combustor and heat exchanger size and cost estimates.

2.4 Pulverizing and Drying Tests

In the original program plan defined in Phase I of the program, a risk was defined, "Pulverization and drying of coal lowers efficiency by using too much CO_2 or heat." Design modifications in Phase I and analysis in Phase II removed the need for this testing.

The original concerns, when the risk was first defined, were that pulverizing to the fine coal size may be difficult, and drying would consume a significant amount of parasitic energy and contribute to increased cost of electricity (COE). This risk was addressed in Phase I by modifying the design to utilize waste heat from the air separation unit (ASU) in the form of warm N_2 to dry the coal during pulverization, rather than a parasitic load from the combustor or generators. This effectively mitigated the original concern in Phase I about reducing cycle efficiency, but introduced a new concern for Phase II: the dried coal would now be mixed with N_2 gas, which was expected to complicate the flue gas CO_2 purification process.

Large quantities of nitrogen in excess of what is fixed in the coal is undesirable in the oxygen blown PFBC combustion process and CO_2 has been planned to pressurize and convey the coal from the high pressure lock hopper feed system into the combustor. There was concern however that the nitrogen held up in the atmospheric coal storage tank and pulverized coal void space located at the entrance to the lock-hopper could become an issue. It was thought that a new invention might be required to somehow eliminate the N_2 gas and replace it with CO_2 prior to injecting the coal/gas mixture into the combustor.

During Phase II, analysis indicated that the nitrogen gas mixed in with the coal was only a few percent of the nitrogen naturally present within the coal, so it should not significantly impact the system. It was determined that the extra nitrogen can be removed with the existing gas cleanup system that was provided by Linde. It was also determined that commercial off the shelf equipment could be used for the dryer and pulverizer, so there was no technology development needed.

The nitrogen gas content concern was addressed by comparing the percentage of nitrogen trapped in the coal void space at the entrance of the lock-hopper to the amount of fixed nitrogen in the coal. The fixed nitrogen percentage from a variety of Illinois basin coals were examined, including: Danville, Baker, Herrin and Springfield [Resource Assessment of the Springfield, Herrin, Danville, and Baker Coals in the Illinois Basin, Chapter 5 -Characterization of the Quality of Coals from the Illinois Basin, R.H. Affolter and J.R. Hatch, U.S. Geological Survey Professional Paper 1625-D]. The median fixed nitrogen mass percentage was 1.2% and a maximum value of 2.7%. The analysis indicates that the void space nitrogen represents less than 3.8% of the maximum fixed nitrogen observed in Illinois basin coals, i.e. approximately 0.1% nitrogen or less.

3.0 Design

3.1 Pilot Design - PFBC

At the heart of the Oxy-PFBC pilot plant is the Oxy-PFBC itself; it handles the oxy-fired combustion of coal, is the primary sulfur capture mechanism, extracts heat energy from the combustion, cools the flue gas in preparation for recycle treatment, and removes large ash particles. The pilot unit consisted of a fluidized bed combustor, an in-bed heat exchanger, the convective heat exchangers, and the bed ash removal system. Due to height constraints of the test facility building, the combustor and heat exchangers were housed within two pressure vessels; the main PFBC vessel on the right, and the Convective Heat Exchanger #2 (CHX 2) vessel on the left as shown in Figure 3-1. Within the main PFBC vessel a refractory lined stainless steel column contained the combustor, in-bed heat exchanger, and Convective Heat Exchanger #1 (CHX 1). The CHX 2 vessel contained a stainless steel column that houses CHX 2. Flue gas flows between vessels via a double walled duct. Below the main PFBC vessel, was a valve train required to depressurize and remove bed ash from the bottom of the bed.

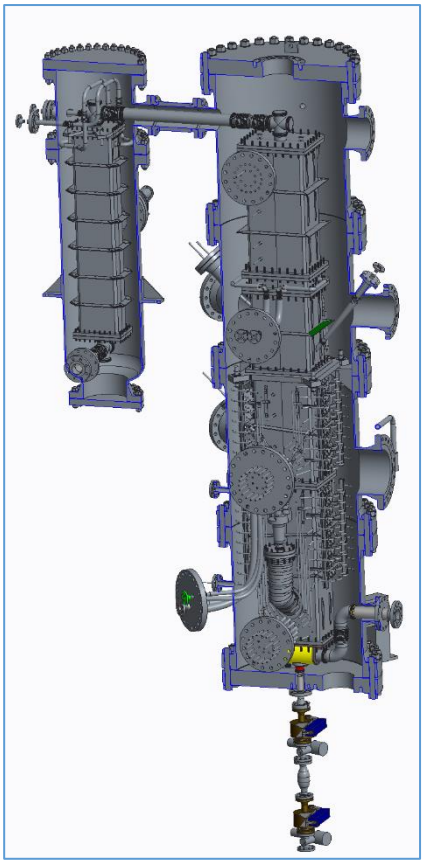

Figure 3-1: PFBC

3.1.1 Pressure Vessels

The main pressure vessel is a carbon steel, ASME Section VIII Div. 1 pressure vessel. The internal dimensions are approximately 1.25m in diameter, and 5.7 m tall. Due to constraints on facility crane height, the vessel was divided into four spools, which allowed for the simultaneous build-up of the pressure vessel and the refractory lined combustor. The top and bottom heads of the vessel were capped off with blind flanges. To protect the vessel, the combustor seals in the flue gas and was surrounded by an inert CO_2 blanketing gas. The inner wall of the combustor wasalso lined with mineral wool insulation, which protected the vessel shell from excessive heat radiating from the combustor.

The CHX 2 vessel is a carbon steel, ASME Section VIII Div. 1 pressure vessel. The internal dimensions are approximately 0.75m in diameter, and 3.2m tall. This vessel is built in two spools. The top head is a blind flange, and the bottom is a domed head with an 18” nozzle opening. To protect the vessel, the CHX 2 spool seals in the flue gas and is surrounded by an inert CO_2 blanketing gas.

The pressure vessels support numerous feed through lines for process and feed flow paths. Various blind flanges with openings were located throughout the vessels; the blind flanges were either bored through and welded to piping, or tapped with a pipe thread to allow for the installation of a Swagelok bore through fitting for tubing (the fittings were subsequently seal welded). To facilitate the connection of feed through ports with the piping/tubing inside the vessel, flex hoses were typically employed. This allowed for connection of the hose to feed through port before closing off the blind flange. Flex hoses typically used JIC fittings, or threaded pipe end connections. The various feed through ports and their sizes are shown below:

- Bed Ash: 2” pipe

- Coal/Sorbent: 3/8 tube
- Recycle Gas: 4” pipe
- Natural Gas: 1” pipe
- Burner Air: 2” pipe
- Solids Port: 3/4” tube
- Dilution CO_2: 1/2” tube
- DPT Ports: 1/2” tube
- Interstitial Pressurization: 1/2” tube
- IHX Coolant: 1/2” tube
- Bed Material Supply: 1-1/4” pipe
- CHX Coolant: 1-1/4” pipe
- Flue Gas Crossover

Additional feed through for electrical components was required as well. Electrical and instrumentation connections were fed through using Conax fittings with factory installed lead wires; the fittings installed onto the Swagelok borethrough fittings. Some of the electrical feed through connections include:

- Spark Ignitor Port
- Flame Detector
- Thermocouples
- Bed Headers

3.1.2 Combustor

The combustor, free board, and CHX 1, which are exposed to the hottest temperatures, all resided in a refractory lined column (Figure 3-2). The column consisted of a stainless steel shell lined with an insulating refractory material on the interior. The refractory lining reduced the shell skin temperature down to 480°C (versus a 950°C process temperature). Due to limitations on crane height, the column was broken up into five sections; each section was bolted together and sealed with a Vermiculite gasket. The refractory lining was also designed to withstand the abrasive and corroding environment of the bed.

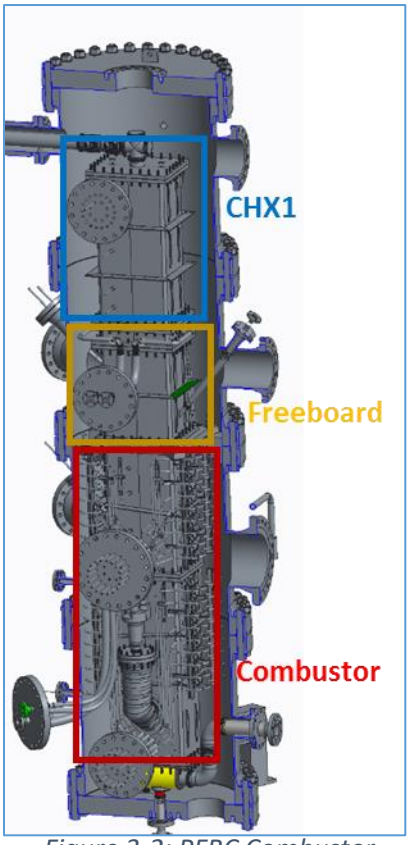

Figure 3-2: PFBC Combustor

At the bottom of the column was the recycle/fluidizing gas injection assembly. This area contained the recycle gas inlet duct, the windbox, and the tuyures (Figure 3-3). The recycle gas (which had been premixed with oxygen) entered the pressure vessel through a feed through port, and was directed to the windbox via the recycle gas inlet duct. The s-shaped duct allowed for the recycle feed through port and windbox to be located at different elevations, thus saving the need to extend the pressure vessel enough to accommodate a port below the windbox. A bellows expansion joint in the duct accommodates thermal growth of the combustor shell

relative to the pressure vessel. Due to velocities in the duct, the bellows expansion joint had an internal liner in order to prevent excessive vibrations. Band clamps were used on either side of the inlet duct, and were sealed with a Vermiculite gasket. The band clamps required only one nut to install, thus saving space inside the pressure vessel. After the recycle gas passed through the inlet duct, it entered the barrel shaped windbox. The windbox functioned as a manifold, distributing gas flow evenly between the two tuyeres. Two pipes leaving the top of the windbox functioned as the bottom of tuyeres. These pipes feed through a stainless steel plate, which functioned as the bottom of the bed. Due to the presence of pre-combusted recycle gas just above the plate, the temperature at the plate was not hot enough to require refractory lining. Two bubble caps were connected to the windbox to form the tuyeres. The bubble caps were designed to be easily changed out and replaced; they were held in place with band clamps and sealed with a Vermiculite gasket.

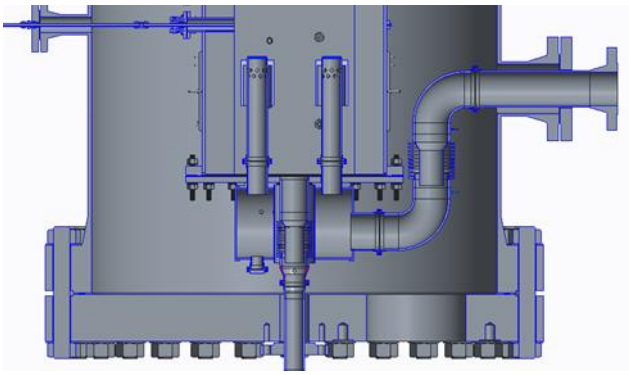

Figure 3-3: Recycle Gas Inlet and Fuel Injector

Located above the tuyeres, but before the first set of in-bed heat exchanger tubes, is the fuel/sorbent injector. The injector is a 3/8" stainless steel conveying line that penetrates through the refractory wall and terminates at the entrance of the bed, it relies upon jet penetration of the coal/sorbent mixture into the bed to provide proper mixing of the combustibles. The cool conveying gas keeps the metallic injectors ports cool. The coal/sorbent conveying line is fed into the pressure vessel through a Swagelok lock bore through fitting. To allow for growth of the combustor relative to the vessel wall, the conveying line enters the combustor through a graphite packing seal. This allows for the conveying line to move freely, seals in flue gas, and doesn't introduce protuberances into the coal/sorbent pneumatic transport line (such as bellows or steam loops).

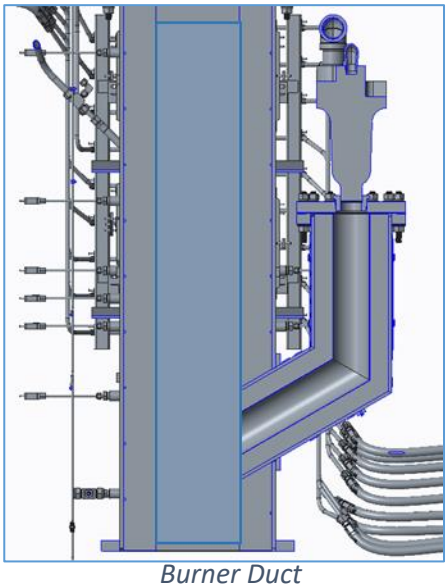

Burner Duct

A natural gas burner provides preheat to the bed, allowing for warm up of the bed, refractory, and the therminol cooling system. The natural gas burner is attached to a burner duct (large duct on the right in Figure 3-4, with burner on top), which directs the hot gas flow into the bed. Because both the burner and duct are housed inside the pressure vessel, there are no hot pressure vessel feed through pipes, and the burner can be operated at pressure. The burner is a high velocity air burner made by Fives North American. Ignition is conducted by spark plug, and the flame is monitored via a flame rod. Burner natural gas, air,

ignition harness, and flame rod wire are all fed into the pressure vessel. The burner duct is insulated with a vacuum formed ceramic fiber material, and lined with a Hastelloy sheath. The ceramic fiber has a high tolerance for thermal shock loading due to the natural gas burner, while the Hastelloy sheath protects the ceramic fiber from the high velocity gases.

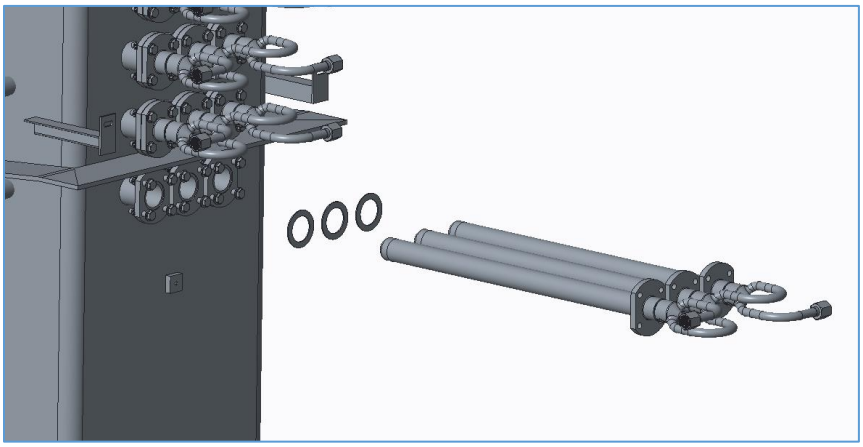

Figure 3-5: In-Bed Heat Exchanger Row

The combustion section of the bed is filled with the in-bed heat exchanger. The in-bed heat exchanger not only regulates bed temperature, but the presence of the tubes help break up bubbles and helps mitigate bed chugging. The heat exchanger consists of thirty-six rows of tubes; each row contain three coaxial tubes (Figure 3-5). Cooling of the bed happens in parallel between rows; coolant entering the vessel travels to the first tube in a row, travels down the outer annulus of the tube then turns around and travels through the inner annulus, then exits the tube and repeats in the second then third tubes of the row before leaving the vessel. Coolant lines which feed each row are manifolded outside the pressure vessel, thus each row has its own set of feed through ports on the vessel. This allows for flexibility in operation of the in-bed heat exchanger, allowing for therminol, air, or no coolant at various levels in the bed. The in-bed heat exchanger spans two combustor spools; to provide continuity in bed geometry, a set of dummy tubes is placed in the area where the flanges prevent the usage of actively cooled tubes. In some areas of the bed, thermocouples are installed on the surface of the heat exchanger tubes, thus allowing for measurement of the heat transfer coefficient of the bed.

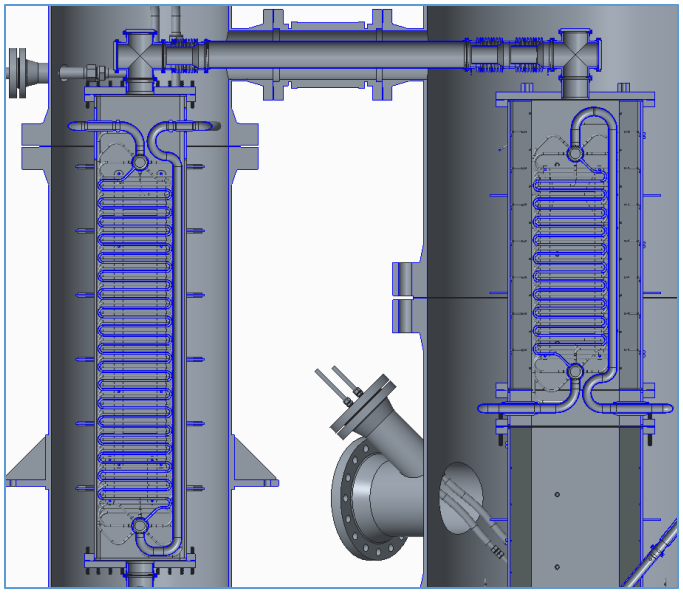

Figure 3-6: Convective Heat Exchangers

Flue gas leaving the bed is cooled in the convective heat exchangers. The convective heat exchangers (CHX 1 and CHX 2) are therminol cooled, coiled heat exchangers (Figure 3-6). Height constraints necessitated splitting up the convective heat exchanger into two parts. CHX 1, which sees hotter flue gas, is located in the refractory lined section above the bed, while the cooler CHX 2 is located in a stainless steel shell inside of the CHX 2 vessel. The duct between the two heat exchangers must feed through two pressure vessels. To do this the stainless duct is insulated with rigid calcium silicate insulation, and fits through the pressure vessel nozzles and the flex hose between the vessels. The flex hose allows for the two vessels to grow at different rates. On either end of the cross over duct are bellows expansion joints which allow for expansion of the combustor and CHX 2 shells.

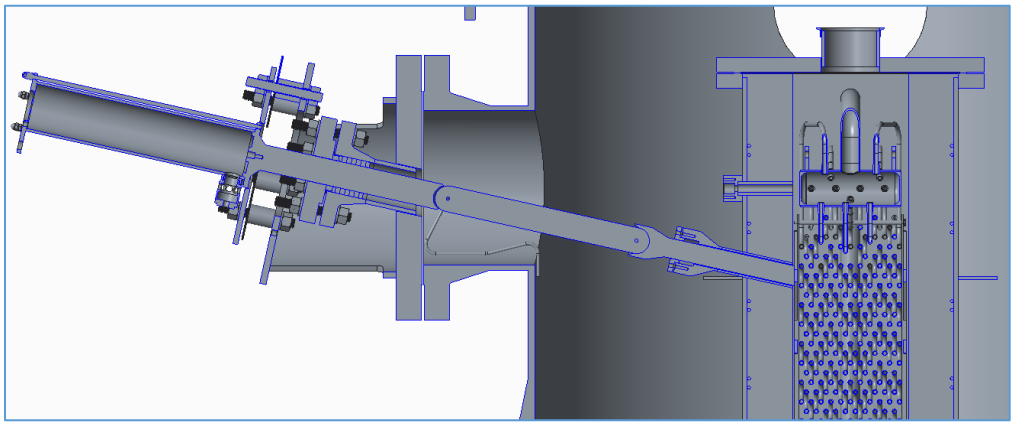

Figure 3-7: Soot Hammer

In order to control heat exchanger fouling due to ash build up, both CHX 1 and CHX 2 are equipped with soot hammers (Figure 3-7). The hammers are pneumatically powered, and are mounted on the pressure vessel flange. The hammer's anvil passes through two packing seals, one on the pressure vessel and one

on the flange. To allow for offset and thermal growth, the two anvils are connected by a spherical end connecting rod.

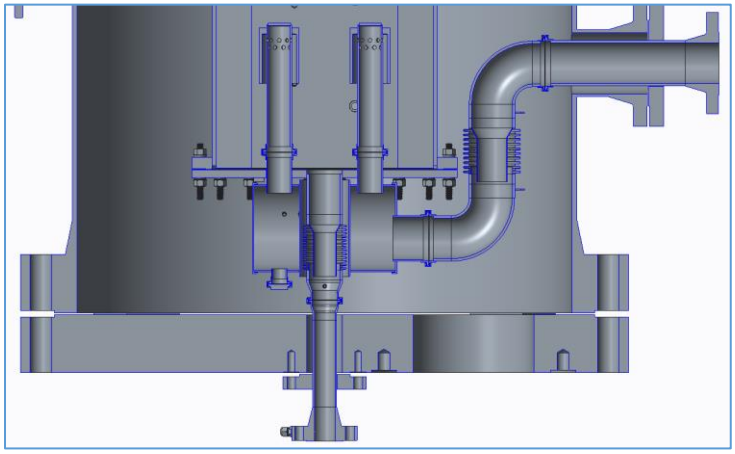

Figure 3-8: Bed Ash Removal

Bed particle removal takes place at the bottom of the bed. The windbox plate (which functions as the bottom of the bed), has a 3" pipe that travels through the windbox barrel and connects with the bed ash feed through port (Figure 3-8). To allow for expansion of the combustor shell, the bed removal pipe has a bellows expansion joint. In order to ensure that bed material removed from the bottom is sufficiently cool, there is a bed ash cooler port located in the pipe. This port injects CO_2 into the bed removal pipe, thus cooling any material in the port.

3.2 Pilot Design - Gas Cleanup and Purification

Linde's CO_2 Purification Unit (CPU) provides a cost-effective method for CO_2 purification (99+% purity) and heat recovery compared with traditional cryogenic CO_2 purification units. Linde's approach uses a Direct Contact Cooler (DCC) for complete HCl removal, a Liconox® to remove SOx and NOx by 95% and 90% respectively, and a De-oxidation reactor (De-Oxo) that can reduce the O_2 below 100 ppm, while increasing net efficiency by heat integration with the power cycle (see Figure 3-9).

The system design began in November 2014 following a design basis review meeting at CANMET facilities in Ottawa, Canada with the rest of the project team. Linde LLC worked with GTI (formerly AR) and Canmet staff to finalize a facilities requirement document that would be the basis of design for Linde Engineering's basic engineering and the work was kicked off in December 2014.

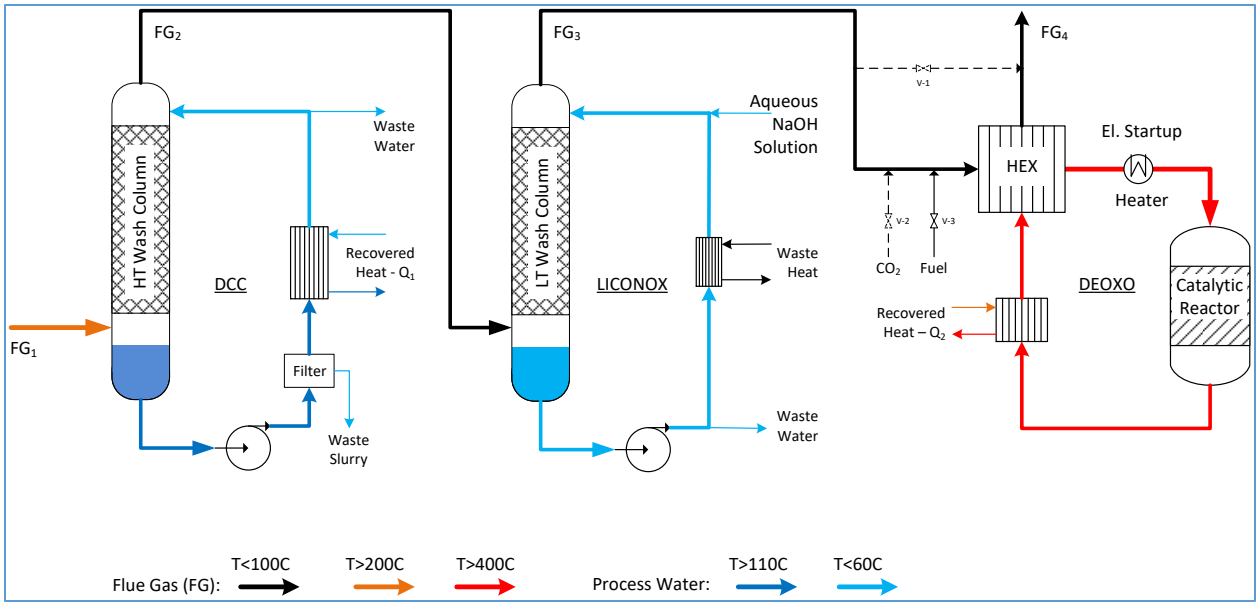

Figure 3-9: Overview of Linde CO_2 purification unit (CPU) process

During an interfaces and plant layout meeting with Linde, GTI and Canmet held in February 2015, it was first recognized that the Linde concept of a 100% pre-fabricated skid would not fit within the allocated space in the Canmet facility. After collaboration with GTI and Canmet, the equipment layout concept was modified from a single pre-fabricated skid to multiple subassemblies to be assembled onsite. The initial layout planned for two pump skids on the ground level; 3 subassemblies on Level 2 for the heat exchangers, piping, and wash water filter; and 3 subassemblies on Level 3 for the heat exchangers, start-up heater and De-Oxo reactor vessel.

Linde and GTI agreed to modify the design of the direct contact cooler to integrate it with the Oxy-PFBC. This mutual decision would eliminate an additional piece of equipment from GTI to quench their flue gas products; however, it also required the materials of construction for the DCC to be more resistant to stress corrosion. The De-Oxo reactor was designed with help from the catalyst vendor. A sulfur guard layer was included in the reactor vessel upstream of the catalyst to reduce the potential for catalyst poisoning. Due to the expected temperature rise in the De-Oxo reactor, the initial configuration of the De-Oxo heat exchanger was replaced by two plate & frame heat exchanges connected in series to reduce the effect of thermal stresses on the heat exchanger material.

The Basic Engineering Design Package (BEDP) was completed and released for approval in April 2015. This package included the

- Preliminary process design,
- Equipment data sheets,
- Piping and instrumentation diagrams, data sheets and specifications,
- Electrical load
- Preliminary layout
- Operating manual, and
- All safety requirements and specifications.

The detailed engineering started immediately with a review of the process and equipment data sheets from the BEDP and a preliminary vendor quotes for the build of Linde's CPU. An additional air supply line to the De-Oxo unit was introduced into the design during detailed engineering to (1) be able to test the De-Oxo unit with a broader inlet gas parameter range as the PFBC flue gas quality parameters are subject to actual testing conditions and (2) to run the De-Oxo unit independently from the PFBC unit to maximize on-stream testing time for the De-Oxo unit.

Throughout the basic and detailed engineering phases of the project, several process and safety meetings were conducted to ensure safe design of the Linde process and equipment selection. This included a Linde HAZOP in February 2015, an overall system HAZOP at Canmet in April 2015, an engineering and design project safety review (PSR3) and 3D model review meeting in August 2015, and a technical risk assessment (TRAS) for the CPU in October 2015, a second HAZOP in April 2016 second 3-D model review in June 2016, a construction and commissioning project safety review in November 2016(PSR4 and PSR5).

The procurement of equipment and materials for the construction of the Linde CPU was carried out on a continuous basis from late 2015 through September 2016. The structural fabrication of the skids began in August 2016 and progressed through the beginning of September. Figure 3-10 and 3-11 show the final versions of skids 1 and 2 in the shop right before shipping. The components on skid 1 include the process condensate cooler for the DCC and associated piping, while skid 2 houses the process condensate filter for the DCC along with piping for the flue gas feed to the CPU. Skid 3 includes the piping for the process condensate from the DCC and wash water from the LICONOX to the respective coolers, along with the feed lines for NaOH and process water. Skid 4 includes feed lines for service water along with other miscellaneous piping. Skid 5 contains the de-oxidation reactor, start-up heater and LICONOX wash water cooler. The last skid, skid 6 holds the fuel and air injection lines to the de-oxidation system.

Figure 3-10. Skid 1 after assembly and ready for shipment

Figure 3-11. Skid 2 ready for shipment

The skids were delivered to the Canmet facility in three shipments between September and October 2016. Installation of the Linde equipment began soon after with the staff at Canmet fitting any loose shipped equipment onto the subassemblies and connecting the piping between modules and the utilities at the battery limit. With remote guidance from the vendor, Canmet also assisted the Linde team with the installation of the catalyst and the sulfur guard bed within the De-Oxo reactor. Figures 3-12 and 3-13 show the location of Module 4 and Module 2 both located on the second-floor mezzanine.

Figure 3-12: Module 4 with process condensate filter

Figure 3-13: Module 2 set in place on second floor

Mechanical completion of the CPU was achieved in February 2017. The CPU subsystem was handed over to Linde Engineering North America to commence pre-commissioning. These activities included: verification of the catalyst installation, piping and instrumentation diagram (P&ID) conformity checks, check of piping, equipment and electrical installations, witness of pressure test for tightness, check of instrumentation and control loops, check of safety integrity systems, resolution of all HAZOP and PSR action items, and completeness of documentation for pilot plant commissioning.

4.0 Analysis

The analysis task consists of four subtasks discussed below: CFD Modeling, Limestone Sulfation Model, Coal Reactivity Model, and Agglomeration Model. More details on each of these tasks are included in Appendices B (Coal Reactivity), C (Limestone Sulfation), D (CFD) and E (Agglomeration Model).

The CFD Modeling task utilized a hybrid approach to develop analysis tools by combining computationally intense CFD analysis with less computationally intense tools. This provided fast turnaround capability for combustor performance analysis and agglomeration analysis to support design activities.

Both the CFD and Limestone models are used to determine combustor residence time requirements for each type of particle. The Coal Reactivity model was validated with test data and embedded within the GTI 1-D PFBC Performance code to support combustor performance calculations. The Limestone Sulfation model was also validated with data and used in a standalone mode now, with plans to integrate it with the 1-D PFBC Performance code in the future.

The Agglomeration Model was developed by Pennsylvania State University, validated against test data available in the literature, and used to predict probability of agglomeration due to slagging in the Oxy-PFBC. The model found low likelihood of slagging if bed temperatures were maintained near the planned 850-900C and the bed had sufficient dolomite to elevate the slagging temperature.

4.1 CFD Modeling

The CFD modeling approach, as originally envisioned, would develop and validate physics models for coal kinetics, limestone kinetics and agglomeration, and add these models to a 3-D CFD code. Investigations into the CFD capabilities showed that our requirements were beyond current CFD and computing capabilities in terms of practical support for the reactor development due to the complexity of the Oxy-PFBC reactor geometry and physics, which include multiple particle types and sizes, multiple gas species, complex chemistry, gas-particle-wall heat transfer, and heat exchanger tube banks.

As a result, the approach was modified to develop two hybrid approaches that combine CFD with tools that are less computationally intense: the 1-D PFBC Performance Code, and the Agglomeration Model (Figure 4-1). The tools were developed, validated and are currently in use at GTI. In addition, the first 3-D CFD analyses of the full pilot scale Oxy-PFBC reactor was completed. The coal kinetics, limestone kinetics and agglomeration physics models were also developed, validated and incorporated into these codes.

The primary benefit of the revised approach is that the tools enable fast turnaround analysis that supports design and optimization efforts. The GTI 1-D PFBC Performance Code combines coal kinetics and fluidized bed thermal transport models. The thermal transport model can utilize input from CFD analysis or test data to calibrate the code for a given configuration. The Agglomeration Model includes coal, limestone and ash thermochemistry models, and input from CFD for bed hydrodynamics. These approaches provide the appropriate physics modeling with quick turnaround time to support analysis and design activities necessary for scaling up to demo and commercial scales.

The 1-D PFBC Performance Code, coal reactivity, and limestone sulfation physics models were validated with test data. The 1-D PFBC Performance Code was enhanced by adding an Axial Diffusion Model to better capture thermal energy transport provided by the fluidized bed. CFD can provide an input to the code to calibrate energy transport for new configurations. The 1-D PFBC Performance Code was successfully validated against test data from the Grimethorpe PFBC Plant in England. The coal kinetics model within the code was validated for oxy-fired pressurized conditions against test data from Pennsylvania State University.

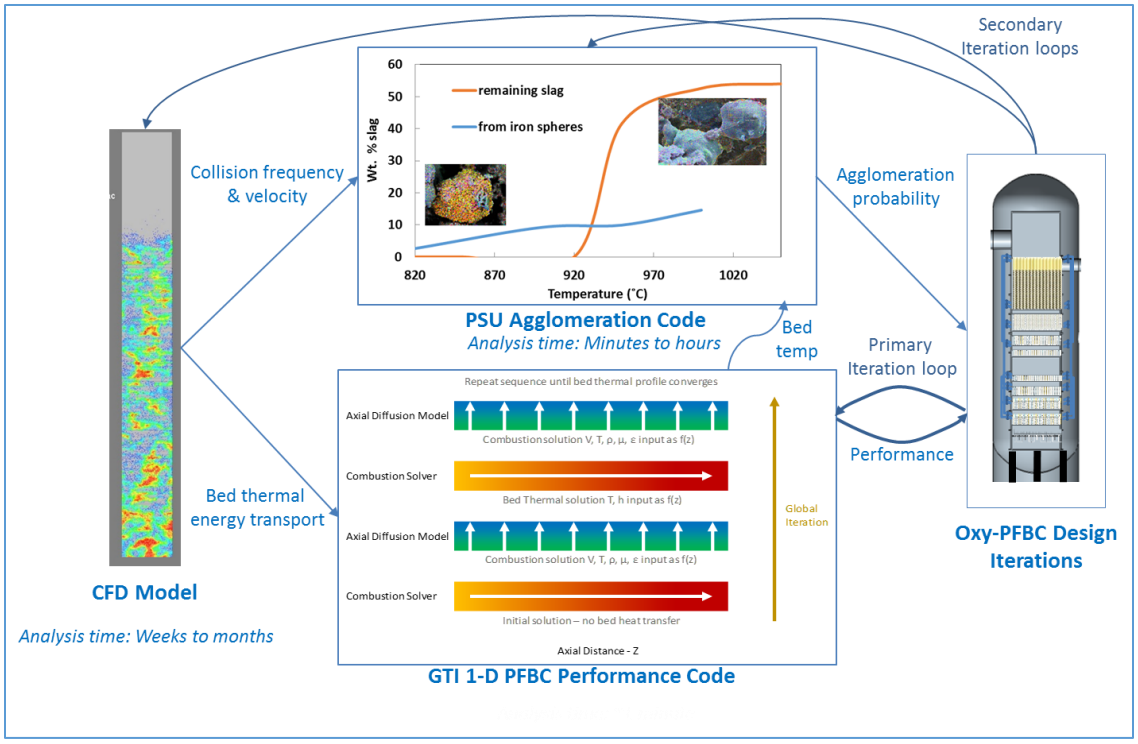

Figure 4-1. Hybrid Modeling Approach Enables Rapid Design Iterations.

The CPFD Barracuda® CFD code was applied to the full reactor configuration. Multiple particle types (coal, dolomite) and particles sizes (5 sizes for coal, 2 for dolomite) were modeled. These results have provided insight into the three-dimensional flow fields that dominate the injection-end of the reactor. This work also provides a foundation to add additional physics to future computations. Chemistry will be demonstrated at a future time, but no issues are anticipated based on previously demonstrated code capabilities.

The fluidized bed physics are, by nature, three-dimensional, and time dependent – or unsteady. The CPFD Barracuda® CFD solutions capture this behavior and, as such, there is no converged, or steady, solution. A fixed bed of particles is impulsively fluidized by the gas flow. The solution is then progressed in time until a cyclical, or periodic behavior is obtained. The solution is then run further in time and data is collected for flow visualization, and engineering parameters of interest.

Two solutions using the CPFD Barracuda® CFD code were run whose results are shown in the following figures. Both used an isothermal bed condition of 1000°K. All gas flows were modeled. These included the main combustible gas mixture, the fuel feed gas, and purge gas flows. The first solution used only the large fluidized bed particles, while the second solution added the fuel feed with the smaller elutriated limestone particles and the elutriated coal particles. A boundary condition was set such that any particle reaching the reactor upper surface would be removed from the computation, i.e. elutriated. Figure 4-2 shows a reactor cross section view from the first solution as a snapshot in time. The color contour show particle volume fraction. The fluidized bed is operating as desired in the bubbling regime, and at the desired bed height which submerges the entire heat exchanger. Figure 4-3 shows a reactor cross section view from the second solution as a snapshot in time. This view is a detail at the top of the bed showing the freeboard region. The large fluidized bed particles are colored green, the smaller

elutriated limestone particles are colored white, and the elutriated coal fuel particles are colored red. Both Figure 4-2 and 4-3 are actually still views from animations that show the dynamic nature of the particles. Some of the green particles are ejected up into to the freeboard area, but – as desired – only a negligible number are elutriated out of the top of the computational domain. Many of the smaller white and red particles are elutriated, as intended.

The CPFD Barracuda® CFD model was designed to extract engineering parameters at spatial locations matching instrumentation ports in the GTI Pilot Plant reactor. Figure 4-4 shows pressures as a function of time. Following from the discussion above, the solution was judged to have attained a periodic behavior at 20 seconds. The pressure data from that point onward are of interest. The pressure oscillations are relatively benign, consistent with a stable bubbling bed.

CFD is also an integral part of the agglomeration modelling approach. CFD is run to determine the collision velocity and frequency between fluidized bed particles for a given operating condition. These results are used as input to the Agglomeration Model, which then computes the probability of particle agglomeration at a particular bed temperature. As the solution is marched in time, it predicts when – or if – the bed will de-fluidize, and defluidization time was predicted within 11% compared to test data. The results show a very low probability of agglomeration in the GTI Pilot Plant with 300°C of operating margin. The slag formation temperature was influenced significantly by the presence of dolomite bed material.

The full report detailing the 1-D PFBC Performance Code modeling, CPFD Barracuda® CFD modeling, and Agglomeration Model analysis can be found in the Appendix.

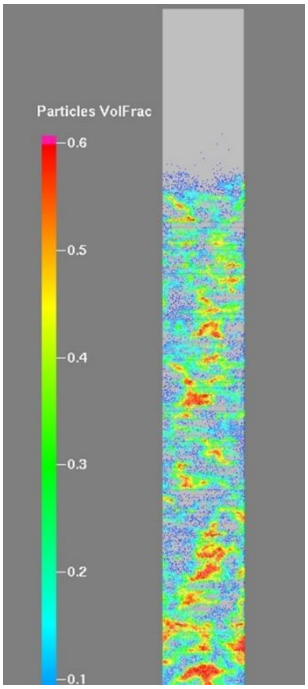

Figure 4-2. Barracuda Solution Fluidized Bed Particle Volume Fraction

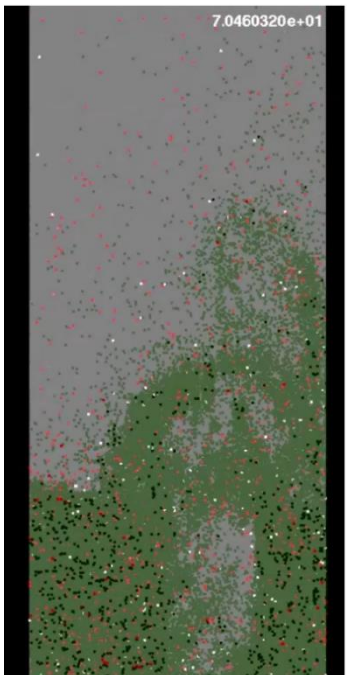

Figure 4-3. Barracuda Solution Fluidized Bed Particle Freeboard Ejection

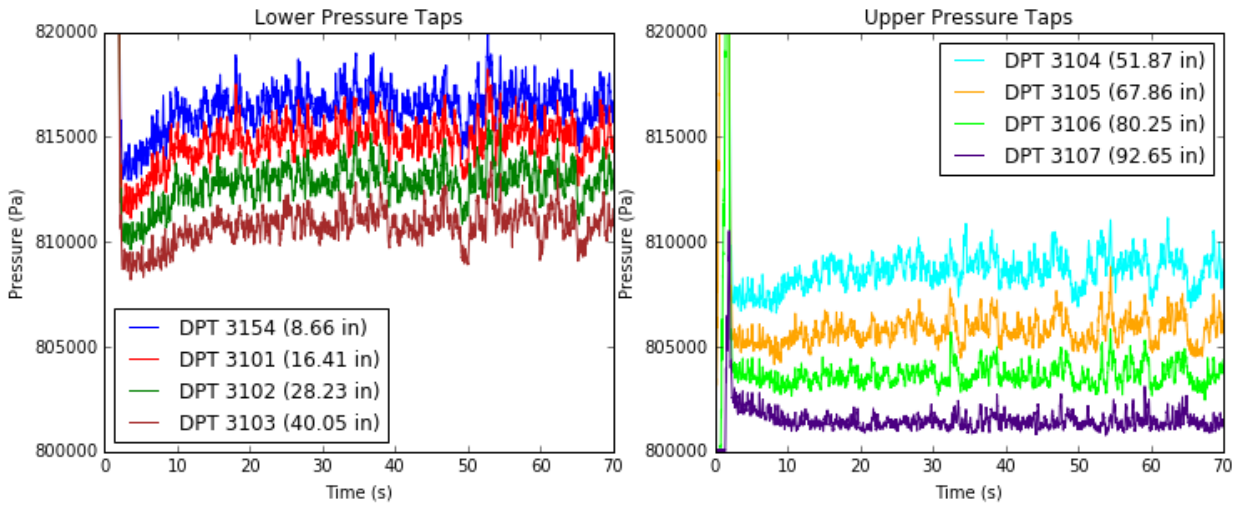

Figure 4-4. Barracuda Solution Pressure-Time History

4.2 Limestone Sulfation Model

Removal of gaseous sulfur oxides (sulfur dioxide, SO_2, and sulfur trioxide, SO_3, or SOx) from air fired coal combustors has been generally accomplished over the years with the use of calcined limestone (i.e., lime, CaO). Usually, this lime is hydrated to calcium hydroxide [$Ca(OH)_2$] by the addition of water (within a pre-injection slaking process) for subsequent post combustion injection into the combustor's flue gas. The use of pressurized fluidized bed combustors (PFBCs) for the coal combustion reactor has the potential of eliminating the limestone's calcination and slaking pre-processes by injecting the limestone ($CaCO_3$) directly into the combustor for direct SOx removal. The GTI oxy-fired PFBC (for economical post combustion carbon dioxide, CO_2, capture and sequestration) uses direct injection of limestone into the combustor as the combustor system's primary SOx removal process.

Penn State completed twelve tests on four limestones in order to provide sulfation data to GTI on its oxy-fired PFBC design. The experimental apparatus was a small pressurized fluidized bed reactor (PFBR) contained within a constant temperature electrically heated furnace. The PFBR operated at a pressure of approximately 7.89 atm and at temperatures between 825 and 875°C. The fluidization gas composition was nominally 92 vol% carbon dioxide (CO_2), 7 vol% oxygen (O_2) and 2,400 parts per million dry (ppm-dry) or 0.24 vol% sulfur dioxide (SO_2). The fluidization gas flow rate to the PFBR was approximately 5 standard liters per minute (slpm) and its superficial gas velocity within the PFBR was on the order of 1.4 cm/s. Four granular limestones were tested – identified as Graymont, Michigan, Dolomite-A, and Dolomite-B – which had been pulverized to a particle size of minus 200 mesh (or minus 74-micron). In such a bed, the coal particle residence times are on the same order as the gas (i.e., seconds) rather than minutes (as is the case with conventional fluidized bed designs). The Penn State testing was designed to help determine whether elutriated micron sized limestone particles can be injected into the bed (similar to the micron size coal particles) or whether they need to be introduced as millimeter sized bed stabilization particles. The results indicate that the limestone needs to be injected into the bed as millimeter sized particles due to the relatively slow sulfation kinetics of the limestones tested.

Figure 4-5 shows the effective instantaneous SOx reaction rate, k_{eff} , time history for the four limestones tested at the temperatures of 825, 850, and 875 °C. This figure shows all effective reaction rates are zero at time zero (t = 0.0) and begin increasing to a maximum value before slowly decreasing as time increases. The initial increase in k_{eff} is most likely due to the initial particle heat-up period whereby the particle temperature, T_p , has yet to reach the reactor temperature after being introduced into the hot PFBR. The subsequent decrease in k_{eff} is due to the limestone's conversion of calcium carbonate (CaCO3) to gypsum (CaSO4) within the particles over time -- so that there is less calcium carbonate surfaces for reaction.

The Gas Technology Institute (GTI) sulfation kinetic model was used to correlate the Penn State University (PSU) experiments on the various limestone feedstocks. The GTI sulfation kinetic model used for test data correlation assumes: (1) the gas flow through the PFBR is one-dimensional uniform plug flow (PF), and (2) the thin layer of limestone mass within the fluidized bed recirculates under well-stirred-reactor (WSR) conditions. The PF/WSR kinetic model was shown to reasonably correlate the experimental test data. The rate determining step (RDS) activation energies, E_{sox} , and the pre-exponential constants, A_{sox} , are found for each limestone from the Penn State PFBR experiments according to the first-order forward RDS kinetic rate constant, k_{sox} , where

$$k_{sox} = A_{sox} \exp\left(\frac{-E_{sox}}{R\,T_p}\right) \tag{3}$$

The activation energy of the sulfation's rate limiting reaction step was found to be 24.1 kcal/mol for all four limestones with pre-exponential velocities ranging from 4.6 cm/s (for Dolomite-B) to 746 cm/s (for Dolomite-A). These kinetic parameters can then be subsequently used in the GTI generalized pressurized fluidized bed combustor (PFBC) performance model.

The full report detailing the Limestone Sulfation Model analysis can be found in the Appendix.

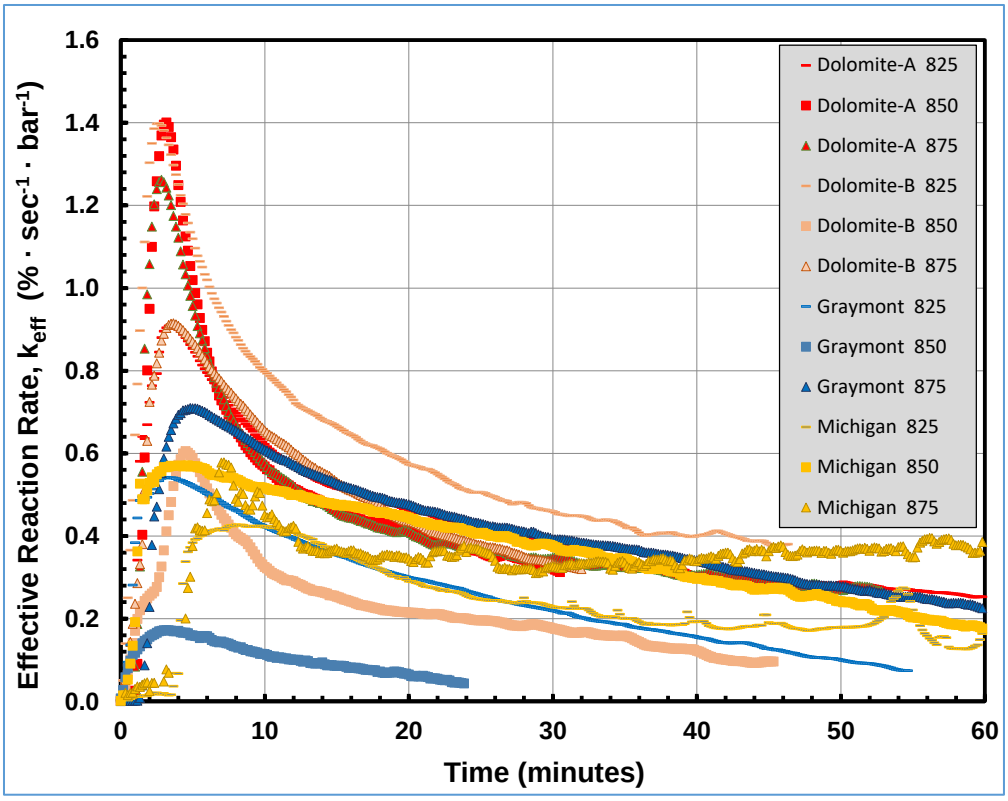

Figure 4-5. Limestone Sulfation Reaction Rate Histories

4.3 Coal Reactivity Model

The Gas Technology Institute (GTI) 1-D Pressurized Fluidized Bed Combustor (PFBC) kinetic performance code was updated with coal reactivity test data generated by Penn State University (PSU) in their fluidized bed laboratory reactor, using numerical simulation code written for the PSU reactor with coal chemistry formulations found in the Gas Technology Institute (GTI) 1-D PFBC kinetic model. The main purpose of the PSU coal reactivity experiments is to measure the devolatilization and char-O_2 oxidation reaction rates from bituminous coal in a fluidized bed setting and determine whether these rates are consistent with those predicted from the coal chemistry formulations used by the GTI 1-D PFBC kinetic performance code.

The PSU experimental apparatus was a small oxy-fired PFBC having a cross-sectional flow area of about 20-cm^2 contained within an electrically heated furnace. The PFBC operated at a pressure from atmospheric to approximately 7.89 atm. Furnace wall temperatures were set between 800 and 875ºC. The oxy-fluidization gas composition contained between 5.3 and 16.0 vol% oxygen (O_2) with the balance being carbon dioxide (CO_2) gas. The fluidization gas flow rate to the PFBC was 3.0 to 6.3 standard liters per minute (slpm) with superficial gas velocities on the order of 1.4 cm/s. The Illinois #6 bituminous particle sizes for the initial runs were nominally 74-microns but increased to approximately 177-microns for the later experiments. The amount of Illinois #6 bituminous coal mass delivered to the PFBC for each batch run -- after the oxy-fluidizing gas had achieved furnace temperature conditions – ranged between 3.2 to 5.0 grams.

The type of data collected from each test is shown in Figure 4-6. The exiting concentrations of oxygen and carbon dioxide gas (in vol%) is continually measured along with the exiting carbon monoxide and

sulfur oxide gas (in parts per million, ppm). These concentrations are subsequently used together with the measured fluidizing gas flow rate to determine the coal's moisture-ash-free (maf) weight loss history from a PSU data reduction analysis. These maf weight loss histories are then divided by the initial maf mass of bituminous coal placed into the reactor to provide the coal's maf mass conversion history, as seen in Fig. 4-7.

As seen in Fig. 4-7, the coal particle's 9.01 wt% moisture is vaporized within approximately 30 seconds after introduction into the furnace's fluidized bed. However, it takes the particles approximately another 2-minutes before their temperature increases to the point that organic devolatilization is initiated near 260°C. This devolatilization period last for approximately another 4 to 8 minutes before the particle has essentially completed the pyrolysis process and reached the ASTM D5142 proximate analysis' 46.4 wt% maf conversion value. The reactor model indicates that during pyrolysis the oxygen gas concentration at the coal particle surface is reduced by the outward flow of pyrolysis gases -- such that the exothermic char-O_2 reaction is very low during this period. Following the pyrolysis period, it takes another 10 to 20 minutes (or even longer in some cases) to complete the char-O_2 oxidation process.

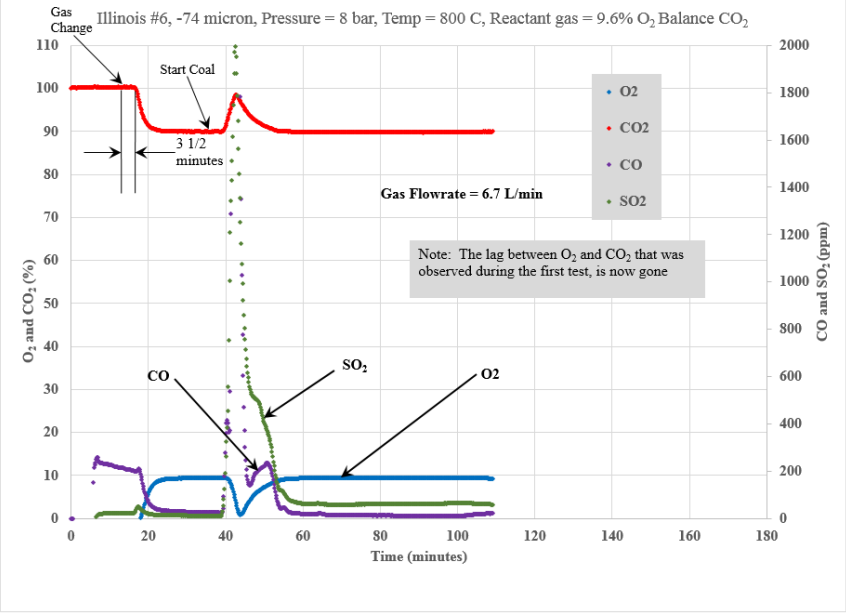

Figure 4-6. Typical Raw Data from a PSU Coal Reactivity Test (Jan 26, 2015 Checkout Run).

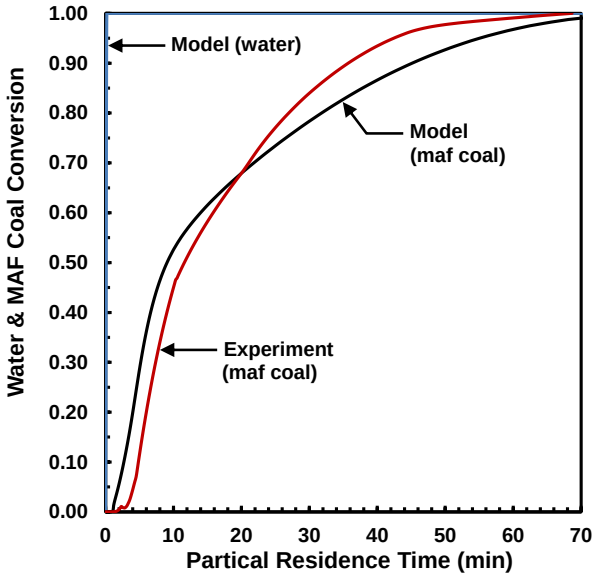

Figure 4-7. PSU Coal Reactivity Test – Run No. 7
(Furnace Temp = 800ºC; Pressure = 8 barg; Particle Size = 177 µm; Inlet Oxygen = 16 vol%)
($\dot{Q}_{rad,in}$ = 100 Watts)

It was found for elutriated fluidized bed reactor systems, that the GTI 1-D entrained flow coal reactor performance model could reasonably predict reactor performance in these more complex multi-dimensional fluidized recirculating flow reactors. The ability to predict performance with a simpler 1-D entrained flow analysis is due to the fact that the small reacting particles are traveling with the fluidizing gas directly through the reactor without any appreciable recirculation. Hence, their residence time through the fluidized bed is measured on the order of seconds (similar to that of the reacting fluidization gas) rather than in minutes had their particle diameters been large enough to remain gravimetrically at all times within the bed.

The GTI transient coal reactivity kinetic model used for PSU test data correlation assumes: (1) the gas flow through the PFBC is one-dimensional uniform plug flow (PF), and (2) the thin layer of coal or char mass within the fluidized bed recirculates under well-stirred-reactor (WSR) conditions. This PF/WSR kinetic model was shown to reasonably correlate the experimental test data by the adjustment of only one model parameter – i.e., the radiation heat transfer rate from the upper freeboard furnace section into the lower 0.25-cm thick fluidized bed layer. The radiation heat transfer rate into the bed was found to be on the order of 200 Watts. All other model parameters were taken from ASTM ultimate/calorific analyses and historical kinetic parameters for bituminous coal devolatilization and heterogeneous char-O_2 oxidation as used by GTI since the 1980's whose origins are from the laboratory work conducted at the Massachusetts Institute of Technology and West Virginia University -- among other institutions.

The full report detailing the Coal Reactivity Model analysis can be found in the Appendix.

4.4 Agglomeration Model

An Agglomeration Model was developed at Pennsylvania State University to predict agglomerate growth in a fluidized bed system. The model was developed based on testing two-particle collisions for sticking. The chemistry of the formation and rheology of the viscous liquid that can bind particles on collision was

studied using computational thermodynamics, while the physical properties that define particle motion are studied using computational fluid dynamics. The agglomeration model developed comprises a mathematical code that uses these inputs on the binder's chemical properties and particle physics to track changes in particle sizes over time.

In order to correctly incorporate the agglomerate growth kinetics for the entire particle size distribution, the determination of a distribution of collision frequencies is required. The collision frequency is calculated based on the kinetic theory of granular flow taking into account the particle granular temperature. The granular temperature required for the calculation is obtained using CFD with the software – MFIX (Multiphase Flows with Interphase eXchanges). This is an open-source software which has been validated for multi-phase simulations in gasifiers and combustors. The mass and momentum balance equations as well as the Schaeffer frictional model are solved to obtain the particle velocities and granular energy using the Eulerian-Eulerian method.

The amount of slag-liquid is determined by the ash chemistry and operating conditions such as the temperature and gaseous atmosphere. The viscosity of the slag-liquid formed helps to determine if the viscous dissipation of the particles' kinetic energy would be sufficient to result in sticking. The viscosity of the slag-liquid is dependent on the chemical composition of the liquid. The extent of particle wetness depends on the amount of liquid, the contact angle and the particle size. FactSage™ thermodynamic equilibrium simulations (computational thermodynamics) based on quasi-chemical computations are used to obtain the amount of slag-liquid formed at equilibrium under a given temperature condition. The chemical composition of the slag obtained from FactSage™ calculations was used to calculate the slag viscosity.

Figure 4-8 shows the rate of growth of agglomerates obtained using the Penn State ash agglomeration model. It is seen that initially, the size of the agglomerates increases rapidly and then begins to stabilize as the frequency of collisions begin to decrease. This modeling methodology is proposed as a more realistic method to obtain particle growth kinetics than assumption of a constant collision frequency or an arbitrary dependence on the number of particles in the system. Figure 4-9 shows the predictions made using the model with the incorporation of the amount of slag. It is seen that as the amount of slag increases, the probability of wet collisions increases and hence the rate of agglomeration increases. At the end of 10 hours, the particles begin to defluidize if 15% slag is present in the system, while their average diameter is only about 4000 µm if 5% slag is available.

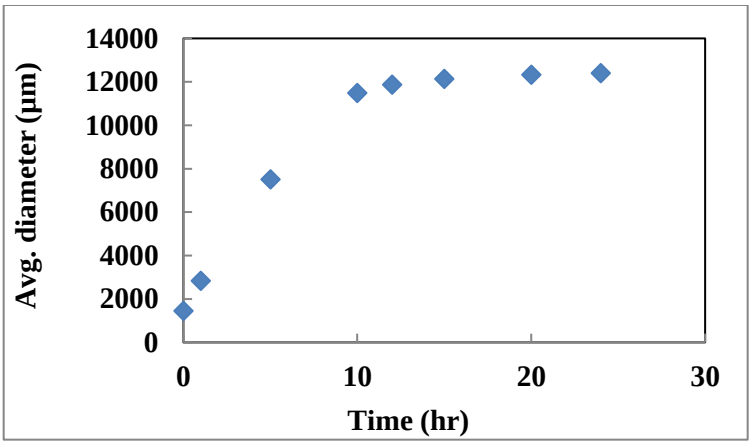

Figure 4-8: Agglomerate growth rate predicted using the ash agglomeration model

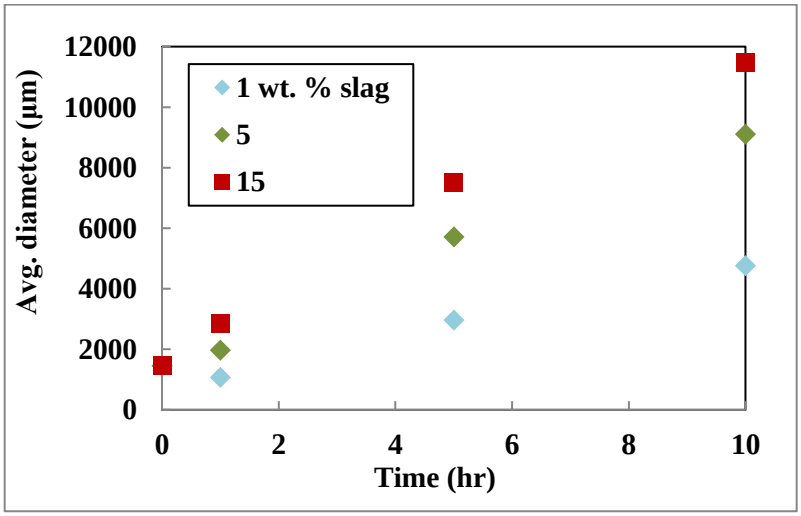

Figure 4-9: Effect of amount of slag on agglomerate growth

The Penn State Agglomeration Model was validated using experimental test data from the literature, and the mechanism of agglomerate growth was validated by studying agglomerates that were formed in CANMET's small scale reactor. Based on a comparison of the results to the literature, the model was modified to simulate a semi-continuous process to better represent real conditions. Additionally, it was recognized that ash particles are likely to be at higher temperature than the measured average bed temperature due to char burning. Hence the simulations were performed with ash particles at higher temperatures, instead of the bulk bed temperature. With these modifications the simulation results obtained were comparable to the experimental results reported in the literature. The agglomerate samples were cut and polished and observed under a scanning electron microscope and the elements present in them were mapped across a cross section of the agglomerate. The results showed the presence of regions that formed slag-liquid at low temperatures initiating agglomeration and also other highly molten regions that are likely to cause propagation at higher temperatures. This supported the model phenomenological mechanism that suggested that agglomeration begins at the particle-level around low-melting particles at a relatively lower temperature and subsequently propagates in the bed.

The propagation may be due to higher temperatures that result from bed instabilities and dead zones arising from the initiation of agglomeration. This is believed to be due to higher temperatures experienced by included mineral particles embedded in hot char particles or local variations in the gaseous atmosphere causing reducing conditions which lower the melting point of some minerals.

Simulations to predict the agglomeration tendency using GTI specified operating conditions were performed. The agglomeration model predicts that the probability of agglomerate growth at conditions in the GTI pilot Oxy-PFBC is low in the specified bed temperature range of 800-900 °C, since in the presence of a bed with 90% sulfated dolomite, slag formation begins only at temperatures above 1,200 °C (see Figure 4-10). A bed with ash alone begins to form slag at lower temperatures of 900 °C, while a bed with 90% dolomite and 10% ash forms slag above 1200 °C. Hence, the proportion of ash and sorbent in the bed is likely to significantly impact the probability of agglomerate growth.

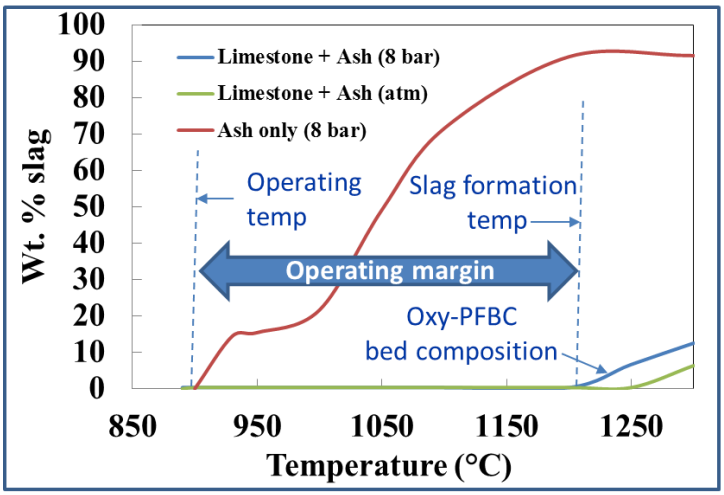

Figure 4-10. Agglomeration analysis indicates significant operating margin at anticipated Oxy-PFB operating conditions.

The full report detailing the Agglomeration Model analysis can be found in the Appendix.

5.0 Pilot Test

5.1 Pilot Fab

The PFBC pressure vessel was fabricated by Titan Metal Fabricators, two other pressure vessels were fabricated by Johansing and Royal Welding. Mott fabricated the filter vessel and pulse back system. All combustor hardware was fabricated by Hales Engineering, which included five assemblies that comprise the majority of the PFBC assembly in the pressure vessel. The combustor sections were shipped to Resco for application of the refractory. Convective heat exchangers were fabricated by Tube Bending Incorporated (TBI). Global Boiler Works worked on the pneumatic hammers used with the convective heat exchangers in order to mitigate the risk of fouling. Fly ash pressure letdown valves were used from Everlasting Valve. Figures 5.1-1 through 5.1-11 show the various fabricated components for use in the pilot plant.

All GTI hardware was installed at the pilot test facility by late 2016. The balance of plant installation, including bulk oxygen, carbon dioxide, and nitrogen tanks, exterior pipe rack, interior plant piping, heat trace and insulation continued through the beginning of 2017. All of the Linde skids had arrived by late 2016 and installation and piping was completed by early 2017. The original 2015 estimated cost of

material was $1,497k compared with a budget of $1,880k and the estimated cost of equipment through mid-2016 was $1,595k.

Figure 5.1-1. MSK1 Fly Ash Filter Vessel Delivered at CANMET (shown during fabrication)

Figure 5.1-2. Fly Ash Pressure Letdown Valves Delivered at CANMET

Figure 5.1-3. Solids sampling cyclone delivered at GTI

Figure 5.1-4. PFBC Pressure Vessel

Figure 5.1-5. Fly Ash Lock Hopper Vessel

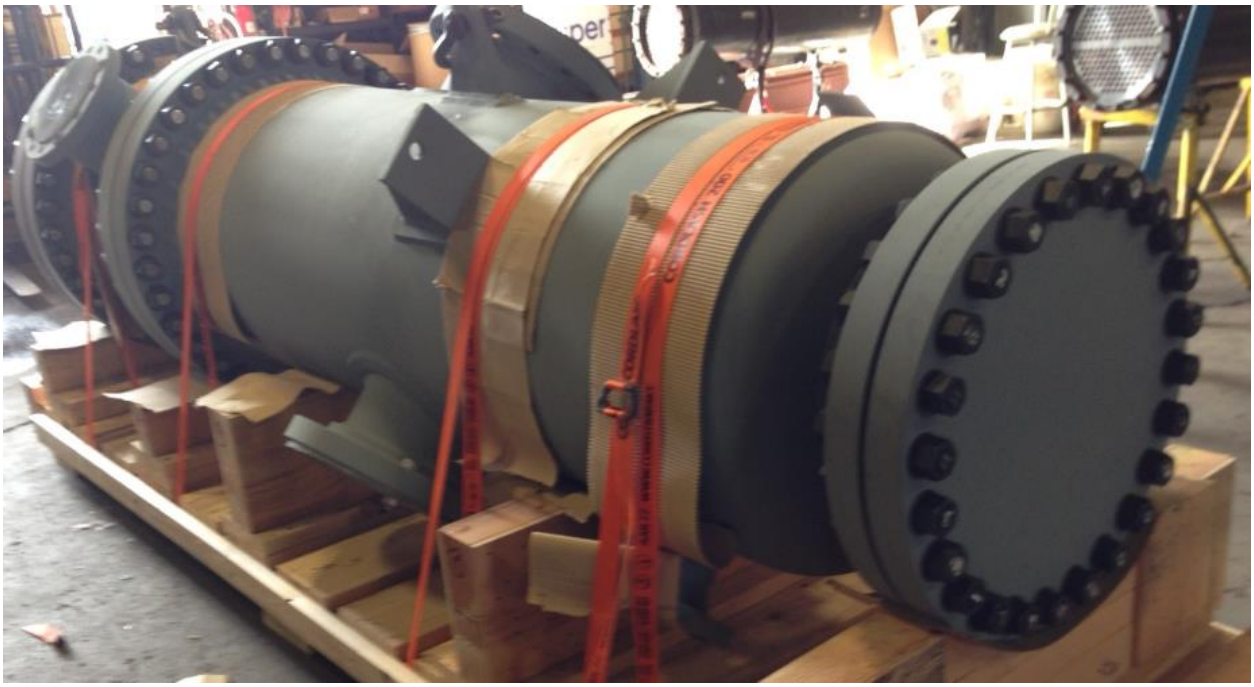

Figure 5.1-6. HEX 2 Pressure Vessel

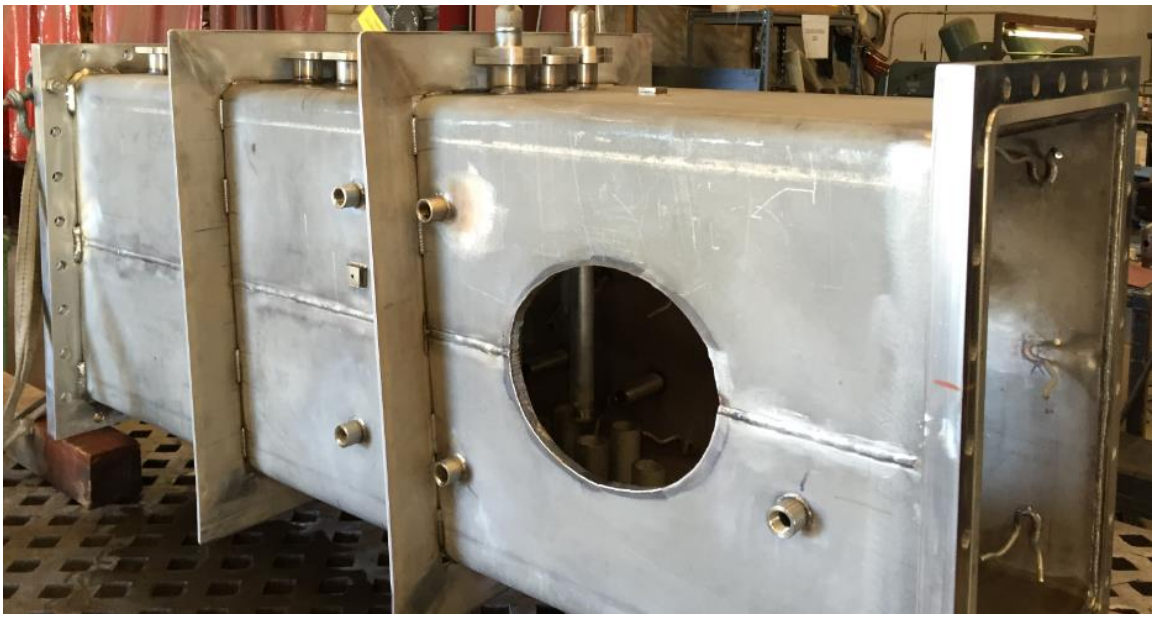

Figure 5.1-7. Combustor Spools

Figure 5.1-8. Heat Exchangers

Figure 5.1-9. Combustor sections assembled and ready to install.

Figure 5.1-10. Fly Ash filter vessel in place.

Figure 5.1-11. PFBC Pressure vessel bottom sections (red) and CHX2 (gray) in place.

5.2 Test Planning & Instrumentation

5.2.1 Design Premise

A Design Premise document was created near the start of the project that defined the purpose of the pilot plant and included an operating concept and approach to testing, including cold flow and hot tests, startup and shutdown. In addition to this document, a set of design trades which must be completed to commercialize the technology, including knowledge gaps which are critical to that commercialization, was outlined, and this in turn was used to identify specific tests which must be performed in the pilot plant in order to gain insight into those commercial plant conceptual trade-offs. These broad scope "knowledge attainment" needs were further analyzed to prioritize tests according to risk, taking the approach that the likelihood of hardware damage must be minimized as the test program progresses, and each test should refine operating constraints for the pilot as well as design constraints for a commercial plant. Based on this methodology, the test plan was defined in terms of one-week long "campaigns".

A test data analysis and attainment plan was also created. This plan took all of the knowledge gaps and predictive analytics which are being used in the design effort, and developed a set of equations, parameters and analytical approaches to validate hardware performance. These formed the basis of the instrumentation list and the specific tests which were to be performed to validate the system performance and anchor predictive design models.

During the first quarter of 2015, a documentation and planning organizing structure was formed. The hierarchy of documents is shown in Fig. 5.2-1. The documents at the top two tiers, PFBC Pilot sizing and Requirements Flowdown, and the PFBC Verification plan, form the basis for hardware designed and fabricated, and the test planning documents. The verification plan contains all of the knowledge gaps required to successfully design a commercial Oxy-PFBC, based on the technical risks identified at the program level. The details of experiment design and pilot plant flexibility which allowed the required data to be gathered was regularly discussed in team meetings, and the test plan (instrumentation in particular) was developed to reflect these needs. A hazard analysis review (HAZOP) identified in clarity the control schemes which must be in place for all the components and systems in the pilot plant. The test matrix was also outlined in the PFBC Verification Plan in terms of knowledge gaps and data requirements.

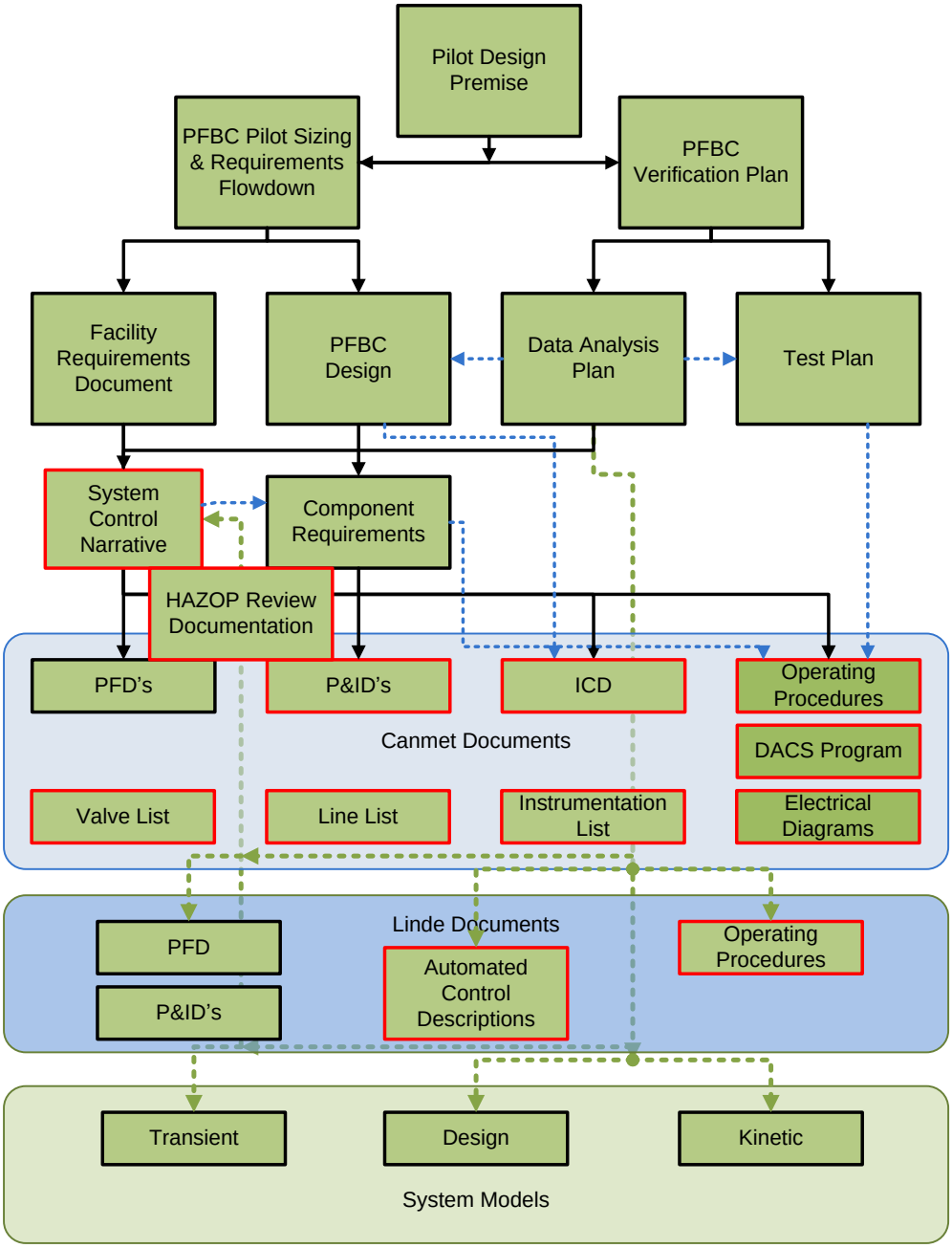

Figure 5.2-1: Oxy-PFBC Pilot Test Documentation Tree

5.2.2 Control Narrative

The Control Narrative was developed that described control logic and transient operation procedures. A transient model was used to add substantial detail to the startup and control sequences drafted in the Control Narrative. The transient model was developed in order to study start-up, shutdown, and upset conditions that the PFBC was expected to experience during normal testing. This enabled the user to derive the flow conditions required for the facility feed systems and to explore various control schemes

for stable operation. The model only calculated the conditions in the combustor and recycle system, including pressure control and recycle compressor operation. It assumed the heat exchanger performance is as designed. If found to be different, the model could be altered to match actual performance. Although the model in its un-anchored state is a rough approximation of reality, it was useful for planning how to control transient behavior. Various control methods were tested for each controlled variable, with varying effects on response time, overshoot, and settling time.

The first section of the Control Narrative gives a description of the process, normal start-up and shutdown procedures, as well as shutdown procedures in the event of a power outage or emergency. The second section gives a description and purpose of each individual system of the PFBC, process control equipment used in that system, and the control system strategy and logic used to operate that system. Once complete, the control narrative was used to develop software controls in the data acquisition and control system (DACS) used at the Canmet pilot plant. Control room viewing screens for the DACS were created which show the current state of valves, pressures, temperatures, and flow rates, and provides input screens for operator inputs.

The Control Narrative document is included in the Appendix.

5.2.3 Matlab Transient Model

The transient model was used to explore ramp rates and reasonable slew rates and rates of change for flow, pressure, temperature, etc. The transient model allowed for experimentation with various flow ramp schedules and control schemes in order to determine which choices were most stable and what a smooth, well controlled startup would look like. The transient model has demonstrated that controls for a PFBC with recycle must be managed with great care when changing pressures and increasing flow rates. Rates of change for the system with recycle are more complex than changes for a system without gas recycle (e.g.: TIDD plant), because of the critical relationship between recycle flow and oxygen mole% content at the injection point in the PFBC. These two cannot be changed independently without causing difficulties for the PFBC operator. Thus, pressure, fuel flow, oxygen flow, and recycle compressor speed must always be in balance with each other.

The transient model was written in the Mathworks Matlab software language. The PFBC was modeled as four main sections including the combustor, convective section, flue, and recycle line and used the dimensions and material properties found in the pilot PFBC. The model calculates such things as gas thermodynamic properties and concentrations, the bed height and density, the velocity of gas through the bed required for fluidization, refractory temperatures, calcination temperatures, and heat transfer among others. In its final configuration, the code was setup to read in from an Excel spreadsheet flowrates of coal, oxygen, burner natural gas and air, recycle flow, bed height, and combustor pressure versus time. The code would then take these inputs and march through time to calculate the transient progression of the operation of the PFBC and the operating parameters of interest.

Consultation with Canmet and experts at GTI led the team to a multi part start sequence which transitions through various heat sources, including electric heaters, air-fired natural gas, a combination of air-fired natural gas and oxy-fired coal, and finally oxy-fired coal. A shutdown sequence was also developed. The input operating parameters for the startup and shutdown sequences were used to write operating procedures to run the pilot plant. Figure 5.2-2 shows some results of the transient model startup versus time after the PFBC was heated to a given temperature by the electric heaters.

The bed solid inventory temperature was monitored to see what margin existed between it and the minimum temperature to calcinate the dolomite which is calculated using the CO_2 partial pressure. Bed mass was calculated based on bed height, the removal of material through the bed drain or elutriated out of the bed, and the relative amounts of olivine sand originally in the bed and dolomite injected with the coal. The minimum velocity to fluidize the bed (Umf) is calculated based on fluid and particle properties, and the refractory temperature is monitored so that it follows near to the maximum heat up rate of 55 degC per hour as recommended by the refractory manufacturer.

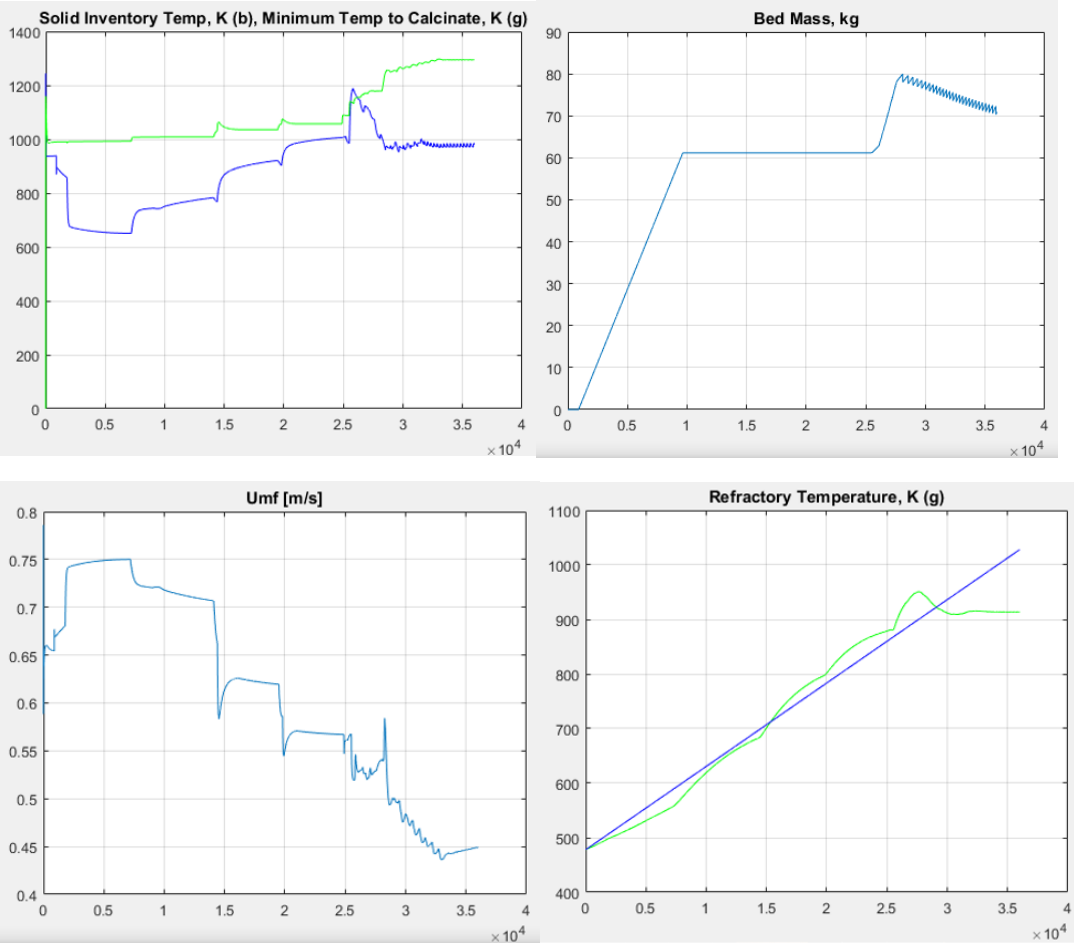

Figure 5.2-2: Transient model startup outputs including bed solid inventory temperature and minimum temperature to calcinate, bed mass, minimum fluidization velocity (Umf), and refractory temperature versus time (secs).

5.2.4 CANMET subscale ("mini-bed") natural gas-fired fluidized bed

In addition to the transient model, CANMET elected to build a sub-scale natural gas-fired 100kW atmospheric fluidized bed with recycle in order to demonstrate the logic and startup sequence in a real system prior to full operation of the pilot. Significant risks were identified and mitigated through the mini-bed tests (designed to be 1/10th scale of the PFBC pilot, and geometrically similar):

1. Line plugging due to coal with higher than requested surface moisture, and larger than planned dolomite particles.
2. Robust startup procedures needed to address potential issues with adhesion of sorbent material to surfaces, coal ignition, and transition from natural gas to coal burning.
3. Agglomeration risk at planned operating conditions

5.2.5 P&ID and instrumentation, valve, line lists

In the first quarter of 2016, the P&ID was finalized, along with the line list, valve list and instrumentation list. Line and valve lists were analyzed against the Pilot Sizing and Requirements, and the system performance model (Unisim simulation model), as well as the control narrative startup and shutdown procedures to verify that all lines were appropriately sized for all operational scenarios. The instrumentation lists were assessed with respect to the required data analysis, which has been outlined in the Verification Plan and were detailed, equation by equation, in the Data Analysis Plan.

5.2.6 Commissioning plan

The Commissioning plan was developed into a detailed test-by-test procedure. Sub-system commissioning consisted of testing functionality of components of the various systems including the supply and distribution of gas, water, fuel, sorbent, bed material, as well as process gas treatment, solid waste handling, cooling tower and PFBC cooling systems, gas and solids sampling systems, gas analyzers, and heat tracing. After sub-systems were verified for proper operation, PFBC commissioning then commenced. This task consisted of several steps including tuning the pressure control system so that the PFBC pressure and the interstitial pressure surrounding the combustor could be automatically set. Cold flow fluidization tests at several pressure levels were run to verify fluidization parameters needed to run the PFBC, the bed ash removal system was tested and tuned to remove the desired amount of material from the bed, and the bed sample removal system was tuned to sample to correct amount of material. Finally pre-heat and coal ignition tests were run to verify natural gas burner ignition and coal ignition. A more thorough discussion of the PFBC commissioning results can be found in the Testing section.

5.2.7 Oxy-PFBC test matrix

A detailed test matrix was developed which provided suggested test conditions for every 8-hour period during the scheduled 4 weeks of testing. In the exercise of creating the test matrix, it was necessary to revisit the basic design and performance goals of the PFBC, give ranges of operation that cover the range of unknowns in performance provided by various models, and establish logical approaches to these unknowns that prevent damage to hardware. In this fashion, a set of tests which cover the unknowns in such a way as to anchor models, yet also provide guidance for risk levels among components was defined. Figure 5.2-3 shows the test matrix for week 1 testing. Listed by weekday and hour are the description of the test or change to be made, as well as all relevant operating parameters such as bed depth, oxygen %, pressure, temperature, etc.

A set of rules for responding to risky conditions was incorporated into an operating manual. The operating manual was designed as a troubleshooting guide and was to be used in conjunction with system alarms and the test procedure, to move through analytical sequences to establish system health. In this way, the operators and technologists had a defined set of reviews to go through on every shift and for every test

condition, allowing them to become familiar with subsystems while ensuring each subsystem is operating safely. Risks which can cause damage to hardware had alarms built into the DACS to alert operators to systems, and the operating manual gave instructions to clear the conditions which are causing the alarm. In addition, less risky situations which do not cause damage do not have alarms, but were important for scientific examination, and these conditions were specified in the test matrix, and procedures for meeting the requested conditions were also included in the operating manual.

day	time after start	description	bed depth, m	oxygen %	MWth	Pressure kPaa	Bed Temp, C	Ca/S mole	Actively cooled tubes in lower bed	Target U/Umf	Recycle flow, kg/hr	recycle CMH	Coal Flow	Dolomite kg/hr	O2 flow	Linde skid flow	Condensate drain flow
Monday	0	ng start	0	21		100	125	2.5	6	4	276.1	290	24.8	12.6	57.5	79.6	9.9
Startup	4	air off	1.5	20	0.35	200	750	2.5	6	5	633.9	333	43.7	22.1	101.4	140.3	17.5
	4.5		1.5	19	0.41	300	800	2.5	6	4.5	797.6	279	50.4	25.5	117.0	161.9	20.2
	5		1.5	18	0.42	400	800	2.5	6	4	899.0	236	51.8	26.3	120.3	166.4	20.8
	5.5		1.5	17	0.40	500	800	2.5	6	3.5	945.9	199	49.4	25.0	114.6	158.6	19.8
	6		1.5	16	0.39	600	800	2.5	6	3.3	1037.5	182	48.7	24.6	112.9	156.2	19.5
	6.5		1.5	15	0.40	700	800	2.5	6	3.3	1179.5	177	49.2	24.9	114.2	158.0	19.7
Monday	8	baseline start	1.5	14	0.47	800	825	2.5	6	3	1162	153	58.6	29.7	135.9	188.0	23.5
Tuesday1	16	increase power	1.5	14	0.52	800	825	2.5	6	3.3	1278	168	64.4	32.6	149.5	206.8	25.9
		If no agglomeration and carbon burnout is poor, skip higher velocity and start 16% tests sooner.															
Tuesday2	24	increase power	1.5	14	0.55	800	825	2.5	6	3.5	1356	178	68.3	34.6	158.5	219.4	27.4
		If agglomeration is severe at any time, do not increase O2, decrease it instead to 1% less than the max achieved.															
Tuesday3	32	increase O2	1.5	15	0.56	800	825	2.5	8	3.3	1258	165	70.0	35.4	162.4	224.7	28.1
		If agglomeration is severe, do not increase O2, change remaining tests to alter between 13, 14, 15%															
		If agglomeration is moderate or nonexistent, continue testing higher depths to increase carbon burnout.															
Wednesday1	40	increase O2	1.5	16	0.61	800	825	2.5	9	3.3	1238	163	75.5	38.2	175.2	242.4	30.3
		If no agglomeration and carbon burnout is good, stop increasing depth. May go to higher oxygen if there is enough cooling. Otherwise, reduce Ca/S ratio and repeat prior steps.															
Wednesday2	48	increase depth	1.7	14	0.52	800	825	2.5	6	3.3	1278	168	64.4	32.6	149.5	206.8	25.9
Wednesday3	56	increase O2	1.7	16	0.61	800	825	2.5	9	3.3	1238	163	75.5	38.2	175.2	242.4	30.3
Thursday1	64	increase depth	1.9	14	0.52	800	825	2.5	6	3.3	1278	168	64.4	32.6	149.5	206.8	25.9
Thursday2	72	increase O2	1.9	16	0.61	800	825	2.5	9	3.3	1238	163	75.5	38.2	175.2	242.4	30.3
Thursday3	80	increase depth	2.1	16	0.61	800	825	2.5	9	3.3	1238	163	75.5	38.2	175.2	242.4	30.3
Friday1	88	increase O2	2.3	16	0.61	800	825	2.5	9	3.3	1238	163	75.5	38.2	175.2	242.4	30.3
Friday2	96	final/off	2.5	16	0.61	800	825	2.5	9	3.3	1238	163	75.5	38.2	175.2	242.4	30.3

Figure 5.2-3: Test matrix for week 1 testing.

5.2.8 Mass and energy balance, health monitoring spreadsheets

Detailed mass and energy balance spreadsheets, as well as health monitoring calculations were created that use data taken during pilot testing to confirm plant performance. Figure 5.2-4 through 5.2-6 show some of the detail of these spreadsheets. The mass balance takes into account all the mass flows of gas and solids into and out of the PFBC and does an elemental balance on the carbon, hydrogen, nitrogen, sulfur, oxygen, and ash to make sure all the inputs and outputs are in balance. If there is a mismatch in inputs and outputs, these calculations can help to troubleshoot and pinpoint if and where there is an error in instrumentation. Figure 5.2-4b shows the mass elemental balance for carbon and oxygen for a test period from July 26, 23:40-00:20 when the PFBC was at the full operating pressure of 800 kPaa. While the measured mass into and out of the PFBC are similar, data is missing and the balances are incomplete since time run at the full load steady-state operating condition was short (targeted data attainment periods are 8 hours in duration to ensure steady-state operation) and operating complications prevented collection and analysis of solid material (unburned coal, ash, dolomite) leaving the PFBC used in the mass and energy balances. Unburned coal was estimated based on carbon conversion as described in the next paragraph.

Similar calculations are done for the energy balance to make sure the input and output energy are in balance, to ensure all the instrumentation is functioning properly and to help provide information on the various flows of energy in the system. Since solid samples were not available from the outlet of the PFBC

for the July 26 period from 23:40-00:20, an estimate of carbon conversion was calculated based on the flows of coal and gases into and out of the PFBC. As the carbon in the coal is combusted, oxygen is consumed and carbon dioxide is generated. Equations for these chemical reactions and flows were written that describe how much oxygen and carbon dioxide enter and leave the PFBC, which provide estimates of how much carbon in the coal combusted. Figure 5.2-5c shows the carbon conversion estimates from July 26, 23:40-00:20. Since some of the flows into the PFBC are not entirely steady during this time period, and it takes time for combustion gas to flow through the system and into the gas emissions analyzers, the averages instead of the instantaneous values are used in subsequent calculations, which are within 2% of each other.

The carbon conversion estimate was used to estimate the mass of unburned coal that exited the PFBC for the mass balance and was also used to estimate how much energy from the coal was released in the PFBC. This was used in the energy balance to determine the energy flows into the PFBC compared to how much energy leaves through such components as the in-bed heat exchangers, convective heat exchangers, combustor walls, and flue gas. Figure 5.2-5b shows the energy balance spreadsheet totals from the July 26, 23:40-00:20 time period and Figure 5.2-5d shows the major system energy flows versus time. While the energy totals going into and out of the PFBC are within 5%, again it is lacking data from solids analysis exiting the PFBC, and the calculation to estimate heat loss to the walls in the in-bed heat exchanger section appears high and may improve as more thermocouples to better measure combustor temperatures are installed for subsequent testing.

The health monitoring spreadsheet shown in Figure 5.2-6 was used in real-time during testing to observe various temperatures and fluidization parameters versus predictions to make sure the PFBC is working according to plan and to verify that the process is under control.

	A	B	C	D	E	F	G	H	I	J	K	L	M	N
1	**Elemental Balance Details**	**Purple: Coal Feeder**	**Red: PFBC and CHXs**			**Blue: Filter**								
2										**Inputs**				
3	P&ID Flow/Weight Transmitter		WT-1601	WT-1701	FT-2121	FT-2125	FT-2101	FW-3301	Process: BedA	WT-1901	FT-2126	FT-2127	FT-2124	FT-2123
4	**Stream Description**	Molecular Weight [kg/kmol]	**Coal Feed**	**Sorbent Feed**	**Coal Feed Pressurizing CO2**	**Coal Feed Conveying CO2**	**Oxygen Tank Feed**	**Compressor Recycle Flow (Emissions from AT-5402, A-F) (Not used in total mass balance)**	**Bed Ash Inlet CO2 to Lockhopper (during solids letdown)**	**Bed Material Feed (should be 0 during a data attainment period)**	**Bed Material Pressurizing CO2 (should be 0 during a data attainment period)**	Interstitial Pressurizing CO2 Gas Flow to PFBC (and bed lockhopper pressurization)	**Bed Solids Cooling CO2**	**CO2 to Bed Solids Letdown (changed to flow from interstitial space)**
5	Mass Balance, kg/hr	Linked to o	92.5	45.9	2.5	70.6	188.5	1553.4	0.0	0.0	0.0	0.6	8.6	0.0
6														
7	**Solids Composition [wt %]**													
8	Moisture, %		7.00											
9	Ultimate Analysis, Dry													
10	Ash (750ºC), %		10.91											
11	Carbon (C), %	12.01	70.21											
12	Hydrogen (H), %	1.008	5.16											
13	Nitrogen (N), %	14.01	1.34											
14	Sulfur (S), %	32.065	3.40	0.03						0.03				
15	Oxygen (O), %	15.999	9.28											
16	Clorine (Cl), %		0.33											
17	Coal Trace Element: Fe2O3													
18	Coal Trace Element: Na2O													
19	Coal Trace Element: TIO2													
20	Calcium Carbonate (CaCO3), %	100.0869		54.50						54.50				
21	CaMg(CO3)2, %	184.4												
22	CaMg2(SO4)3, %	376.87												
23	Calcium Sulfate (CaSO4), %	136.14												
24	Magnesium Carbonate (MgCO3), %	84.3139		45.00						45.00				
25	Magnesium Sulfate (MgSO4), %	120.366												
26	Magnesium Oxide (MgO), %	40.304												
27	Silica (SiO2), %	60.08		0.30						0.30				
28	Iron Oxide (Fe2O3), %	159.69		0.07						0.07				
29	Alumina (Al2O3), %	101.96		0.08						0.08				
30	**Total, %**		**100.62**	**99.98**						**99.98**				

Full Instrument List | OPCCall | Linde | **Mass Balance** | Energy Balance | IBHX Tubes Heat Transfer | Run Summary | Particle Analyses | IBHX | Fluid Bed | Defluidization | Acid Dew Point | DP En

Figure 5.2-4a: Mass balance spreadsheet calculations.

Elemental Balance, kmols/hr		Total In	Total Out	Total Output/Input, %
Carbon (C)		7.46	7.39	99.1%
Oxygen (O)		18.20	17.13	94.1%

Figure 5.2-4b: Mass elemental balance for carbon and oxygen from July 26, 23:40-00:20.

	A	B	C	D	E	F	G	H	I	J
1	Note: For RefProp pressure units of Mpa	Purple: Coal Feeder		Red: PFBC and CHXs		Blue: Filter		Inputs		
2	Reference Temperature 25 degC, Pressure 100 kPa			Coal In		Sorbent		CO2 from Solids Distribution (Conveying minus Vent)		
3				Illinois #6						
4	Stream Description	Molecular Weight [kg/kmol]	HHV, kJ/kg (negative = exothermic)	Mass flow rate, kg/	Temperature In, de	Mass flow rate, kg/	Temperature In, de	Mass flow rate, kg/l	Temperature In, de	Pressure In, kPa
5	P&ID #:			WT-1601	TE-2120 (at CO2 con	WT-1701	TE-2120 (at CO2 con	Post Process	TE-2120	PT-2502
6	Measured data:	Linked to other Sheets (Red)		92.5	23.31785636	45.9	23.31785636	64.6466145	23.31785636	1033.500935
7	Tube: On=1, Off=0									
8	Air Enthalpy In, kJ/kg									
9	Air Enthalpy Out, kJ/kg									
10	Therminol Enthalpy Out Minus In, kJ/kg									
11	Coal, Illinois #6		-30506							
12	Water Heat of Vaporization at 25 degC, kJ/kg		2443.02							
13	Gas Flows measured by emissions analyzers									
14	CO2 mass flow, kg/hr, and other properties	44.01								
15	CO mass flow, kg/hr, and other properties	28.01	-10102.96323							
16	H2O mass flow, kg/hr, and other properties	18.015								
17	NO mass flow, kg/hr, and other properties	30.006								
18	O2 mass flow, kg/hr, and other properties	31.9988								
19	SO2 mass flow, kg/hr, and other properties	64.06								
20	Solids Composition [wt %]									
21	Moisture, %									
22	Ultimate Analysis, Dry									
23	Ash (750ºC), %									
24	Carbon (C), %	12.01	-32766.19484							
25	Hydrogen (H), %	1.008	-358050.5952							
26	Nitrogen (N), %	14.01								
27	Sulfur (S), %	32.065	-9257.508186							
28	Oxygen (O), %	15.999								
29	Calcium Carbonate (CaCO3), %	100.0869	1781.332022			54.5				
30	Calcium Sulfate (CaSO4), %	136.14	-3691.714412							
31	Magnesium Carbonate (MgCO3), %	84.3139	1194.049854			45				
32	Magnesium Sulfate (MgSO4), %	120.366	-3155.043783							
33	Silica (SiO2), %					0.3				
34	Total, %					99.8				
35										

Full Instrument List | OPCCall | Linde | Mass Balance | Energy Balance | IBHX Tubes Heat Transfer | Run Summary | Particle Analyses | IBHX | Fluid Bed | Defluidization | Acid Dew Point | DP Errors | HQ

Figure 5.2-5a: Energy balance spreadsheet calculations.

	Total In	Total Out	Total Output/Input, %
Energy (Compressor), kW	2.84449		
Energy (Heat Transfer), kW	-0.8339	645.1901	
Energy (Heat of Vaporization), kW		30.89313	
Energy (Combustion (HHV)), kW	723.084	87.95737	
	Total	Total	Total
	725.094	764.0406	105.37%

Figure 5.2-5b: Energy balance spreadsheet totals from July 26, 23:40-00:20.

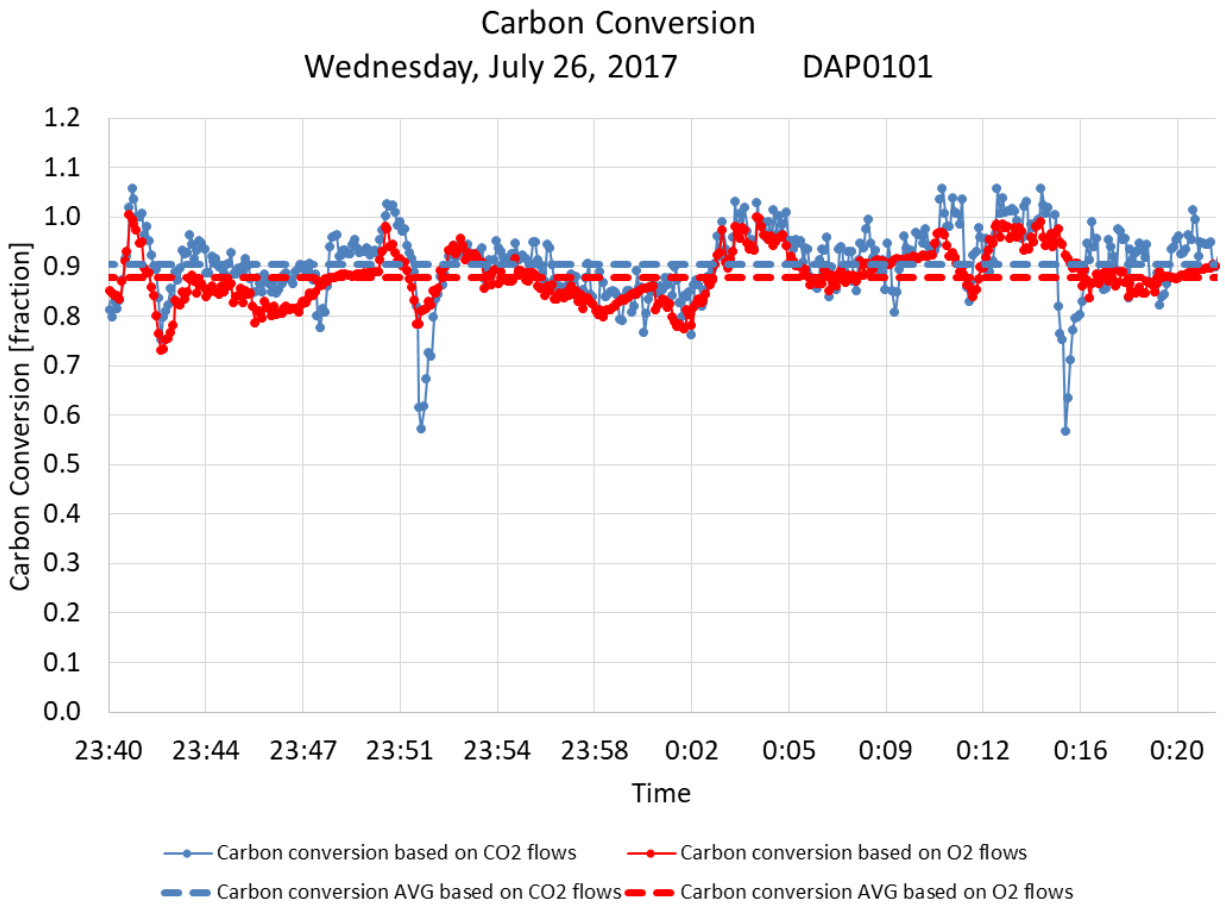

Figure 5.2-5c: Carbon conversion used to estimate coal heat release from July 26, 23:40-00:20.

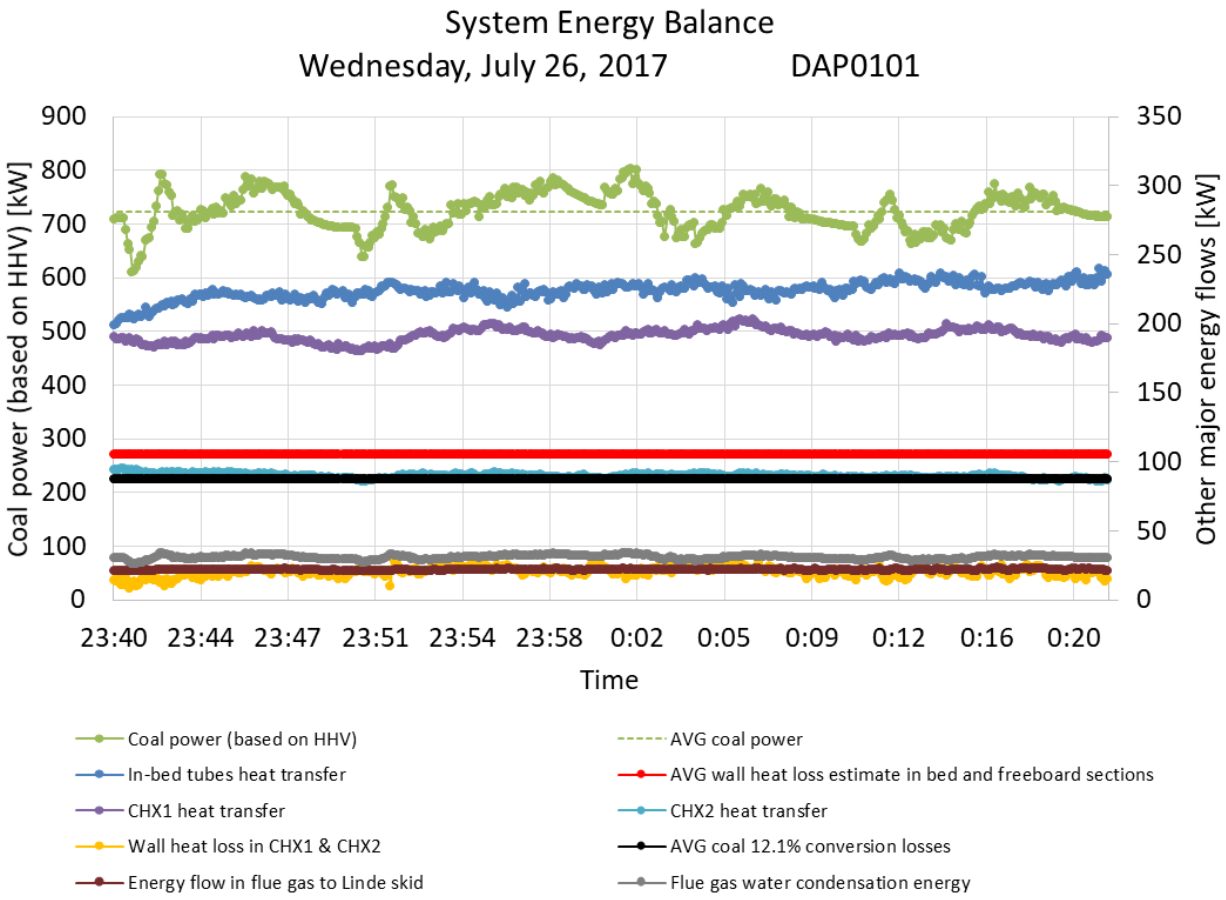

Figure 5.2-5d: Major system energy flows from July 26, 23:40-00:20.

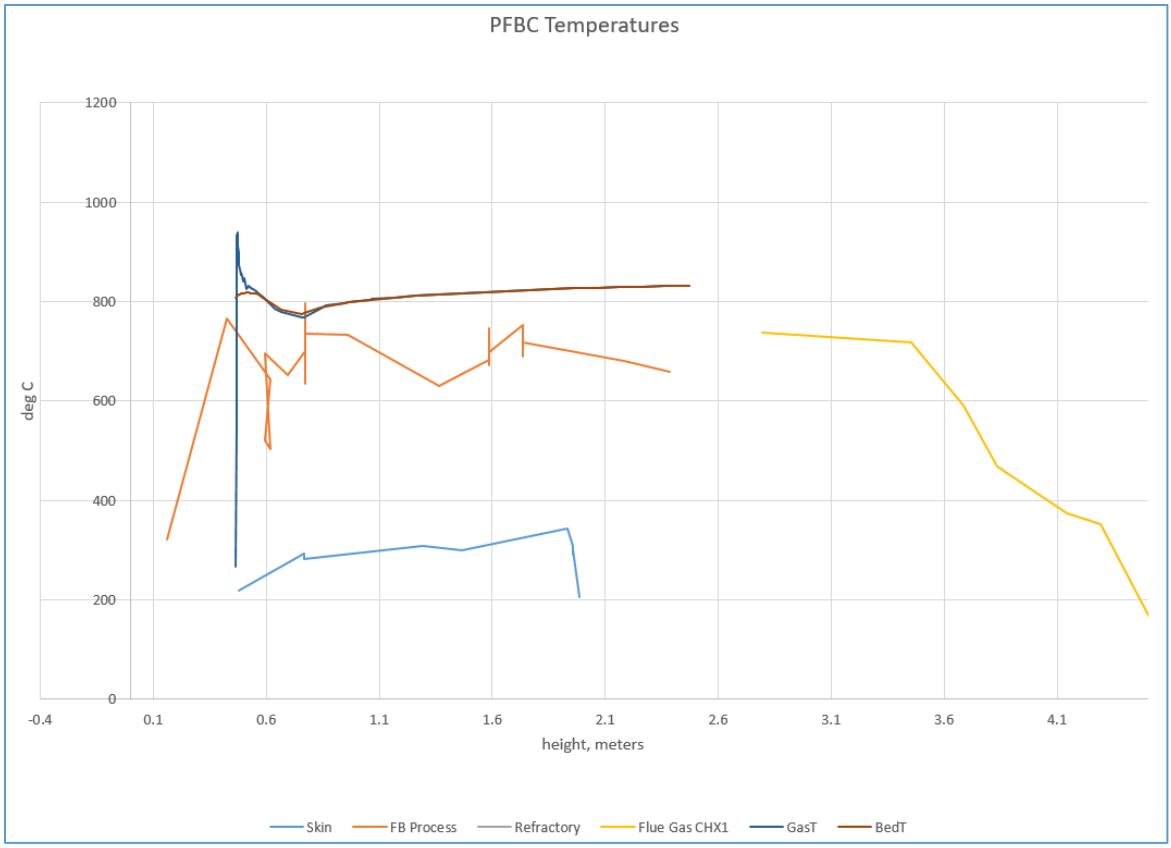

Figure 5.2-6: Health monitoring of combustor temperatures at various heights versus predicted gas and bed temperatures.

5.3 Engineering Construction

Initial tasks performed at CanmetENERGY included development of a block flow diagram (BFD) to identify all the major pilot facility systems, generation of a process simulation model of the 1 MWth Oxy-PFBC operating at up to 15 bar(g) and 950°C to determine preliminary heat and material balances, creation of a process flow diagram (PFD) to identify all major heat and material streams, and development of a draft piping and instrumentation diagrams (P&ID) to aid in determining a major equipment list for the pilot facility. The information was used, in conjunction with GTI's modeling results, to form a design basis and help define the battery limits of the facility. Several process simulation test conditions were generated to better understand the practical operational limits of the facility and to define equipment design specifications. The initial process simulation test parameters that were evaluated include: PFBC temperature, PFBC freeboard pressure, firing rate, inlet O_2 concentration, outlet (excess) O_2 concentration, and PFBC inlet gas superficial velocity.

After an initial assessment by Canmet and GTI, further refinement to the BFD and PFD was performed to incorporate changes in supply / process requirements and to more accurately define scope requirements between the project partners. A more detailed set of P&IDs was created that incorporated all the known facility requirements and was modified to incorporate equipment that falls under GTI and Linde scope. After a review of the initial process simulation test conditions, modifications to the simulation assumptions were performed to better represent the conditions expected during pilot-plant operation. Several additional simulation test cases were generated, where the results have been

summarized in a document entitled “CANMET Unisim Balance Conditions – REV02.” This document provides details on flow rates, composition, pressure, temperature, and other pertinent properties for all the major process streams. In conjunction with GTI’s modeling efforts, the PFBC process simulation model was utilized to determine overall cooling requirements for the pilot-plant, along with cooling splits between the major heat exchangers for several different cooling media. Based on the initial studies, the requirements for several systems including bulk gas supply, solid fuel and sorbent supply, electrical demand, and elements of the cooling systems were defined.

During the first quarter of 2015, Canmet completed the basic engineering for the balance of plant including definition of available site utilities including water and electricity, operating temperatures, flows and pressures for all process streams, approved pilot plant process flow sheets, pilot plant heat and material balances, and specifications for major equipment items including vessels, tanks, compressors, pumps, heat exchangers, and process cooling systems. Detailed engineering proceeded to include site plot plan, materials of construction selection, mechanical flow sheets (process and instrumentation diagrams), de-commissioning activities for the existing gasifier pilot facility, new plant construction schedules, and detailed equipment and instrumentation specifications. Canmet also completed the installation of a glycol to air heat exchanger and associated piping, carbon dioxide bulk storage vessel and piping, infrastructure for the supply of high and medium pressure oxygen, nitrogen, carbon dioxide, and natural gas.

During the second quarter of 2015, Canmet completed piping sizing and material selections for balance of plant, process and instrumentation diagrams, detailed equipment and instrumentation specifications, detailed project costing based on supplier quoted costs, engineering and design of building modifications, and de-commissioning of the existing gasifier pilot facility. Detailed engineering activities included detailed plot plan including piping isometrics, building modifications, mechanical equipment installation and electrical system integration, and procurement of required instrumentation, piping and fittings.

During the third quarter of 2015, the detailed engineering for the balance of plant had been completed and procurement activities had started. The structural design work for the pilot facility mezzanines and equipment support was completed. Canmet was also granted Canadian Federal Government funding for the construction of a new exterior bulk gas supply piping system, equipment support and process bay retrofit, and renovations to the control room for the pilot facility. This funding enabled Canmet to purpose build the pilot plant area rather than trying to make the pilot plant suit the space available.

During the fourth quarter of 2015, with the completion of the detailed engineering for the balance of plant, procurement activities had been the main focus. The procurement contracts for tubing, piping, valves and instrumentation required for the construction of the pilot facility were awarded.

During the first quarter of 2016, Natural Resources Canada finalized the process piping and electrical routing in the process area as shown in the figure below. The required procurement of tubing, piping, valves, instrumentation and contractor services required for the construction of the pilot facility were then completed. All necessary design registrations with the Technical Standards & Safety Authority (TSSA) were completed for the pilot facility.

As of the end of March 2017 mechanical installation was substantially complete and electrical installation was complete. The mechanical work included completion inspections, piping system testing,

and certification of the piping systems for use. The electrical work included installation of all control and power wiring for the pilot plant, and connection to the DACS control system. The programming for the control system was completed in February 2017, and the commissioning of the DACS control system input and output signals was also completed. This includes control system loop checks, as well as cold and hot flow commissioning activities for the pilot plant.

As of mid-2017, commissioning activities were complete and system operation had commenced. In addition to the main combustor system, the auxiliary plant system were fully commissioned including bulk material (sorbent and fuel) systems, pneumatic fuel injection system, heating and cooling systems, bulk gas systems, and ash handling systems.

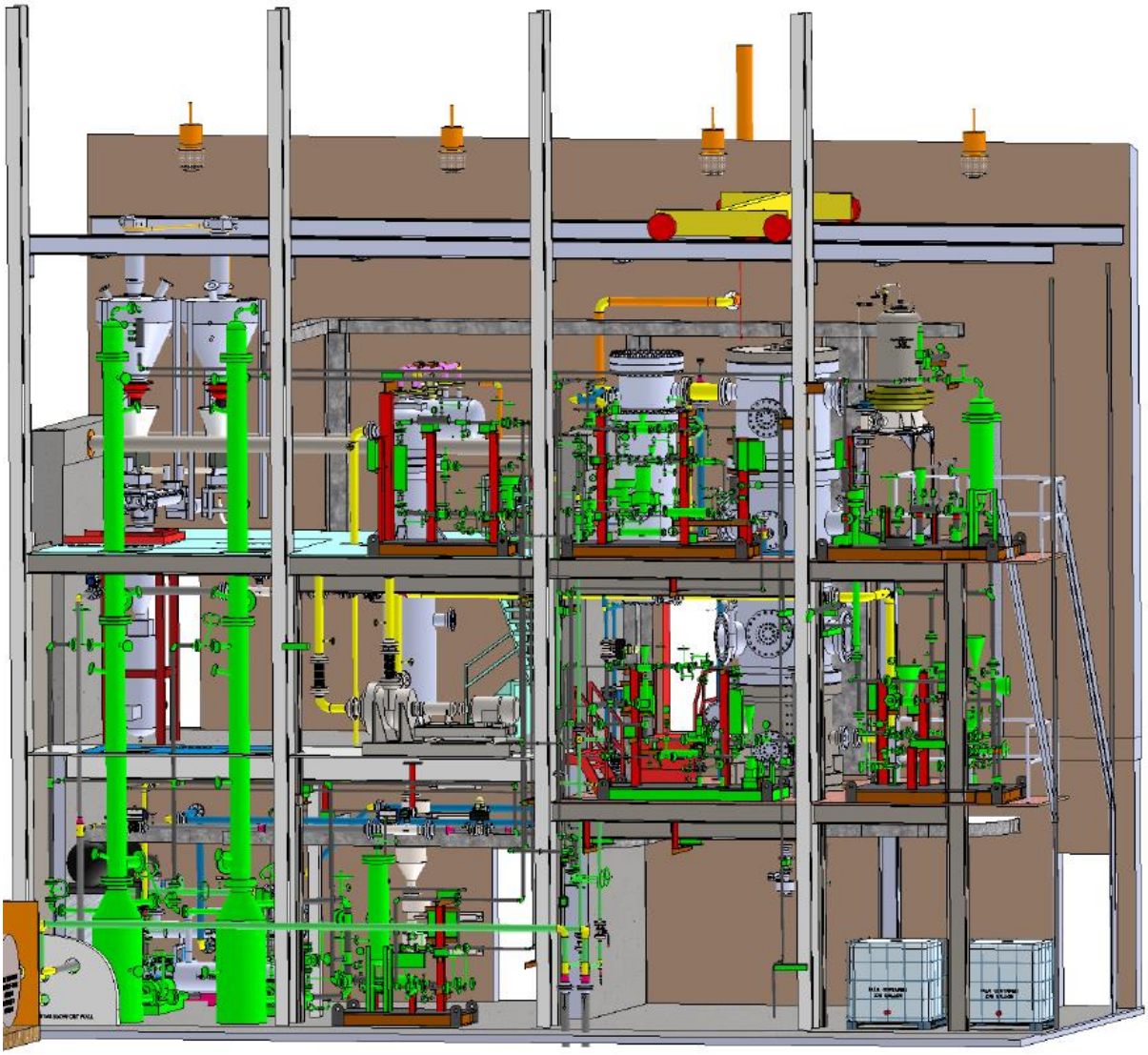

Figure 5.3-1 – Model of Oxy-PFBC pilot plant at the CanmetENERGY facility in Ottawa, Canada

5.4 CO_2 Purification Unit (CPU) Testing

The commissioning of the Linde CO_2 purification unit (CPU) was completed in April 2017. A pre-start up safety review meeting was conducted and a comprehensive comparison was performed on the as-built system installation against the final P&ID and design intent. The Linde CPU successfully demonstrated readiness for performance testing with flue gas from oxy-coal combustion of GTI's Oxy-PFBC. Table 5-1 gives a brief overview of the parameters of interest that were investigated during commissioning and the test results.

Table 5-1: CO_2 Purification Unit commissioning tests and results

Parameter or Relationship	**How achieved**	**Implications of Test**
DCC Temp & Condensate Flow control	Test performed with heated air and flue gas of natural gas combusted with air	Systems working
DCC Level & Temp Trips	Test performed with water	Systems working
LICONOX® Temp & Condensate Flow control	Test performed with heated air	Systems working
LICONOX® Level & Condensate Flow Trips	Test performed with water	Systems working
DEOXO start up heater & HEX	Test performed with air	Systems working
DEOXO O_2 conversion, along with Temp and Composition (HC & O_2) trips	Tested with synthetic FG	Systems working

Integrated operations with the Oxy-PFBC demonstrated that the DCC performed as expected. The column completed over 120 hours of cooling of flue gas from the Oxy-PFBC, with flue gas from coal and oxygen based combustion, as well as air/natural gas and air/coal-based combustion. During these campaigns, the DCC was run with flue gas flow rates between 200 – 400 kg/hr, flue gas inlet temperatures of 190 – 220 °C and pressures between 4 and 8 bara. In all cases, the column demonstrated performance as per the design. The flue gas outlet temperature was reduced to between 45 and 55°C, depending on the water circulation rate. The discharge pH of the condensate was maintained close to neutral with addition of caustic as needed.

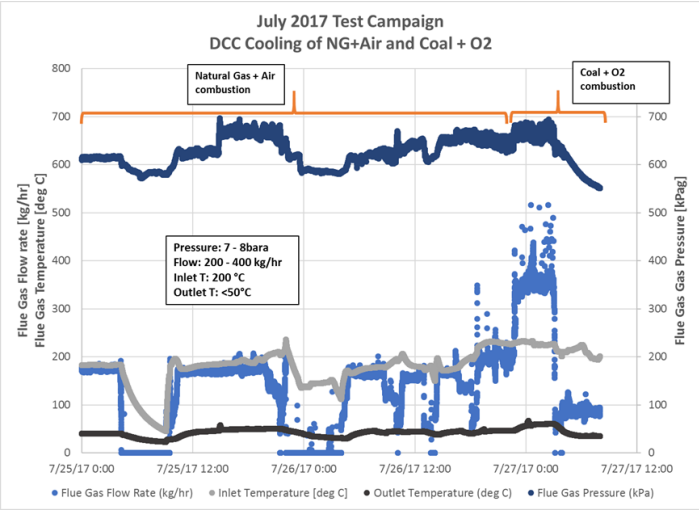

Figure 5.4-1. Performance of Direct Contact Cooler with natural gas and air combustion and coal and oxygen

Figure 5.4-1 demonstrates sustained cooling with the DCC column over a period of 60 hours. During this campaign, coal and oxygen were combusted at design flow and pressure for approximately 4 hours. Under design conditions, the DCC cooled

approximately 400 kg/hr of flue gas from 200°C to 55°C at 8 bara pressure.

The CO_2 purification unit (CPU) underwent independent tests in 2018 without the PFBC using a synthetic flue gas mixture of CO_2 and air, with trace amounts of contaminants SO_2 and NO. The CPU completed an extended duration test in October 2018 where it ran without interruption for over 3 full days. The objective of these tests was to collect performance data of the Liconox and Deoxo, which had not previously been tested with the boiler. Since the DCC performance had been previously validated with oxy-coal combustion, it was modified to heat the gas mixture to 60°C and saturate it with to simulate the inlet conditions to the Liconox that would be expected under operation with the combustor. Approximately 200 hours of test time was accomplished and over 41 tonnes of synthetic flue gas processed.

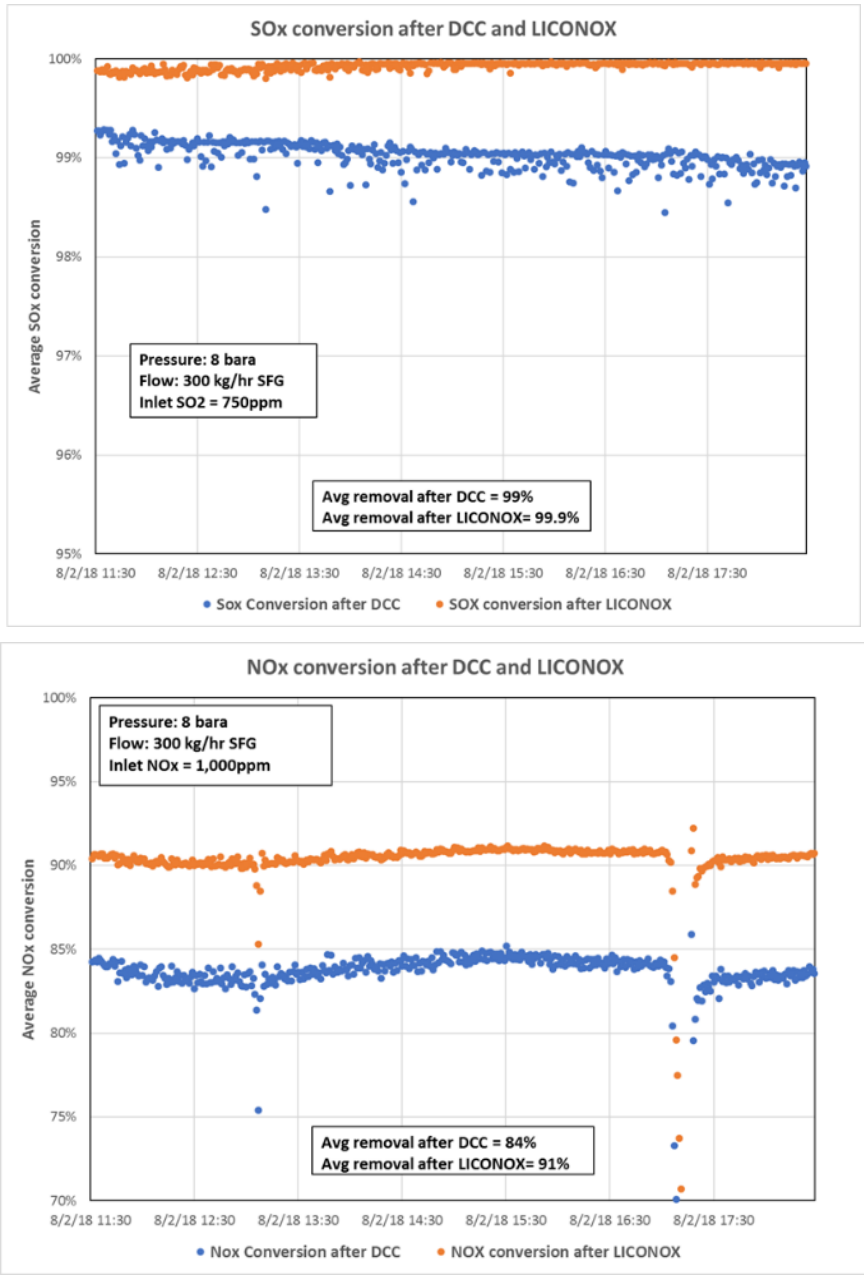

Figure 5.4-2. Removal of SOx and NOx in the DCC and Liconox using a synthetic flue gas mixture

Inlet NO and SOx concentrations varied between 500 – 1000 ppmv and inlet SO_2 between 500 – 750ppmv. Test results shown in figure 5.4-2 demonstrated that a significant amount of SOx and NOx were removed in the DCC before target SOx and NOx removal was achieved after the Liconox.

Simulated tests of the Deoxo also demonstrated stable performance with natural gas fuel, achieving removal of 2 mol% oxygen and average oxygen slip below 100 ppmv. Lower concentrations of oxygen in the product gas may be attainable with further optimization of process control that could not be accomplished during these tests. Figure 5.4-3

shows a representative example of 20 hours of testing, in which the outlet oxygen content varies, but an average concentration of 53 ppmv is achieved.

The initiation temperature of the deoxidation reaction was found to be around 315°C, about 50 degrees lower than anticipated, allowing a higher temperature rise and extent of deoxidation reaction while staying within the maximum allowable working temperatures of the vessel materials. As Figure 5.4-4 demonstrates, once steady state was achieved, the temperature profile within the reactor remained stable over the length of the test.

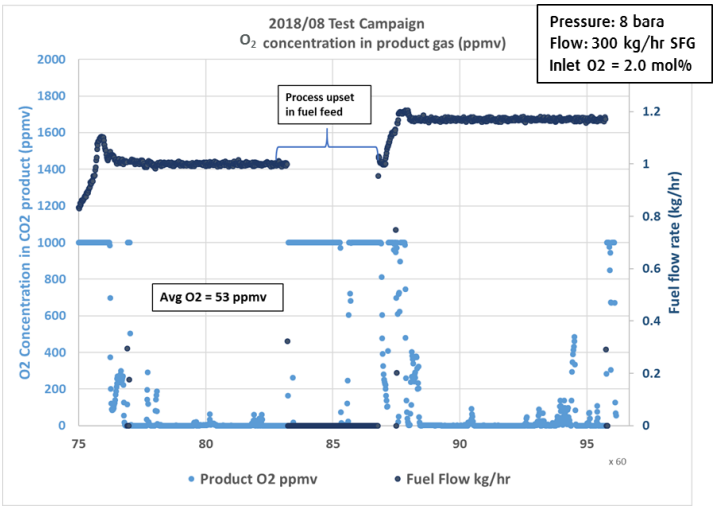

Figure 5.4-3. Oxygen removal in the Deoxo with synthetic flue gas

Table 5.4-2 provides a summary of the CPU performance attributes against the design targets. The Linde CPU met or exceeded all design targets with synthetic flue gas, except where facility limited or for those targets that could only be addressed through longer testing or with flue gas contaminants from coal.

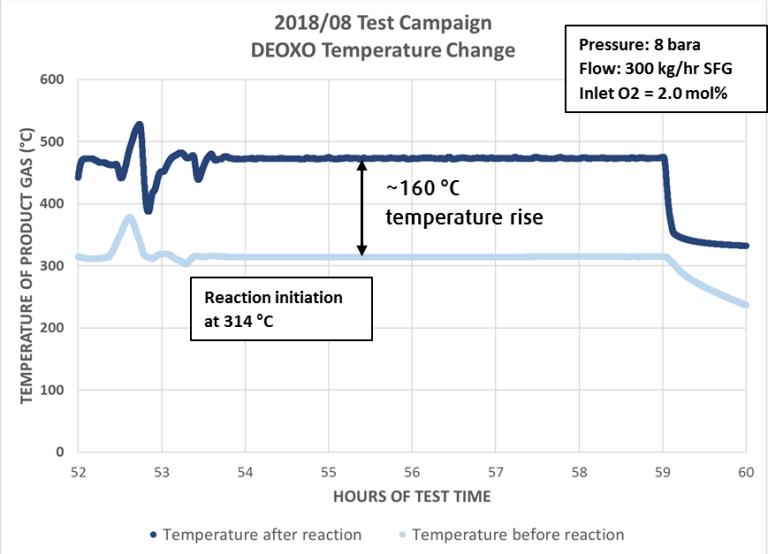

Figure 5.4-4. Stable temperature profiles within the deoxo reactor

	Performance Attribute	Design Target	Performance against target
1.	Plant Capacity (kg/hr)	1 MWth	Demonstrated with 300 kg/hr of CO2 contained in synthetic flue gas (SFG) and 400 kg/hr of flue gas with limited oxy-coal combustion
2.	CO2 purity	> 95% dry basis	Achieved target removal of contaminants (SOx, NOx, O2)
3.	Operating pressure	8 - 16 bar	Achieved up to 10 bar due to facility limit
4.	DCC exit temperature	< 60 °C	Achieved < 50°C with boiler flue gas
5.	Oxygen removal	Up to 2 %	Achieved 2% removal with natural gas
6.	Oxygen slip	< 100ppm	Achieved. Average O2 slip was <100 ppm during test campaigns with SFG
7.	Sulfur capture	>95% after LICONOX	Achieved. Average SOx capture >99% during tests with SFG
8.	NOx capture	>90% after LICONOX	Achieved. Average NOx capture up to 94% during tests with SFG
9.	HCl capture	Complete removal	Not measured
10.	Validation of design features	(i)DCC Materials of construction (ii) De-oxo catalyst (iii) De-oxo sulfur guard (iv) Controlled temperature rise of deoxo temp ~ 100 °C	(i)Limited testing completed with duplex stainless steel (ii) Achieved design space velocity at 300 kg/hr and 10 bar (iii) No degradation of catalyst performance observed (iv) Achieved. Demonstrated lower reaction activation temperature and temperature rise of 160 °C

Table 5.4-2. Summary of Linde CPU performance

5.5 Testing

5.5.1 Oxy-PFBC commissioning tests

Commissioning tests included testing of individual components prior to testing systems or subsystems. Once components were determined to function properly, the Oxy-PFBC combustor was tested as a subsystem to gradually expand the Oxy-PFBC operating envelope. The Linde Liconox and De-Oxo units were commissioned separately (as discussed in section 5.4), and were not included as part of the Oxy-PFBC subsystem during commissioning tests. There were four primary Oxy-PFBC commissioning tests as described below. The initial commissioning test was conducted to evaluate bed behavior and utilized cold gas flow at atmospheric and full operating pressure (700 kPa gauge). The second test evaluated operation of the bed removal system at operating pressure. The third test evaluated the ability of the natural gas burner to heat the injector region of the combustor to coal ignition temperatures. Finally, the fourth test evaluated the ability to ignite coal and sustain burning.

5.5.1.1 Cold flow tests at atmospheric and elevated pressure

Cold flow tests were run to determine the minimum fluidization velocity at 100 and 700 kPa gauge pressure. 150 kg of olivine 30-60 sand bed material was loaded into the PFBC before the start of the testing. For 100 kPag test, fluidization air was supplied from the air compressor and flowed into the recycle line upstream of the windbox and into the combustor through the tuyeres. For the 700 kPag test, in addition to the air supply, the recycle compressor was turned on at the upper range of what the air compressor could supply to get data in the higher velocity range. The data from these tests is shown in the following figure. The velocity of gas was calculated using the mass flow of air, density, and cross sectional area of the combustor. The pressure drop across the bed is the sum of all the pressure delta

sensors spanning the height of the bed. The minimum fluidization velocity is found from the plots at the point where the increase in bed pressure with velocity reaches a local maximum. This value is found to be about 0.37-0.38 m/s at 100 kPag and 0.25-0.26 m/s at 700 kPag.

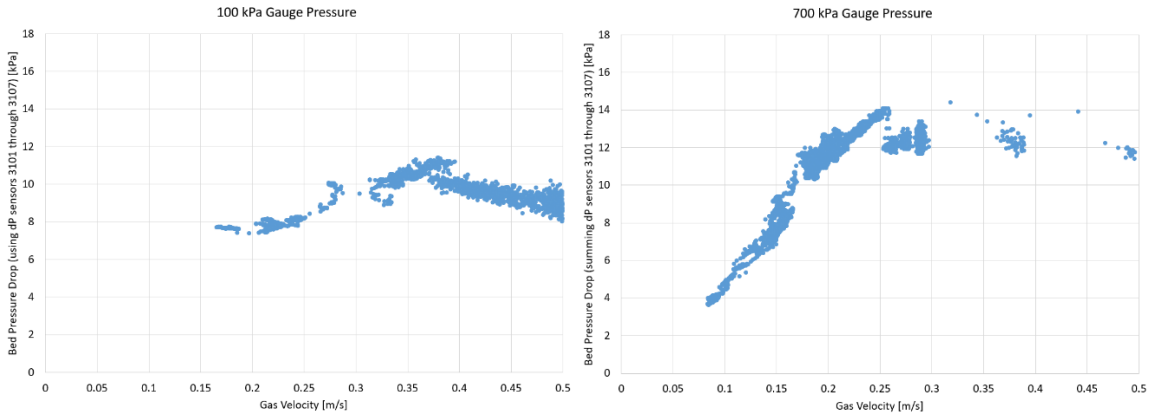

Figure 5.5-1: Cold flow testing to determine minimum fluidization velocity at 100 and 700 kPag.

5.5.1.2 Bed letdown testing

Bed ash removal testing was conducted to determine bed ash valve timing in order to target approximately 1 kg of bed ash removed for each cycle of the system. Testing was conducted at 700 kPag and with air supplied through the recycle line to the combustor, such that the velocity in the bed was 0.48 m/s and U/Umf was 1.84. 125 kg of olivine was initially loaded in the combustor for bed material. The following figure shows the amount of time the bed ash valve was open in seconds versus the amount of olivine bed material that fell into the bed ash lockhopper during that cycle. Based on this test, a valve open time of about 12 seconds would allow the approximately 1 kg of bed ash to be removed for each lockhopper cycle.

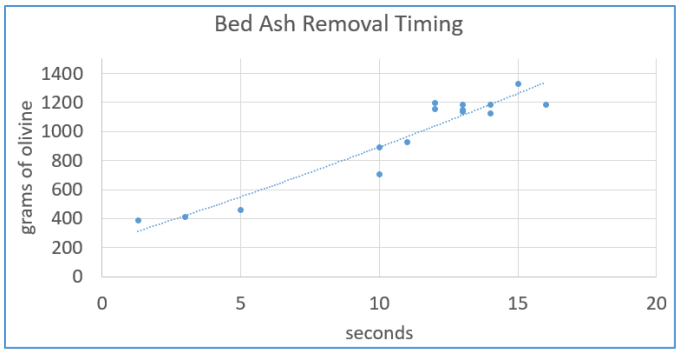

Figure 5.5-2: Bed ash removal testing to determine valve open timing in seconds.

5.5.1.3 Natural gas ignition test

The key test objectives for the natural gas ignition test were to demonstrate: 1) That the natural gas burner could be successfully ignited and monitored using a flame rod despite the lack of the ability to see the flame (a first for Canmet), and 2) That the temperature of the PFBC in the region of the coal injectors could be successfully heated to above the coal ignition temperature of 750°C. Ignition was successful and the flame rod worked as expected. For this test, no bed was present, the recycle blower was running, the cooling system was enabled, and combustor was slightly above ambient pressure. The following figure shows the process temperatures inside the combustor. The burner is turned on around 9:00 and most of the temperatures increase close to the desired rate of 55°C/hour, shown as the red line. However, past 11:00 the rate of temperature increase tends to decrease for most of the thermocouples. Just before 15:00, it was attempted to heat the injector zone (TE_3132/PV, gray line) to coal ignition temperatures by turning off the recycle blower, a technique demonstrated in the mini-bed test. This worked, however the overall system temperatures were not significantly altered during this time, due to large heat loads being dumped to the glycol system. Both key test objectives were successfully met, however due to the learnings of this and subsequent tests, the natural gas supply was switched to a higher supply pressure. This allowed for more rapid heating of the combustor as well as startup and transition to oxy-fired coal at a higher pressure, closer to the combustor operating pressure.

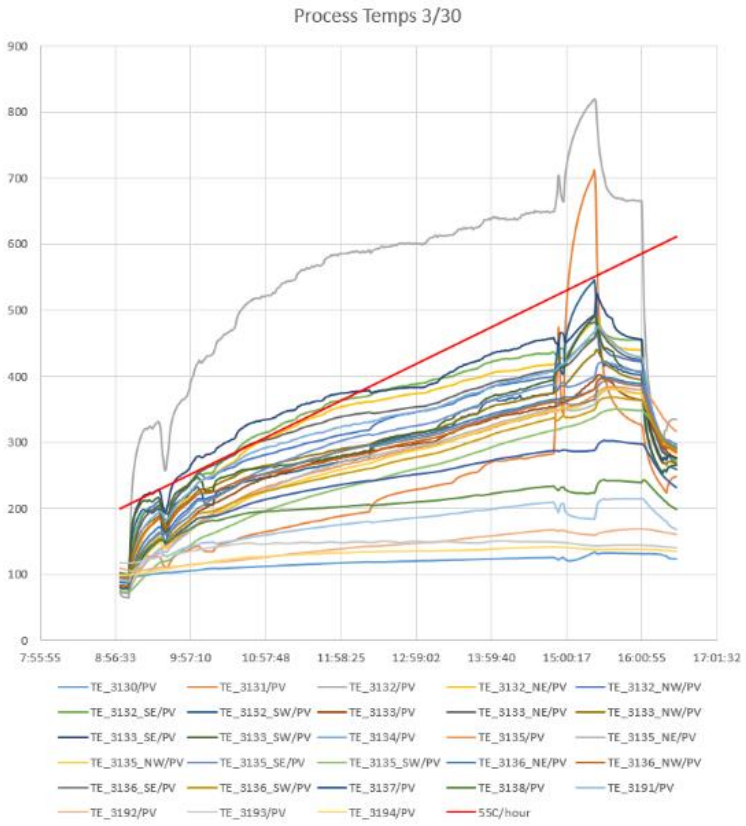

Figure 5.5-3: Process temperatures in °C during March 30 natural gas ignition test.

5.5.1.4 Air-fired coal ignition testing

The 1 MW_{th} Oxy-PFBC was successfully commissioned on April 27, 2017. Commissioning included component testing followed by Oxy-PFBC system testing that demonstrated successful ignition and sustained burning with coal. Coal ignition was robust and repeatable. The coal ignition testing was accomplished by feeding air through the recycle line to the combustor to provide the extra oxygen for coal combustion. Air instead of oxygen was used because the oxygen supply that normally would have been fed to the recycle line still had piping that was under construction and not yet complete.

The coal ignition testing utilized startup procedures developed in the 50 kW_{th} oxy-FBC "mini-bed". The natural gas burner was used to preheat the combustor for approximately twelve hours. Temperatures in the injector zone were further increased by shutting off the recycle blower several hours prior to coal injection. Test parameters that were varied during ignition testing included mass flow rates for coal, natural gas, oxidizer and recycle gas, as well as bed material mass in the combustor. Combustor pressure was slightly above atmospheric at 30 kPag. Six of seven attempted ignition tests were successful. Five of the tests achieved sustained burning, with typical coal combustion test times of 20-30 minutes.

Representative data from one of the tests is shown in the following figures. The thermocouples in Fig. 5.5-4 are listed in order from the lowest position on the left to the highest position in the bed on the right. The red line, TE_3132/PV, which is located near the coal injector, shows very quick temperature increase and levels off close to 875°C. Figure 5.5-5 shows the gas composition near the fly ash filter. As coal combustion starts, the O_2% decreases, the CO_2% increases, and since the oxidizer for this test was air, nitrogen would be a majority of the remainder of the gas composition, which is not measured by the gas analyzers. Carbon monoxide is seen to increase as coal combustion is initiated, and then gradually starts to decrease as temperatures in the combustor increase.

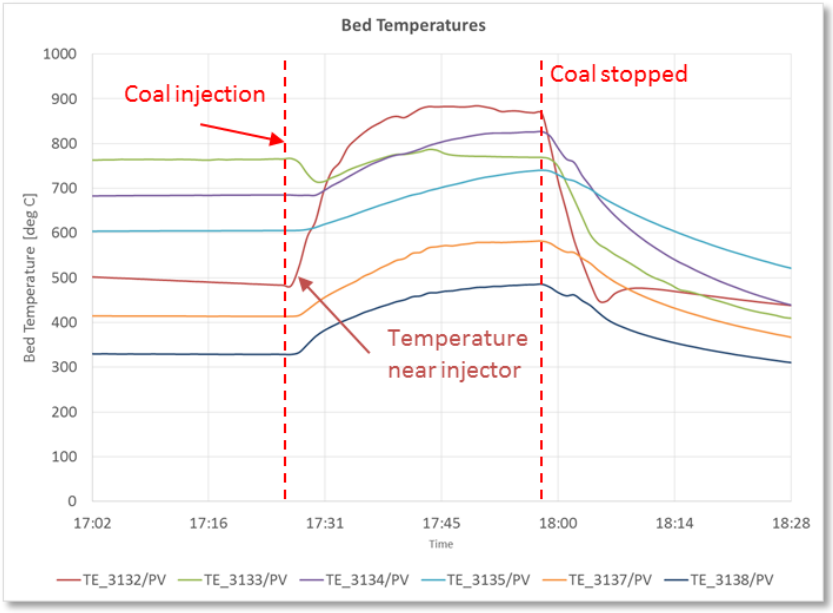

Figure 5.5-4. Fluidized bed temperatures in the combustor indicating successful coal ignition and burning for over thirty minutes.

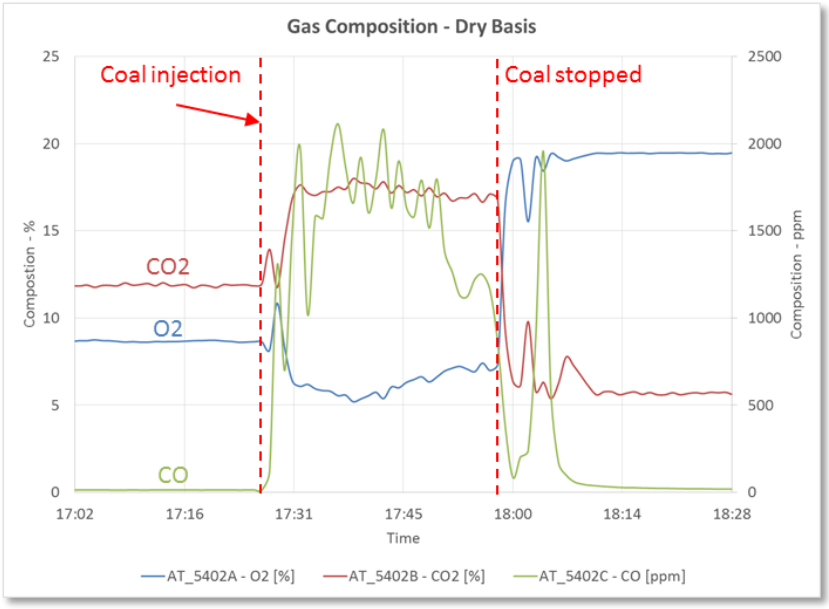

Figure 5.5-5. Production of CO_2 and CO in the combustor provide verification of successful coal ignition and burning.

5.5.2: Performance Testing

5.5.2.1 Test 1: Testing of high pressure NG burning, coal ignition and burning with oxygen

The first phase of testing after commissioning was conducted which demonstrated high pressure natural gas combustion capability and coal ignition with oxygen. A high pressure natural gas supply was added to the natural gas burner to allow the combustor to achieve higher temperatures and pressures at ignition to achieve cleaner coal burning with reduced fouling risk and better bed fluidization. It also allows more rapid combustor heatup. This test also demonstrated that ignition of the coal with oxygen is possible.

Figure 5.5-6 shows the combustor process temperatures during warm-up, several oxy-fired coal attempts, and cooldown for one of the test days performed during late May. After the initial electric heatup period, the natural gas burner was turned on around 10:20 and many of the process temperatures are seen to rise at much quicker pace than in prior tests with low pressure natural gas. Thermocouples in the lower bed near to the coal injector (TE-3132 through TE-3133_SW) reach higher temperatures, in the range of the 750°C coal ignition temperature, within 6 hours after burner startup. The recycle blower was kept off during warmup and turned back on just prior to the start of coal injection.

Several runs with coal injection were performed where the process temperatures in the figure are seen to rise quickly around 16:40, and 19:50 through 22:00, with the longest sustained run being the last one of 40 minutes duration. Each run was interupted when the coal flow would stop on its own even though the Macawber feed system was running. It was determined that the coal feed line into the combustor was not being plugged, so the problem was somewhere in the Macawber feed system. Similar problems

had been occurring on the prior test day of May 25, so these series of tests were suspended so that the coal feed system problem could be investigated and fixed.

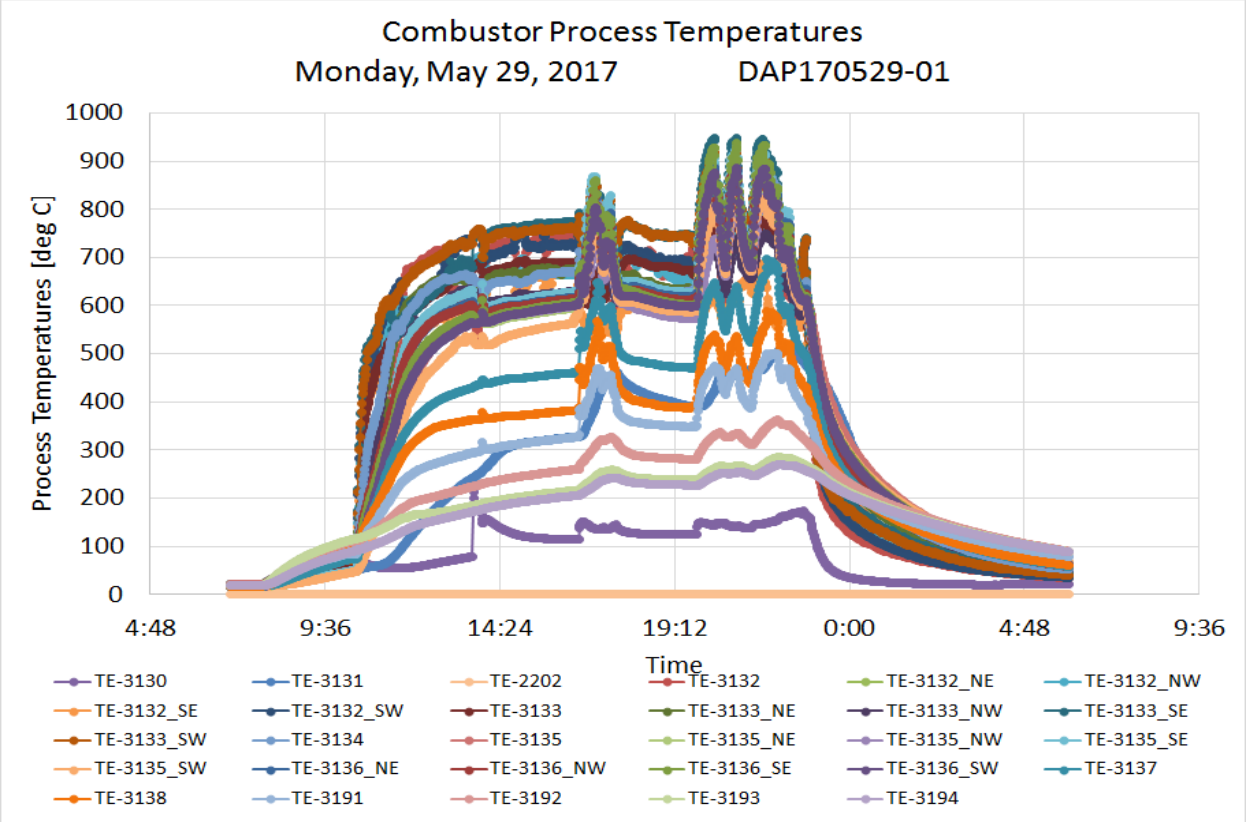

Figure 5.5-6: Combustor process temperatures during warm-up, several oxy-fired coal attempts, and cooldown.

5.5.2.2 Fuel cold flow testing

As a result of these first tests, there was extensive testing of the Macawber pneumatic injection system in June 2017. Cold flow testing revealed that the coal/dolomite mixture was bridging in the Macawber lockhopper. The lockhopper sits above the injection vessel tank and receives the coal/dolomite mixture from a surge bin vessel above it at atmospheric pressure. The lockhopper is then pressurized with CO_2 gas until it reaches the pressure of the injection vessel, and then the valve between the lockhopper and injection vessel opens allowing the coal/dolomite mixture to flow into the injection vessel, which then feeds the mixture with an auger into the injection line running to the combustor.

The lockhopper includes an internal sparger tube that is meant to fluff and agitate the coal/dolomite mixture just before the valve opens between the lockhopper and injection vessel to allow the mixture to flow move freely and to prevent bridging, see Fig. 5.5-7. As received by the manufacturer, the sparger tube did not match the engineering drawing, when installed the tip of the tube was near enough to the valve at the bottom of the lockhopper, and had too many holes such that CO_2 velocity through the holes was lower than desired. A new sparger tube was designed by the team and fabricated by Canmet that featured a curved tube so that the tip was closer to the valve at the bottom of the lockhopper when

installed. The tube had fewer holes and they were located in closer proximity to the tube tip so that the CO_2 velocity would be higher and would agitate the coal/dolomite mixture nearer to the valve better to enhance the flow above the valve. As a preventative measure, the red surge bin located above the Macawber lockhopper was modified to include air slides on its internal wall to promote better flow of the coal/dolomite mixture from the surge bin to the Macawber lockhopper, see Fig. 5.5-8.

After these system modifications, the injection system was successfully operated at different pressures and flow rates to confirm the viability of sustained longer term operation. An example of the test results is shown in Fig. 5.5-9, where the coal/dolomite mixture is being fed from the Macawber system into a vessel at 700 kPag back pressure. Each time the conveying weight (gray) increases rapidly, coal/dolomite mixture is being fed from the surge bin into the Macawber lockhopper, followed by a spike in the CO_2 convey gas (orange line) which is also fed to the lockhopper to pressurize it until it is equal to the injection vessel pressure. The coal/dolomite mixture then flows into the injection vessel when the valve opens. The steady downward slopes in the conveying weight (gray) show that the Macawber system steadily decreases in weight as the auger in the injection vessel continuously delivers coal/dolomite mixture to the injection line where it flows to the combustor.

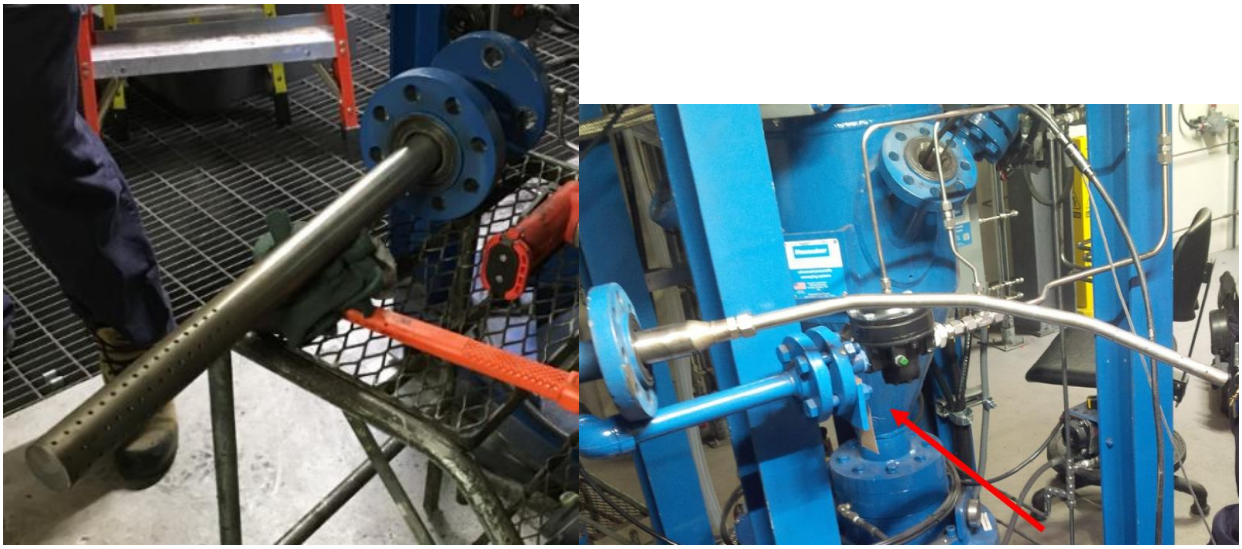

(a) (b)

Figure 5.5-7: (a) Macawber lockhopper sparger tube as fabricated by the manufacturer, (b) sparger tube as designed and fabricated at Canmet. The arrow points to where in the lockhopper the tip of the newly designed sparger tube is located.

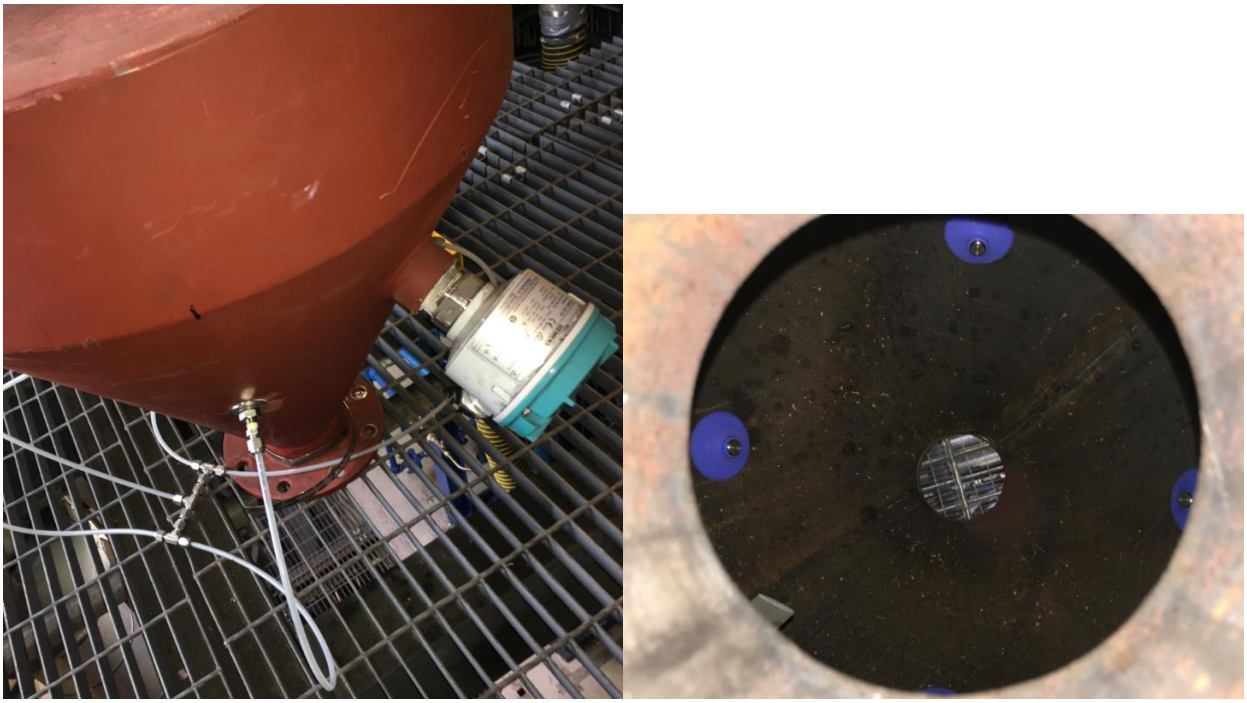

(a) (b)

Figure 5.5-8: (a) Red surge bin with sits above and feeds the Macawber lockhopper, (b) purple air slides installed which help the material to flow more easily by flowing gas along the surge bin wall.

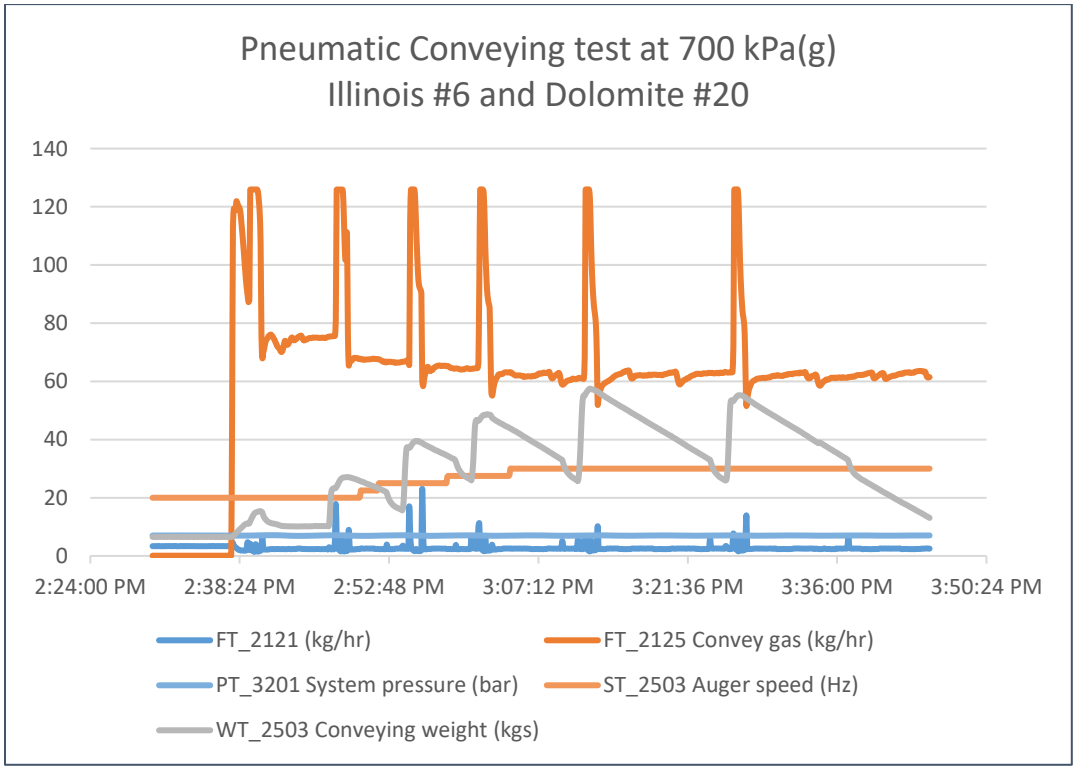

Figure 5.5-9. Illinois #6 and Dolomite #20 blend conveying test into 700 kPag back pressure.

5.5.2.3 Test 2: Testing of oxy-combustion at full operating pressure in July

A second test of the 1 MW_{th} Oxy-PFBC was completed during the week of July 24, 2017. This follows an earlier test in May. Hardware changes that had been implemented for this test included:

- New sparge tube installed in Macawber fuel feed lockhopper, slide valves installed in surge bin.
- In-bed heat exchanger Therminol tube rows 8, 11, and 17 were plumbed and turned on for additional bed cooling, for a total of 13 active cooling tube rows.

This test demonstrated oxy-combustion at the full operating pressure of 700 kPag. Figure 5.5-10 shows the process temperatures in the combustor during oxy-fired coal testing. Once the natural gas burner is turned off (sky blue line), the combustor is run in oxy-fired coal mode for the following 9 hours. It took several hours to bring the combustor up to full operating pressure. During 18:22 to 20:46 as the combustor pressure was being raised, the operators observed a decrease in the temperature of several thermocouples, including about a 100°C drop in TE-3132 near the fuel injector. The pressure was decreased and the temperatures were seen to recover. Then some adjustments were made in the recycle flow, oxygen supply, and finally continual increases of coal/dolomite flow with increases of pressure to keep temperatures hot enough in the combustor to reach the 700 kPag operating pressure.

After over an hour at 700 kPag pressure, there were troubles with starting the bed ash drain system as no material was coming out of the system and it appeared to be plugged at the bottom of the combustor. Attempts to clear the plug using blasts of CO_2 through the drain system cooled the lower bed, and the pressure was decreased to about 630 kPag while trying to stabilize combustion in the combustor. At about 3:00, temperatures in the combustor began to rapidly decrease and it was discovered that the coal/dolomite convey line between the Macawber fuel injection system and the combustor had developed a hole due to erosion at a kink in the tubing. Figure 5.5-11 shows the location of the hole on the tubing and a cutaway view of the hole. This caused a shutdown of testing.

This test also demonstrated combustor sulfur capture of greater than 99%, with 95% in the bed (Figure 5.5-12), and >99% downstream of the combustor fly ash filter and prior to the Linde CO_2 purification equipment. This exceeds the goal of 90% sulfur capture upstream of the CO_2 purification equipment.

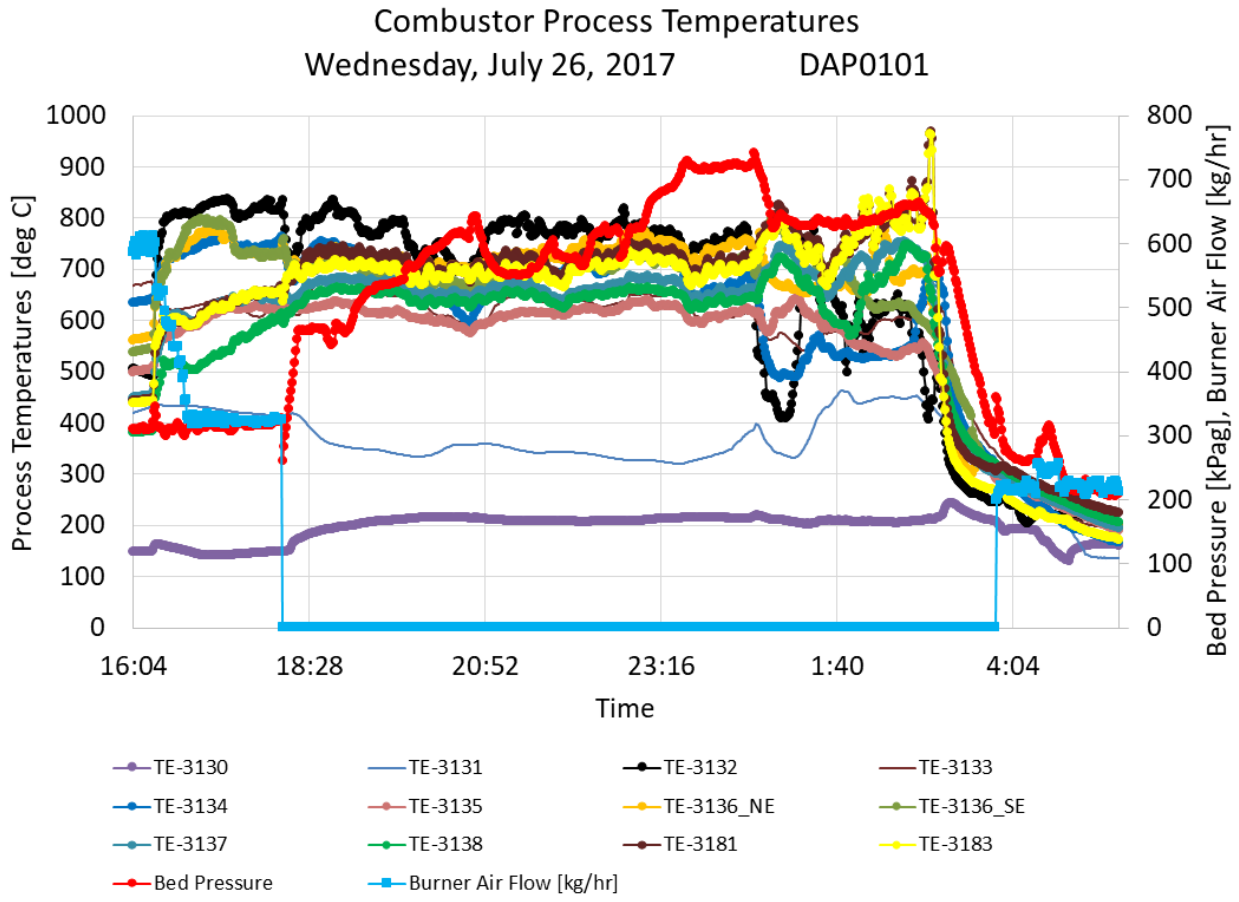

Figure 5.5-10: Process temperatures in the combustor during oxy-fired coal testing.

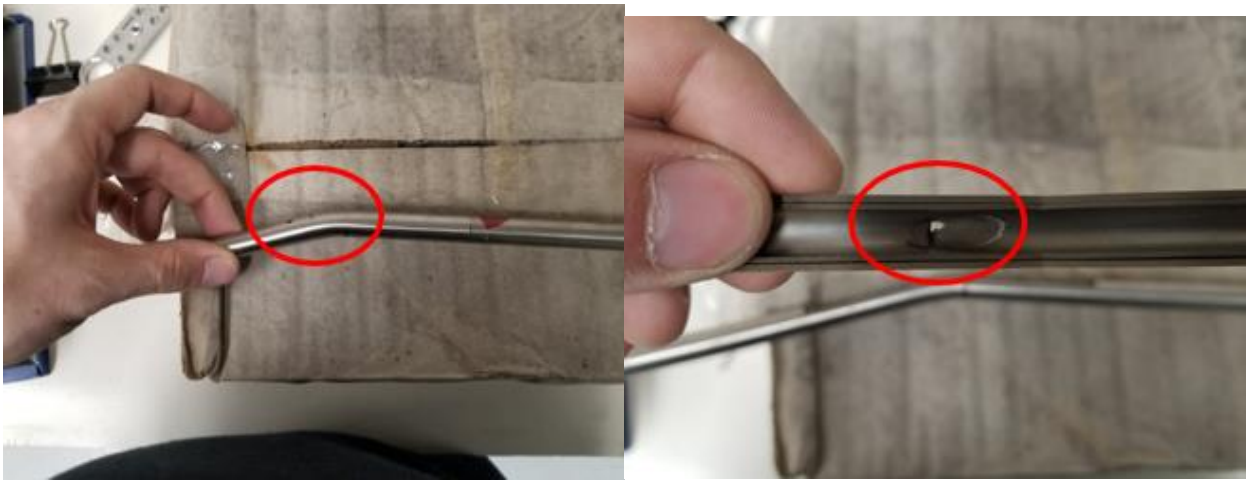

Figure 5.5-11: Hole formed by erosion in coal/dolomite convey line at a kink in the double-walled tubing.

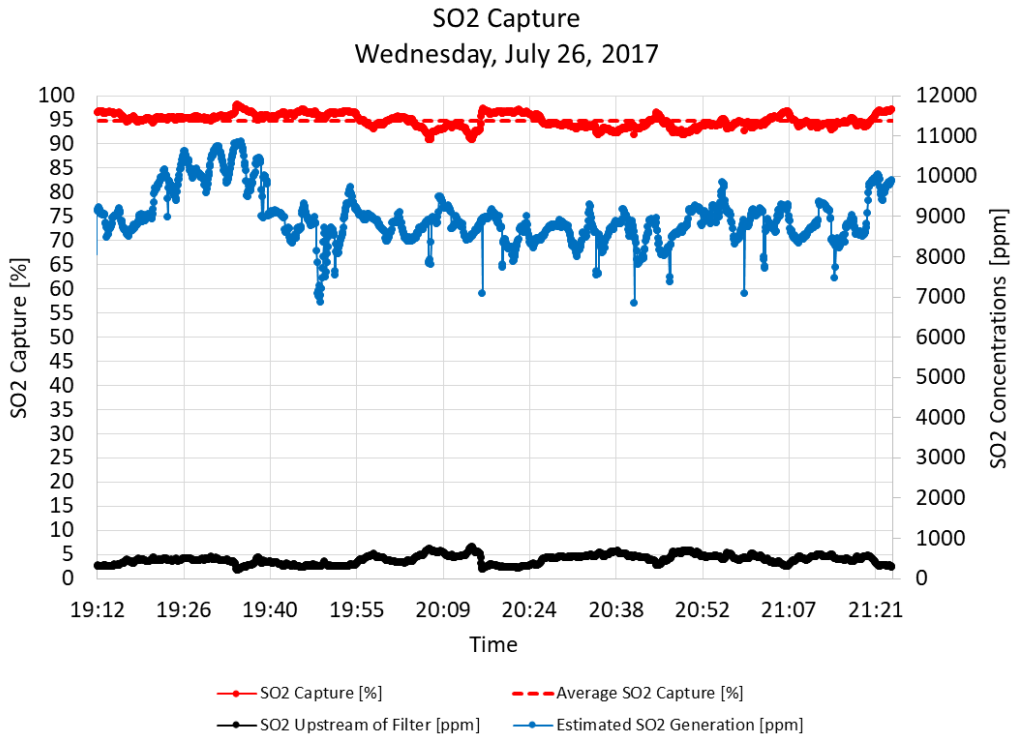

Figure 5.5-12. The Oxy-PFBC achieved an average of 95% sulfur capture during testing.

The test had six issues that were identified during testing, and have been addressed since that time. These items and the mitigation activities are listed below:

- Burn injury: A Canmet person was injured when hot bed material was inadvertently released due to the coal/dolomite convey line not being connected to the PFBC during test operations. While cleaning the material, additional hot material was ejected, even though the fuel shutoff valve was thought to be closed. This material landed on the person's hand, resulting in a burn. *Mitigation:* Procedures were changed including adding the requirement to log lines that are disconnected or require leak testing, to insure that lines are not activated prior to testing. In addition, people entering the test cell must have a partner that is in sight and in radio communication at all times. GTI personnel will now have Nomex (fire retardant) lab coats, similar to what Canmet personnel currently have.
- Coal line erosion: Coal eroded a hole through the feed line, which stopped the test. *Mitigation:* New rig was built to enable larger radius bends for conveying line. Erosion was only detected in the line near sharper radius bends. Conveying gas mass flow will be reduced, which should reduce max velocity by ~20% and max erosive force by ~40%. Tubing with double wall thickness is now used.
- Fly ash filter element damage: Damage was caused by overcooling combustor which led to unburned coal on the filter, leading to overheating of filter. *Mitigation:* Broken filter elements replaced. Larger bed material will be used to limit bed expansion and overcooling. Therminol tubes (which are always cooling) will be reduced from 3 tube banks to 1, with the remainder of cooling provided by air cooled tubes that can be switched on and off as needed.

- Inability to drain bed material: Agglomerates were formed that clogged the drain line, preventing bed height control.
  Mitigation: Put in place new procedures that are expected to reduce the likelihood of agglomeration. Bed drain modified to reduce risk of agglomerates clogging the drain. Existing agglomerates broken up and removed by fluidizing the bed in cold flow operation for several days.
- Fly ash fabric filter: A new fabric filter is needed downstream of the atmospheric pressure conveying line.
  Mitigation: Fabric filter was replaced.
- Fly ash vessel drainage issue due to control system software bug.
  Mitigation: This was corrected during the test.

Post-test operations led to an additional issue: failure of the shaft seal on the recycle blower on September 6. The seal was replaced. However, during the week of September 25 which was the next planned testing campaign, the shaft seal broke again during routine shimming of the recycle blower to reduce vibrations. Repairs for the shaft seal caused the next test campaign to be pushed back to the week of October 23.

Post-test inspections also found significant agglomeration formations had developed in the lower bed section. To clean out the agglomerates, cold flow fluidization with olivine bed material was used to try to mechanically break up and loosen the agglomerates lodged between cooling tubes. In between fluidization runs, the bed ash drain system was also removed and long metal rods were inserted up into the section with cooling tubes to poke at and dislodge the agglomerates. The agglomerates seemed to be of two distinct types, smooth and triangular in shape with one cylindrical side suggesting they formed on the leeward side of the cooling tubes, and coarse with small bed particles stuck together to form clinkers of various sizes, see Fig. 5.5-13. A majority of the agglomerates were cleaned out of the bed before the following test campaign, and work continued trying to understand under what conditions they formed.

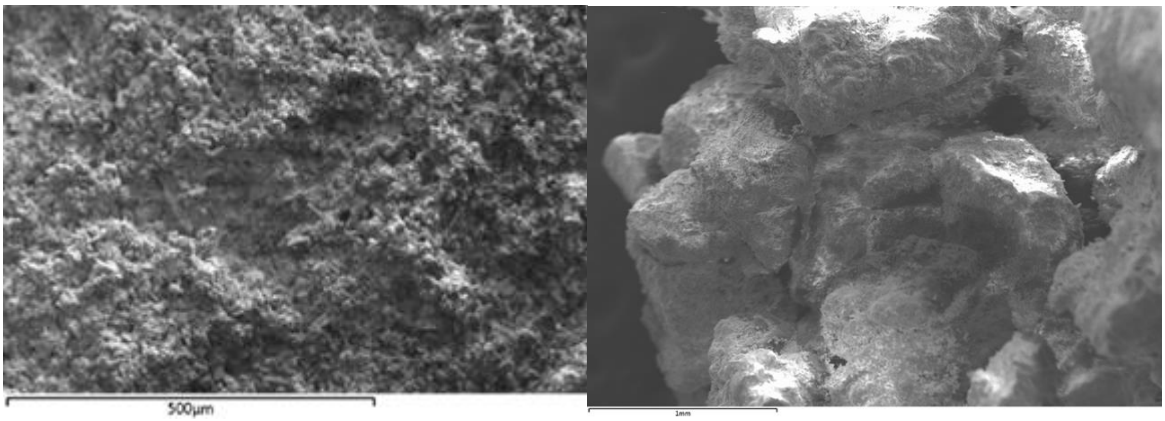

Figure 5.5-13: Agglomerates discovered after testing came in two types, smooth (left) and coarse with small bed particles stuck together (right).

5.5.2.4 Test 3: Testing of oxy-combustion in October

A third test of the 1 MW_{th} Oxy-PFBC was conducted during the week of October 23, 2017. Hardware changes that had been implemented for this test included:

- A bed ash tube retrofit, such that the bed drain tube extended several inches above the bottom of the combustor to deter larger agglomerates falling to the bottom from entering and clogging the bed ash tube.
- A smaller orifice was installed in the CO_2 gas supply line that conveys the coal/dolomite mixture from the Macawber feed system to the PFBC such that the velocity would be decreased to reduce the chance of convey line erosion.
- In-bed heat exchanger Therminol tube rows 27-29 and 31-35 which had been actively cooling in the July test were drained, cleaned and capped to allow the upper bed to increase in temperature and possibly increase carbon conversion.
- Trickle purges for the bed pressure delta sensors changes from CO_2 to N_2 gas to reduce the chance of agglomerates forming near the pressure sensing lines.
- 2.0" orifice installed in flue gas line downstream of the recycle blower.

The first half of the week was spent verifying that the recycle blower was working correctly in the speed range required for testing and a Flowserve technician came on-site to check on the newly installed shaft seal and to troubleshoot some squeaking noises. By the latter half of the week the combustor was started through the warmup heating sequence. There were some delays due to the natural gas burner flame rod initially not sensing the flame, and several times the coal/dolomite mixture stopped flowing from the Macawber fuel feed system and time was spent re-starting that system.

There were three periods during which there was extended running in oxy-fired coal operation, termed DAP0201, DAP0202, and DAP0203. The following figures show the process temperatures during these tests, the pressure did not reach full operating pressure. As can be seen, once the natural gas burner is turned off (sky blue line), there is a wide range in process temperatures throughout the bed, much more so when compared to the data from July (Fig. 5.5-10). In all three runs, the temperature nearest to the coal/dolomite injector, TE-3132, drops considerably once the burner is turned off. The temperatures in the lower bed, TE-3132 through TE-3135, are generally cooler than the temperatures in the upper bed, TE-3136_SE through TE-3138, and the temperatures above the upper bed in the freeboard, TE-3181 and TE-3183, are seen to read the hottest. In normal operation, it is expected that the bed temperatures would be fairly uniform throughout the bed. After the third test, the PFBC was shutdown to investigate possible damage to the combustor from high temperatures experienced during the test.

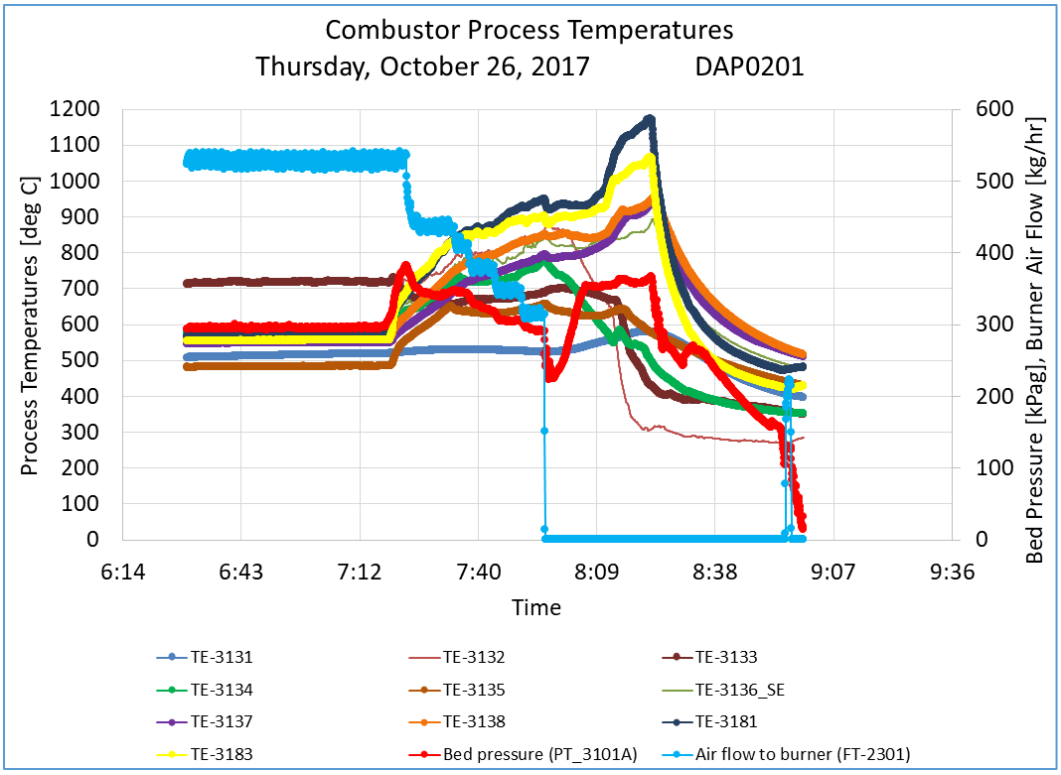

Figure 5.5-14: Process temperatures for DAP0201 during oxy-fired coal operation.

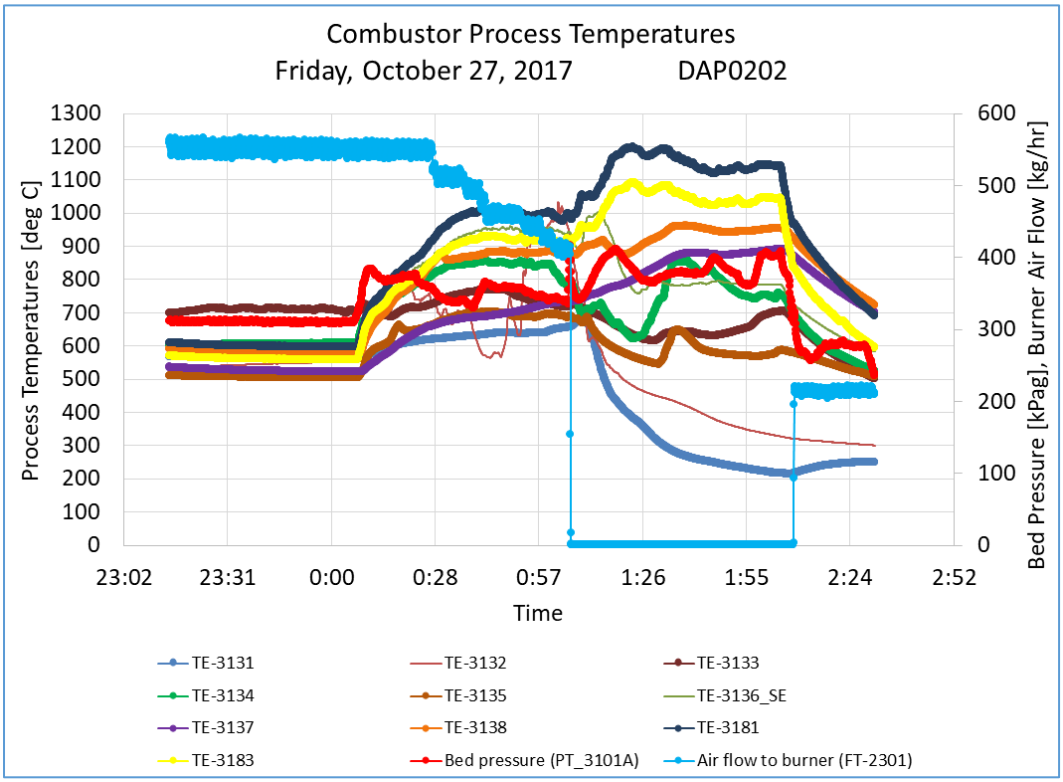

Figure 5.5-15: Process temperatures for DAP0202 during oxy-fired coal operation.

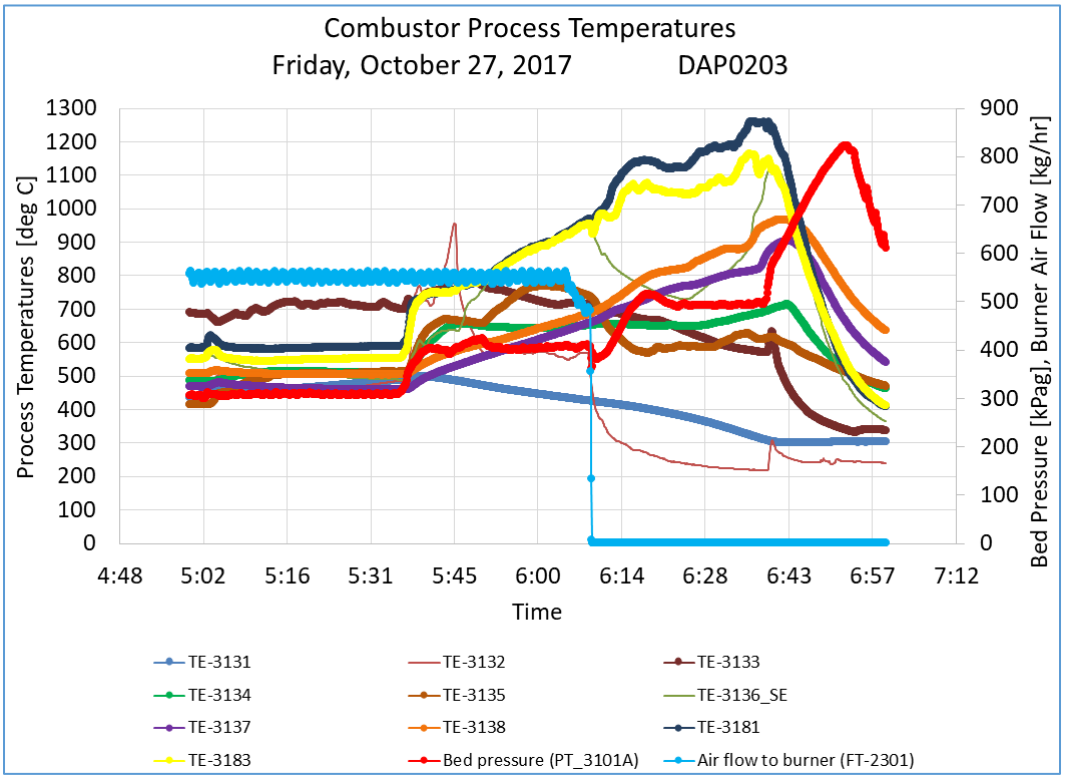

Figure 5.5-16: Process temperatures for DAP0203 during oxy-fired coal operation.

5.6 Test Analysis

5.6.1 Analysis of oxy-combustion at full operating pressure in July

Some key analyses of oxy-fired coal operation at full operating pressure are presented here. Figure 5.6-1 shows various bed properties. The average bed density is about 300-400 kg/m3, whereas the expectation was to achieve bed densities in the 600-800 kg/m3 range. Thus, the bed was almost double the desired volume, exposing 8 more tubes than desired to the bed. This had the effect of increasing the heat transfer out of the bed, and possibly lowering the carbon conversion by over-cooling the bed.

Calculations of carbon conversion indicated performance that was significantly less than the goal of 99%. Equations to compute carbon conversion are based on the flow of CO_2 or O_2 into and out of the PFBC. Calculations based on CO_2 flows are noisier due to more flowmeter inputs. Assumptions such as the complete conversion of Hydrogen in the coal to H_2O and Sulfur in the coal to SO_2 were used to derive the equations.

Figure 5.6-3 shows the heat transfer rates from the in-bed heat exchanger tubes. All the air tubes were turned off during this period. There is a fairly narrow range of heat transfer throughout the bed, ranging from 14-15 kW in rows 1 and 2 to 19-20 kW in rows 8 and 17.

Figure 5.6-4 shows a zoomed in view of process temperatures in the lower bed (TE-3132 through TE-3133_SW) and in the upper bed (TE-3135_NE through TE-3136_SW) for thermocouples not located adjacent to cooling tubes. The temperatures in the bed show a fairly wide range from 500-775°C. Data from other fluidized beds would suggest the range in temperatures should be in the tens of degrees instead. Also, temperatures are cooler than the target range of 825-875°C for the bed.

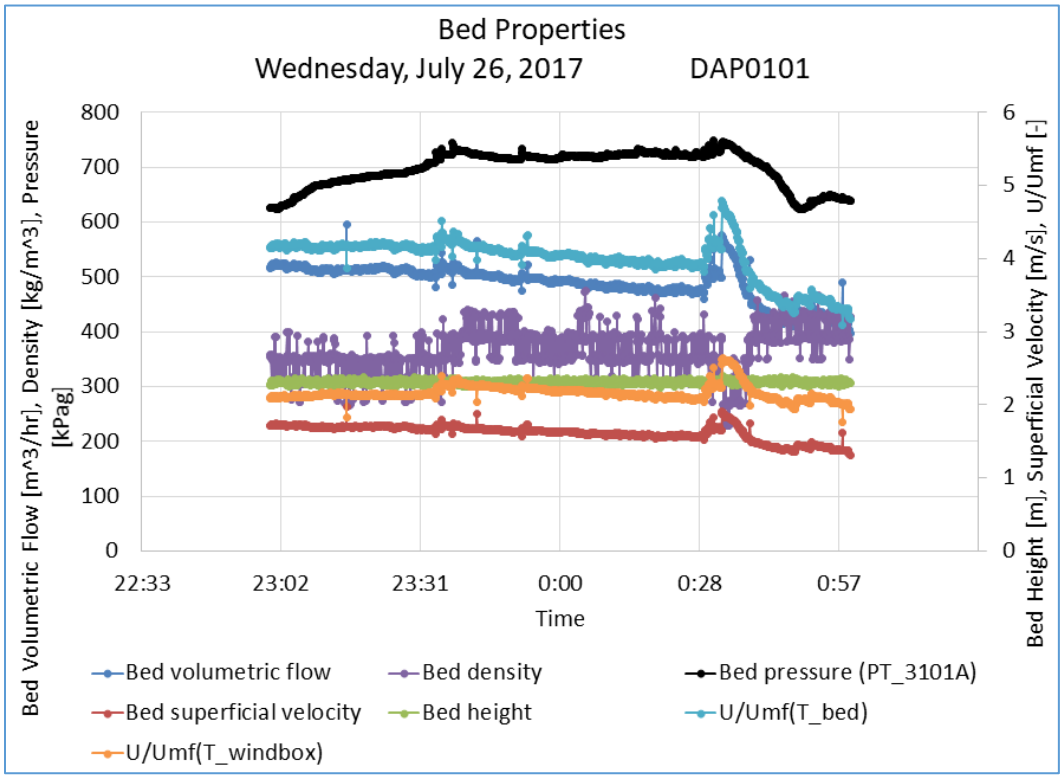

Figure 5.6-1: Bed properties during full operating pressure.

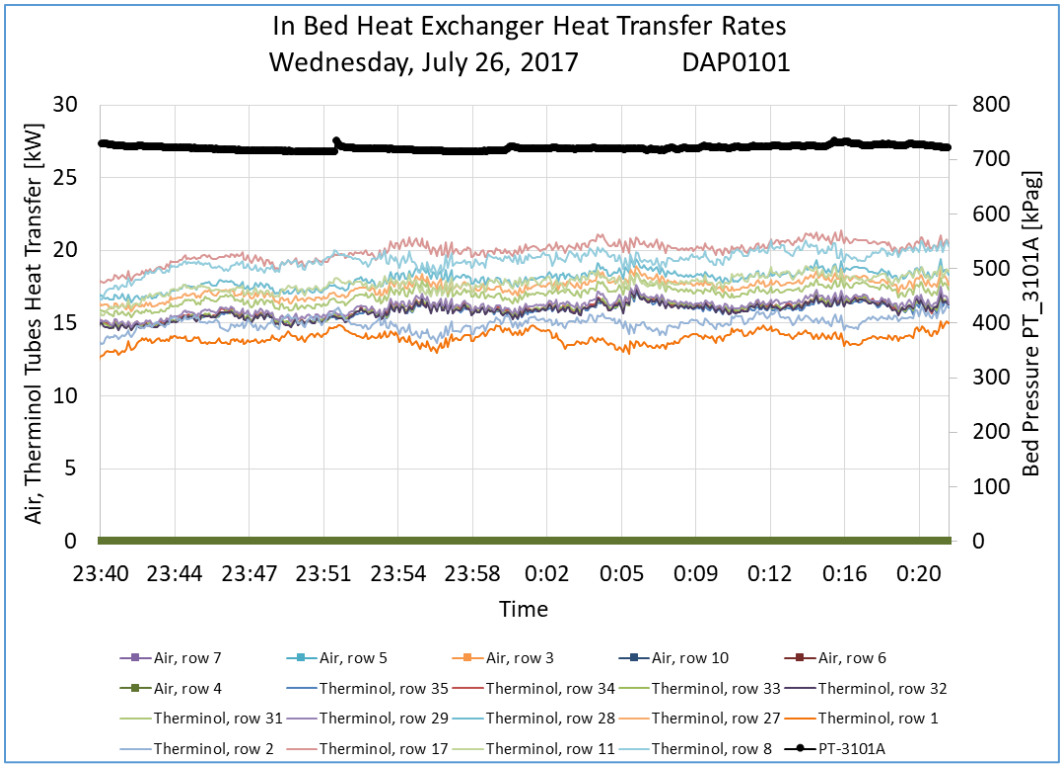

Figure 5.6-3: Heat transfer rates from in-bed heat exchanger tubes.

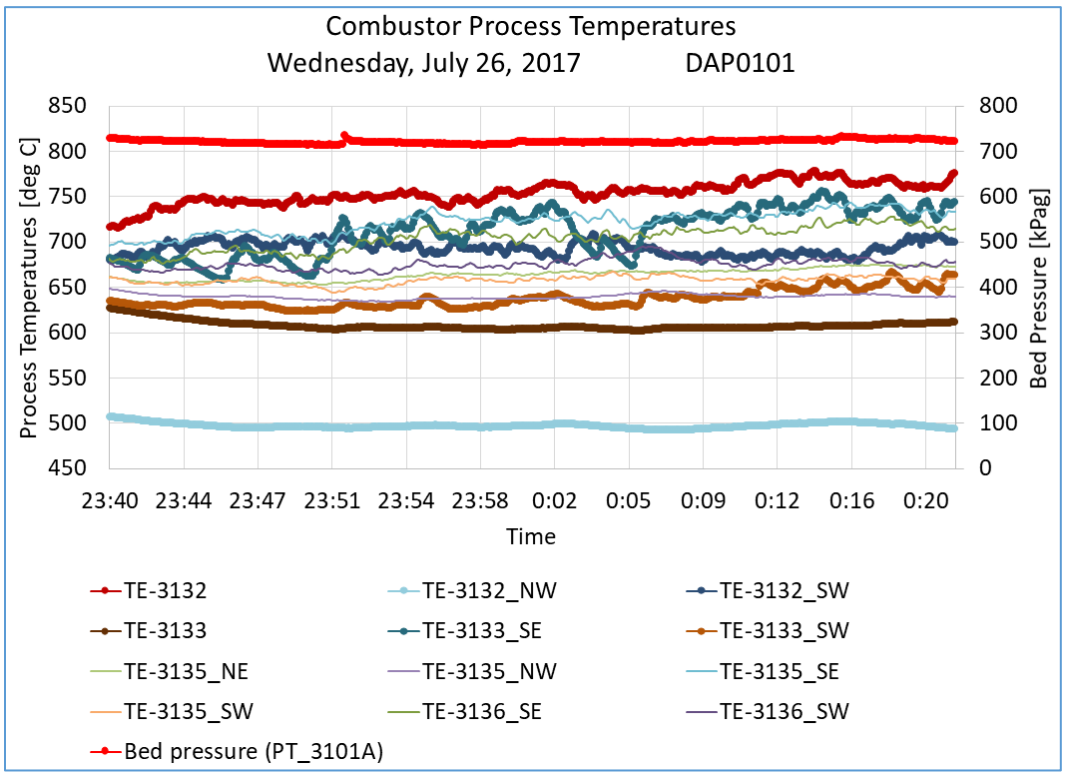

Figure 5.6-4: Process temperatures in the lower bed (TE-3132 through TE-3133_SW) and in the upper bed (TE-3135_NE through TE-3136_SW). Thermocouples not adjacent to cooling tubes.

5.6.2 Analysis of oxy-combustion in October

Some key analyses from the second test, DAP0202, which ran the longest in oxy-fired coal mode, is presented here. Similar bed dynamics and temperature profiles were seen in all three of the October tests. Figure 5.6-5 shows the various bed properties. The average bed density is about 200 kg/m3, whereas the expectation was to achieve bed densities in the 600-800 kg/m3 range. This is true even though the superficial velocity and U/Umf are similar at the same bed pressure to the test in July. The bed densities were not uniform throughout the height of the bed, which may be an indication that remaining agglomerates from the prior test in July and additional agglomerate growth in October changed the cross-sectional area in certain bed regions, causing areas of higher and lower gas velocity resulting in bed non-uniformity.

Figure 5.6-6 shows the heat transfer rates from the in-bed heat exchanger tubes. With the upper bed Therminol tubes turned off for these tests, there were five remaining tubes in the lower bed providing cooling. As soon as the natural gas burner (sky blue line) is turned off, the Therminol heat transfer rates rapidly decrease. Looking at Fig. 5.6-7 showing the combustor process temperatures, this corresponds to a decrease in a number of temperature readings in the lower bed (TE-3132 through TE-3133_SW). Shortly after the recycle blower was decreased, as can be seen by the bed volumetric flow and U/Umf in Fig. 5.6-5, to attempt to bring the combustion back to the lower bed. The heat transfer to Therminol tube rows 8, 11, and 17 increase, however rows 1 and 2 just above the coal/dolomite injector do show any heat transfer. Many of the lower bed process temperatures also continue to decrease. Similar dynamics occurred for all three of the October tests, where coal burning and higher temperatures appeared to favor the upper bed.

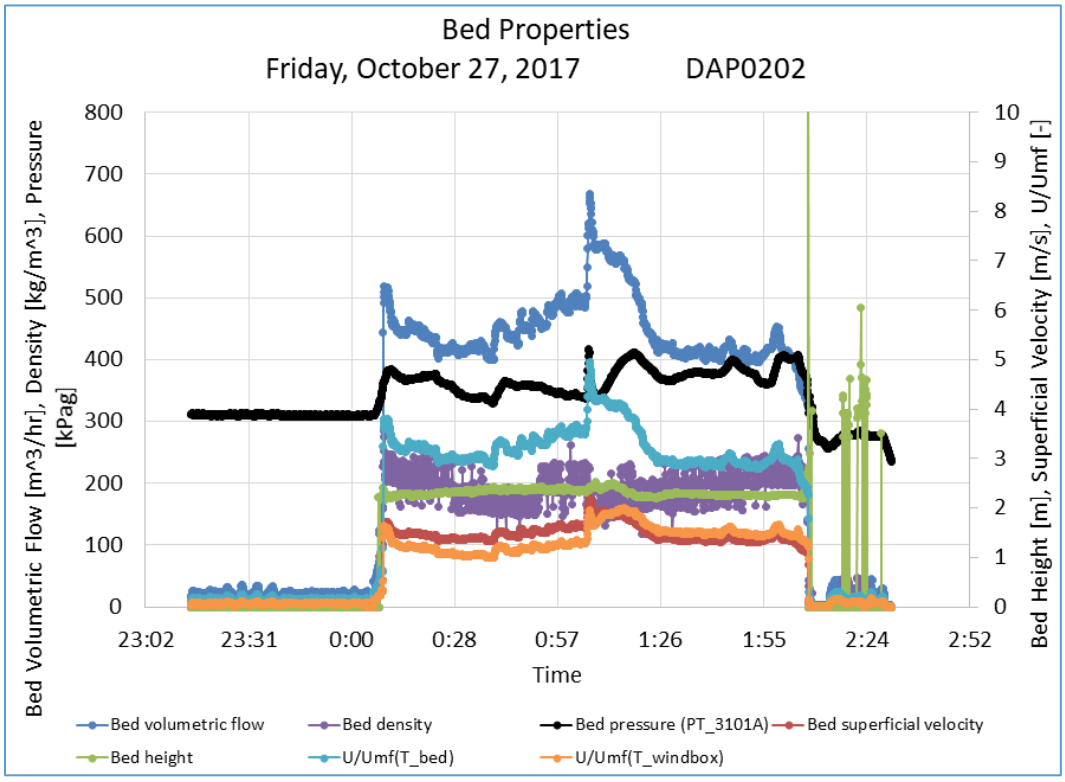

Figure 5.6-5: Bed properties during DAP0202.

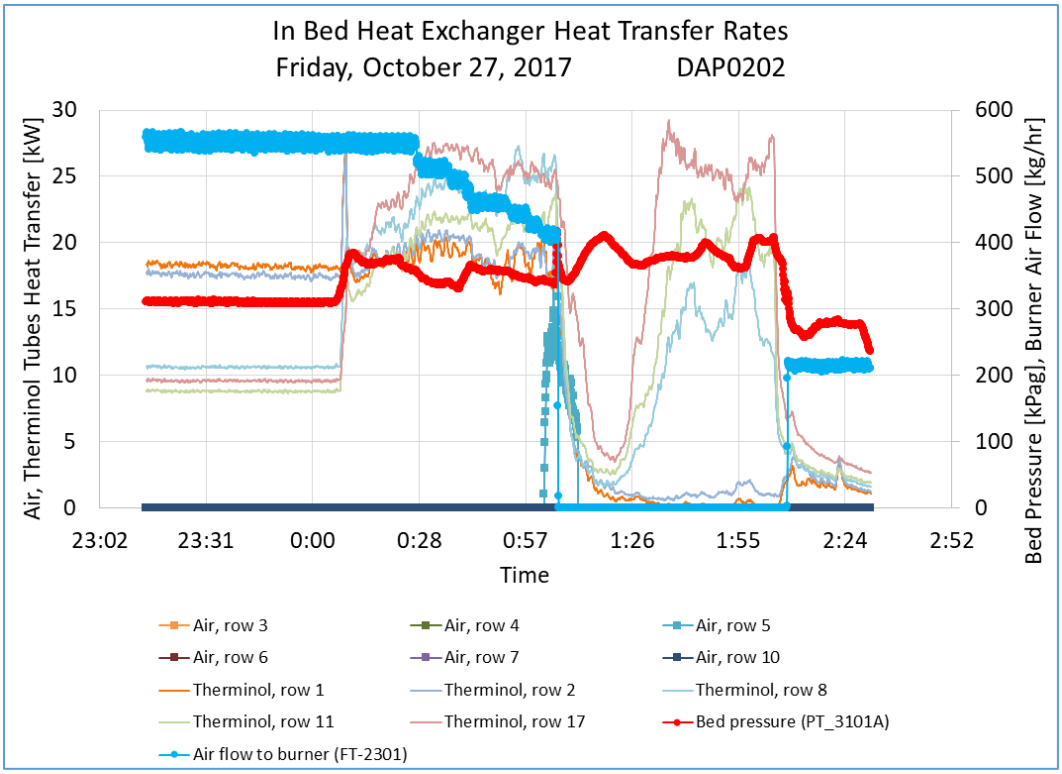

Figure 5.6-6: Heat transfer rates from in-bed heat exchanger tubes.

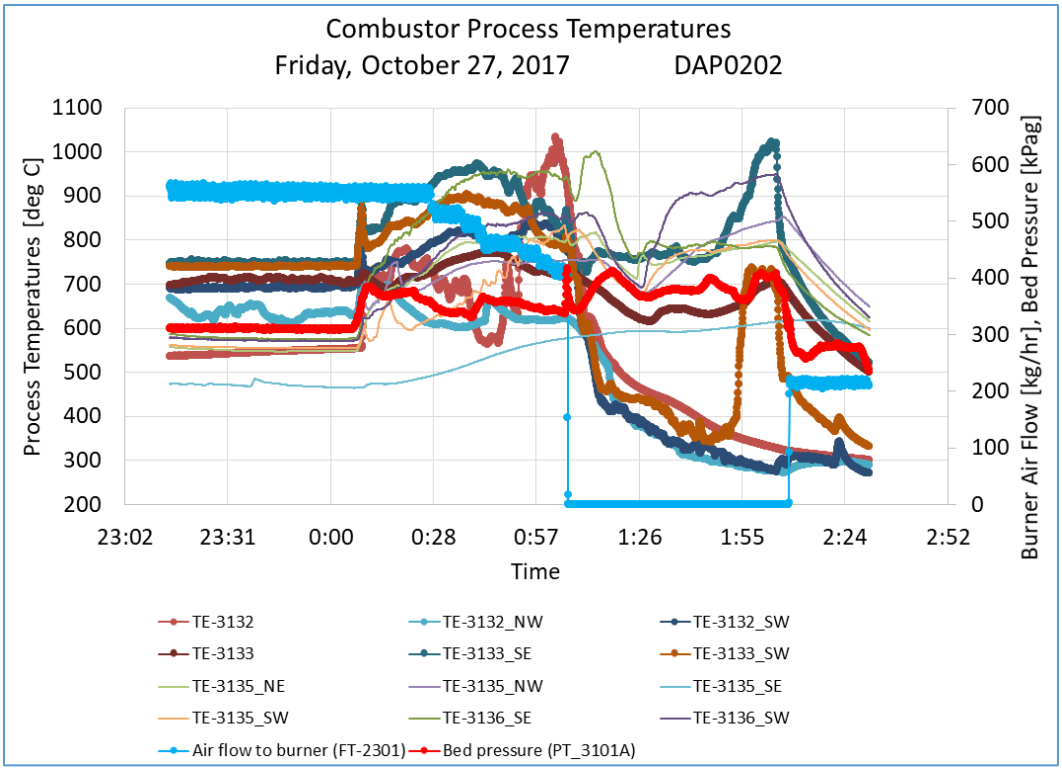

Figure 5.6-7: Process temperatures in the lower bed (TE-3132 through TE-3133_SW) and in the upper bed (TE-3135_NE through TE-3136_SW). Thermocouples not adjacent to cooling tubes.

5.6.3 End of testing

After the final test, the team conducted an incident investigation. During the final of the three October tests, high temperatures in the freeboard section of the combustor and abnormal pressure delta measurements in the bed section was the cause for the shutdown of testing. Inspection of the combustor with a borescope the following day revealed sections of the combustor with slag buildup.

5.7 Incident Investigation

During the Oxy-PFBC test in October, 2017, the combustor unexpectedly experienced significant heat release above the fluidized bed due to combustion in the freeboard region, where there were no heat exchanger tubes to remove heat and few temperature sensors. This was accompanied by low bed density and low carbon conversion performance. The freeboard burning resulted in catastrophic damage to the combustor through excessive temperatures that melted internal combustor components and led to coal ash melting (slag) that clogged the combustor. The root cause analysis found that the freeboard burning, low bed density and low carbon conversion all had the same primary cause: some heat exchanger tubes were too close to the combustor wall, leading to bed material collecting on top of the heat exchanger tubes near the wall and insulating temperature sensors there. As a result, average temperature readings were significantly lower than core combustor temperatures, resulting in erroneous calculations of gas density and velocity, which led to significantly higher gas velocities in the fluidized bed than realized at the time of testing. The higher gas velocities caused reduced coal residence time and lowered bed density, both of which led to reduced carbon conversion, burning in the freeboard region and ultimately to hardware damage. The lack of temperature sensors in the freeboard area, and the insulation of other sensors throughout the fluidized bed, led to the failure of the system to shut down in a high temperature situation, as intended.

There were other unresolved operational issues addressed by the root cause analysis (RCA) process, such as agglomerate formation, bed drain malfunction, safeguards inadequate to prevent damage, intermittent flame detection for the natural gas burner, CO_2 blower vibration, and coal mass flow variability. In addition, two additional issues that were resolved during testing, filter fire and coal feed line erosion, were also evaluated with RCA. RCA was conducted by reviewing all available data from the hot fire tests, as well as data from design, construction and cold flow tests. In late January, 2018, findings were reviewed by a team of non-advocate experts while DOE personnel were present. Twelve problem statements were developed with root cause analysis conducted for each.

The review team found that there were not any problems identified that indicated there were inherent problems with the technology (i.e. no “showstoppers”). There was general consensus on the root causes of the problems identified and the set of corrective actions. The details of the RCA are provided below.

5.7.1 Process for the investigation

The Root Cause Analysis process to understand the cause of abnormal combustor operation has multiple parts. It begins with constructing problem statements which are as specific as possible in order to avoid combining multiple problems into one study, and to focus the analysis. If a problem statement is too broad, it is difficult to identify a single problem. The team started with three problem statements.

A detailed timeline was constructed around the test data to shed light on problems, and as the investigation progressed, this led to refinement of the problem statements. Often, as in this case, a close look at the data leads to identification of new or unknown problems, which are then defined in new problem statements. The timeline used all available resources: test data, logbooks, personal recollection, dated records, emails, reports, etc. to combine a chronological account that extends back to design, construction, commissioning and cold flow tests.

Knowledge gained from assembling the timeline was then sorted to identify which facts are relevant to which problems, and theories are also included which, through team discussion, led to new areas of investigation, which included expansion of the timeline, destructive and nondestructive examination of hardware, and additional forensic testing.

The PFBC was carefully disassembled so as not to destroy any evidence, with each step documented to aid in the investigation and to provide guidance in improving the PFBC design and operation.

Once the set of problem statements was final, it became necessary to study other similar reactors which had been designed and tested in the past in order to compare the Oxy-PFBC to historical data, and identify differences in the old versus new test data.

When the complete set of knowledge of the Oxy-PFBC and historical data was assembled and discussed in meetings with non-advocate experts, the team found broad agreement and consensus on the root causes of the problems identified.

The team and reviewers were able to then assemble a set of corrective actions which would have to take place to produce an Oxy-PFBC which would function as intended. All of these steps and the results are described in the sections which follow.

5.7.2 Problem statements

This is the final list of problem statements. It should be noted that items 3, 4, 5, 7, 8, 9, 10, 11 and 12 were all identified prior to the catastrophic damage, and steps had been taken to improve multiple systems throughout the calendar year 2017 as each item was identified. This report is a catalog of the steps taken in the past and what else (if anything) would need to take place in the future. Some of these items are considered to be closed.

1. PFBC in Oxy-Combustion mode produces triangular or wedge-shaped agglomerates of very fine material on upper surface of tubes. Unclear if they are cold, hot or all tubes at this time. “Mostly” (60-70%) dolomite source. (in July, uncertain in October)

2. PFBC in Oxy-Combustion mode produces ovoid coarse sand agglomerates, sometimes trapping coal, which can smolder. Contains all materials present in bed, but still 60% dolomite source (Ca, Mg oxides, carbons, sulfurs). In July, uncertain in October.

3. In October, PFBC with natural gas burner off (oxy-combustion mode) promotes freeboard burning, and cannot maintain high temps near fuel injector. Burning occurs in upper section of bed and in the freeboard.

4. Bed ash removal system is not removing material. [Pipe installed which is presumed to allow coarser material to collect elsewhere so smaller particles exit the bottom]

5. Filter burning unburned coal in July test [partially addressed procedurally with filter cleaning before introducing air at end of test, will also be addressed by low carbon conversion above]

6. Safeguards/Alarms/Procedures are insufficient to prevent catastrophic slagging and HEX melting in combustor.

7. Startup heater flame detection was intermittent on October 26.

8. Solid Fuel blending system does not have steady flow or steady mix. (Dolomite is found to have wide variation in PSD.)
9. Solid Fuel pneumatic injection system is prone to plugging and erosion. (Partial fix in Aug: smaller orifice, lower velocity.)
10. Fly Ash Everlasting valves are intermittent. Ball valves work well but are slow. Multiple programming issues with filter and fly ash cleaning system.
11. In July Carbon conversion is only 85-87% - Fault tree combined with item #3
12. Blower vibrates unacceptably at speeds higher than 80%, causing seal failure

5.7.3 Relevant facts from testing and forensic investigation

A timeline overview is presented below. More detailed findings from a second-by-second timeline investigation are presented in separate tables, organized by problem statement.

- Commissioning tests
    - Robust and repeatable ignition of coal, ability to sustain combustion with air
- May 2017 test
    - *Changes:* Upgraded natural gas supply pressure (3 bar) to achieve higher ignition temps. Oxygen supply in place.
    - Demonstrated ability to ignite and sustain combustion with oxygen at elevated pressure
    - Linde CO2 Purification Unit (CPU)
        - All modules demonstrated to be functional
        - De-Oxo unit achieves performance goals with synthetic flue gas
    - *Issues:*
        - Intermittent coal supply. Difficulty draining bed.
        - Found one instance where agglomerated (presumed to be sintered) sand in lower bed was broken up in one large burp, causing cooling in bed and quenching.
        - Natural gas startup burner wall was damaged in the last test, and sheet metal pieces blocked flow out of the bed ash system. This had to be disassembled to remove the bed ash.
- July 2017 test
    - *Changes:* Modified coal feed system to provide more consistent feeding and address erosion found during feed system testing

- Demonstrated oxy-combustion at full operating pressure (8 bar)
- Captured 99% of sulfur prior to Linde CPU (goal of 97%)
- Achieved good burning throughout bed in one test

➢ *July 2017 Issues:*

- Coal line erosion stopped test.
- Lower bed density than expected, leading to greater than expected bed expansion and overcooling of combustor.
- Agglomerates in bed. No slag.
    - Found one instance where agglomerated (presumed to be sintered) sand in lower bed was broken up in one large burp, causing cooling in bed and quenching.
    - Found another instance where agglomerated (presumed to be sintered) sand in lower bed was broken up in one large burp, releasing unburned fuel and caused a spike in temperatures in center of bed.
- Lower carbon conversion than expected (86% vs. 99%).
- Difficulty draining bed – could not control bed height, leading to overcooling.
- Filter fire due to inadequate filter purging and poor carbon conversion.

➢ October 2017 test

- *Changes:*
    - Removed agglomerates through cold operation of bed. Small amounts remained.
    - Less bed material, coarser particles.
    - Replaced seal for CO_2 recycle blower (2^{nd} time).
- Attempted to achieve good carbon conversion without overcooling combustor and without blockage due to agglomerates as in July test by reducing bed velocity and reducing the number of cooled tubes.
- Achieved oxy-combustion at full operating pressure on three occasions. Carbon conversion was not improved.
- *Issues:*
    - Every test resulted in freeboard burning, despite making incremental improvements to operating method (startup temp, velocity).
    - Significant agglomerates leading to blockage, poor bed behavior and slag deposits.

- Difficulty maintaining burning in lower bed.
- Autoshutdown procedures did not operate as expected, leading to slagging in combustor and melting of multiple inactive HEX tubes

Fault trees and supporting data

For each problem statement, fault trees were created, and then facts gleaned from a detailed second-by-second timeline investigation plus post-test inspections and forensic tests were assembled into knowledge charts, which identify the relevance to fault tree branches, and the quality of the data. These charts of facts, opinions and questions are shown below, organized by problem statement. The cause trees are arranged so that root causes are at the bottom of each branch, and effects are above them. A summary of the causes is also presented. Figures 5.7-1 and 5.7-2 show legends for the problem statement fault tree box colors and knowledge chart data quality definitions, respectively.

Since many of the problem statements were found to have common causes with similar solutions, the proposed mitigations are presented in a subsequent section, and linked back to multiple cause chains.

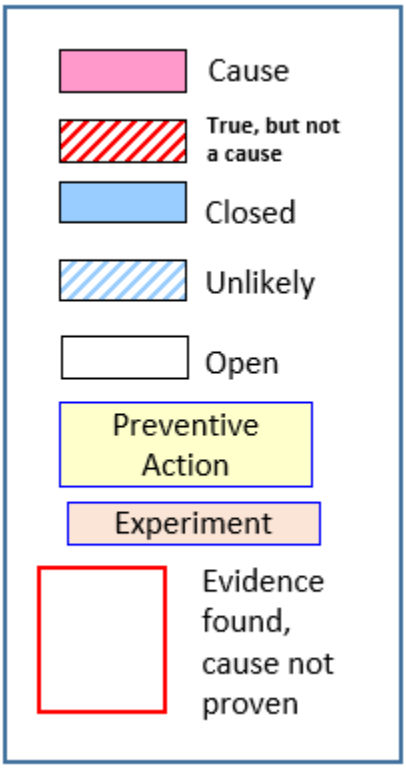

Figure 5.7-1: Problem statement fault tree legend.

Data Quality	Definition
1	Supporting data exists
0	Data is inconclusive
-1	Supporting data does not exist

Figure 5.7-2: Problem statement knowledge chart data quality legend.

Problem statement 1 (Fine agglomerates): PFBC in Oxy-Combustion mode produces triangular or wedge-shaped agglomerates of very fine material on upper surface of tubes. Unclear if they are cold, hot or all tubes at this time. “Mostly” (60-70%) dolomite source. Observed in July test, uncertain in October test.

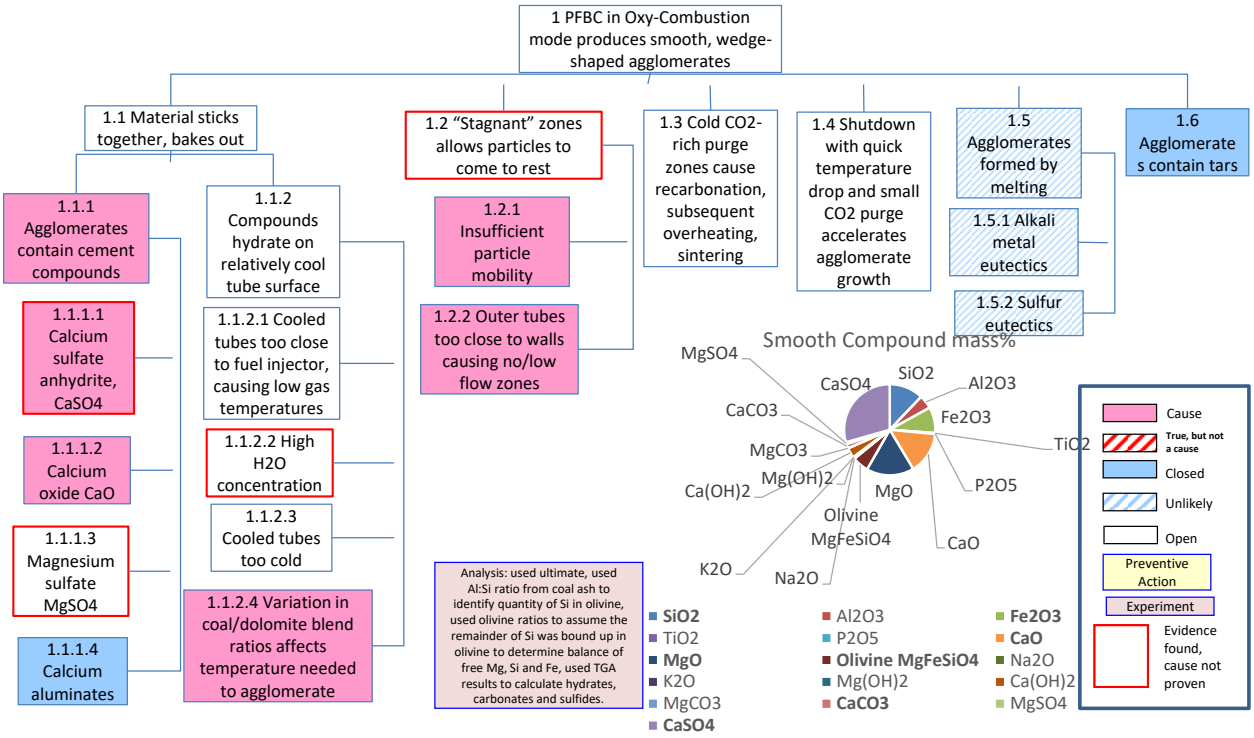

Figure 5.7-3: Problem statement 1 fault tree.

Table 5.7-1: Problem statement 1 knowledge chart.

Fault Tree ID	Fault tree branch/title	Question or Data Item	Quality
1.0, 2.0	Smooth & Coarse agglomerates	Are coarse and wedge shaped agglomerates independent of each other?	0
1.0, 2.0	Smooth & Coarse agglomerates	Some wedge agglomerates found stuck inside coarse agglomerates	1
1.0, 2.0	Smooth & Coarse agglomerates	So far, no coarse agglomerates found inside of wedge agglomerates	1
1.0, 2.0	Smooth & Coarse agglomerates	Most wedge agglomerates are not stuck to coarse agglomerates	1
1.0, 2.0	Smooth & Coarse agglomerates	Agglomerates found above first two cooled tubes, up to row 9	1
1.0, 2.0	Smooth & Coarse agglomerates	Locations of agglomerates not known yet for October tests	1
2.1	Cement compounds	Cements form due to t, pp changes?	0
1.1.1.2, 2.1.1.1	Ca(OH)2	Ca(OH)2 in agglomerates	1

1.1.2, 2.1.1.1	xxx, Calcium hydroxide	Agglomerates caused by overcooled zones	0
2.1.1.2	CaSO4-H2O	Unknown if hydrates of CaSO4 were previously present	-1
1.1.1.3, 2.1.2	MgSO4	MgSO4 in agglomerates	1
1.1.1.4	Calcium aluminates	Calcium aluminates not present	1
1.1.2, 2.1.1.1	xxx, Calcium hydroxide	Agglomerates caused by overcooled zones	0
1.1.2.4	Variation in coal/dolomite blend ratios affects temperature needed to agglomerate	Temperature needed to agglomerate affect by coal/dolomite ratio	1
1.2.1	Insufficient particle mobility	Wedge shape agglomerates have tube radius	1
1.2.1	Insufficient particle mobility	Stagnant zone on top of tubes	1
1.3, 2.4.1	xxx, Cold CO2 purge results in low O2	Agglomerates may be influenced by high CO2 partial pressure	0
1.5	No evidence of low melt temperature compounds	Low temperature eutectics not found	0
1.5.1, 2.2.2	xxx, Alkali & other eutectics	Alkali eutectics not found	0
1.5.2	Sulfur eutectics	Sulfur eutectics not found	0
1.6	No evidence of tars found	No tars found in either agglomerates	1
1.1.1.2, 2.1.1.1	Ca(OH)2	Ca(OH)2 in agglomerates	1
1.1.2, 2.1.1.1	xxx, Calcium hydroxide	Agglomerates caused by overcooled zones	0
2.1.1.2	CaSO4-H2O	Unknown if hydrates of CaSO4 were previously present	0
1.1.1.3, 2.1.2	MgSO4	MgSO4 in agglomerates	0

Table 5.7-2: Illinois Lab X-Ray Diffraction (XRD) Results

Compound Found	172515-002 Oxy-PFBC July 27 2017 Test Agglomerate Granular
Anhydrite ($CaSO_4$)	~96
Calcite ($CaCO_3$)	~1
Quartz (SiO_2)	~1
Dolomite ($Ca(Mg)CO_3$)	~2

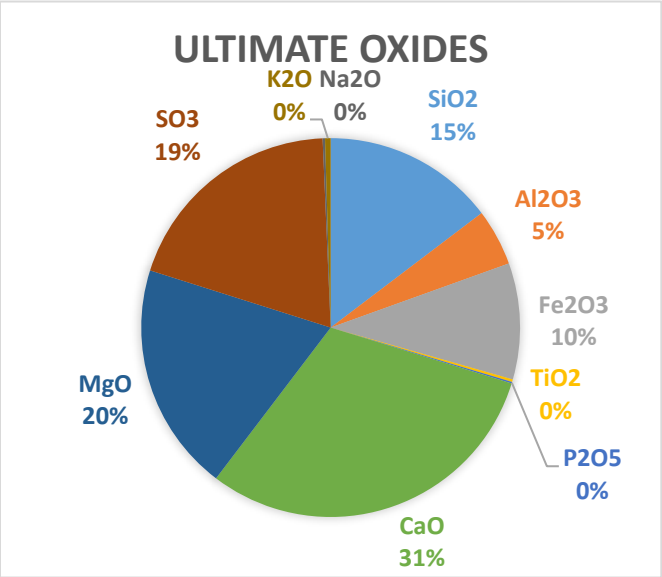

Figure 5.7-4: Illinois Lab X-Ray Diffraction (XRD) Results

Table 5.7-3: Canmet Lab Results

Chemical compound		% Chemical Compound	
Magnesium Oxide	MgO		18.8
Anhydrite	Ca(SO4)		57.0
Magnesioferrite, syn	MgFe2O4		2.8
Hematite, syn	Fe2O3		1.0
Quartz, syn	SiO2		2.7
Crystallinity (%)			82.3
Amorphous (%)			17.7

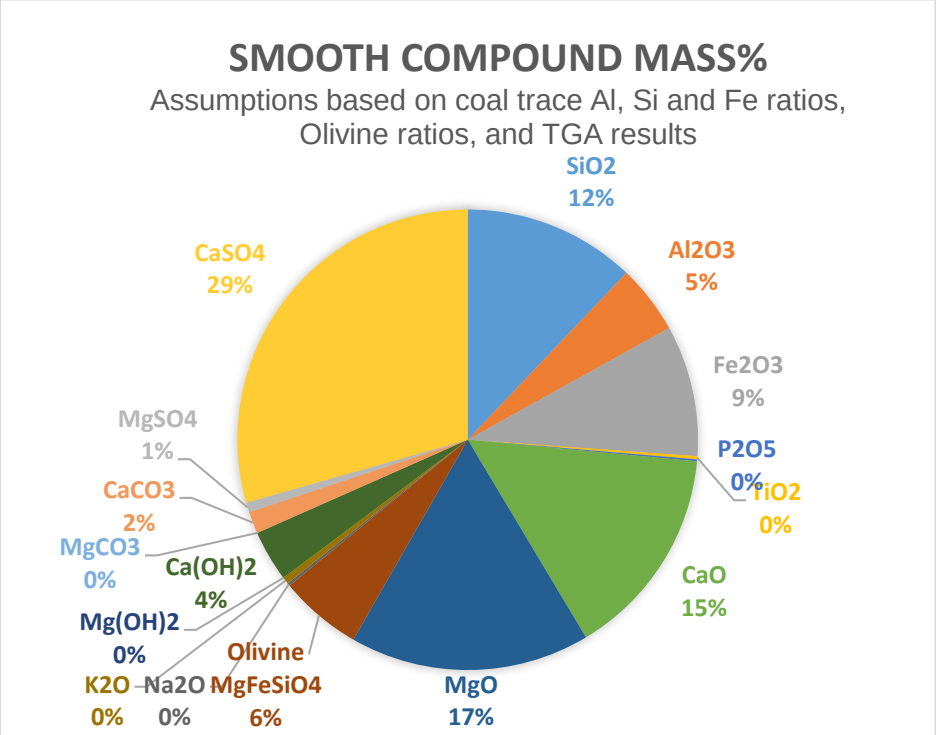

Figure 5.7-5: Canmet Lab Results

In summary, the problem of fine agglomerates was attributed to cementitious compounds undergoing a large temperature swing. The calcium particles were able to calcine to CaO during parts of the cycle where CO2 partial pressure was below the calcination/recarbination temperature for CaCO3. They were all triangular or deltoid in shape because they could find a foothold to stick to the small stagnation surface on the top of the heat exchanger tubes. An additional cause, which shows up in the cause chains for problem statement 3 (freeboard burning), is the startup sequence was being operated at low absolute pressure due to a limitation on natural gas inlet pressure, which meant the burner was operating above the calcination temperature during low pressure operation, when the system was designed to operate below the calcination temperature at high pressure.

Problem statement 2: Coarse agglomerates PFBC in Oxy-Combustion mode produces ovoid coarse sand agglomerates, sometimes trapping coal, which can smolder. Contains all materials present in bed, but still 60% dolomite source (Ca, Mg oxides, carbons, sulfurs). Occurred in July test, uncertain in October test.

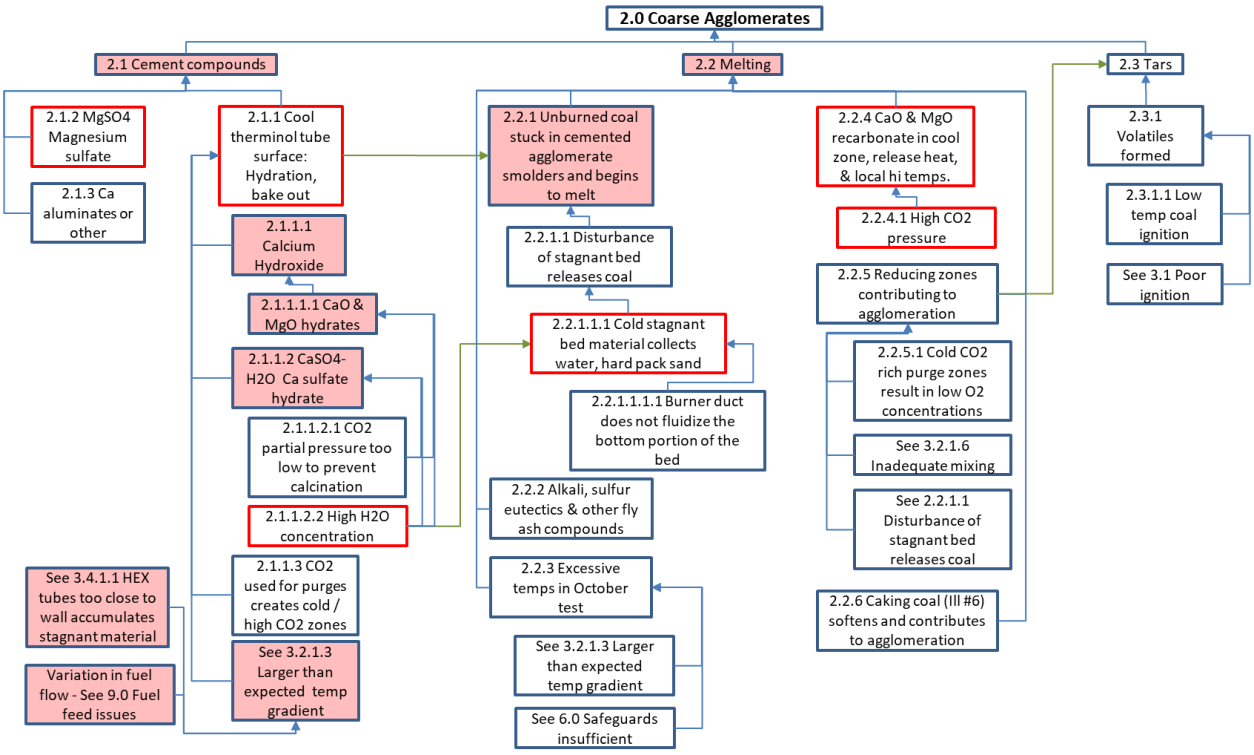

Figure 5.7-6: Problem statement 2 fault tree.

Table 5.7-4: Problem statement 2 knowledge chart.

Fault tree ID	Fault tree title	Specific Data Item	Data quality
Agglomeration formation			
1.0, 2.0	Smooth & Coarse agglomerates	Are coarse and wedge shaped agglomerates independent of each other?	0
1.0, 2.0	Smooth & Coarse agglomerates	Some wedge agglomerates found stuck inside coarse agglomerates	0
1.0, 2.0	Smooth & Coarse agglomerates	So far, no coarse agglomerates found inside of wedge agglomerates	1
1.0, 2.0	Smooth & Coarse agglomerates	Most wedge agglomerates are not stuck to coarse agglomerates	1
1.0, 2.0	Smooth & Coarse agglomerates	Agglomerates found above first two cooled tubes, up to row 9	1
1.0, 2.0	Smooth & Coarse agglomerates	Locations of agglomerates not known yet for October tests	1
2.0,	Coarse agglomerates	Coarse agglomerates irregular in shape	1
2.0,	Coarse agglomerates	Unknown what starts coarse agglomeration	0
2.1	Cement compounds	Cements form due to t, pp changes?	0
1.1.1.2, 2.1.1.1	Ca(OH)2	Ca(OH)2 in agglomerates	1
1.1.2, 2.1.1.1	xxx, Calcium hydroxide	Agglomerates caused by overcooled zones	0
2.1.1.2	CaSO4-H2O	Unknown if hydrates of CaSO4 were previously present	-1
1.1.1.3, 2.1.2	MgSO4	MgSO4 in agglomerates	0
2.2	Melting	Coarse agglomerates appear to contain melt material	0
2.2	Melting	Agglomerates in middle center bed contained some coal which was subsquently released, causing sintering and high temps. This appears to be when coarse agglomerates grew larger and formed some slag.	0
2.2.1.1	Disturbance of stagnant bed releases coal	Coal gets stuck in lower bed and later comes out to burn, if there is enough oxygen.	1
2.2.1.1	Disturbance of stagnant bed releases coal	In July, there were three separate incidents showing high DP across tuyeres.	1
2.2.1.1	Disturbance of stagnant bed releases coal	In October high DP across tuyeres was seen without a shutdown or olivine injection prior to the behavior	1
2.2.1.1	Disturbance of stagnant bed releases coal	Two of the July events ended with a breakup of some blockage and a resulting high temperature excursion.	1
2.2.1.1.1	Cold stagnant bed material collects water	Under certain circumstances, reducing blower speed to bring bed into the fuel injector region does not result in effective area decrease (after many hours of operation) which suggests that when all material is hot, it doesn't plug tuyeres, also suggesting that plugging is related to cold temperatures.	0
2.2.1.1.1	Cold stagnant bed material collects water	Water may be condensing in the bed sand at the bottom, holding it together in a tighter mass	0
2.2.5	Reducing zones contribute to agglomeration	Partially reducing environments may exist	0
2.2.6	Caking coal (IL No.6) softens and may contribute to agglomeration	Caking coal (IL No.6) softens and may contribute to agglomeration	0

Table 5.7-5: Illinois Lab X-Ray Diffraction (XRD) Results

Compound Found	172515-002 Oxy-PFBC July 27 2017 Test Agglomerate Granular
Anhydrite ($CaSO_4$)	~35
Calcite ($CaCO_3$)	~60
Quartz (SiO_2)	~2
Dolomite ($Ca(Mg)CO_3$)	~2

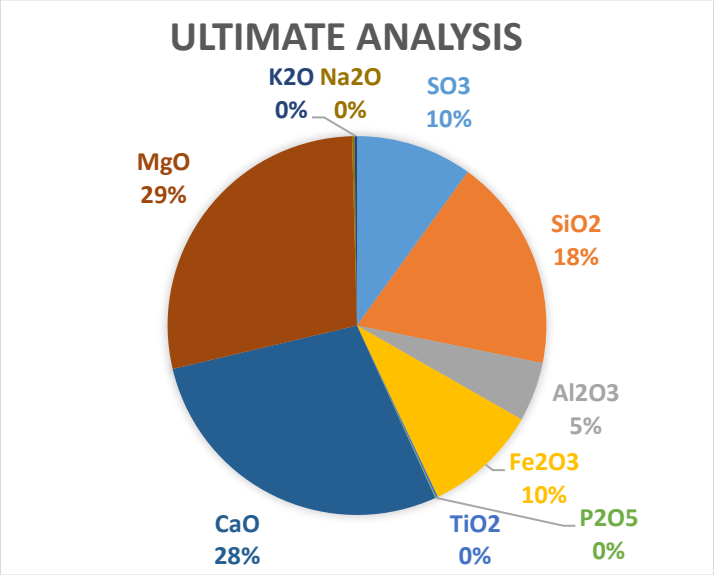

Figure 5.7-7: Illinois Lab X-Ray Diffraction (XRD) Results

Table 5.7-6: Canmet Lab Results

Chemical compound		% Chemical Compound
Calcium Carbonate	Ca(CO3)	13.4
Anhydrite	Ca(SO4)	56.6
Periclase, syn	MgO	22.2
Hematite, syn	Fe2O3	0.6
Quartz, syn	SiO2	1.4
Crystallinity (%)		94.2
Amorphous (%)		5.8

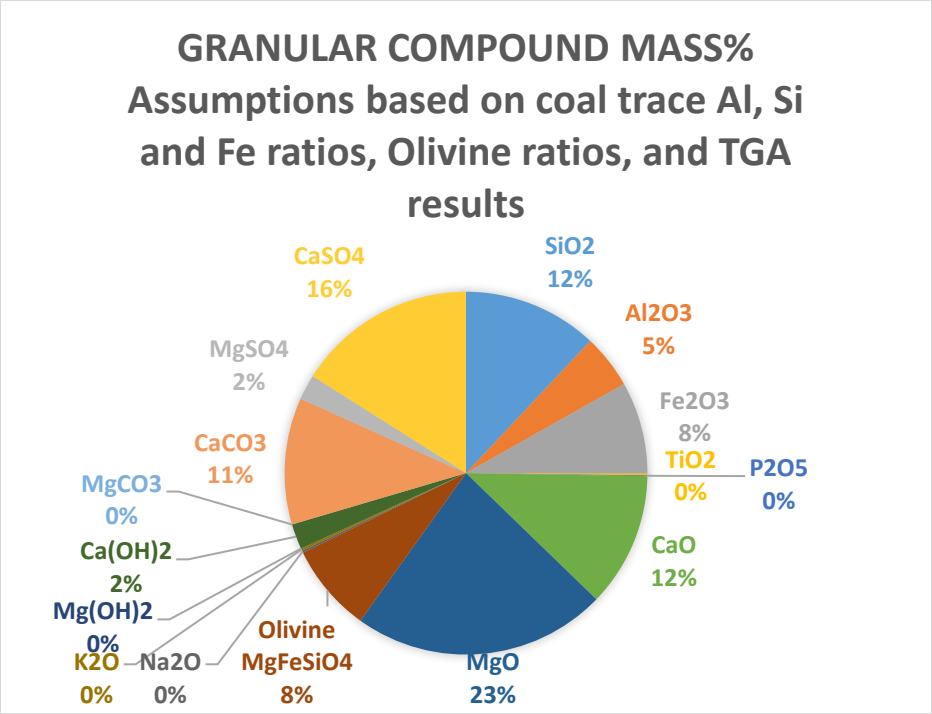

Figure 5.7-8: Canmet Lab Results

In summary, the coarse agglomerates cause was somewhat ambiguous, as these appeared to have at least two or three causes. First is the overly tight tube packing, in particular the distance from tubes to the wall of the reactor, which prevented sand particles from moving. These stagnant areas were able to cement together in some places due to cementing (cause 1), and also were able to contain unburned coal, which could smolder and cause locally high temperatures, causing sintering or local melting (cause 2). A third proposed cause was a melt reaction which was observed in other pressurized combustors in the past in which both oxidizing and reducing zones could switch the valence of Sulfur in Calcium Sulfite/Calcium Sulfate and produce liquid CaO. Since there were multiple causes proposed, the appropriate mitigation will include adjustments to the test sequence to isolate the three possible causes.

Problem statement 3: Freeboard burning In October test, PFBC with natural gas burner off (oxy-combustion mode) promotes freeboard burning, and cannot maintain high temps near fuel injector. Burning occurs in upper section of bed and in the freeboard.

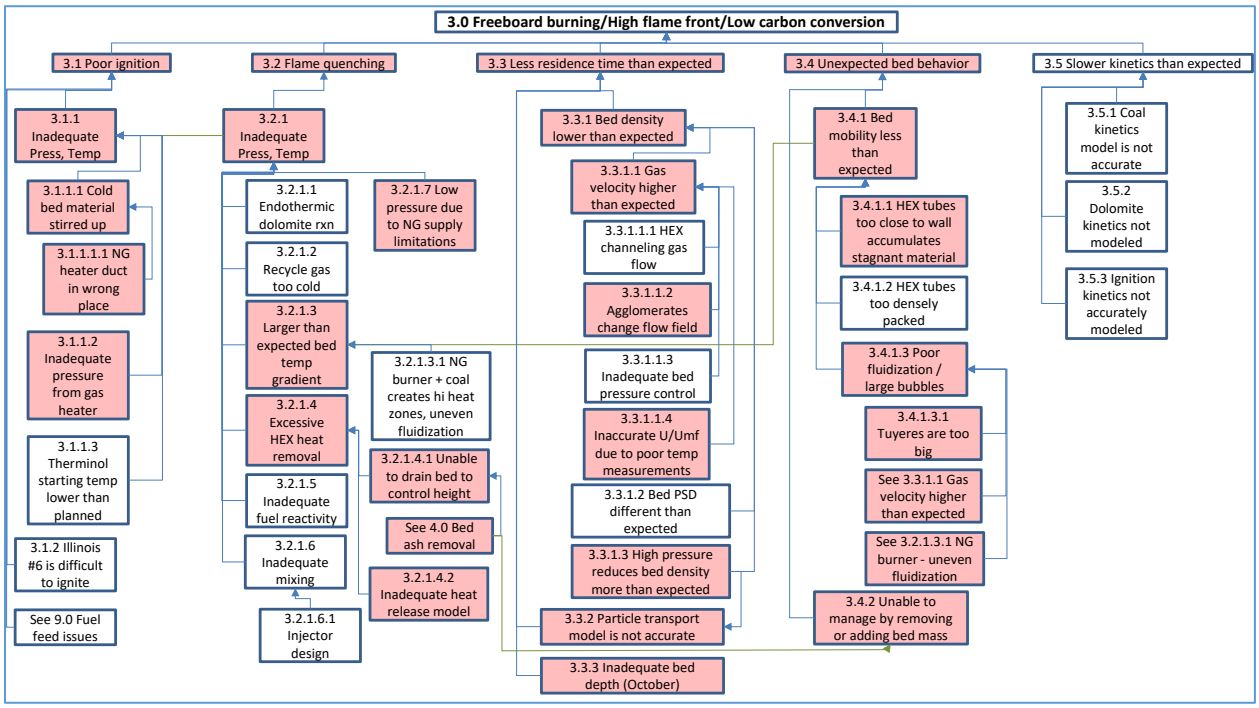

Figure 5.7-9: Problem statement 3 fault tree.

Table 5.7-7: Problem statement 3 knowledge chart.

Fault tree ID	Fault tree title	Specific Data Item	Data quality
Bed mobility / behavior			
3.1.1.1.1, 3.2.1.3.1	NG heater duct in wrong place; NG burner + coal creates hi heat zones, uneven fluidization	Burner duct is altering the bed solid distribution and bubble dynamics	1
3.2.1.3	Larger than expected temp gradient	TC's which are not near tubes show wider variation than a fluidized bed "should" exhibit.	0
3.2.1.3.1	NG burner + coal creates hi heat zones, uneven fluidization	Bed density near injector appears to be worse when burner is on, suggests burner bubble prevents particles from moving down.	0
3.3.1	Bed density less than expected	Bed density is lower than expected, lower than cold flow test rig	1
3.3.1.1.2	Agglomerates change flow field	Agglomerates have altered the flow dynamics, bed lifting up higher	1
3.3.1.1.2	Agglomerates change flow field	7/26 morning start shows a second incident of partial blockage, which also partly clears	1
3.3.1.1.2	Agglomerates change flow field	It is possible that chunks form in the region of the lower bed and are thrown up into the IHX area, where they grow	0
3.3.1.1.2	Agglomerates change flow field	7/25 is the earliest evidence of the IHX tubes acting as a classifier, pushing material up and allowing lower bed to empty	0
3.3.1.1.2	Agglomerates change flow field	During normal bed operation, classification/segregation of material gradually worsens over a period of many hours, even in the best conditions.	1
3.4	Unexpected bed behavior	In tests prior to agglomeration, the bed does not consistently act as designed.	1
3.4.1.1, 1.2.2	HEX tubes too close to wall	Bed material not flowing down due to plugging between tube and wall	0
3.4.1.1, 1.2.2	HEX tubes too close to wall	Tubes were built closer to the wall than intended.	0
3.4.1.2	HEX tubes too densely packed	Is in-bed hex too dense? Need to understand bed mobility/heat transport as designed.	-1
3.1.4.3	Poor fluidization / large bubbles	DPT3102 is an early indicator of bed fluidization control, bubbling stability	0
3.4.1.3.1	Tuyeres are too big	Tuyeres are causing larger bubbles than expected	0

Fault tree ID	Fault tree title	Specific Data Item	Data quality
3.0,	Low carbon conversion	First test in July has very poor performance, as low as 20-40% to start	0
3.0,	Freeboard burning/high flame front	In tests prior to agglomeration, we do not get burning as expected (C conversion)	0
3.1.1.1	Cold bed material stirred up	Recycle blower stirs up cold bed material and quenching burning	1
3.1.1.2	Inadequate pressure from gas heater	Warm up is being conducted at half the pressure targeted for PFBC operation	1
3.1.2	Illinois #6 difficult to ignite	Illinois #6 is more difficult to ignite than other coals	1
3.2.1.1	Endothermic dolomite rxn	Dolomite thermodynamics not included in models	1
3.2.1.4	Excessive HEX heat removal	Too much cooling near the fuel injector	0
3.2.1.4	Excessive HEX heat removal	Two therminol rows near fuel injector are overcooling bed, prevents or quenches devolatization.	0
3.2.1.4.2	Inadequate heat release model	Coal devol / ignition kinetics modelling is not accurate	0
3.2.1.6	Inadequate mixing	Not enough oxygen near fuel	0
3.3	Less residence time than expected	fine coal does/does not have the residence time predicted	1
3.3.1	Bed density less than expected	Fine coal char burning will/won't be improved with denser bed. Fuel holdup parameter for 1-D PFBC code analysis assumes 700 kg/m3 bed versus 350 kg/m3 actual.	0
3.3.1.3	Elevated pressure reduces bed density more than expected	Bed density during combustion is roughly 350 kg/m3 (but highly variable) compared to assumed density of 700 kg/m3 based on Cold Flow Rig data and CFD analysis at pressure.	1
3.3.1.2	Bed PSD different than expected	Dolomite changes size after heating in furnace in Canmet furnace tests	0

Fault tree ID	Fault tree title	Specific Data Item	Data quality
3.3.1.1.3	Inadequate bed pressure control	Only 3 operator stations. Data accessibility is compromised (must interrupt operator to access raw data).	1
3.3.1.1.3	Inadequate bed pressure control	24 possible control screens, 30 data screens, only 8 screens available.	1
3.3.1.1.3	Inadequate bed pressure control	Recycle flowmeter is too large for rated duty.	1
3.3.1.1.3	Inadequate bed pressure control	Filter DP is significant enough to alter flow through blower after cleaning. If not corrected in time, filter pulsing can result in 15-35% flow change and 25 minutes of disruption or more.	1
3.3.1.1.3	Inadequate bed pressure control	Procedures need to be clearer to avoid confusion	1
3.3.1.1.3	Inadequate bed pressure control	Uncontrolled mass flows and recycle flow are making the burning problems worse.	1
3.3.1.1.4	Inaccurate U/Umf	Test U/Umf calculation is based on average temp in bottom of combustor (multiple thermocouples against wall that are buried by stagnant bed material and instrumented tube thermocouples in core of flow). Only instrumented tube is accurate. Using instrumented tube data results in U/Umf and bed densities that are in line with cold flow data.	1
3.3.2	Particle transport model is not accurate	Coal transport might be incorrectly modeled	0
3.3.3	Inadequate bed depth (October)	Bed depth reduced in October due to concerns of overcooling the bed as happened in July. Post test analysis indicated that high gas velocity and inadequate bed depth both contributed to inadequate residence time for burning in the bed	1

The causes for freeboard burning are multiple:

The primary cause of freeboard burning, and the resulting damage to the combustor, was that multiple wall temperature sensors were insulated by bed material that was resting on heat exchanger tubes near the walls (see Figure 5.7-10). The chain of events start with insulated temperature sensors which read 200-400°C lower than actual temperatures based on temperature readings during the test compared to the interior combustor temperatures deduced by observation of component materials that melted. The average temperature from all sensors was used to compute the average combustor gas density and gas flow velocity. As a result, real time gas velocity calculations were erroneous and showed lower velocity than reality. The tests were run with higher gas flow velocities than intended, leading to lower bed density, reduced fuel residence time and lower carbon conversion. The high gas velocities continued to push the burning zone into the upper portion of the combustor and made it difficult for the flame front to move lower. (Figure 5.7-11) Core temperature readings (near the bottom of the combustor) were low since there was no burning there, further contributing to the calculation that showed low combustor

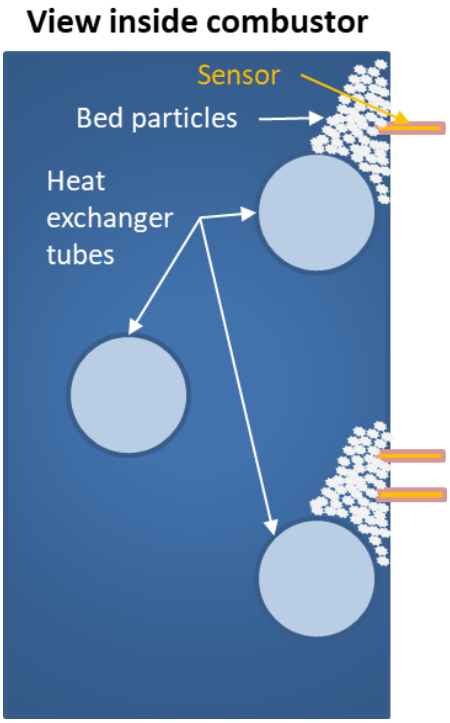

Figure 5.7-10. Bed particles rest on heat exchanger tubes and near the wall and insulate temperature sensors

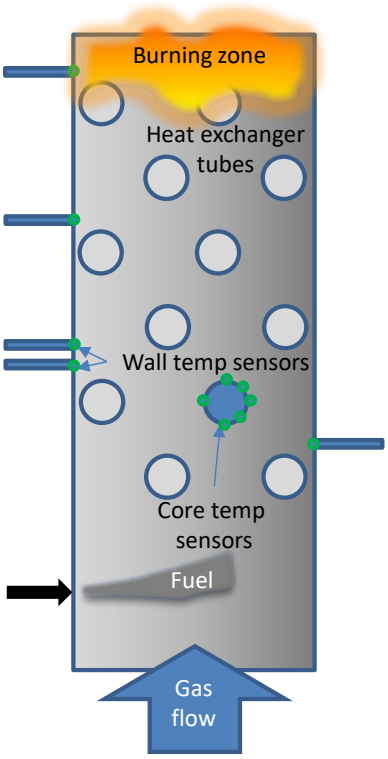

Figure 5.7-11. Low temperature readings led to higher than realized gas velocities and burning above the bed.

Note: Figures are for illustrative purposes only. They are not to scale and do not the show actual combustor internal configuration.

temperatures despite robust burning at the top of the combustor (where there were few sensors). Bed density measurements identified significantly lower bed density than expected and also identified a large void at the bottom of the combustor. The bed density and void was consistent with cold flow test data at U/Umf velocities of 4.5 to 5. The intended velocity in the hot fire test was 3-3.5. This data verified the hypothesis that the gas velocity in the hot fire test was significantly higher than realized during testing and was due to erroneous temperature measurements.

Low pressure NG system causes long periods of lower pressure/high velocity operation during startup. This increases the bed velocity to almost double the design velocity. Pressure control and recycle flow control have significant lag times, and this is extended due to manual operation. As a result, significant pressure swings were possible and happened, leading to uncontrolled bed velocity.

Lower than expected bed density and density distribution is not even vs. height or width, and this is consistent with channeling flow due to tubes being too close to the wall, allowing particles to block the gas flow near the wall. Borescope inspection shows agglomerates were concentrated on edges of bed.

Lab tests indicate that over time, the bed particle size was changing because no additional coarse bed material was being added in the solids feed systems.

Problem statement 4: Bed ash system not removing material Bed ash removal system is not removing material. Pipe was installed which was presumed to allow coarser material to collect elsewhere so smaller particles exit the bottom.

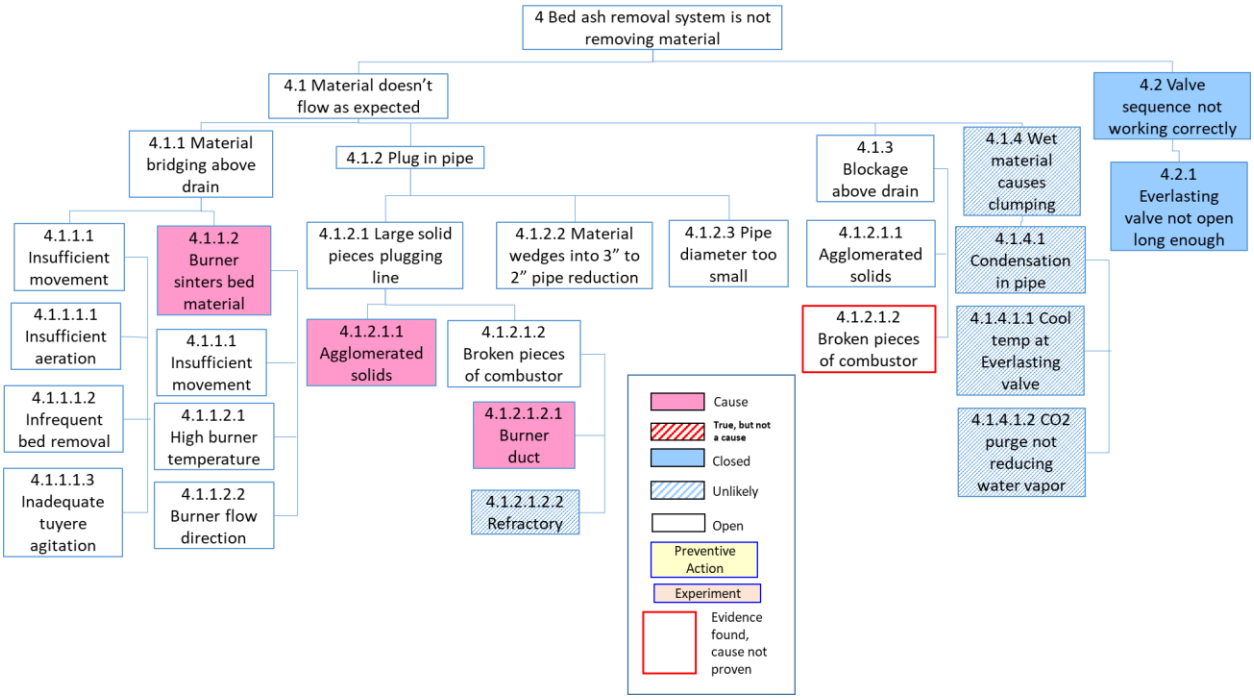

Figure 5.7-12: Problem statement 4 fault tree.

Table 5.7-8: Problem statement 4 knowledge chart.

Fault tree ID	Fault tree title	Specific Data Item	Data quality
Bed drain issues			
4.1.2.1.1	Agglomerated solids	Agglomerates prevented removal of bed material sample in 7/27 test	1
4.1.2.1.1	Agglomerated solids	Bed drain did not work in July due to agglomerates	0
4.1.2.1.2	Broken pieces of combustor	Bed drain did not work in May due to metal from combustor	1
4.1.1.2	Burner sinters bed material	Burner operation with still bed results in packed lower bed that is stuck together for hours, affecting tuyere flow. Does not require dolomite to cause this.	1
		April bed drain worked	1

In summary, the bed ash system appeared to be plugged by large agglomerates and pieces of sheet metal, and the bed burner issue was also implicated in sintering bed material, creating blockages in the lower reactor. The solutions will be to operate the bed burner close to the target system temperatures (i.e. full recycle and full pressure) and to integrate the burner flow with the recycle flow so there are not temperature striations within the lower bed.

Key insights include: The system worked during cold tests and warmup only tests but would not drop material during first coal tests.

Significant agglomerates were found in non-working cases, with evidence of local sintering.

Problem statement 5: Unburned coal ignites on fly ash filters Unburned coal burned on the filter in the July test. This was partially addressed procedurally with filter cleaning before introducing air at end of test, will also be addressed by low carbon conversion above. No additional filter fires occurred after new procedures were implemented.

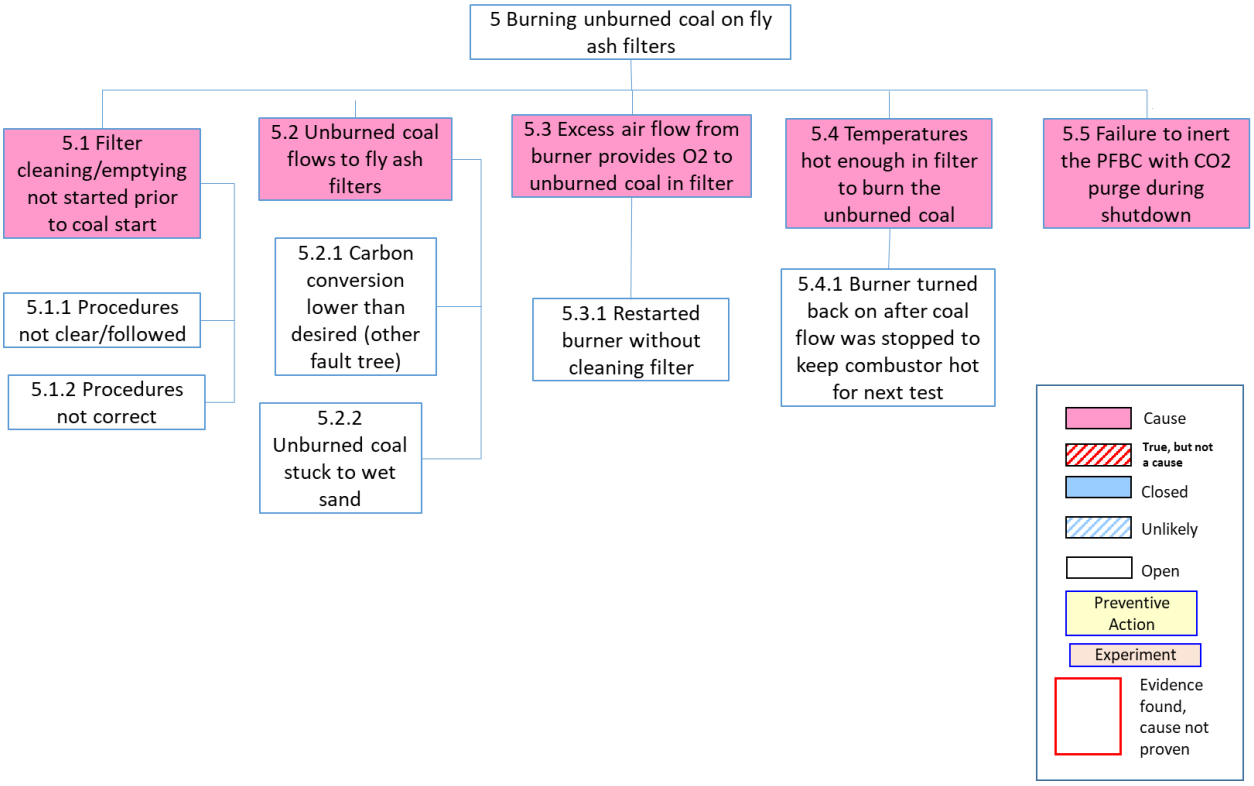

Figure 5.7-13: Problem statement 5 fault tree.

Table 5.7-9: Problem statement 5 knowledge chart.

Fault tree ID	Fault tree title	Specific Data Item	Data quality
Bed drain issues			
5.1.1	Filter fire	Filter cleaning system was not started prior to initiating coal in March, April or July 25.	1
5.2	Filter fire	Significant unburned carbon left the bed and deposited on filter	1
5.3	Burner restart	Burner operation initiated without cleaning filter or dumping fly ash vessel.	1
5.1	Resolution of filter fire issue	Numerous restarts in October following correct procedure did not produce a filter fire.	1

In summary, the cause of the filter damage was inattention to procedures, which specified cleaning the filters prior to introduction of coal, and continuation of cleaning prior to re-introduction of air, oxygen or coal. An air purge was initiated to prepare for burner restart after a shutdown, but the filter cleaning cycle had not been started, as directed by the procedure. Shift change between warm-up and re-start is a possible contributing cause.

Problem statement 6: Safeguards were insufficient to prevent catastrophic damage

Safeguards/Alarms/Procedures are insufficient to prevent catastrophic slagging and HEX melting in combustor.

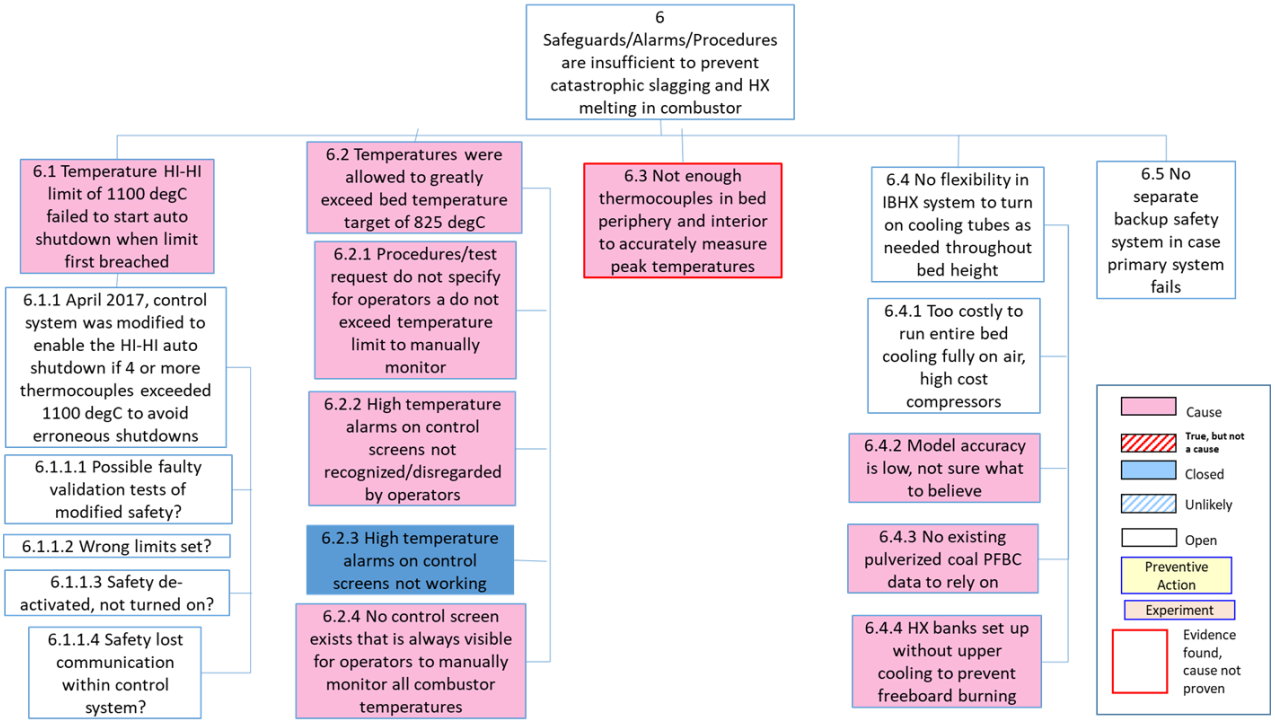

Figure 5.7-14: Problem statement 6 fault tree.

Table 5.7-10: Problem statement 6 knowledge chart.

Fault tree ID	Fault tree title	Specific Data Item	Data quality
6.1	Temperature HI-HI limit of 1100 degC failed to start auto shutdown when limit first breached	Autoshutdown did not work despite exceeding temp limits in combustor. Were requested temps (1000C) programmed in? Yes.	1
6.1	Temperature HI-HI limit of 1100 degC failed to start auto shutdown when limit first breached	Was the right voting/averaging calculation programmed in correctly? Actual voting requires 4 TC's, maybe should reduce.	1
6.3	Not enough thermocouples in bed interior to accurately measure peak temperatures	Some TC's are too close to cooled tubes to give good bed temp.	0
6.2.1	Not clear what is appropriate action to take	Only 3 operator stations. Data accessibility is compromised. (must interrupt operator to access raw data)	1
6.2.4	Data hard to see.	24 possible control screens, 30 data screens, only 8 screens available	1
6.2.2	Alarms disregarded.	Operators distracted by other concerns. High pressure to obtain data for proposal. Unsure what to do when things deviate from prediction.	1
6.2.1, 6.2.2	Not clear what is appropriate action to take.	No thorough formal data review between coal starts.	1
6.4	Manual control of HX banks (air cooled portion)	Tubes turned on or off based on observation. Sometimes goes unnoticed.	1
6.4.4	No HX to cool flue gas before freeboard	HX set up for October run eliminated top of bed cooling (inappropriate decision to deal with bed density issue, inaccurate model used as a guide).	1

In summary, there are several contributing causes to the insufficient safeguards.

There are 4 separate systems: Linde, Canmet, fuel mixing, and fuel/sorbent injection with separate control stations. The filter and heat trace system also have separate digital control stations which must be periodically attended to.

There is a large quantity of data spread over more screens than 5 people can reasonably watch.

Essential functions are in 6 different locations on two floors.

Predictions have not matched the observed behavior (DP, Temps, char burnout, bed expansion).

It is difficult to formulate a plan which covers unexpected results.

Actual temperatures were at least 200 C hotter than any measured temperature.

Indications of combustion gas leaking into air vent manifold (from air cooled tubes) recorded but not alarmed, not discovered until weeks later.

Too many (4) HIHI temps are required in control implementation to cause a shutdown.

Problem statement 7: Flame detection was intermittent Startup heater flame detection was intermittent on October 26.

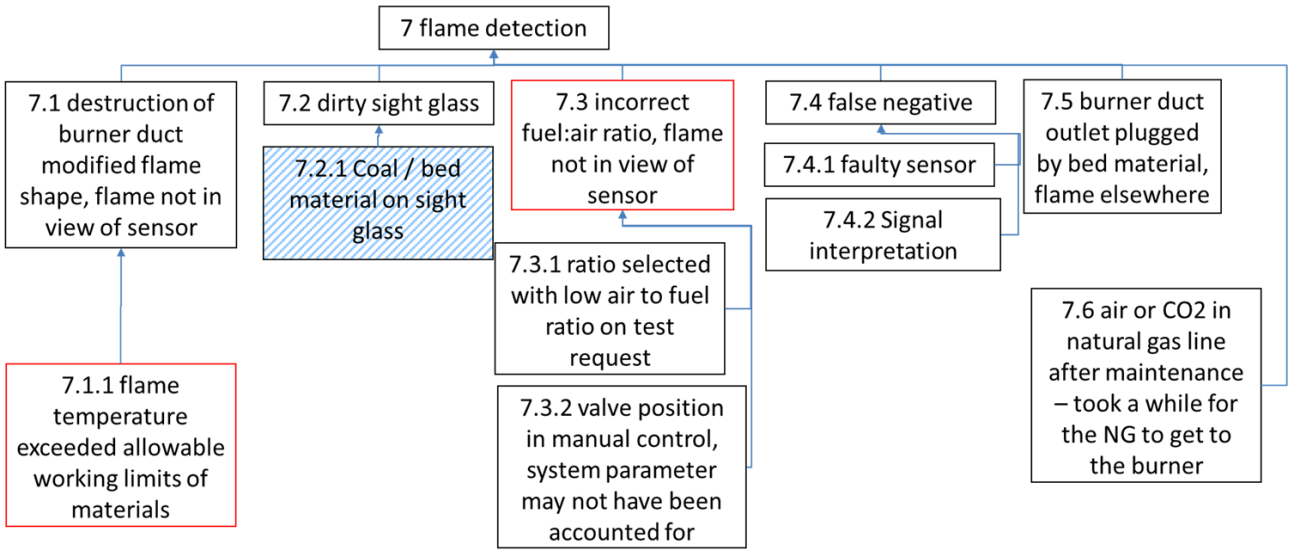

Figure 5.7-15: Problem statement 7 fault tree.

Table 5.7-11: Problem statement 7 knowledge chart.

Fault tree ID	Fault tree title			Specific Data Item	Data quality
7.1	destruction of burner duct modified flame shape, flame not in view of sensor	flame sensor	1	Changes in flame position can cause flame sensors to fail to detect that a flame is present, based on past experience with flames that we can see and all other systems ok	
7.1.1	flame temperature exceeded allowable working limits of materials		1	Adiabatic flame temperature sometimes out of allowable range - actual flame temperature not known	
7.2	dirty sight glass	none avail	0	Combustors much easier to diagnose when there is optical access to the flame to see position and colour	
7.2.1	coal / bed material on sight glass	none avail	0	50 kW oxy-FBC has sight glass at duct elbow with otherwise same geometry - stayed clean for 25+ operations with bed material only as high as top of duct at injection point to bed. Unlikely to be the cause.	
7.3	incorrect fuel:air ratio	natural gas flow, burner air flow, pressure of combustor	-1	low air:fuel ratios can cause soot formation. Incorrect air:fuel ratio can cause light off failure. Need to know flows, pressures at time of failed ignitions. Compare with successful ignitions.	
7.3.1	ratio selected with low air to fuel ratio on test request	natural gas flow, burner air flow, pressure of combustor	-1	Can the burner ignite at the full range of allowed air:fuel ratios? Can't test now...	
7.3.2	valve positions in manual control, parameter may not have been accounted for	natural gas flow, burner air flow, pressure of combustor	1	Burner mass flow rates controlled manually by operators - valve positions set to spec'd position. Need to know if there was a difference in the other burner system parameters.	
7.4	Faulty sensor	flame sensor	-1		
7.5	burner duct outlet plugged, flame elsewhere	none avail	0	bed material sintering is sometimes seen at the outlet of the 50 kW oxy-FBC burner duct	
7.6	air or CO2 in NG line after maintenance - took a while for the NG to get to the burner.		-1	Was the burner purged for maintenance? How long does it take for the NG line to fill with NG after maintenance? Is a method in place for ensuring the line is filled with NG?	

Summary:

Flame detection DID work dependably for all previous tests. Temperatures were too high for UV/IR detectors electronics to function as currently installed. Replacement of sensor (and spark plug) was not possible without teardown. Preventative maintenance difficult. Alternate methods of detection are recommended.

Problem statement 8: Fuel blending mass flow variability Solid Fuel blending system does not have steady flow or steady mix. (Dolomite is found to have wide variation in PSD.)

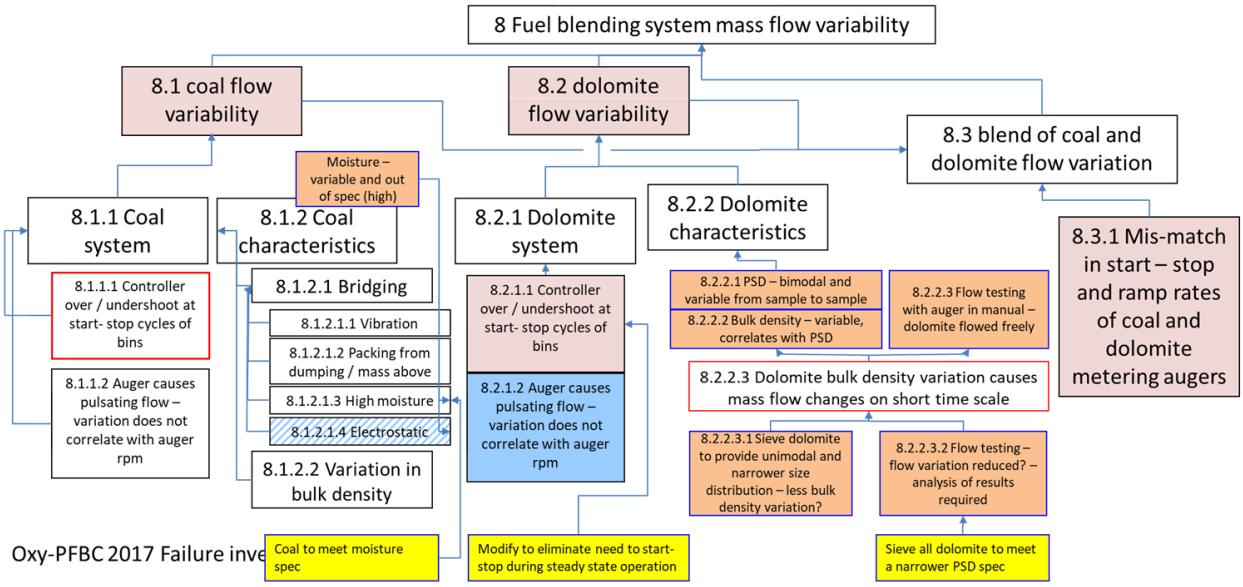

Figure 5.7-16: Problem statement 8 fault tree.

Table 5.7-12: Problem statement 8 knowledge chart.

Fault tree ID	Fault Tree Title	Specific data item	Data quality	How K,N,O,T
8	Fuel blending system mass flow variability		0	
8.1	coal flow variability	loss in weight feeder signal	1	measured coal flow rate changes from set point
8.1.1	coal system variability	loss in weight feeder signal	1	K - coal flow is variable
8.1.1.1	controller over / undershoot at start-stop cycles of bins	loss in weight feeder signal	1	K - Manual testing of dolomite system - local controller consistantly over / under shooting at start - stop. N - to know if this is also happening for the coal system O - System designed to go through periods without mass flow signal due to need to fill hopper, not likely to be able to avoid under/overshoot.
8.1.1.2	Auger causes pulsating flow	Auger speed, weight signal	0	N - correlation visible between flow rate and auger rotation - there should be some, but is it of an important amplitude?
8.1.2	Coal characteristics		0	
8.1.2.1	Bridging followed by bridge collapse		1	K - Coal can bridge large gaps (> 4") given suitable conditions K - agitators commonly used to alleviate bridging issues / powder bulk density variability N - is the agitator running in the coal supply? Speed? Working?
8.1.2.1.1	Vibration causing packing		1	K - level sensors are vibratory, vibration in plant. Vibration causes densification which can make bridging worse.
8.1.2.1.2	Packing from dumping / mass from above		0	
8.1.2.1.3	High moisture		1	K - moisture analysis indicates higher moisture content ~6 - 7 wt% than Canmet would normally use for Illinois #6 conveying in small diameter tubing. More commonly use 4 to 5 wt%.
8.1.2.1.4	Electrostatic		0	O -Moisture is high, so electrostatic issues unlikely. Could be cause in future if coal much drier (suface moisture < 0.5 wt% based on journal publication)
8.1.2.2	Variation in bulk density		0	K - minimal variation in PSD of coal O - bulk density variation not caused by differences in PSD K - bulk density varies substantially with vibration, packing, settling time
8	Dolomite flow variability	loss in weight feeder signal	1	K - dolomite flow is variable
8.2.1	controller over / undershoot at start-stop cycles of bins	loss in weight feeder signal	1	K - Manual testing of dolomite system - local controller consistantly over / under shooting at start - stop. N - to know if this is also happening for the coal system O - System designed to go through periods without mass flow signal due to need to fill hopper, not likely to be able to avoid under/overshoot.
8.2.2	Auger causes pulsating flow	Auger speed, weight signal	0	N - correlation visible between flow rate and auger rotation - there should be some, but is it of an important amplitude?

In summary:

Coal mass flow variability can result in variations in fuel/oxygen mixture ratio which can potentially contribute to agglomeration, or chemically reducing zones which cause corrosion.

The moisture content of coal is higher than desired for reliable flow control.

Agitator in hopper feeding blender is not optimized for coal (minimizing bulk density variation).

Can't collect data in manual mode—unable to troubleshoot or sufficiently test system.

Dolomite bulk density is not uniform, reasonable to predict flow change vs time (need to analyze).

Startup variation cannot be programmed out without more sophisticated level sensing. (now operated on/off to HI sensor)

The recommended course of action for this pilot system is to separate fuel and sorbent systems and eliminate the blending, which would reduce uncertainty by large measure.

Problem statement 9: Fuel plugging and erosion Solid Fuel pneumatic injection system is prone to plugging and erosion. (Partial fix in Aug: smaller orifice, lower velocity.)

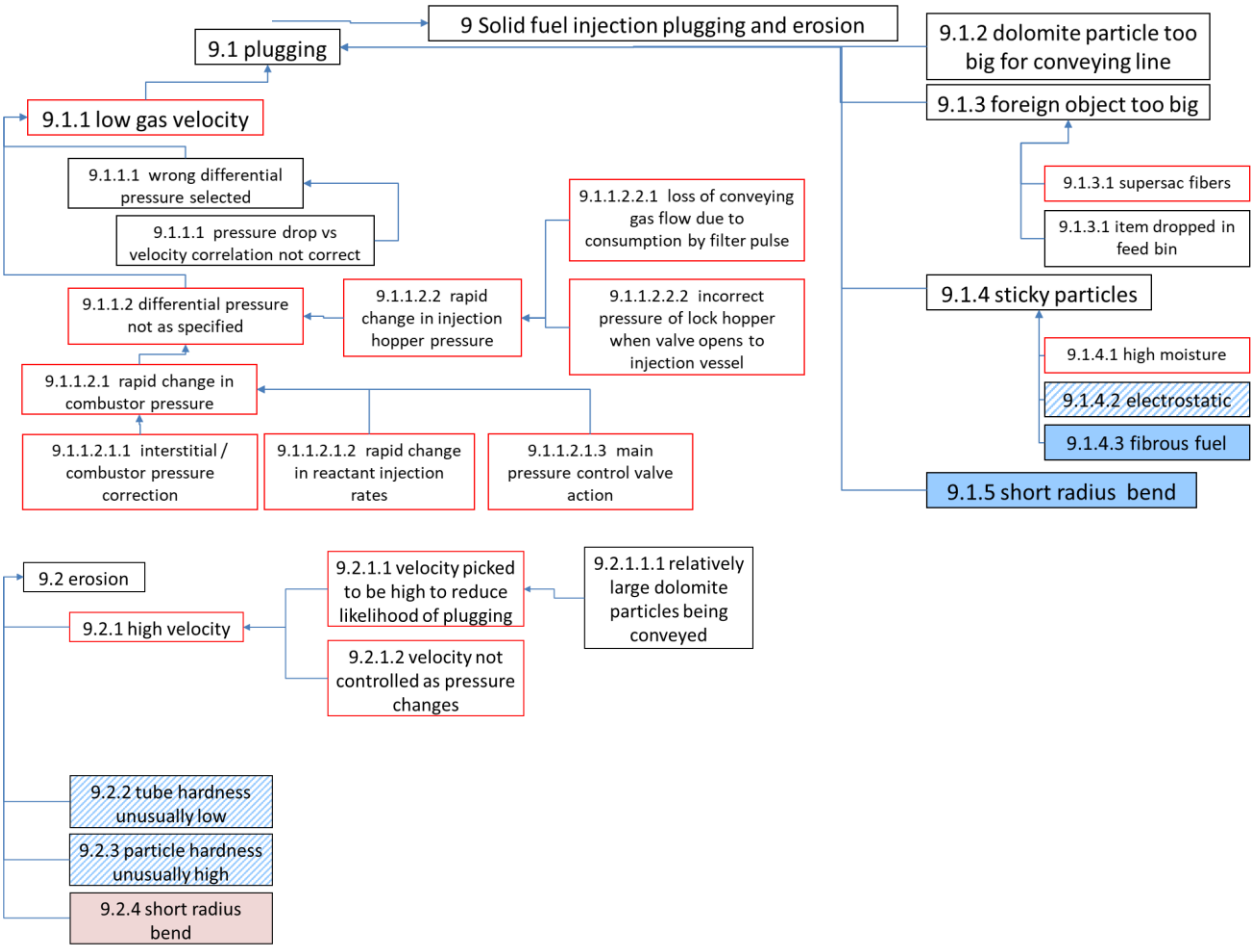

Figure 5.7-17: Problem statement 9 fault tree.

During testing, there were multiple times where fuel flow stopped due to plugging in the fuel feed system. In addition, there were multiple times when erosion in the coal feed line led to failure of the feed system to deliver fuel to the combustor.

In summary, there were significant pressure oscillations from multiple sources (lockhopper cycle, filter pulses, PFBC backpressure, interstitial pressure control valve), the DP from injector to PFBC too low at times (incorrect limits), there is no surge capacity in the piping, and the filter pulses were not coordinated (and can't be).

Suspected density variation of material (see problem statement 8 above) is exacerbated by not having screens in the blender supply hoppers.

In addition to these sources of variation, there were high velocities in the tubing due to low pressure startup, and higher velocity recommended to move large dolomite particles, which are harder and have more erosive impact.

The solution for problem 8 to separate the systems will go a long way to fixing the problem. Some additional changes to the programming and volume of gas supply will also reduce uncertainty in the fuel flow. Erosive forces in the feed line can be reduced by increasing the facility natural gas pressure which will allow the Oxy-PFBC to start at higher pressure, thus reducing pressure drop and velocity in the solids feed line.

Problem statement 10: Fly ash removal system intermittent Fly Ash Everlasting valves are intermittent. Ball valves work well but are slow. Multiple programming issues with filter and fly ash cleaning system.

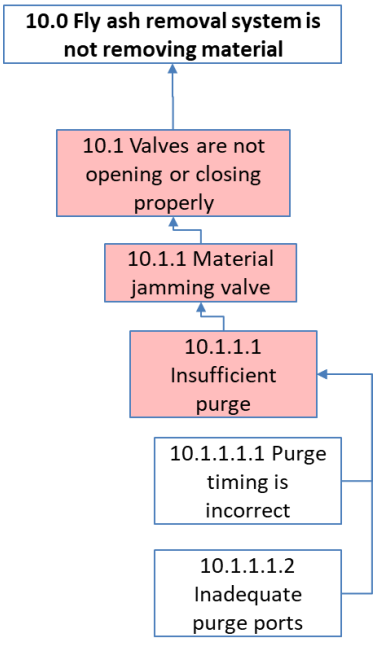

In summary, the purge programming has to be corrected to activate every time valve opens or closes.

The team must consider purge port modification prior to next start.

Figure 5.7-18: Problem statement 10 fault tree.

Problem statement 11 (Low carbon conversion) was combined with 3. In July Carbon conversion is only 85-87%.

Problem statement 12: Blower vibration above 80% Blower vibrates unacceptably at speeds higher than 80%, causing seal failure.

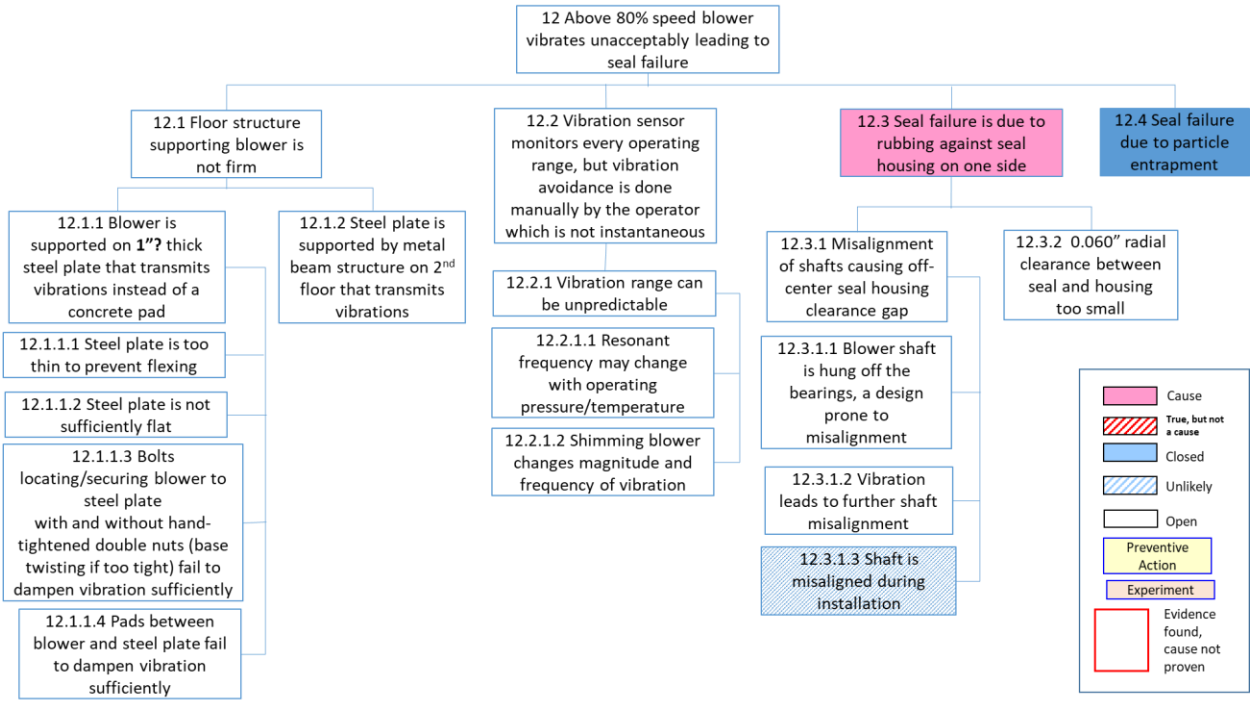

Figure 5.7-19: Problem statement 12 fault tree.

Table 5.7-13: Problem statement 12 knowledge chart.

Fault tree ID	Fault tree title	Specific Data Item	Data quality
12.1	Damage occurred during flow tests.	Blower seal broken twice: August and September	1
12.2	Data confirmation/avoidance	Vibration monitors confirm that vibration is unacceptable over 80%	1
12.3	Support structure	Sometimes shimming the motor/blower structure removed the vibration, allowing operation between 80-100%	1
12.2	Fabrication	Blower did not have excessive vibration during setup at manufacturer	1
12.5	Harmonic level	Blower harmonics are 40% and 80%	
12.4	Floor is vibrating at blower harmonic	Blower is on 2nd floor with structural steel support. I-beams do not directly transfer loads to the 1st floor.	1

In summary, although a range of operation was found for the system as built, there were no viable options for correcting vibrations once they started, except for a complete shutdown. Therefore, moving the blower to the first floor with a firm concrete base was selected as the most viable long term option.

5.7.4 Historical design data

A review of public and proprietary literature which became available to the GTI team found that there were useful design data from several fluidized bed combustors with internal heat exchangers which became invaluable in developing mitigations for these problems and their causes. The descriptions of these combustors and the experiments which provided particularly useful data are shown in Table 5.7-14 below.

These designs had relevance to multiple problem statements, which should be obvious from the evidence already presented in section 5.7.3 with timeline data and cause trees, and will become even more clear in 5.7.5 where the RCA conclusions are described and corrective actions prescribed. The primary areas of interest are the fuel injectors, heat exchanger design, and startup burner design.

Table 5.7-14: Historical FBC's and experiments of interest to the Oxy-PFBC

Name	General Description	Interesting experiments
Pressurized:		
Leatherhead	~1-3 foot scale went through at least six different design iterations. I, III and VI have the most published data. Some were dry feed, others paste. Many tests with Ohio coal and dolomite.	Found that IBHX can prevent particle mobility and increase bed temperature gradient even if tubes are uncooled. More open bed provides more constant bed temp.
Grimethorpe	2 meter square, tests at 8, 10, 12 bar with 3 different heat exchanger designs. Dry feed, also used Ohio feedstocks.	As with Leatherhead, found that dense heat exchanger depressed bed temp and reduced carbon conversion. ¼" top size coal. Finned tubes at bottom to reduce erosion.
NYU	~30 inch round FBC with small in bed HX. Dry gravity feed coal underbed. Startup burners were below the grid.	Tested horizontal and vertical HEX tubes.
Non-pressurized:		
Rockwell "Air Heater Experiment"	Atmospheric combustor with air used as IBHX working fluid.	Multiple iterations of fuel injectors gives good basis for fuel distribution and oxygen partial pressure results across bed.

The information presented below is arranged by component, to make it easier to compare the oxy-PFBC design to the various historical combustor solutions.

A. Burner
    a. Multiple test rigs were operated with burners similar to that used in the PFBC pilot without notable problems in the reports (Leatherhead, Rockwell). It is unclear why a similar design was insufficient for the PFBC pilot, but better integration with the bed air injection grid is a likely problem, due to asymmetric flow, so the best course of action will be to integrate the PFBC recycle flow with the burner flow prior to grid injection.
B. Gas Grid
    a. The number of holes per square foot is considerably less than the range of grid orifices in any of the historical pilot plants, so the PFBC pilot will increase the number of holes by a factor of 8 and design the grid to be a minimum of 30% of the bed pressure drop.
C. Fuel Injector
    a. The fuel injector design is similar to some of the Leatherhead and other commercial air-fired coal plants, but backup injectors similar to the Rockwell plant have been fabricated and are available for testing.
D. In-Bed Heat Exchanger
    a. The in-bed heat exchanger (IBHX) is more dense than prior IBHX's, and the wall gap is smaller than any of these other designs. The first course of action will be to move the outer rank of tubes farther from the wall, so that solids can recycle down the wall without interruption. This is similar to a set of experiments conducted at Leatherhead, where it was discovered that removing the outer rank of tubes improved bed circulation and temperature uniformity.
E. Bed Ash Removal
    a. Bed ash removal systems used in prior PFBC's were not different than this pilot, however the amount of agglomerates is greater. In addition to the corrective actions above, which will serve to reduce agglomerate formation, the suggested course of action is to begin injecting bed material and removing it prior to fuel ignition, to ensure the lower bed is freely moving prior to coal combustion.

5.7.5 Root causes and suggested fixes, organized by problem statement

<u>The root causes of each problem are summarized below:</u>

1. Fine agglomerates are caused by temperature and humidity changes close to the cooled heat exchanger tubes, and secondarily due to a local stagnation point on the top of each tube. More mixing is expected to improve this by making more uniform temperatures, and by increasing turbulence, but due to the open questions about the thermochemical environment in oxy-PFBC combustion, it is prudent to start testing with no dolomite first while using low sulfur coal, and then increase use of dolomite gradually, and to start with hotter coolant (air cooled) prior to starting to use colder coolant (therminol or steam). In this manner, it can be determined the actual limits of humidity and temperature.
2. Coarse agglomerates are caused by a combination of poor mixing and poor recirculation, i.e. tubes too close to the wall of the combustor. The material is able to sinter, often with coal sticking to the interstices and smoldering, which begins a more aggressive melting environment. Designs of the burner duct, the fuel injector, the heat exchangers, and possibly the oxygen injection systems are all contributing factors which must be addressed.

3. The freeboard burning, low bed density and low carbon conversion all had the same primary cause: the heat exchanger tubes were too close to the combustor wall, leading to bed material collecting on top of the heat exchanger tubes near the wall and insulating temperature sensors there. The low temperature readings led to erroneous calculations of gas density and velocity, which led to significantly higher gas velocities than intended. This resulted in reduced coal residence time and lowered bed density, both of which led to reduced carbon conversion, burning in the freeboard region and ultimately to hardware damage. This is closely related to the cause of problem statement 2, and must be addressed by increasing the gap between the wall and the closest heat exchanger tubes, and by adding temperature probes with thermowells that extend away from the wall to avoid potential insulation by stagnant bed material. Another contributing factor is the initialization of coal flow at 3- 4 atmospheres, which results in gas velocity that is double the maximum velocity desired. The solution to this is to change the startup burner system so the Oxy-PFBC can be started at the full pressure of 8 atmospheres and operated as designed. See problem statements 7 and 9.

4. The bed ash removal system was not robust when agglomerates and debris were present. This design should be improved while also resolving problems 1 and 2. The system has already been improved to include warmed CO_2 for purging, and an inlet pipe elevated off the floor of the bed to reduce likelihood of clogging by larger objects. Suggested improvements include adding grill or lump diverter at the inlet pipe. In addition, there should be an easier method of draining larger agglomerates between tests, and possibly increased pressure drop across the drain valves, if possible (this becomes a safety issue, so may not be practical in a pilot of this size). Eliminating the diameter reduction in the drain is also desirable.

5. Filter burning was caused by a combination of low carbon conversion and inadequate filter cleaning procedures. This was successfully addressed by starting filter cleaning earlier, and ensuring that it continued after completion of each test.

6. Safeguards/Alarms/Procedures insufficient to prevent catastrophic slagging is caused by instrumentation which was not inserted deeply enough into the bed to provide complete information about the center of the combustor. This is related to the inadequate mixing and close tube-wall spacing in problem statements 2 and 3. More thermocouples deeper in the bed and lower alarm limits must be provided. An improved combustion model to help justify appropriate limits would address a contributing cause.

7. Startup heater flame detection intermittency was only partially understood to be related to absolute pressure, so adequate corrective actions will include alternate methods of detection which do not have failure modes dependent on pressure (thermocouple readings, for example, would be one such alternate method). The natural gas startup system must be redesigned to operate across the full range of pressures from 1-8 atmospheres, absolute, with flame detection systems which are reliable across the same pressure range.

8. Fuel and dolomite flow issues are exacerbated by flowing a blend of fuel and dolomite. For assured flow measurement and steady flow delivery, these systems must be separated and gas flow measurements must be divided to logically separate different failure modes.

9. Solid Fuel pneumatic injection system plugging and erosion is partially addressed by the solutions to problem 8 above, but in addition, high velocities in the fuel line must be reduced by starting fuel flow only at high pressure, thus, the solution to this problem is also tied into the natural gas startup system, which was designed only to operate from 1-4 atm absolute.

10. Fly Ash Everlasting valve intermittency is caused by inadequate purging of the valve bodies. The purges must have additional ports and sufficient programming to ensure the purges are operating any time the valves move.

11. Carbon conversion of 85-87% is attributed to inadequate mixing of fuel and oxygen, high velocity, and overcooling of the bed. These causes are all expected to be improved when the corrective actions for items 1, 2, 3, 8, and 9 are incorporated.

12. Blower vibration is caused primarily by resonance between the motor/pump, which has an overhung bearing, and the floor support, which is structural steel. The damage risk is partially mitigated by adjusting speed by altering the inline orifice size and adding a vibration sensor to alert operators to an issue, but this is insufficient to prevent the problem from happening in the middle of a test. Long term solutions must include placing the blower on a concrete base, and future systems should be designed with a fan which has bearings on both the inlet and outlet, so the rotating mass is not overhung.

<u>General</u>

In addition to the above numbered problems, some common cause issues were identified during the investigation. These are situational awareness and control issues which were found to be due to four primary causes: Too many pages of data display to choose from on eight control room screens, insufficient documentation of or training for alarm and automatic cutoff setpoints, and too many control devices being operated in manual mode to ensure operation at the desired setpoint, and finally, there were not formal data reviews after each test shutdown, which led to multiple restarts within a week without being absolutely sure about resolution of problems encountered.

5.7.6 Corrective actions, organized by operational system

The following corrective actions were developed with the assistance of a non-advocate team of fluidized bed experts who reviewed the root cause analysis. They are organized here by operational system, in contrast to the previous section which presented them according to problem statement.

1. Coal Feed Reliability/Stability (Separate Fuel and Dolomite/Bed Material)

    A. Provide separate fuel and dolomite feed systems to reduce coal flow rate uncertainty from current 30%+ to <5%

        1) Eliminate mixer (coal only)

        2) Separate CO_2 measurement for injection and lock hopper

    B. Address coal feed intermittency issue for stable test operations

        1) Adjust timing on lock hopper equalization to prevent overpressure

        2) Add surge vessel to prevent starvation of CO_2

3) Add valve rate limits on filter pulseback system for repressurization

2. Fluidization Gas Distribution

    A. Need substantially more orifices (24x-64x).

    B. Minimum of 1/3 total pressure drop should be through the orifices.

3. Bed Temperature Monitoring and Control

    A. Need better instrumentation (thermowell) in bed to understand environment and protect the combustor (in some cases, our wall measurements were 200-400C less than actual temps in the combustor core).

    B. Need ability to adjust bed height to control bed temps (need working bed drain and fill systems).

    C. Need to be able to start coal combustion at full operating pressure of 8 atmospheres so Oxy-PFBC is operating at the design pressure and flow conditions. Requires modification to the natural gas facility supply pressure and the startup burner system.

4. Fluidized Bed Hydrodynamics (In-Bed Particle Mobility, Bed Density, Dolomite Size Distribution)

    A. Poor bed density and mobility adversely affects carbon conversion, agglomeration. Address with modified HEX tube pattern/wall gap, coarser dolomite (with separate feed system), modified gas distribution. Validate with cold flow rig testing and CFD (to scale results to pressurized hot flow).

    B. Reduce gas flow velocity to design conditions by using improved temperature sensors (thermowell) in the bed to calculate average combustor gas properties.

5. HEX Density and Operational Flexibility

    A. Explore changes to HEX tube density to improve bed mobility (see item 4) and temperature uniformity in the bed while minimizing reduction in power density.

    B. Need to retain ability to adjust heat removal in various parts of bed.

6. Startup and Transition to Operating Conditions

    A. Increase natural gas supply pressure so we can start at full pressure and avoid long transition period at low pressure / high gas velocities.

    B. Start at 750C and transition to coal combustion at full operating pressure in ~30 minutes (rather than hours required now).

7. Improved Bottom Removal System

    A. Revise design to enable drainage even with some agglomerates of FOD in system.

    B. Add “grizzly” (i.e. grill or strainer) to drain to keep larger chunks out of lockhoppers.

C. Add 5-6 psi pressure drop through drain to help material flow and remove flow area reduction in the lockhopper system.

D. Eliminate area reduction in drain system.

8. Startup Burner Pressure and Reliability

   A. Modify flame detection system and ignitor for more reliable operation at pressure.

   B. Validate that burner can operate at pressure of 8 bar (vs. 3 bar used now).

9. Test Program Design – Start Simple and Establish Stable Combustion Operation

   A. Initial testing should be done with low sulfur subbit coal (PRB) and no dolomite to avoid agglomeration issues while learning to operate combustor.

   B. Next move to low sulfur bituminous coal with no dolomite.

   C. Once we are confident with PFBC operations, move to fuel with sulfur and dolomite.

6.0 Commercialization Plan

6.1 Demo Plant Economics

Multiple demo plant concepts have been developed with potential partners, and cost estimates for these plants were developed. This includes a 60 MWth (20 MWe) plant that can create power and chemicals while capturing the CO_2, and a 15 MWth plant to demonstrate the combustion/CO_2 purification technology without producing power or capturing the CO_2.

The commercialization plan includes completion of the pilot plant, followed by a demo or larger scale pilot plant and after that, a commercial plant, as shown in figure 6-1 below.

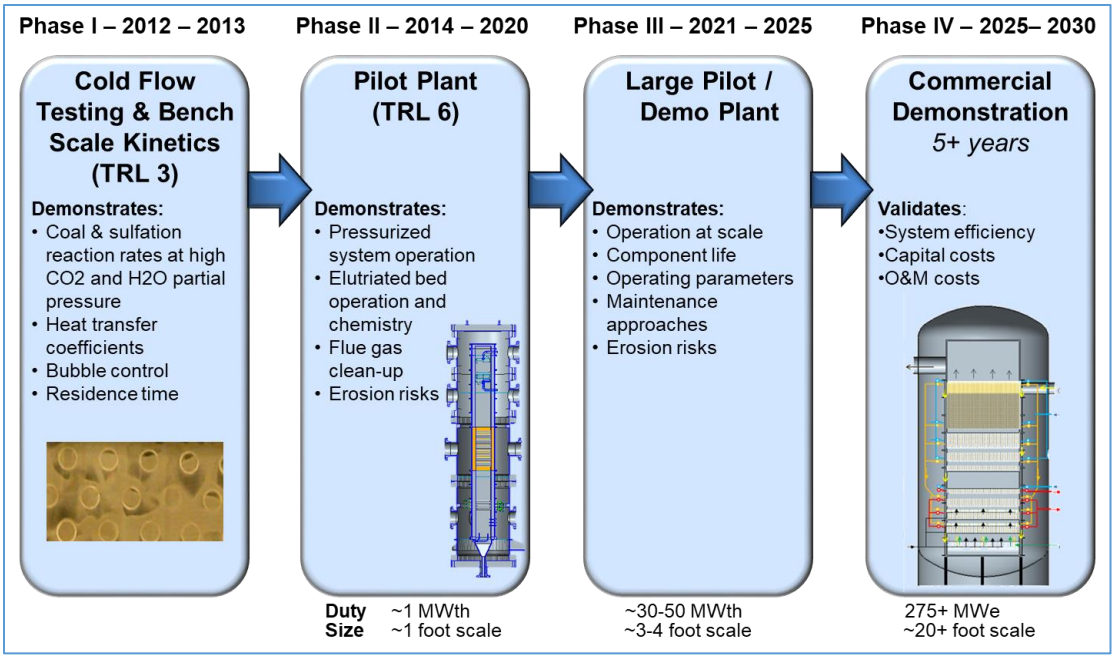

Figure 6-1. Oxy-PFBC Commercialization Plan

Estimates were developed through the use of vendor budgetary estimates for bare equipment cost whenever possible. However, one significant exception is the bare cost of the combustor that was developed as a bottom-up estimate by GTI. The total installed cost was then arrived at by multiplying the bare equipment cost by greenfield installation factors estimated by GTI (see Table 6-1), and later validated by one of the demo plant partners and their in-house EPC contractor based on their experience installing facilities at their site. The installation factors were more conservative than those used in standard DOE cases, but more aggressive than comparable quotes to GTI on similar equipment from EPC contractors like Jacobs.

Table 6-1. Installation factors for demo plant to produce power and chemicals.

Equipment Type	Installed Cost Factor
Materials Handling	2.50
Pulverizer	2.20
Vessels & Silos	2.50
Cyclones & Filters	3.00
Recycle Compressor	2.50
Combustor	3.00
Steam System	2.50
Solid Service Valves	1.35
Analytical Instruments	2.00
Feed System Structure	1.30
CO2 Purification and Drying	3.00
Total	2.72

6.1.1 Estimate approach

A Class 4 estimate was developed for the 60 MWth plant using budgetary costs from vendors for most items. The Combustor cost was developed in-house. The boiler feed water (BFW) Circulation Pump costs were obtained from Aspen Cost Estimator. Cost for two small cyclones and one bag filter were entered as an allowance. The estimate includes 6 analytical instruments (i.e. gas chromatographs for emissions monitoring).

Total Installed Cost was then obtained by multiplying the bare equipment cost by a factor based on information from both the DOE standard case studies (DOE/NETL-2007/1291) and from previous cost studies done for GTI by Jacobs. The total effective installed cost factor is 2.72 as shown in Table 6-1, as compared to a value of 1.99 (with contingencies) for the CO_2 Removal and Compression subsystem from DOE Case 12, or 3.55 (without contingencies) for a Jacobs estimate for an GTI commercial scale hydrogen generator. The total installed cost factor is an average ratio to take each piece of equipment to a ready to use installed item and includes all of the following:

- Home office engineering
- Field labor construction and supervision
- Piping, insulation, painting, piling, concrete, pipe racks, cables, wiring, etc
- General instrumentation (control and isolation valves excluding solid service valves)

The GTI selected factors are applied as follows:

- Packaged units (Pulverizer, Turbine and Condenser System): factor of 2.2
- Solid Service Valves: factor of 1.2 for materials plus 80 hours engineering @ $100/hr per tag service, plus 20 hours field installation per valve @ $45/hr (including supervision)
- Analytical Instrumentation: factor of 2.0
- Combustor and Filters: factor of 3.0
- All others: factor of 2.5
- The structure cost was estimated assuming bare cost of $4.71/ft3 of volume space and installed cost of $6.12/ft3 of volume space (1.3 factor) based on prior data with similar structures size. An allowance of $150,000 was added for bare cost of one elevator.

Table 6-1 includes the equipment that was to be provided by GTI for the power/chemical plant. As a result, it does not include oxygen systems, since oxygen was to be provided by the facility. If an oxygen system were to be included, the factor would be 3.0, and this would increase the total effective installed factor at the bottom of the Table 6-1. The 3.0 factor for the combustor, filter, CO_2 purification and drying, and oxygen system is broken down as shown in Table 6-2. The breakdown of the 2.5 factor used for most other equipment is shown in Table 6-3.

Table 6-3. Breakdown of installation factor for combustor, filter, CPU and O_2 system.

Cost category	Factor	Cum factor
Bare equipment		1.0
On-site installation:	1.5	1.5
EPC cost	1.1	1.7
Instrumentation	1.1	1.8
GTI oversight	1.1	2.0
Process contingency:	1.3	2.6
Project contingency:	1.15	3.0

Table 6-4. Breakdown of installation factor for other equipment with 2.5 factor.

Cost category	Factor	Cum factor
Bare equipment		1.0
On-site installation:	1.5	1.5
EPC cost	1.1	1.7
Instrumentation	1.1	1.8
GTI oversite	1.1	2.0
Process contingency:	1.1	2.2
Project contingency:	1.12	2.5

Estimates for a 15 MWth system were also developed. The component costs were estimated by scaling the components from the 60 MWth demo plant using a scaling exponent value of 0.68. In addition, plant operation costs were estimated based on historical data from similar GTI scale pilots (R-Gas™, U-Gas®, & National Carbon Capture Center). Consumables (oxygen, coal, limestone/dolomite, etc.) and utility usage are estimated on a bottoms-up basis. Repair, rework and maintenance costs are based on historical data.

6.2 Demo Plant Permitting Assessment

GTI defined a task to assess risks associated with getting a permit to build and operate a demo plant due to an experience with a previous demo plant partner that indicated that there could be significant resistance to the plant from local residents and state political leaders. This task should assess the risk, and define mitigation steps if necessary.

GTI worked with a potential partner to develop a demo plant concept and cost estimate. The partner had a viable business case and management support to carry the project forward. They conducted a preliminary assessment of the permitting risk as part of the preparation for seeking management approval for the project. Their assessment was that the permitting risks at the site were low due to several factors: 1) The site is in a rural location with low probability of affecting neighboring residents, 2) The site had already received permits for similar DOE-funded projects without any significant difficulties, 3) State political resistance is unlikely since the state government is supportive and was willing to consider providing funding to the project. It was felt that no significant mitigation activities were required at that time.

If the project is moved to a different site, the risk assessment will need to be reconsidered.

6.3 Commercial Plant LCOE Refinement

The team evaluated a number of different options and compared them to DOE Case 11 (greenfield supercritical pulverized coal (SCPC) without CO_2 capture) and DOE Case 12 (SCPC with post combustion capture)[1,2,3] using the DOE/NETL guidelines.[4] The Oxy-PFBC predictions for COE, were updated to reflect the component and system test results through 2017, but no change was seen relative to earlier Phase I predictions (see Figure 6-1). Carbon conversion is still an operational issue that needs to be addressed prior to finalizing COE predictions. An alternate proprietary architecture was developed that shows significant improvement in COE, with projected COE of 1.2 times DOE Case 11, compared to 1.3 for the current system.

The COE updates are based on test results through 2017. Testing at the 1 MWth scale demonstrated the ability to meet or exceed all performance targets with the exception of carbon conversion. The carbon conversion target is expected to be met in 2018 after operational issues are addressed. The performance targets of interest were for carbon conversion, in-bed sulfur capture, filter sulfur capture, direct contact cooler sulfur capture, bed temperature, NOx after direct contact cooler, acid dewpoint, water pH in condensed flue gas effluent, O_2 level in de-oxo system, and heat captured at high temp to achieve target efficiency. The updated COE predictions assume all target levels of performance are achieved, including carbon conversion, and as a result are unchanged from earlier projections[3]. The predictions will be updated again at the conclusion of pilot scale performance testing necessary to correct operational issues and achieve relevant performance metrics for carbon conversion.

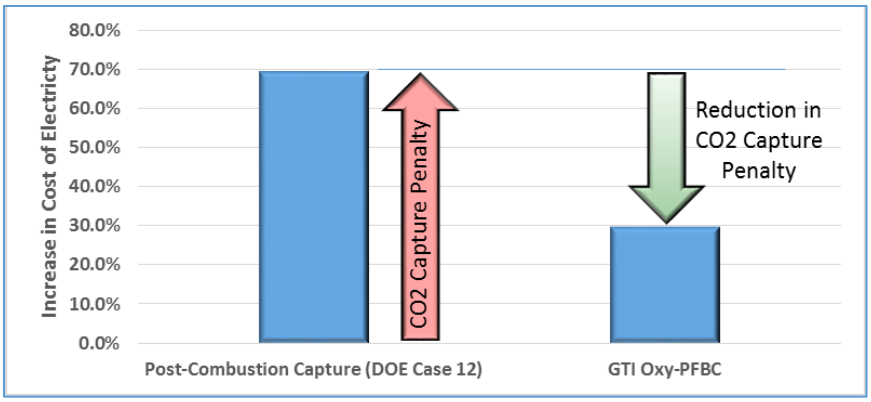

Figure 6-2. GTI Oxy-PFBC reduces the CO_2 capture penalty through lower cost combustor and gas cleanup equipment

In addition to the performance targets discussed above, there were some minor changes to the system that affected cost. First, an oversight in estimating cost of the combustor in the Phase I estimates was corrected, increasing COE by roughly 2%. Secondly, the favorable performance impact of including a quasi-isothermal de-oxo reactor was included. The quasi-isothermal feature captures heat from the deoxidations process that can be used in the cycle for better performance. The quasi-isothermal de-oxo technology is expected to be tested in 2019 with the 1 MWth pilot to validate performance predictions. The quasi-isothermal de-oxo technology reduces COE by roughly 2% thus offsetting the COE increases due to the combustor CapEx impact mentioned earlier.

DOE Case 12 increases the cost of electricity by 70% (the CO_2 capture penalty) relative to Case 11. The GTI Oxy-PFBC is predicted to eliminate 57% of the CO_2 capture penalty in cost of electricity for DOE Case 12 as shown in Figure 6-1. The Oxy-PFBC is predicted to achieve a COE increase of 29.9 and 31% over a plant without CO_2 capture (DOE Case 11) with 90 and 98.3% CO_2 capture, respectively. Primary contributors to reduced cost of electricity include reduced capital costs of the combustor and CO_2 capture system. The combustor is one third the size and less than half the cost of a traditional combustor, while the ASU and CO_2 purification systems cost significantly less than the post combustion CO_2 capture system they replace. These two items are projected to reduce capital costs by nearly half a billion dollars for a commercial scale plant (550 MWe). Technologies that can further reduce cost of electricity are currently under evaluation.

These results indicate that the Oxy-PFBC system can exceed the DOE goals of less than 35% increase in cost of electricity while capturing at least 90% of the CO_2. If the benefits of revenue or tax credits for captured CO_2 are factored in, the GTI baseline system with 90% CO_2 capture is predicted to break even with the no-capture case at a CO_2 price of $30/ton. To put this in perspective, proposed legislation in the

United States would provide a credit of $35/ton for EOR applications and $50/ton for permanent sequestration. The World Bank Group reported in 2016 that carbon prices around the world ranged from less than $1/ton to $137/ton, with roughly three fourths of the CO_2 market priced at less than $10/ton. Markets at $25/ton or greater included France ($25/ton), Denmark ($26/ton), Tokyo ($31/ton), Norway ($53) and Switzerland ($137/ton). Carbon pricing is a growing trend which is projected to cover roughly 13% of total greenhouse gas emissions in 2017, compared to less than 5% in 2011, the last year before rapid growth started. If China's national carbon trading system is put in place in 2017 as planned, then 22% of global emissions will be covered by carbon pricing.

An alternate proprietary architecture was developed that shows significant improvement in COE, with projected COE of 1.2 times DOE Case 11, compared to 1.3 for the current Oxy-PFBC system. GTI worked with another technology provider and conducted a bottoms up analysis consistent with the DOE methodology used on other TEA analyses discussed earlier in this report. A patent application was submitted on the new architecture. To achieve these reduced COE levels, technology in addition to the Oxy-PFBC will need to be advanced, including achieving both cost and performance targets.

6.4 Commercial Plant Market Development

The Commercial Plant Market Study is complete. The study includes four primary sections: 1) Global Electricity Market, 2) Carbon Capture Regulations, 3) Value Chain Mapping / Voice of the Customer, and 4) GTI Business Case. The study identified market opportunities in regions where coal is inexpensive relative to natural gas, countries have implemented CO_2 emissions regulations or markets, and the countries have resources to invest in new power generation. Opportunities were identified in Japan and China where an Oxy-PFBC plant would have substantial OpEx advantages relative to a natural gas combined cycle (NGCC) plant. The market for the Oxy-PFBC technology in North America is currently challenged by relatively inexpensive natural gas and lack of regulations in the United States, but is projected to improve by the time the Oxy-PFBC is first available to sell on the commercial market in the late 2020's, and ramps up production during the 2030's.

GTI had significant market pull for the Oxy-PFBC technology demonstrated in November 2017, in support of a proposal. A pitch package was developed as part of this activity and presented to a number of potential investors and commercialization partners. This led to the development of multiple large pilot scale plant concepts at different host sites. This culminated in a proposal to the US DOE in response to the Funding Opportunity Announcement DE-FOA-0001459, "Pre-Project Planning for Advanced Combustion Pilot Plants." GTI had five companies from three countries competing for the opportunity to host the large scale pilot plant. The program, if awarded, will downselect to one host site during the first year of the program.

7.0 Conclusions and Recommendations Future Work

7.1 Conclusions

The Oxy-PFBC technology development has made significant progress, with successful completion of key component testing, as well as design, fab and testing of a 1 MWth pilot scale plant. Testing demonstrated the ability to hit all performance targets to date, with the exception of coal conversion. To achieve the project objectives of achieving TRL 6 to enable scale up to a large pilot scale plant, additional work is required to resolve issues uncovered in pilot scale testing, especially issues associated

with low carbon conversion. It is expected that resolving these issues will allow all performance metrics to be achieved within the current combustor size, thus validating current cost of electricity projections.

The Oxy-PFBC provides the potential for significantly lower cost coal power generation and is projected to exceed the DOE goals of >90% CO_2 capture with less than a 35% increase in COE relative to DOE Case 11 (supercritical Rankine cycle with pulverized coal and no carbon capture). Two key components that are the primary drivers of lower CapEx and therefore lower cost of electricity are: 1) a compact combustor, and 2) low cost gas cleanup. The key challenges that must be met to achieve a low cost combustor are: the coal reactions must be achieved within the limited residence time available in the combustor, the limestone must absorb sufficient sulfur, and the in-bed heat exchanger must be able to extract sufficient heat within the smaller combustor. The key challenges for low cost gas cleanup are: the Linde CO_2 Purification Unit must have flue gas from the combustor that is sufficiently low in sulfur, and the De-Oxo unit must be able to remove sufficient excess oxygen to achieve purity specs for CO_2 pipelines.

Pilot testing at the 1 MWth scale demonstrated key performance metrics that drive projected cost of electricity at the commercial scale. The combustor exceeded sulfur capture goals with 99% capture compared to a goal of 90% capture. The in-bed heat exchangers provided sufficient heat extraction as predicted. The CPU achieved its goals when utilizing simulated flue gas. The DCC and Liconox systems were able to remove the required amount of additional sulfur, and the new technology, the De-Oxo reactor, was successful in removing sufficient O_2 to achieve CO_2 pipeline specs, with 99% O_2 conversion. The DCC was tested with actual flue gas from the Oxy-PFBC, but actual flue gas testing of the Liconox and De-Oxo modules was not achieved during this series of tests.

The key performance metric that still needs to be validated in future testing is carbon conversion. The investigation found that the temperature sensors were insulated by stagnant bed material, leading to higher gas velocities in the combustor than realized at the time of testing. Modifications to the sensors and combustor hardware will be required to achieve the desired performance in future testing. Component testing, in the form of pressurized elutriation testing to determine coal residence time and coal kinetics testing to determine reaction rates in the Oxy-PFBC environment, give confidence that target coal conversion rates can be achieved once the temperature sensor issue is resolved.

Commercialization activities included development of large pilot/demo scale plant concepts at the 5 and 20 MWe scales with potential host site partners. Five host sites in three countries expressed interest in hosting a large scale pilot site as part of a proposal response to a US DOE opportunity. The TEA was updated for a full scale commercial plant, and still indicates a commercial scale COE of 1.3 times a no capture plant (DOE Case 11). An alternate proprietary architecture was developed that has the potential to reduce COE to 1.2 times a no capture plant. These COE estimates assume no economic benefit for the CO_2 captured.

7.2 Recommendations for Future Work

The team recommends that the hardware should be repaired and upgraded as recommended by the Incident Review Board, and testing resumed to achieve the desired combustor operation and performance.

The next step of large scale pilot/demo plant development will proceed after successful 1 MWth pilot testing.

8.0 Acknowledgements

US DOE:
This material is based upon work funded in-part by the United States Department of Energy under Award Number DE-FE0009448.

This report was prepared as an account of work sponsored by an agency of the United States Government. Neither the United States Government nor any agency thereof, nor any of their employees, makes any warranty, express or implied, or assumes any legal liability or responsibility for the accuracy, completeness, or usefulness of any information, apparatus, product, or process disclosed, or represents that its use would not infringe privately owned rights. Reference herein to any specific commercial product, process, or service by trade name, trademark, manufacturer, or otherwise does not necessarily constitute or imply its endorsement, recommendation, or favoring by the United States Government or any agency thereof. The views and opinions of authors expressed herein do not necessarily state or reflect those of the United States Government or any agency thereof.

GTI would like to acknowledge Robin Ames and John Rockey of the National Energy Technology Laboratory at the United States Department of Energy

CANADIAN GOVERNMENT:
This work was supported by the Government of Canada's Program of Energy Research and Development, and the ecoENERGY Innovation Initiative program.

PROVINCE OF ALBERTA:

A portion of the project funding was also provided by:

GTI would like to acknowledge Duke DuPlessis and Maureen Kolla of Alberta Innovates for their support of the project and its goal of achieving affordable clean fossil fuel power generation.

TEAM MEMBERS:
The development and testing of the Oxy-PFBC and CO_2 purification technologies requires support and teamwork from a number of individuals with the diverse expertise and capabilities necessary to make the project a success. GTI would like to acknowledge the following people for their contributions (in alphabetical order):

From GTI: Bruce Brian, Alexander Cruz, Anthony Eastland, Mark Fitzsimmons, William Follett, Patrick Frye, Scott Halloran, Douglas Heim, Megan Huang, Michael Kutin, Jeff Mays, Sergio Meza, Shinjiro Miyata, Don Stevenson, Dr. Ganesan Subbaraman, Scott Trybula and Derek Wissmiller.

From Linde: Dr. Alexander Alekseev, Ron Arias, Makini Byron, Devin Bostick, Charlie Davis, Dr. Lars-Erik Gaertner, Crystal Green, Sven Halang, Dr. Stevan Jovanovic, Dr. Krish Krishnamurthy, Harold Kober, Debbi Lacey, Walt Mishkovsky, Frankie Rodriguez, Torsten Stoffregen and Heiko Volk.

From Natural Resources Canada CanmetENERGY: Kelly Atkinson, Steve Bethune, Samantha Bryson, Ryan Burchat, Scott Champagne, David Faguy, Dr. Robin W. Hughes, Dennis Lu, Chris Mallon, David J. McCalden, Alex McCready, Stephen Montero, Gilles Roy, Jeff Slater, Robert Symonds and Yinghai Wu.

From Pennsylvania State University: Dr. Aditi Khadilkar, David K. Johnson and Dr. Sarma Pisupati.

From General Electric: Ray Chamberland, Glen Jukkola (retired) and Armand Levasseur (retired).

From EPRI: Horst Hack and David Thimsen (retired).

From University of Ottawa: Dr. Arturo Macchi, Dr. Poupak Mehrani, Eric Mielke, and Marc-André Séguin.

From Etaa Energy, Inc.: Dr. Kumar Sellakumar.

9.0 References

1. Follett, W., Fitzsimmons, M., Pisupati, S., Sonwane, C., Jovanovic, S., Manley, T., Hiraoka, D., Yows, S., "Development of a Pilot Scale Coal Powered Oxy-fired Pressurized Fluidized Bed Combustor with CO2 Capture", Power-Gen Europe Conference, June 9-11, 2015, Amsterdam, The Netherlands.
2. NETL, "Updated Costs (June 2011 Basis) for Selected Bituminous Baseline Cases," Report No. DOE/NETL-341/082312, U.S. Department of Energy, National Energy Technology Laboratory (NETL), Pittsburgh, PA (August 2012).
3. Fitzsimmons, M., Laurie, J., Manley, T., Swalgen, S., Jovanovic, S., Alekseev, A., Hawkins, S., "Technology Engineering Design and Economic Analysis Report of the Aerojet Rocketdyne Oxygen Fired Pressurized Fluidized Bed Reactor and Regenerative Rankine Steam Cycle Power Plant with Heat Integration," November, 2013, prepared for the Department of Energy, National Energy Technology Laboratory, by Aerojet Rocketdyne, Canoga Park, CA, USA.
4. NETL, "Quality Guidelines for Energy System Studies (QGESS): Cost Estimation Methodology for NETL Assessments of Power Plant Performance," Report No. DOE/NETL-2011/1455, U.S. Department of Energy, National Energy Technology Laboratory, Pittsburgh, PA (Apr. 2011), available online at: http://www.netl.doe.gov/energy-analyses/refshelf/PubDetails.aspx?Action=View&Source=Main&PubId=355

10.0 Publications

The following publications provide public releases of results achieved during the project.

1. Subbaraman, G., "Oxy-Combustion Pressurized Fluidized Bed with Carbon Dioxide Purification", BIXPO 2017, Gwangju, Korea, November 1-3, 2017.

2. Follett, W. W., "Payment Milestone, Project: Advanced Oxy-Combustion Technology Development and Scale Up for New and Existing Coal-Fired Power Plants (Phase II), Milestone: Final Report", delivered to Alberta Innovates, Alberta, Canada, February 28, 2018.

3. Séguin, M., “Fuel Residence Times for Clean Combustion of Coal in a Pressurized Fluidized Bed - Cold Flow Study”, Master’s Thesis, University of Ottawa, Ottawa, Canada, 2017.

4. Follett, W. W., “Oxy-Combustion Pressurized Fluidized Bed with Carbon Dioxide Purification”, U.S. Department of Energy Carbon Capture Technology Meeting, Pittsburgh, PA, August 21-25, 2017.

5. Follett, W. W., “Oxy-Combustion Pressurized Fluidized Bed with Carbon Dioxide Purification”, U.S. Department of Energy Carbon Capture Technology Meeting, Pittsburgh, PA, August 21-25, 2017.

6. Follett, W. W., Fitzsimmons, M. A., Huang, M.T., Jovanovic, S., Byron, M., Krishnamurthy, K., McCalden, D. J., Champagne, S., Hughes, R. W., Symonds, R., Mehrani, P., Macchi, A., Seguin, M., “Pilot Scale Test Results of a Coal Powered Oxy-fired Pressurized Fluidized Bed Combustor with CO_2 Capture and Purification,” Power-Gen Europe Conference, Cologne, Germany, June 27-29, 2017.

7. Follett, W. W., Fitzsimmons, M. A., Huang, M.T., Jovanovic, S., Byron, M., Krishnamurthy, K., Bostick, D., Hughes, R. W., McCalden, D. J., Champagne, S., “Development Status of a Coal Powered Oxy-fired Pressurized Fluidized Bed Combustor with CO2 Capture and Purification”, Clearwater Clean Energy Conference, Clearwater, FL, June 11-15, 2017.

8. Khadilkar, A., Pisupati, S. V., “Unified Model for Prediction of Agglomeration in Fluidized Beds and Validation Attempts of Proposed Particle-level Growth Mechanism of Ash Agglomerates”, delivered to GTI, Woodland Hills, CA, November 28, 2016.

9. “Payment Milestone Report, CFD Analysis Task Complete”, delivered to Alberta Innovates, Alberta, Canada, November, 2016. (See Appendix D)

10. Follett, W. W., “Oxy-Combustion Pressurized Fluidized Bed with Carbon Dioxide Purification”, U.S. Department of Energy Carbon Capture Technology Meeting, Pittsburgh, PA, August 8-12, 2016.

11. Follett, W. W., “Enabling Technologies for Oxy-fired Pressurized Fluidized Bed Combustor Development”, U.S. Department of Energy Carbon Capture Technology Meeting, Pittsburgh, PA, August 8-12, 2016.

12. Séguin, M., Champagne, S., Hughes, R. W., Fitzsimmons, M. A., Macchi, A., Mehrani, P., “Cold Flow Study of the Effect of Pressure and Gas Velocity on Residence Time of Fuel Particles in an Oxygen Fired Pressurized Fluidized Bed Combustor”, Fluidization XV, poster session, Quebec, Canada, May 22-27, 2016.

13. Fitzsimmons, M., “GTI Oxy-PFBC Cold Flow Test Report”, delivered to Alberta Innovates, Alberta, Canada, February 29, 2016. (See Appendix A)

14. Sprouse, K. M., “Penn State Sulfation Tests & Kinetic Analysis”, delivered to Alberta Innovates, Alberta, Canada, February 29, 2016. (See Appendix C)

15. Sprouse, K. M., “Penn State University Coal Reactivity Tests and Analysis”, delivered to Alberta Innovates, Alberta, Canada, January 20, 2016. (See Appendix B)

16. Follett, W. W., “Oxy-Combustion Pressurized Fluidized Bed with Carbon Dioxide Purification”, U.S. Department of Energy Carbon Capture Technology Meeting, Pittsburgh, PA, June 23-26, 2015.

17. Follett, W. W., Fitzsimmons, M. A., Pisupati, S. V., Sonwane, C. G., Jovanovic, S., Manley, T. W., Hiraoka, D., Yows, S. A., “Development of a Pilot Scale Coal Powered Oxy-fired Pressurized Fluidized Bed Combustor with CO2 Capture,” Power-Gen Europe Conference, Amsterdam, The Netherlands, June 9-11 2015.

18. Fitzsimmons, Kutin, Mesa, Hughes, McCalden, Symond, Jovanovic, “Oxy-PFBC Test Plan, Revision A”, Document number TBP-321060, Nov 15, 2015.

19. Fitzsimmons, M., et. al. “Oxy-PFBC Phase I Final Technical Report”, U.S. Department of Energy, DOE/NETL Contract DE-FE-0009448, June 27, 2013.

20. Fitzsimmons, M., et. al., “Technology Engineering Design and Economic Analysis Report of the Aerojet Rocketdyne Oxygen Fired Pressurized Fluidized Bed Reactor and Regenerative Rankine Steam Cycle Power Plant with Heat Integration”, U.S. Department of Energy, DOE/NETL Contract DE-FE-0009448, June 27, 2013.

21. Fitzsimmons, M., Jovanovic, S., “Technology Gap Analysis Report,” U.S. Department of Energy, DOE/NETL Contract DE-FE-0009448, June 27, 2013.

22. Fitzsimmons, M., et. al., “Pressurized Fluidized Bed Oxy-Combustion with Heat Integration”, Oxyfuel Combustion Conference 3, poster session, Ponferrada, Spain, September 9-13, 2013.

11.0 List of Acronyms and Abbreviations

µm – micrometer ($1X10^{-6}$ meters)

3-D – three dimensional

AR – Aerojet Rocketdyne

ASME – American Society of Mechanical Engineers

A_{sox} - Pre-exponential constants for limestone reaction with SO_x

ASTM - American Society for Testing and Materials

ASU – Air separation unit

Atm - atmospheres

bara - Bar absolute

BEDP – Basic engineering design package

Canmet – Natural Resources Canada

CanmetENERGY – Natural Resources Canada

CapEx – Capital Expenditures

CHX – Convective heat exchanger

C - Celsius

CaO – Calcium oxide, lime

CaCO3 – Calcium carbonate, limestone

CaSO4 - gypsum

CCS – Carbon Capture and Sequestration

CDN$ - Canadian dollar3

CFD – Computational fluid dynamics

cm – centimeter

cm/s – centimeter per second

CO_2 – Carbon dioxide

COE – Cost of electricity

CPFD – Computational Particle Fluid Dynamics (company that sells Barracuda software)

CPU – CO_2 purification unit

DCC – Direct contact cooler

DACS - Data acquisition and control system

DeOxo – De-oxygenation

DOE – United States Department of Energy

DOE/NETL - United States Department of Energy National Energy Technology Laboratory

DPT – Differential pressure transducer

EPC – Engineering, Procurement and Construction

EPRI – Electric Power Research Institute

E_{sox} – Activation energy limestone reaction with SO_x

FGD – Flue gas desulfurization

GE – General Electric

GTI – Gas Technology Institute

h – heat transfer coefficient

HAZOP – Hazard and Operability study

HCl – Hydrochloric acid

HEX – Heat exchanger

H_2O - Water

hr - hour

IHX – In-bed heat exchanger

K – Kelvin

kcal - kilocalorie

k_{eff} - Effective reaction rate

kg/m^3 – kilograms per cubic meter

kPaa – kilopascal absolute

kPag – kilopascal gage

kW – kilowatt

kW_{th} – kilowatt thermal

k_{sox} – Kinetic rate constant for limestone reaction with SO_x

LiCONOX – Linde Cold NOx removal

maf – moisture ash free

MFIX - Multiphase Flows with Interphase eXchanges

mm - millimeter

mol - mole

MWe – Megawatts electric

MWth – Megawatts thermal

N_2 - Nitrogen

NaOH – Sodium hydroxide

NGCC – Natural gas combined cycles

NOx – Oxides of nitrogen (NO_2, NO_3, etc.)

O_2 - Oxygen

OpEx – Operational Expenses

Oxy-PFBC – Oxygen-fired pressurized fluidized bed combustor

Penn State – Pennsylvania State University

P&ID – Piping and instrumentation diagram

PF – Plug flow

PFBC – Pressurized fluidized bed combustor

PFBR – Pressurized fluidized bed reactor

pH – Concentration of hydrogen ion

ppm – parts per million

PRB – Powder River Basin

psi – Pounds per square inch

PSR – Project Safety Review

PSU – Pennsylvania State University

R – Universal gas constant

RCA – Root cause analysis

RDS – Rate determining step

SCPC – Supercritical steam / pulverized coal

SFG – Synthetic flue gas

slpm – standard liter per minute

SOx – Oxides of sulfur (SO_2, SO_3, etc.)

Subbit - subbituminous

TEA – Technoeconomic Analysis

T_p – Particle temperature

TRAS – Technology Risk Assessment

TRL – Technology Readiness Level

TSSA - Technical Standards & Safety Authority

U - Velocity

Umf – Minimum fluidization velocity

U.S. – United States

vol% - volume percent

WSR – Well stirred reactor

XRD – X-ray diffraction

12.0 Appendices

Appendix A: Cold Flow Test Report

Appendix B: Coal Reactivity Report

Appendix C: Limestone Reactivity Report

Appendix D: CFD Analysis Task Report

Appendix E: PSU Agglomeration Model Report

Appendix A. Cold Flow Test Report

the Energy to Lead

REPORT

GTI PROJECT NUMBER 21854

GTI Oxy-PFBC Cold Flow Test Report

Report Issued:
February 29, 2016 (non-proprietary version)

GTI Technical Contact:
Mark Fitzsimmons
Institute Engineer
818-813-2728
mark.fitzsimmons@gastechnology.org

Gas Technology Institute
5945 Canoga Avenue, Suite 200
Woodland Hills, CA 91367
www.gastechnology.org

Legal Notice

This information was prepared by Gas Technology Institute ("GTI").

Neither GTI, the members of GTI, the Sponsor(s), nor any person acting on behalf of any of them:

a. Makes any warranty or representation, express or implied with respect to the accuracy, completeness, or usefulness of the information contained in this report, or that the use of any information, apparatus, method, or process disclosed in this report may not infringe privately-owned rights. Inasmuch as this project is experimental in nature, the technical information, results, or conclusions cannot be predicted. Conclusions and analysis of results by GTI represent GTI's opinion based on inferences from measurements and empirical relationships, which inferences and assumptions are not infallible, and with respect to which competent specialists may differ.

b. Assumes any liability with respect to the use of, or for any and all damages resulting from the use of, any information, apparatus, method, or process disclosed in this report; any other use of, or reliance on, this report by any third party is at the third party's sole risk.

c. The results within this report relate only to the items tested.

Table of Contents

Table of Figures

Page

List of Tables

Abstract

In order to mitigate risks in GTI's Oxy-PFBC project, a number of cold flow tests were performed to improve the understanding of pressurized fluidized beds. These tests were selected based on gaps in the literature regarding the prediction of various fluidized bed parameters of interest, and designed to reduce errors in predicting the behavior of fluidized bed designs. The parameters of interest are:

Heat Transfer Coefficient
Fluidization velocity and bed expansion
Bubble size and breakup due to the presence of heat exchangers
Particle velocities and entrainment of fine particles
Particle pressures on exposed surfaces

Tests were performed on a shop-built mockup of a pressurized fluidized bed at Aerojet Rocketdyne (prior to the sale of these assets to GTI in 2015). Although this mockup is not capable of pressures higher than 17 psia, it did serve well to illustrate all of the above behaviors and lend support to a number of correlations in the scientific literature. The knowledge is being used to compare predictions and develop further high pressure tests which are to be performed during commissioning in the Oxy-PFBC Pilot Plant at CanmetENERGY in Ottawa.

Note: This version of the report was edited to remove proprietary data.

Executive Summary

The GTI-led Oxy-PFBC project (previously initiated by Aerojet Rocketdyne) is a collaborative effort between GTI, CanmetENERGY and Linde LLC, which is primarily focused on developing and commercializing carbon capture systems burning pulverized coal (and other carbonaceous feedstocks). During Phase I of this project, Aerojet Rocketdyne (AR) found that the design of a full scale PFBC would be subject to a high risk of not meeting performance targets due to uncertainties in engineering predictions. These uncertainties were due to significant variation in the literature for predicting heat transfer, fluidized bed behavior, particle combustion rates, sulfur capture, solid material entrainment and filtration, and residence times. In some cases there was a lack of published information for the pressures and gas constituents of interest, and in other cases, the scientific papers that existed were in direct conflict with one another. Preliminary designs based on educated guesses from the literature that existed were drawn up, but the uncertainties remained.

AR determined that a significant number of these unknowns could be experimentally determined for the preliminary designs, and validate or refute the predictions, resulting in higher confidence for the pilot and future commercial designs. A test rig was built for atmospheric fluidized bed experimentation which incorporated the features found in many similar experiments described in the literature, and the details of the design matched the pilot plant preliminary designs as closely as possible in order to eliminate as many uncertainties due to mathematical scaling procedures (which are themselves controversial) as possible.

The tests were performed in several stages. The first set of tests was done to obtain basic flow and bubbling parameters for different in-bed tube arrangements and measure in-bed heat transfer coefficient. The second set was done to obtain particle elutriation and entrainment data, and infer particle residence time. A third set of tests was conducted to expand this data set for different particles to further investigate particle residence time. Finally, a few tests were run with a particle pressure sensor to establish a baseline and to determine if a sensor design that would be adaptable to a high temperature PFBC would work.

The tests were very successful, reducing the uncertainties for most of the information sought. Particle velocity and residence time data was in a range expected based on literature, but the tests did not point toward one specific correlation as the best choice, so more tests are recommended at high pressure in order to reduce uncertainties for this aspect of operation.

Introduction

Commercial Design Considerations

The parameters of fluidized bed operation are important to understand because they have direct implications for capital and operating costs for a PFBC. The most important in this respect is the heat transfer coefficient. Together with corrosion rates, erosion rates, and manufacturing technology, this determines how many kilograms of high alloy in-bed heat exchanger pipes are required to transfer heat from the combustion chamber to the steam system. The relationships between heat transfer coefficient and miles of pipe, and the mass of the containing vessel are straightforward, but from an engineering standpoint, the uncertainty in 2012 was +/- 50%, while the experiments performed in this work brought this uncertainty down to +/-10%.

Secondly, the combustion rates for particles in various oxygen atmospheres has been established with drop-tube testing, but the particle residence time in a fluidized bed has not been established for the very fine coal proposed by GTI for the current project. Prior fluidized beds injected 6mm (¼") top size coal, while the Oxy-PFBC project intends to inject a top size of only 0.3 mm. Elutriation predictions based on the literature are even worse than those available for heat transfer coefficient, however they do not have as great an impact on the cost of the design, so they have secondary importance.

Thirdly, bubbling behavior, particle pressures and instability are much more of an art than the above two items, and depend greatly on the bed design and in-bed heat exchangers and baffles, if present. A cold flow test is the only way to establish basic information about bubbling regime transitions, bed expansion at different velocities, and to establish if baffles are required, or can heat exchanger tubes suffice for bubble control. All of these things were measured in the cold flow test, and directly influenced the combustor design and the system pressure balance for calculating recycle compressor power.

The cold flow testing addresses the main challenges to achieving the necessary level of accuracy in sizing the fluid bed heat exchanger (FBHE) for the required heat transfer performance. These challenges include the prediction of the emulsion phase or "bed side" heat transfer coefficient (HTC) to the external surfaces of the tubes and in predicting the particle heat release, sulfur uptake, and particle residence times.

To achieve some flexibility in the design process of a large scale device for technology demonstration, the influence of the superficial velocity and the bed particle diameter for pressurized bed conditions needed to be more completely characterized, since the current literature[1,2,3,4,5,6] yielded very limited usable data for heat exchanger tube bundles, and does not sufficiently explore the effects of these parameters. Concurrently with Phase I of this project, an internally funded research and development (IR&D) project examined these relationships using cold flow sub-scale testing, similar to that described in the paper of Wiman & Almstedt[7].

The experimental cold flow rig is capable of accommodating the typical staggered horizontal tube bundle arrangement, with packing fractions in the range of interest above (0.18, 0.24 and 0.3 were tested based on prior design approaches developed at AR and relying on data from past PFBC's).

Finally, the implications of particle residence time are fundamental to the design of the fluidized bed, in order to balance heat release with heat removal. There is ample literature[8,9,10,11] to indicate that particle temperature and heat release rates can be managed by altering oxygen partial pressure in the PFBC, however this is only 1/3 of the problem. The other 2/3 are the heat transfer coefficient described above, and the particle velocity, which may be inferred from particle elutriation and entrainment, described in the experimental section of this report. Another set of experiments involved indirect measurement of particle velocity by measuring particle holdup in a fluidized bed in a manner similar to the experimental method in reference[12] and the bibliographic references of that paper.

Limitations of Atmospheric Cold Flow

The decision to begin with atmospheric cold flow tests was purely an economic one, but the physical assumptions that led to the decision were sound. The Reynolds number of bed particles in a pressurized hot combustion chamber is nearly identical with that of an atmospheric fluidized bed of air at room temperature. It is therefore reasonable to use this testing as a first approximation for basic bed behavior. The other items, heat transfer coefficient, and particle entrainment, can be scaled from low pressure and temperature to high pressure and temperature, providing that the particles are of similar size and density, because the relationships for Nusselt number and Prandtl number are straightforward calculations to extrapolate the predictions to high pressure and temperature. Thus, for a substantial savings in test costs, a great deal can be learned, and the extrapolated predictions can then be validated or adjusted in pressurized warm bed tests during startup experiments in the full pilot.

The primary purpose of the test rig was to obtain data in attempt to mitigate high risk items of heat transfer coefficients, particle residence time, erosion risks and tube packing density. Many correlations exist for the heat transfer coefficient, but not all of the particular design features of the AR PFBC were matched in the various articles and books studied. Considering the large disparity in opinion on the "best" approach to scaling a fluidized bed, and the literal impossibility of matching all variables in a scaled system, it was deemed necessary to actually replicate some of these test methods and create a test article that meets the AR design requirements.

The fluidized bed was specifically sized to operate in a fluidization regime that matches that of the PFBC commercialized fluidized bed and the Pilot Plant test. When analyzing the Glicksman scaling parameters for the fluidized bed, it became clear that the Reynolds number and Archimedes numbers, and thus the fluidization parameters shown in Figure 1 below, would be very similar between the atmospheric test rig and the

pressurized fluidized bed test rig. The slightly larger box of the dark brown atmospheric rig indicates that this test rig can be used for slower or faster test flows. Larger particles can, of course, be loaded into the test rig, but this has not been done. It is an option for the future if some of the particle reaction and fluidization control risks make it necessary in Phase II.

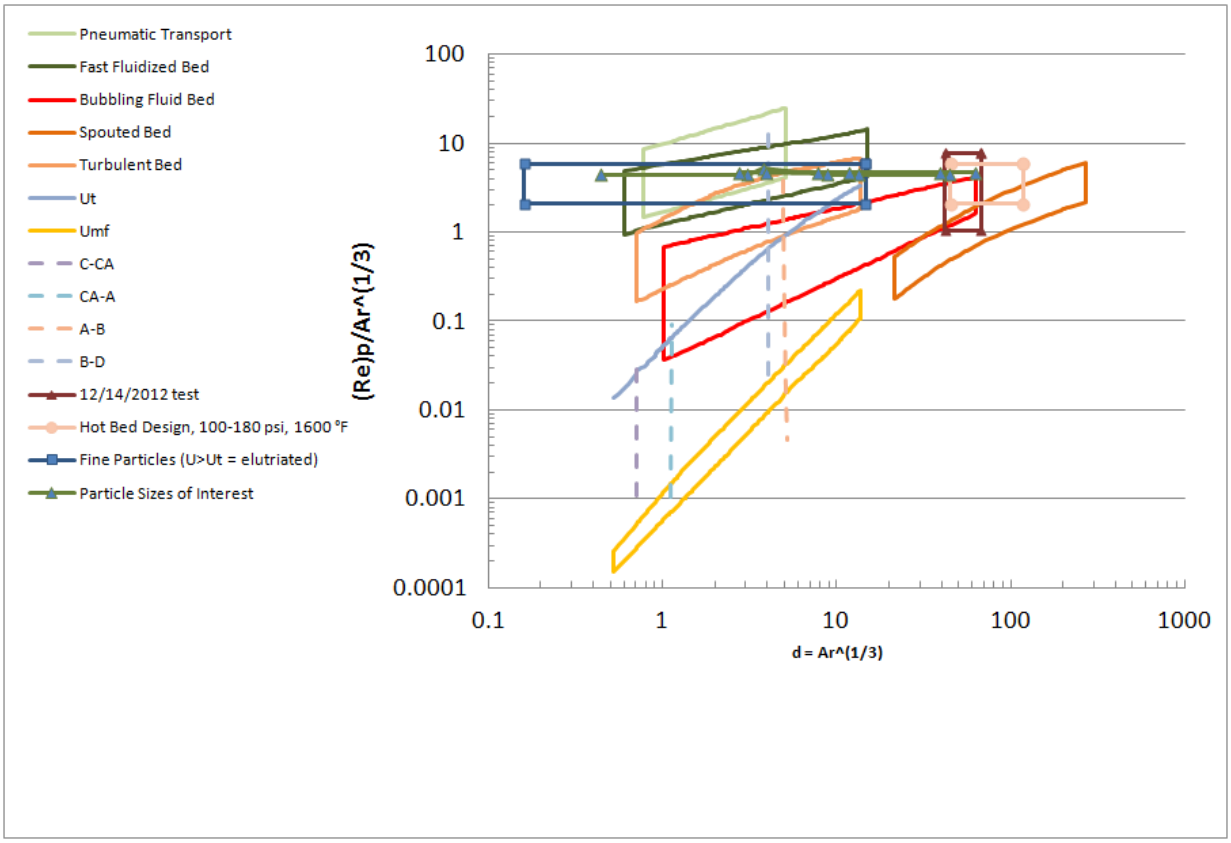

Figure 1: Fluidization Regime Comparison Between Cold Flow Rig and PFBC

Objectives

The test objectives for cold flow testing include:

1) Measure heat transfer coefficient at different bubbling velocities and in different levels of the fluidized bed, and compare these results to correlations in literature.
2) Measure bed pressure drop and volume expansion as a function of flow rate.
3) Measure pressure fluctuations and bubble growth as a function of velocity and heat exchanger packing density, and develop design parameters that minimize fluctuations and bubble growth.
4) Measure particle pressure if possible; examine the utility of particle pressure sensors.
5) Use injector designs similar to the Rockwell tests in 1983 and visually examine the plume. If the plume is very uneven, attempt to measure it.

6) Measure fine particle elutriation rate as a function of superficial velocity and particle size, and compare these results to correlations in literature.
7) The correlation of the data obtained from this sub-scale testing allows bed to tube heat transfer coefficient to be determined to within 10% for a given set of parameters. This will reduce the uncertainty in the overall heat transfer coefficient, U, and the predicted heat transfer surface area for the FBHE to within 5% error during the FBHE sizing process.

Methods

Use Silicon Carbide (SiC) as a coal simulant. It has a similar density and will be easily visible through the acrylic window. Phase I tests showed that limestone had problematic hygroscopic properties, which made it stick to surfaces even in low humidity air.

Examine the heat transfer coefficient near the disengagement level of the bed, and also measure any change when simulated coal (SiC) particles are introduced. Prior tests demonstrated the accuracy of the Molerus correlation to predict heat transfer coefficient on two different particle sizes.

Test variations in the range of space between the "coal" injector and the first bank of tubes of 6" to 24". Prior work in Phase I determined that injector designs may require between 6" and 24" to get complete mixing.

Tests of at least three particle sizes should be performed for elutriation rates.

Plume measurements may be done with video or photographic evidence. If particle measurements are necessary, a sample probe may be used to check the particle delivery.

Determine the relative accuracy and general correlation of particle pressure versus sensor design. A particle pressure sensor from reference 4 appears to be useful to measure gradients from bubble intensity.

Experimental

Basic Description of the Test Rig

In November 2012, a 12" x 20.5" x 20' AFB was constructed at Aerojet Rocketdyne's AR Innovations facility located in Simi Valley, CA.

The test rig was built using mostly non-industrial grade materials, and was intended to be an inert "cold" flow test apparatus. The test rig consisted of the following components: a pressure vessel, an air blower, an air injector/distributor plate, heat exchanger tube simulators, spherical glass fluidized bed particles, an exhaust and filtration system, and instrumentation.

The rectangular pressure vessel had an internal volume of 20.5 inches wide by 12 inches deep by 23 feet tall. The floor, back, and two side walls were constructed of ¾ inch plywood. 2x4s were framed around the plywood, and were spaced every foot in elevation. The seams were sealed with fiberglass and epoxy. The front was made from ¾ inch thick clear Acrylic to allow for visibility into the test rig. The plastic windows were braced with rectangular aluminum bars attached to a flange made of steel angle bracket, which was bolted to the plywood. The pexiglass was sealed with low temperature RTV silicone, which could hold the internal pressure of 2 psi, but still could be removed in order to switch out internal components. The bed particles were made of technical grade borosilicate glass beads, 1 mm diameter, which have approximately the same density as dolomite, the projected pilot plant bed material.

A Sonic 150 centrifugal blower is used to provide air flow to the system. The blower was purchased at Sonic Air Systems in Brea, CA. The supplier mounted the blower to a 20 hp motor owned by AR. The blower was bolted to the floor, and connected to the pressure vessel via a 6 inch PVC pipe. AR's Engineering Development Lab (EDL) calibrated the PVC pipe with a pitot tube flow indicator in order to provide air flow measurements for the system. During initial testing, four different measurements of mass flow were used until the test engineers determined the high range delta pressure transducer was well calibrated and gave very accurate indications of flow. Calibration of the pitot tube and pressure transducer was done with pressurized nitrogen flowing through an orifice calibrated to NIST standards in metrology with an accuracy better than +/- 1%.

Blower motor speed was controlled by a variable frequency drive. There was a manual dial and an on/off switch so that the motor could be turned up or down slowly or rapidly shut down when the switch was flipped.

To inject and distribute air into the fluid bed, an injection system was devised. The injector consists of a welded metal frame with screen on top to keep the bed particles from flowing through. The frame provides about 2 feet of open space between the floor of the pressure vessel and the screen barrier. The screen is built from various

layers of perforated metal sheet, with coarser layers providing rigidity, while the finest layer provides a particle barrier to prevent back flow of bed inventory. Above the frame and screen, a replaceable plywood sheet was fastened in place and sealed around the edges. The plywood sheet had injector bubble caps with orifices sized to produce about 10% pressure drop (bed mass x 0.1) at full flow rate. This was modified later to take out 20% pressure drop to enhance stability.

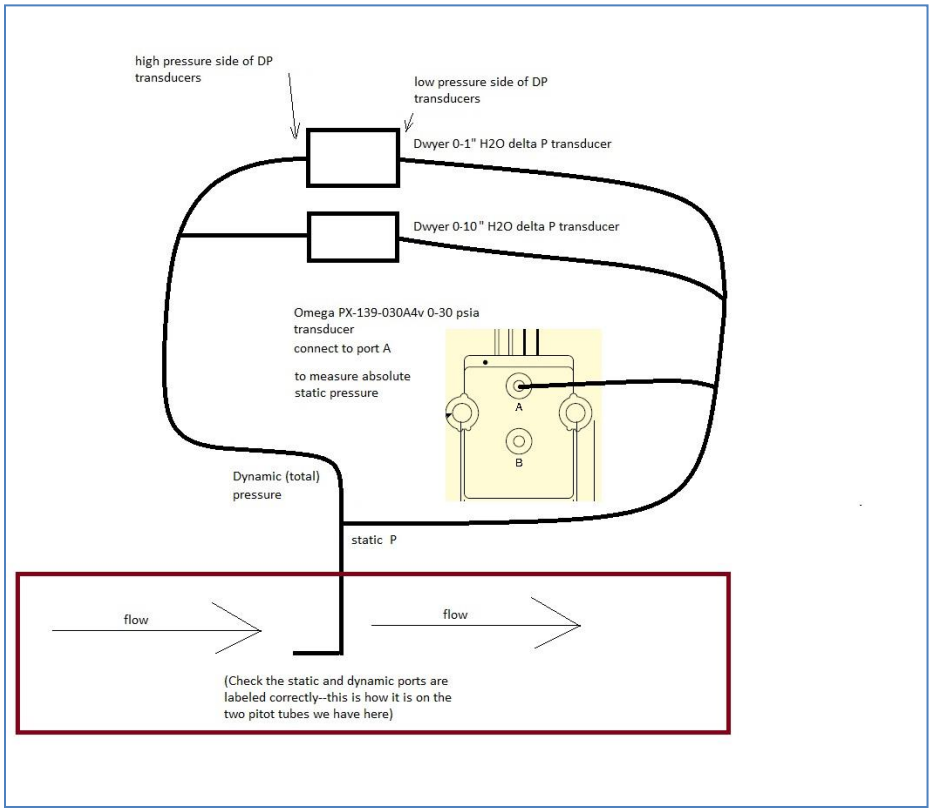

Figure 2. Calibration of Pitot Tube

The frame and screen were built to support the weight of the fluid bed. Air enters the bottom of the pressure vessel side wall, equalizes in the open space, finally trickles through the screen and then through the bubble caps. Initial testing with freshly loaded bed particles was done slowly to determine minimum fluidization velocity (U_{mf}) for a particular bed material and load. This was then analytically matched to the sphericity and void fraction, ε_{mf}.

The fluidized bed particles were 1 mm glass or 1.8 mm alumina beads. Upwards of 500 pounds of beads were fed into the pressure vessel, and filled a space above the injector. The pressure vessel height was high enough to provide sufficient free board to keep the particles from leaving the pressure vessel. The alumina beads were problematic because they tended to grind into a fine buoyant powder when fluidized, and would create a lot of debris within the test facility. As such, the glass beads were

subsequently used for the rest of the tests. The one test with larger beads clearly showed the drop off in HTC as a function of particle diameter.

At the top of the vessel, a hole was cut out to exhaust air from the rig. Originally a filter bolted at the top of the vessel provided filtration, however, the alumina quickly clogged the filter and reduced air flow and pressure drop across the bed. As such, the air was routed through an exhaust duct down to the bottom to the floor of the facility and subsequently outside. The power of the exhaust blower was probably assisting the Sonic blower, extending the operating range of the test unit.

The rig was instrumented to provide pressure, temperature, power, and flow data. Absolute pressure probes installed at the top and bottom, and delta pressure probes in between, provided a pressure map throughout the rig.

Heat Exchanger Designs

One major trade to be decided for the PFBC design was to examine concepts for the heat exchanger designs. Both horizontal and vertical tubes had been discussed as different options for tube packing. Horizontal tubes typically provide for better heat transfer coefficients, but are more prone to erosion. Vertical tubes require baffles for bubble breakup and more tubes, but can be easier to design manifolds for certain steam generator designs. The literature indicates that the primary factor in improving emulsion side heat transfer coefficient is the size and heat capacity of the particles making up the bed. A secondary consideration is packing fraction. A tight packing fraction will allow smaller heat exchangers, but there is theoretically a density at which adjacent tubes do not allow enough particle movement to develop full mixing and thermal equilibrium, which is to say that they interfere with each other, however the various published papers were not unanimous in this. Grimethorpe's data indicates that high packing fractions can be as efficient as lower ones, and due to the GTI projected heat release profile, this is desireable.

Three specific setups were tested, one with vertical tubes and two different baffle designs, and two with horizontal tubes, but with different packing densities.

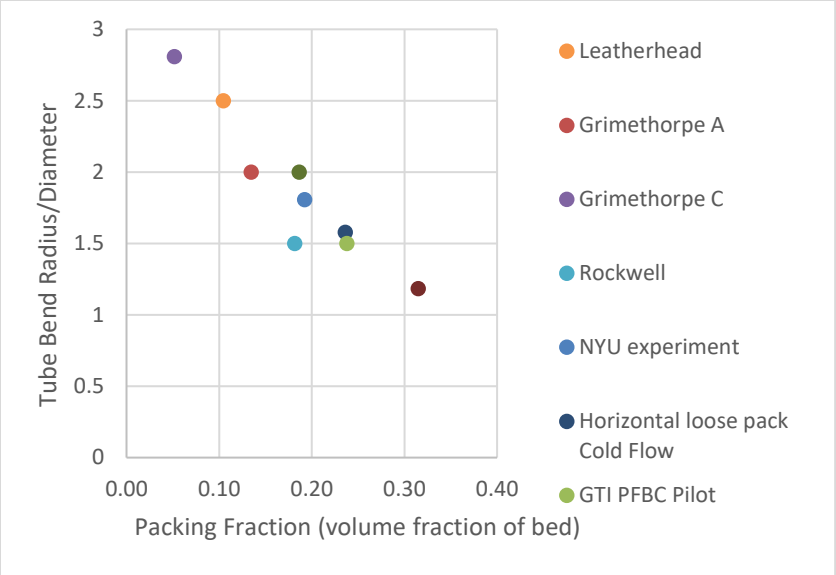

Figure 3: Comparison of Packing Fractions and Bend Radii for Various PFBC's

One of the packing arrangements are shown below in Figure 4.

Pipe bends were not provided in order ease manufacturability and to give a more representative flow pattern in the center of the bed.

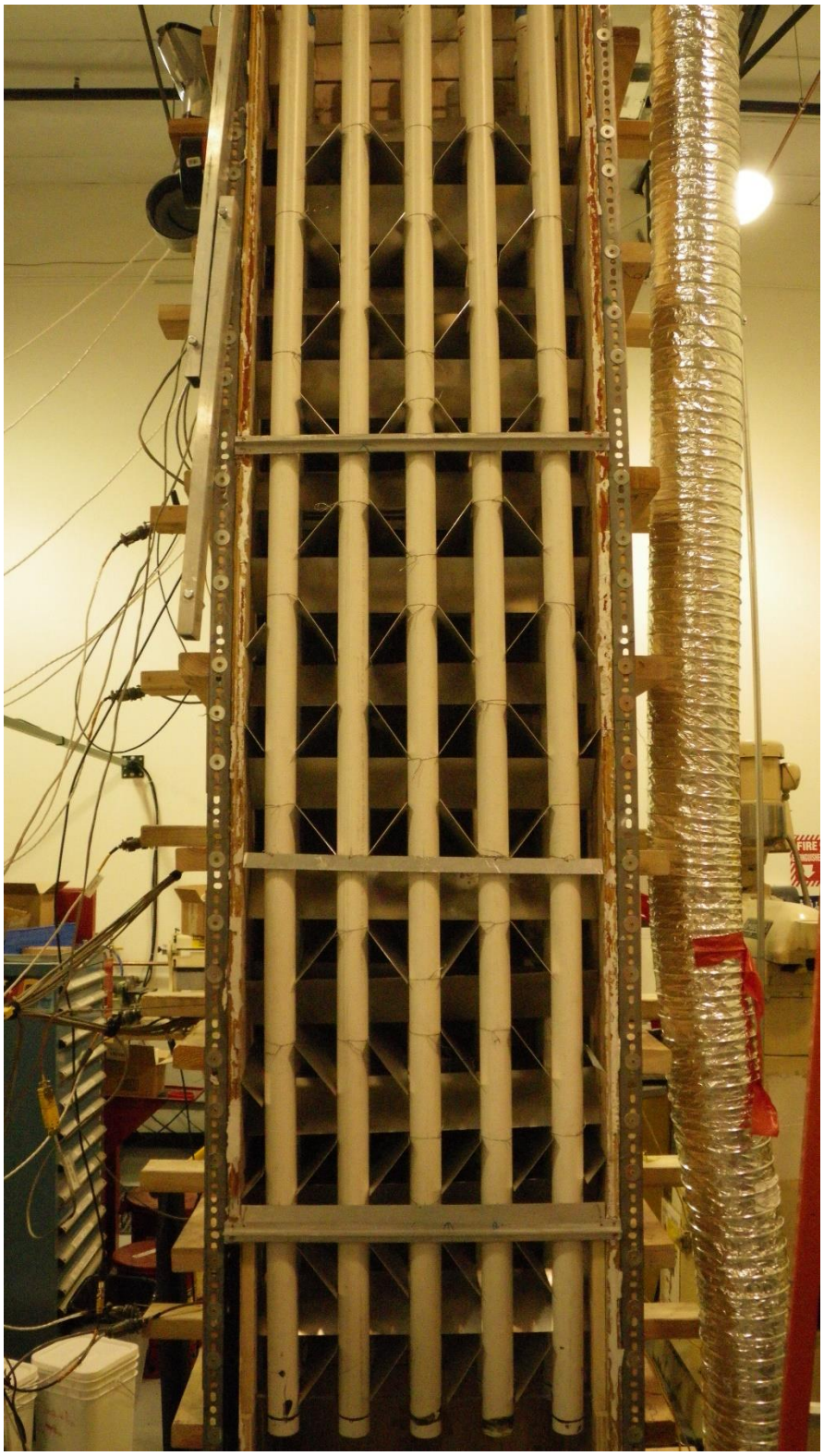

Figure 4: Vertically Installed HEX Tubes With Two Different Baffle Arrangements.

Test Rig for Heat Transfer Measurements

Heat transfer coefficients for different particle sizes and bed packing fractions in the range of interest for the PFBC were measured and compared to predictions from the various correlations in literature. This was done in "reverse" heat transfer fashion: tubes were constructed with internal heaters and heated electrically. The horizontal arrangement of these tubes is shown in Figure 5. The wattage was measured using volt-amp instrumentation, and the surface temperature was directly measured using thermocouples firmly clamped to the tube surfaces. Dozens of thermocouple measurements were also taken at various locations throughout the bed to establish emulsion temperature.

Special tubes were constructed of aluminum pipe the same diameter as the PVC pipe. These tubes held 3 kW hot water heaters which were cemented internally with high heat transfer coefficient silicon carbide castable refractory (St. Gobain GC-904) and they were instrumented with thermocouples. In two places inside the test rig, PVC tubes were replaced with these cement-encased electric hot water heaters. The heater voltage was controlled by a Variac up to 240 volts. Voltage, amps and surface temperature were measured, and the combination of these measurements and the fluid temperature enabled direct calculation of the surface heat transfer coefficient. They were capable of being operated up to 650°F without overheating the bed walls, which is a ΔT of 540-580°F, similar to expected fluidized bed temperature differences in the commercial design.

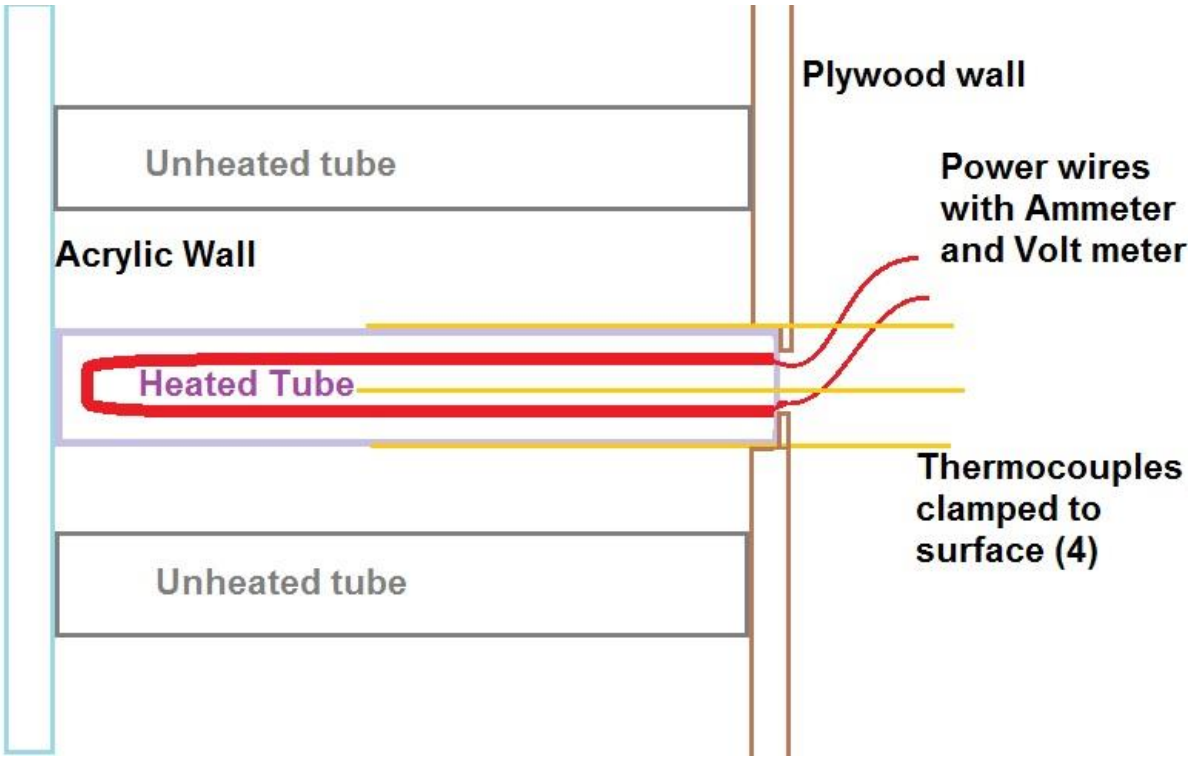

Figure 5: Simplified diagram of heater tubes.

Thermocouples were installed upstream and downstream of each heater, as well as around the heaters themselves. Voltage and current into the heaters was used to calculate heat being pumped into the system.

Particle Elutriation Test Rig

In May 2013, the test rig was modified to conduct testing to mitigate the risk associated with the uncertainty with the current chemical kinetics model. At the time, it was unknown if the coal utilization and/or sulfur capture would be able to meet the target efficiencies. Through testing, AR determined the magnitude of the limestone velocity/residence time through the in-bed portion for various limestone particle sizes.

The eductor and hopper were designed to push granular solids into the fluidized bed, scaled off of the total coal plus limestone feed rate per square foot for a commercial PFBC design condition, and we designed the hopper to hold 20 minutes of inventory at that flow rate. Initially we looked at ordering the eductor from one of two companies, Elmridge or Shutte & Koerting. We settled on using the Shutte & Koerting unit because it was a sturdier steel design and ready to ship, whereas the Elmridge units were plastic and four times as expensive and had a three week lead time. The hopper was locally fabricated out of acrylic to make it easy to see the material flowing out. We did an original test at 60 PSI and measured the feed rate, which was about twice as high as the manufacturer's estimate.
It should be noted that the hopper that feeds the material into the eductor is pressure-equalized with a feed line from the bed to ensure that the hopper doesn't blow dust into the room, which could account for the difference between our measured solids flow and the manufacturer's estimate. The input pressure to the eductor was lowered to 30 psi which then led to an acceptable feed rate.

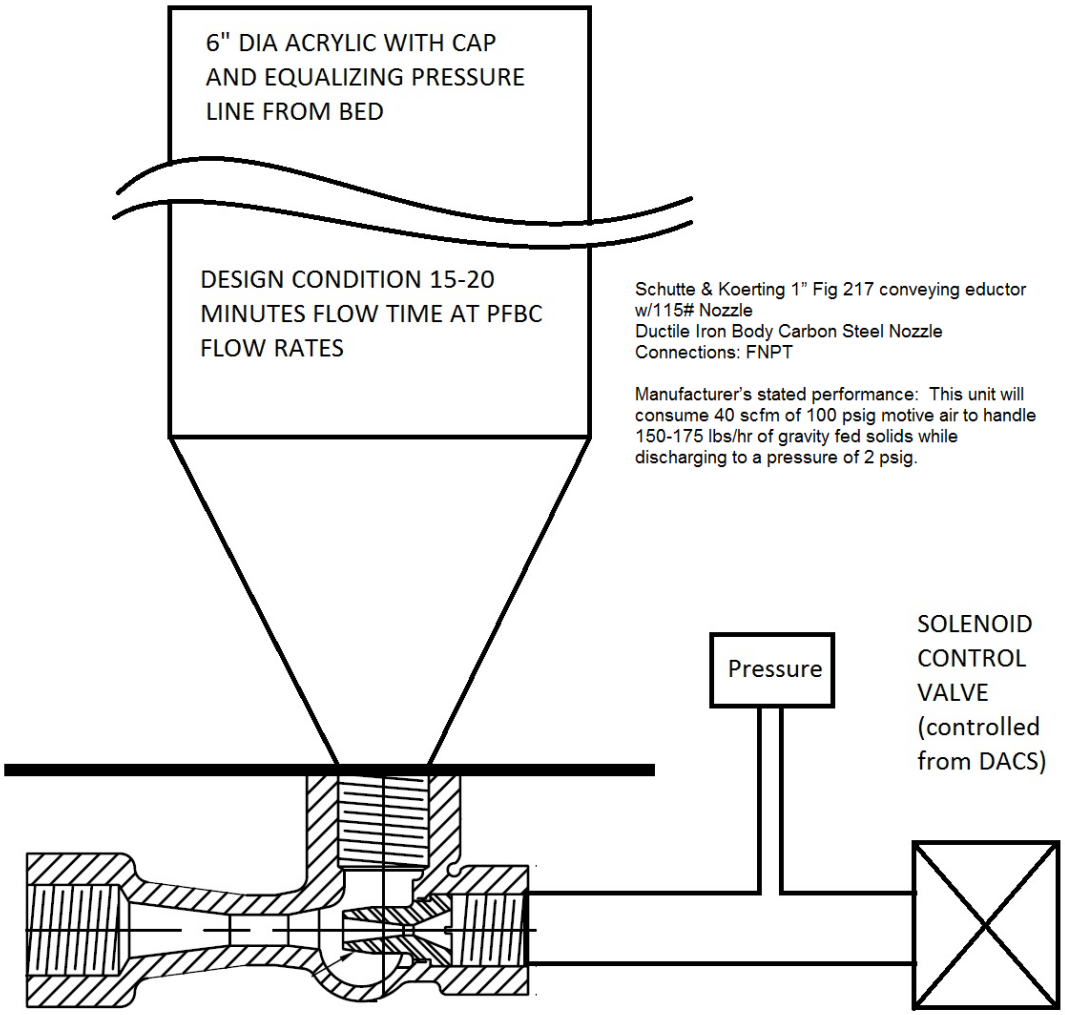

Figure 6: Eductor/hopper assembly for cold flow unit elutriated solids injection

The hopper is used to hold the calcium carbonate. The hopper was designed to hold approximately 60 to 80 lbs of material. The hopper is 6 inches inside diameter and 6' long. The bottom of the hopper is funnel shaped to direct the calcium carbonate into the educator input. The hopper funnel has a 60 degree included angle.

A cyclone is used to remove particulate form the exhaust flow. The exhaust from the top of the column is routed to the cyclone and the particulate drops out of the bottom and the exhaust is routed to four felt filter bags. It was originally noticed that when using one filter bag the bag would clog and increase system back pressure before the test was completed. Additional bags were added to decrease system back pressure.

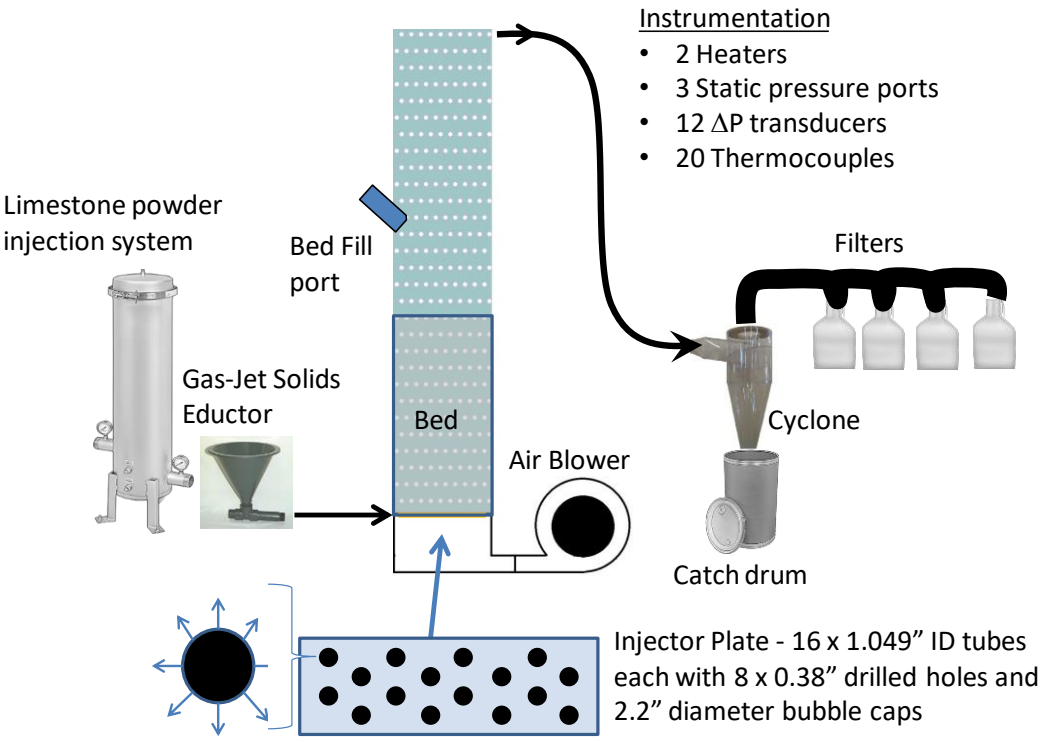

Figure 7: Simplified diagram of test setup

Particle Pressure Measurement "Dragometer"

Another specially instrumented tube was constructed following the design and method described in the paper by Johnson and Flemmer[12]. The tube is machined with slots providing a cushion of air so that a cylinder floats, much like a hovercraft. The slots providing the air are tightly tolerance so that particle pressure which impacts the surface will alter the pressure balance of the air supply. This is detected as offset pressure in the horizontal and vertical axes. See the figures below. The instrument was calibrated in both the horizontal and vertical directions by hanging weights on the ring to develop a relationship between the offset pressure and the magnitude of the signal.

The calibration curves are shown in Figure 9.

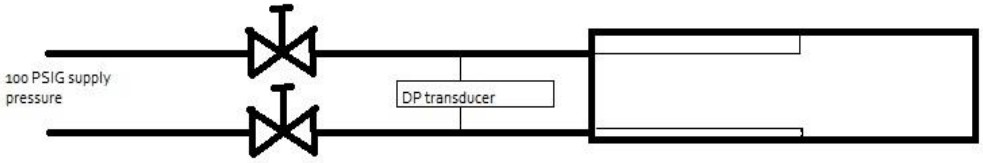

Hand Valves are set to provide about 20 psig to the orifice, which is unchoked.
The valve throats themselves ARE choked as long as the supply pressure
remains well over twice the orifice absolute pressure.

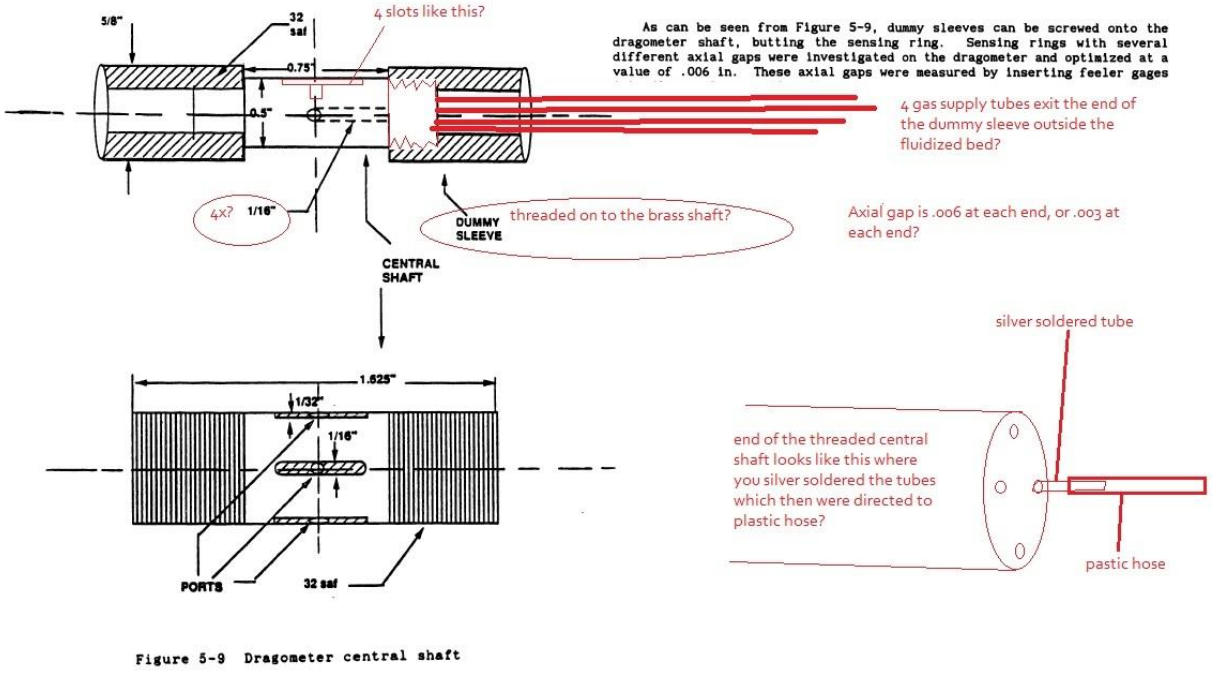

Figure 5-9 Dragometer central shaft

Figure 8 : "Dragometer" Design From Reference

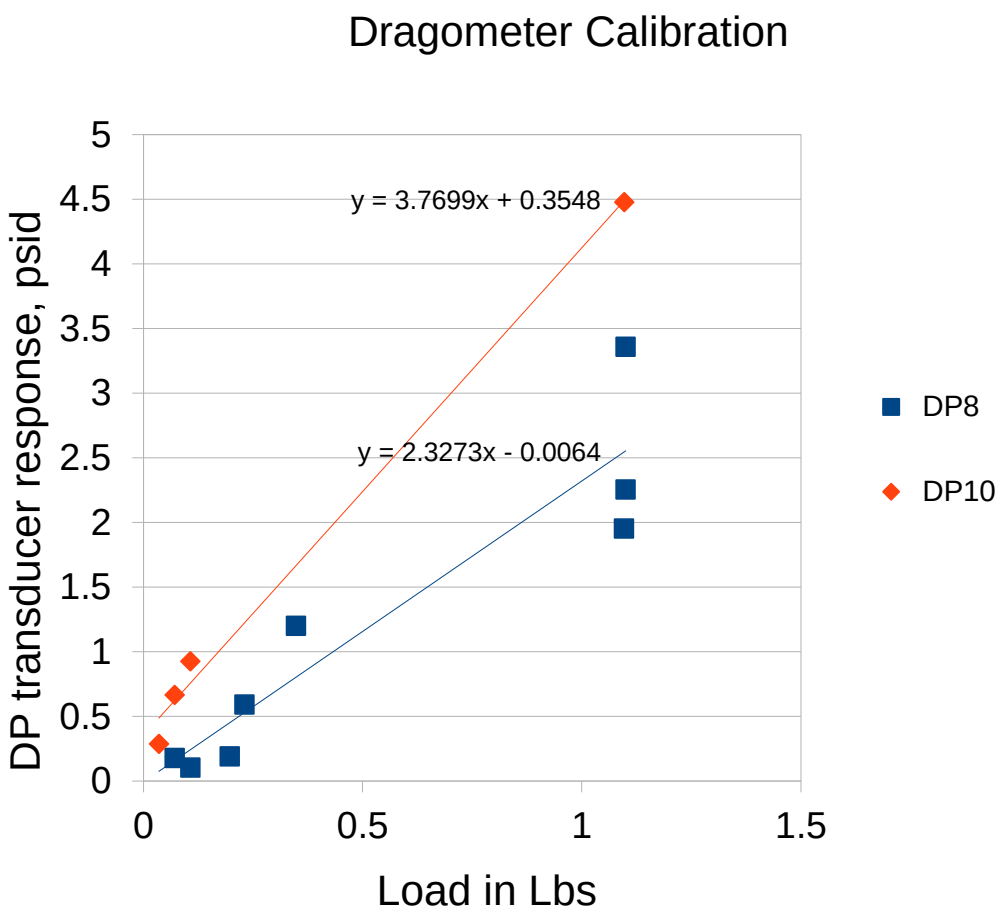

Figure 9: Dragometer Calibration

Figure 10 : "Dragometer" Assembly Prior to Installation

Results and Discussions

Basic Findings from the Cold Flow Testing

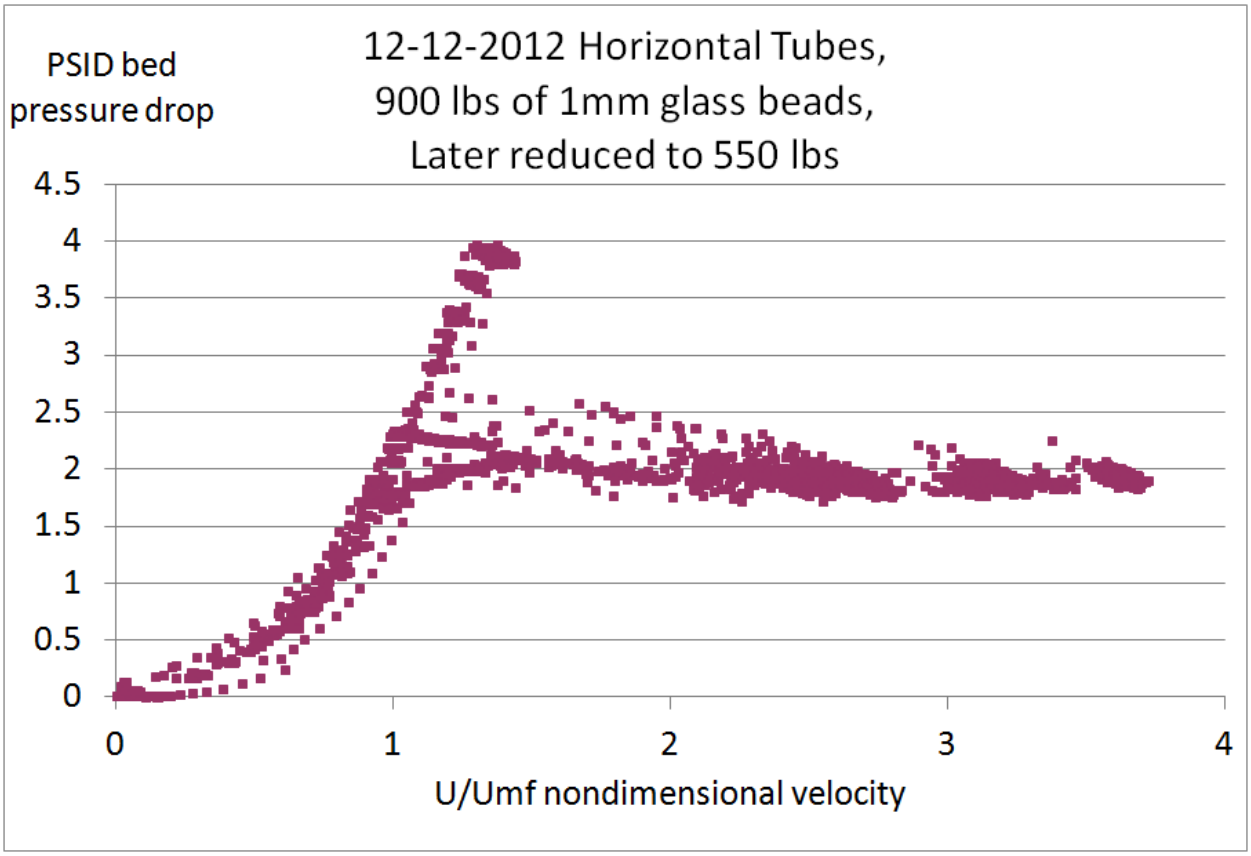

Figure 11 : Determination of Minimum Fluidization Velocity

Figure 11 shows how Umf is experimentally determined. The flow rate is increased until the bed pressure drop no longer increases with increasing flow rate. The inflection point is Umf (defining the x-axis locus U/Umf=1 in the figure). Minimum bubbling velocity, Umb, is just above that, and is defined as the velocity when bubbles appear. This is not visible on the graph. The portion of data which extends up to 4 psi was taken when 900 lbs of material was in the bed. The blower was unable to loft the entire bed at this mass, so 350 lbs were removed, at which time the bed was properly sized for the capacity of the blower, and tests could go all the way up to 3.5x Umf. If higher velocities are desired, the bed could be made smaller in width. The PFBC is designed to operate at 2.5-3.5 * Umf.

The first phase of testing showed a low frequency pressure oscillation in the bed. Modifications were made to the bed that eliminated the issue and led to stable bed operation as shown in Figure 14.

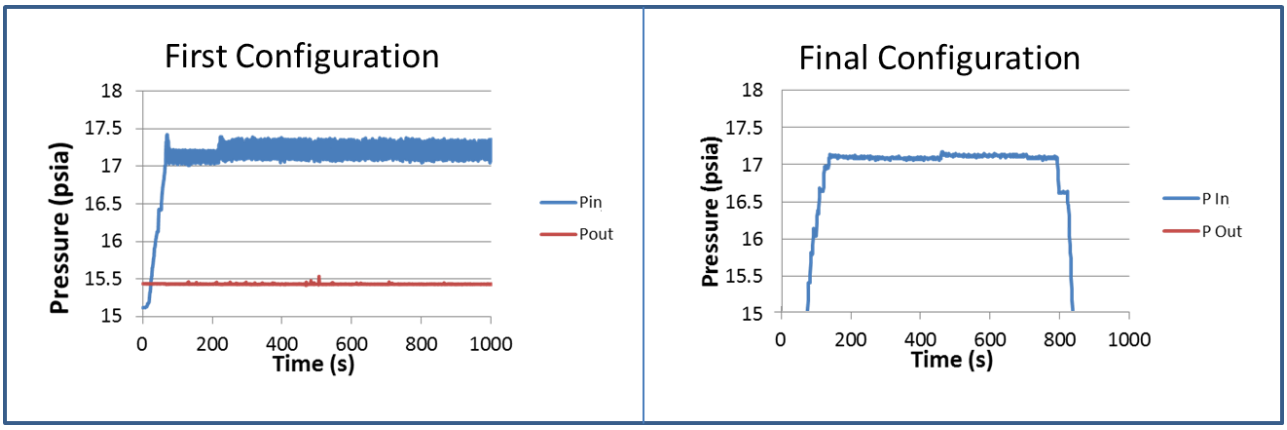

Figure 12: Bed Oscillation Improvements from Design Changes

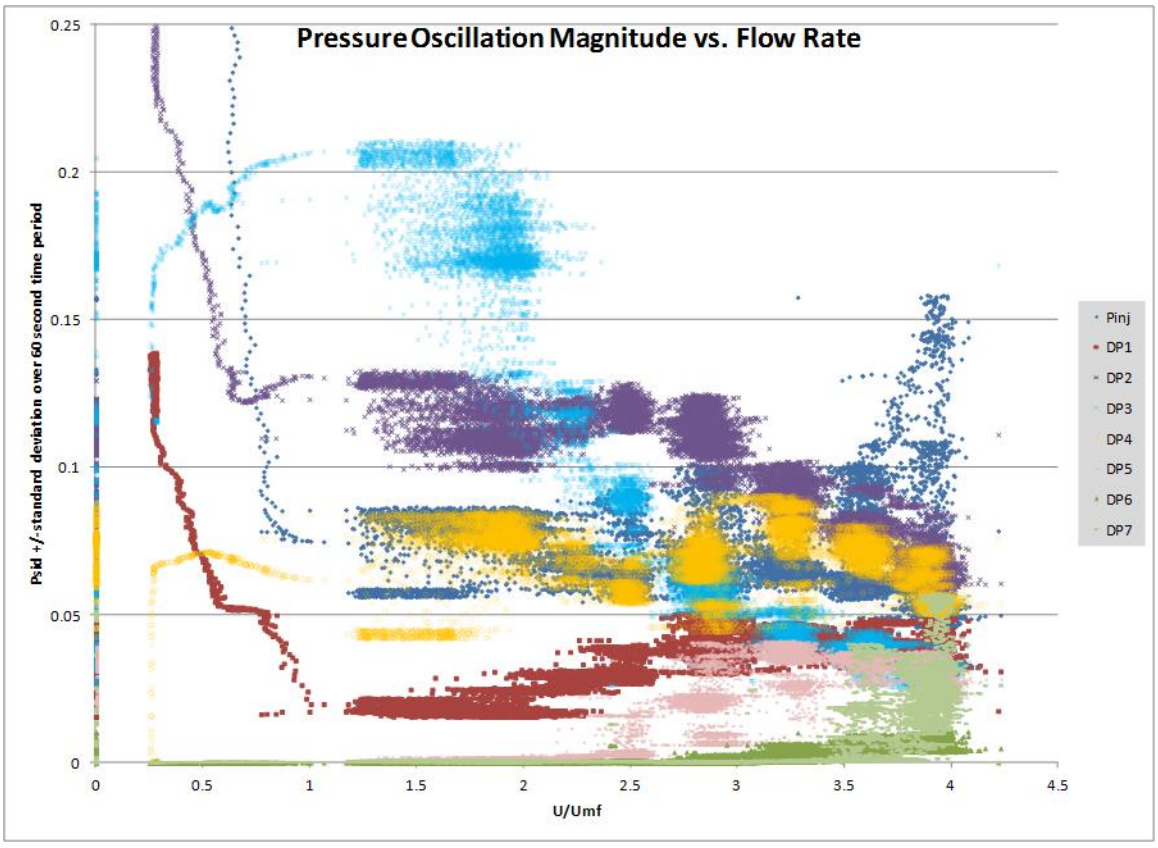

Figure 13: Bed Oscillations as a Function of Flow Rate

Figure 13 shows the instability problem in a different way, as a function of velocity. The Y-axis is plotting the standard deviation or noise level of delta pressure measurements. Between U/U_{mf} of 1.5 and 2.5, the standard deviation of the ΔP is seen to be almost double the magnitude of the pressure transducers at the maximum flow rate of 2.5-4

U/U_{mf}. This is due to the transition from bubbling bed regime to turbulent bed (shown earlier in Figure 1). Between 3.5 and 4 U/U_{mf} a different phenomenon is seen, where the injector pressure drop (dark blue symbols) becomes noisier, which may be signaling the onset of another regime: pneumatic transport. This quiet zone between 2.5 and 4 was selected for the bulk of the tests in this investigation for this reason and because video evidence shows very smooth operation, uniform bubble size, and even distribution of particles in the bed.

Bed Expansion and Height Measurement

Another important basic measurement in a fluidized bed is bed height and mass. It can be shown that the mass is directly measured by the pressure drop across the bed after reaching the minimum fluidizing velocity (see the discussion of Umf above), but the bed height cannot be directly measured in a pressure vessel except by instrumentation. The pressure drop across the vertical direction is nearly linear, and this property can be used to construct a line whose intercept with the freeboard pressure is a reliable indicator of bed height. Physical measurements of the cold flow bed with a ruler can be used to validate these algorithms.

Figure 14 shows a typical graph of bed expansion. As the air flow is increased, the bed begins to expand, and more of the pressure transducers are engaged in measuring fluid bed pressure drop.

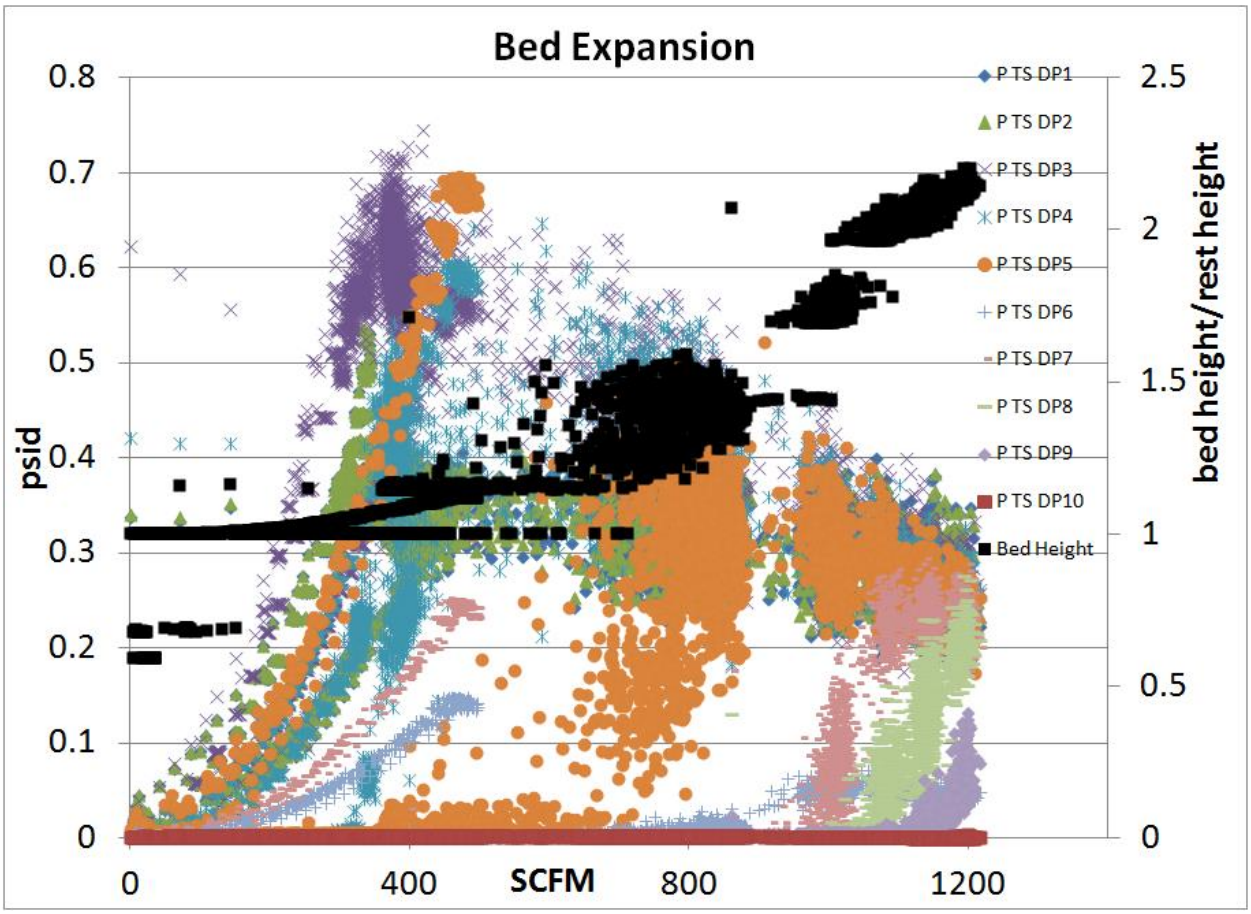

Figure 14: Bed Expansion as a Function of Flow Rate

Two different methods of obtaining a height measurement were employed. The first uses an average pressure drop per foot to obtain a straight-line intercept with the freeboard pressure, and the second method relies on selecting the highest "active" pressure transducer and the known height of that transducer to interpolate a height. This is depicted in Figure 15. All of these methods have noise and idiosyncratic difficulties. It is clear that some sort of averaging will have to be used, and operators will have to use judgement to control bed levels via ash removal valves. A more accurate modeling of the ΔP/ΔH curve as a function of bed depth will improve the calculation (this is discernable as the descending slope of ΔP measurements in Figure 13). This must be obtained in cold flow testing of the actual Pilot Plant bed after construction. Ultimately, thermal stability of the bed will also provide a good secondary indicator of bed level, as the number of immersed heat exchanger tubes increases. The next section on heat transfer measurements describes this phenomenon more deeply.

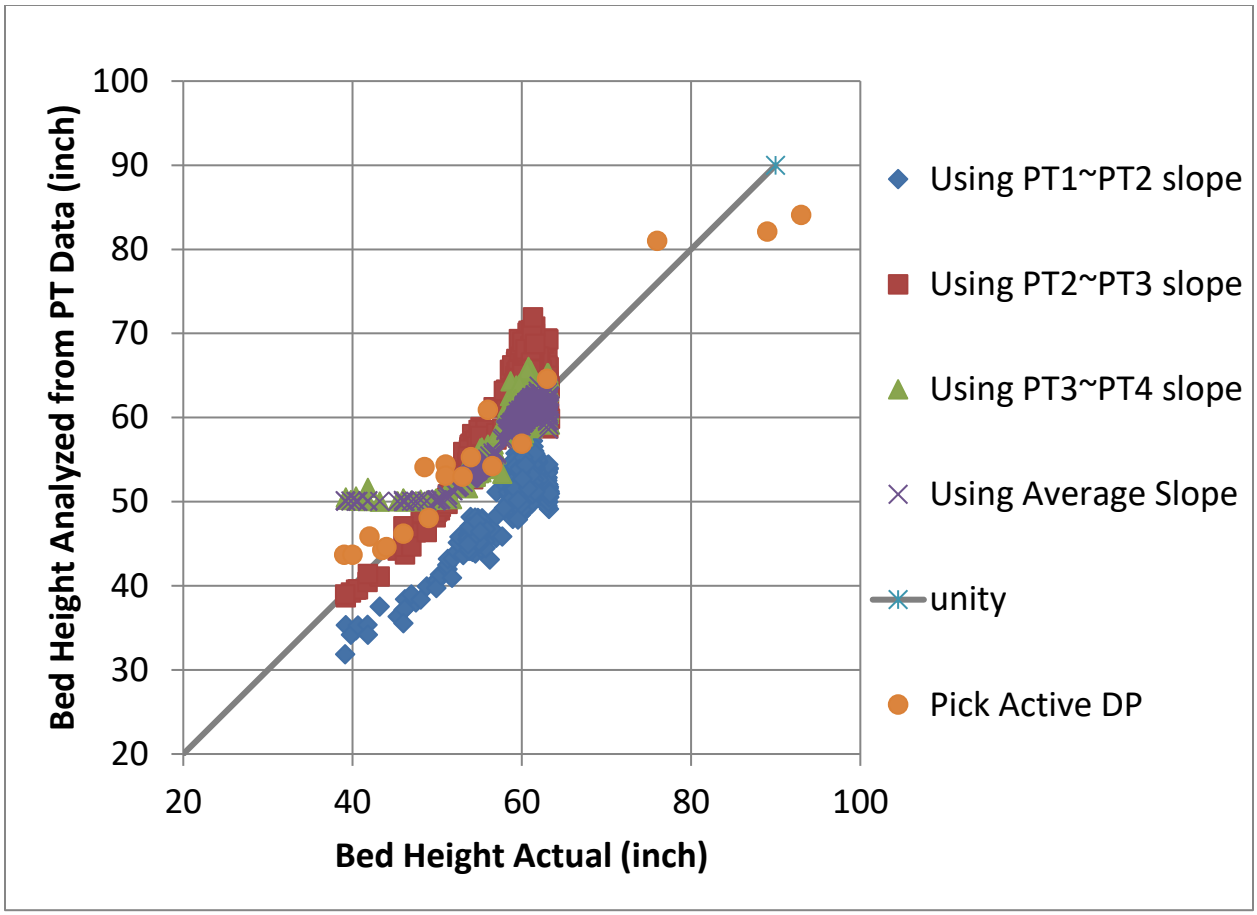

Figure 15: Bed Height Calculation Methods

Heat Transfer Coefficient Measurement

Special tubes were constructed of aluiminum pipe the same diameter as the PVC pipe. These tubes held hot water heaters (3 kW each) which were cemented internally with high heat transfer coefficient silicon carbide castable refractory (St. Gobain GC-904) and they were instrumented with thermocouples. In two places inside the test rig, PVC tubes were replaced with these cement-encased electric hot water heaters. The heater voltage was controlled by a Variac up to 240 volts. Voltage, amps and surface temperature were measured, and the combination of these measurements and the fluid temperature enabled direct calculation of the surface heat transfer coefficient.

The measurement method is as follows: while operating the bed, voltage is turned up to 200 volts. When tube temperatures reach approximately 400-500 °F, the heater is turned down to a voltage which results in no net increase or decrease in temperature. Data taken for the next 10-30 minutes forms the basis of the heat transfer coefficient measurement. Flow velocity is altered and the process repeated, typically with no change in voltage required to restabilize, as the HTC is very flat across a wide range of flow rates.

The fluidized bed particles were 1 mm glass or 1.8 mm alumina beads. Upwards of 500 pounds of beads were fed into the pressure vessel, and filled a space above the injector. The pressure vessel height was high enough to provide sufficient free board to keep the particles from leaving the pressure vessel. The alumina beads were problematic because they tended to grind into a fine buoyant powder when fluidized, and would create a lot of debris within the test facility. After the first such test, these were replaced with glass beads, and the glass beads were subsequently used for the rest of the tests. The one test with larger beads showed the reduction in HTC as a function of particle diameter.

At the top of the vessel, a hole was cut out to exhaust air from the rig. Originally a filter bolted at the top of the vessel provided filtration, however, the alumina beads quickly clogged the filter and reduced air flow and pressure drop across the bed. As such, the air was routed through an exhaust duct down to the bottom to the floor of the facility and subsequently outside. The power of the exhaust fan was probably assisting the Sonic blower, extending the operating range of the test unit.

The first and most obvious thing observed is that all the bed thermocouples were within a degree or two of each other, even those placed within two inches of the heaters. Heat Transfer measurements were in very good agreement with predictions. It will be noted that the upper heaters were often not submerged in the bed. Since they were often in the freeboard zone, they provided a good check against the very well understood and predictable convection coefficient for a cylinder in a free stream.

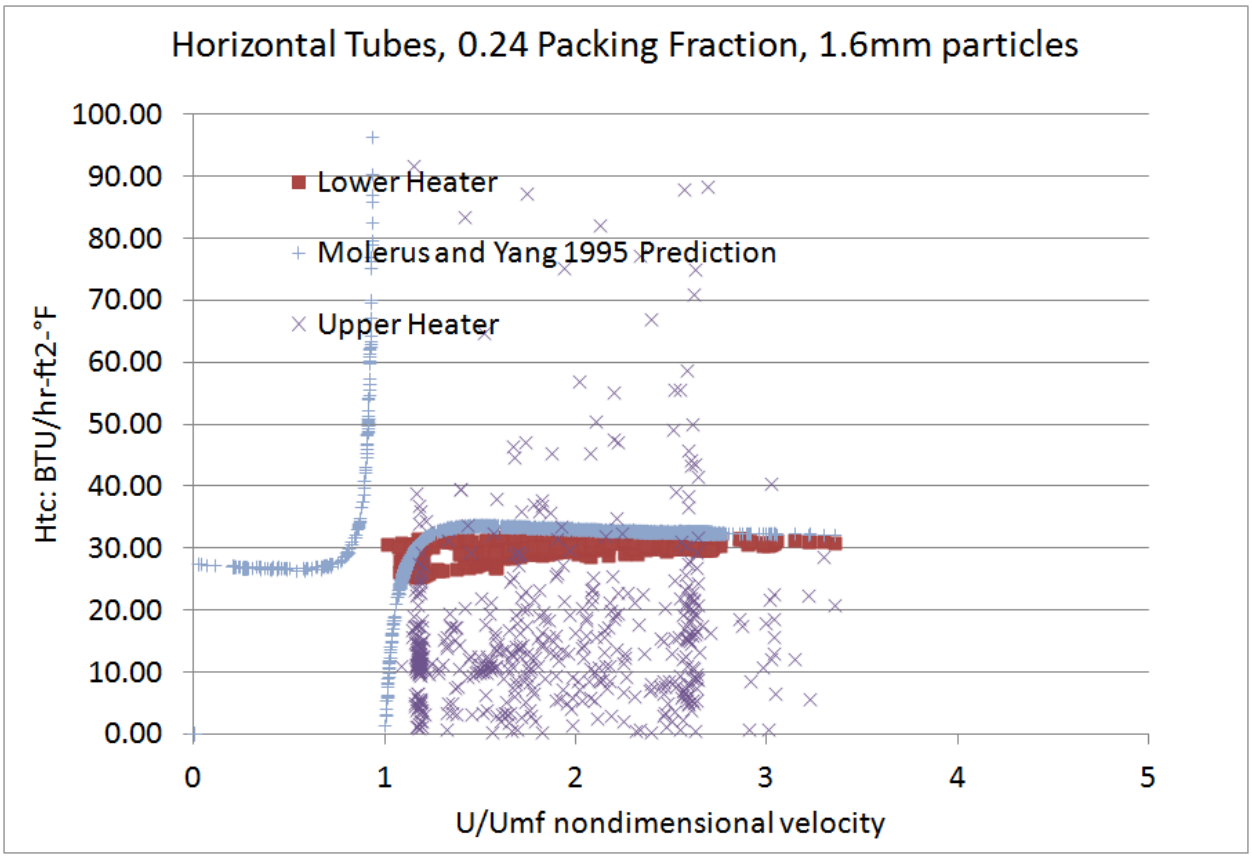

Figure 16: Correlation with HTC Predictions with 1.6 mm particles and 0.24 PF

Figure 16 shows two important effects: the lower heater, which is constantly immersed in the bubbling bed, has very high heat transfer coefficients, and is very stable from low to high velocities; in other words, very predictable. The upper heater, which is located near the interface between the bubbling bed and the freeboard, has very erratic heat transfer coefficient, in other words, unpredictable.

The general effect of bed expansion on heat transfer coefficient is also clearly shown in Figure 17. As the bed expands with higher velocity, the upper heater, originally in the freeboard, enters a splash zone, and then becomes fully immersed. This is illustrated in another way in Figure 18 and Figure 19, which demonstrate two different predictions for bed height as a function of velocity, on proposed by AR Chief Technologist Kenneth Sprouse, and the other proposed by an academic paper by Lofstrand and Almstedt. The previously discussed DP slope and DP transducer select methods of establishing bed height are also plotted. It can be seen that a splash zone exists for several inches above the visually dense bed, which has some effect on the heat transfer coefficient.

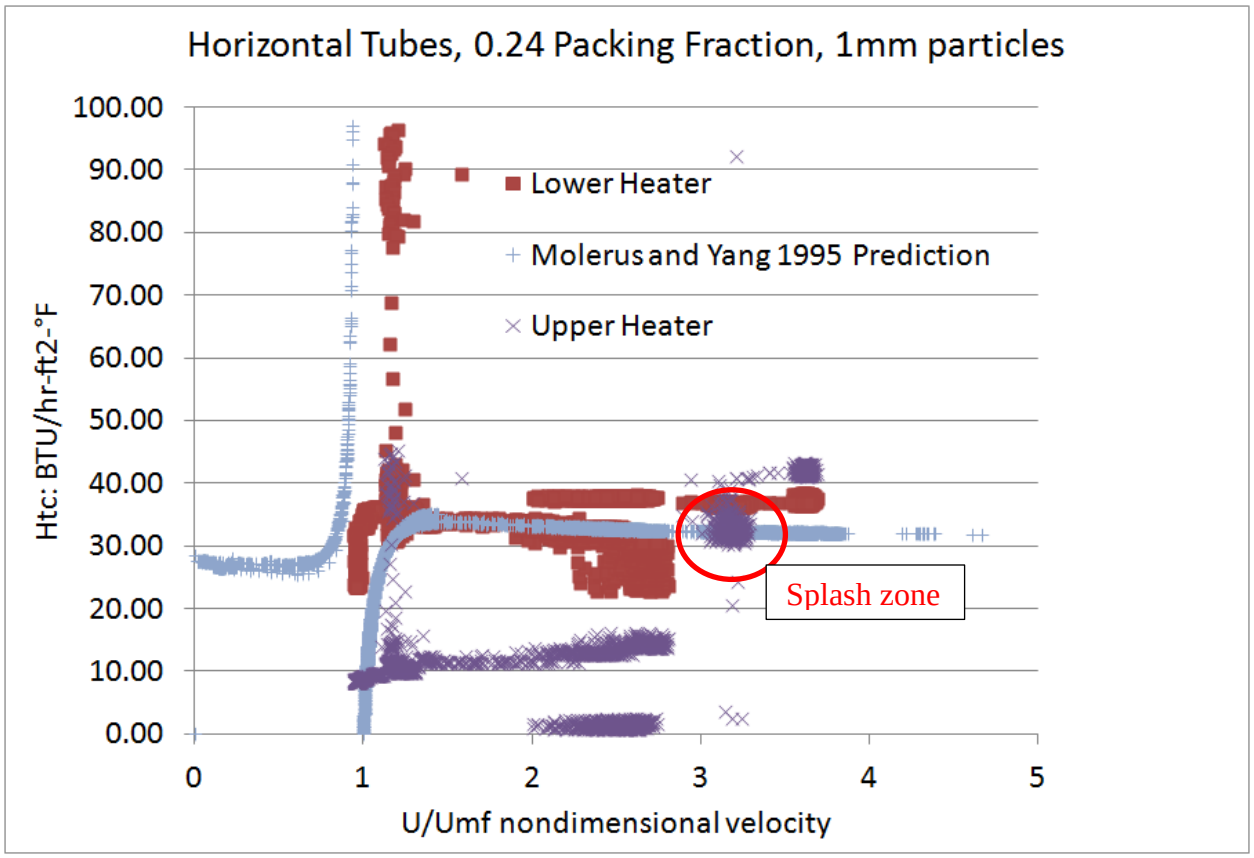

Figure 17: Smaller particle size increases the heat transfer coefficient

Comparing the two different particle sizes at the same packing fraction shows a very clear 10% increase in HTC for in-bed tubes. 1 mm is a reasonable lower practical limit for the inert bed inventory. It is unlikely that reducing the particle size further would allow for proper differentiation between small and large particles required for the AR concept to work. Here the HTC delineation between bubbling bed and freeboard is more obvious: the bubbling bed immerses the upper tube only when U/Umf>3.

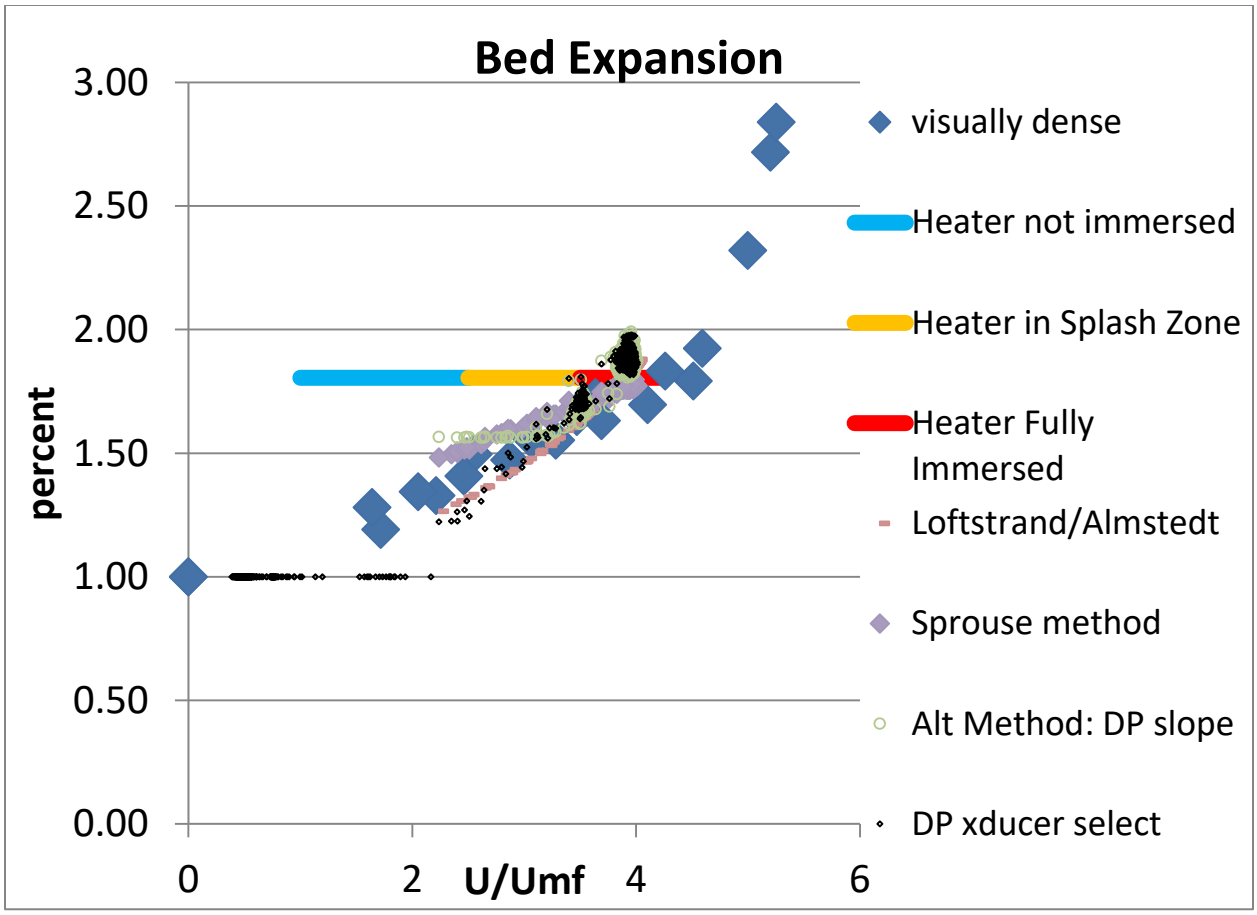

Figure 18: Bed Height Measurement Methods Plotted to Show Upper Heater Immersion, .24 PF

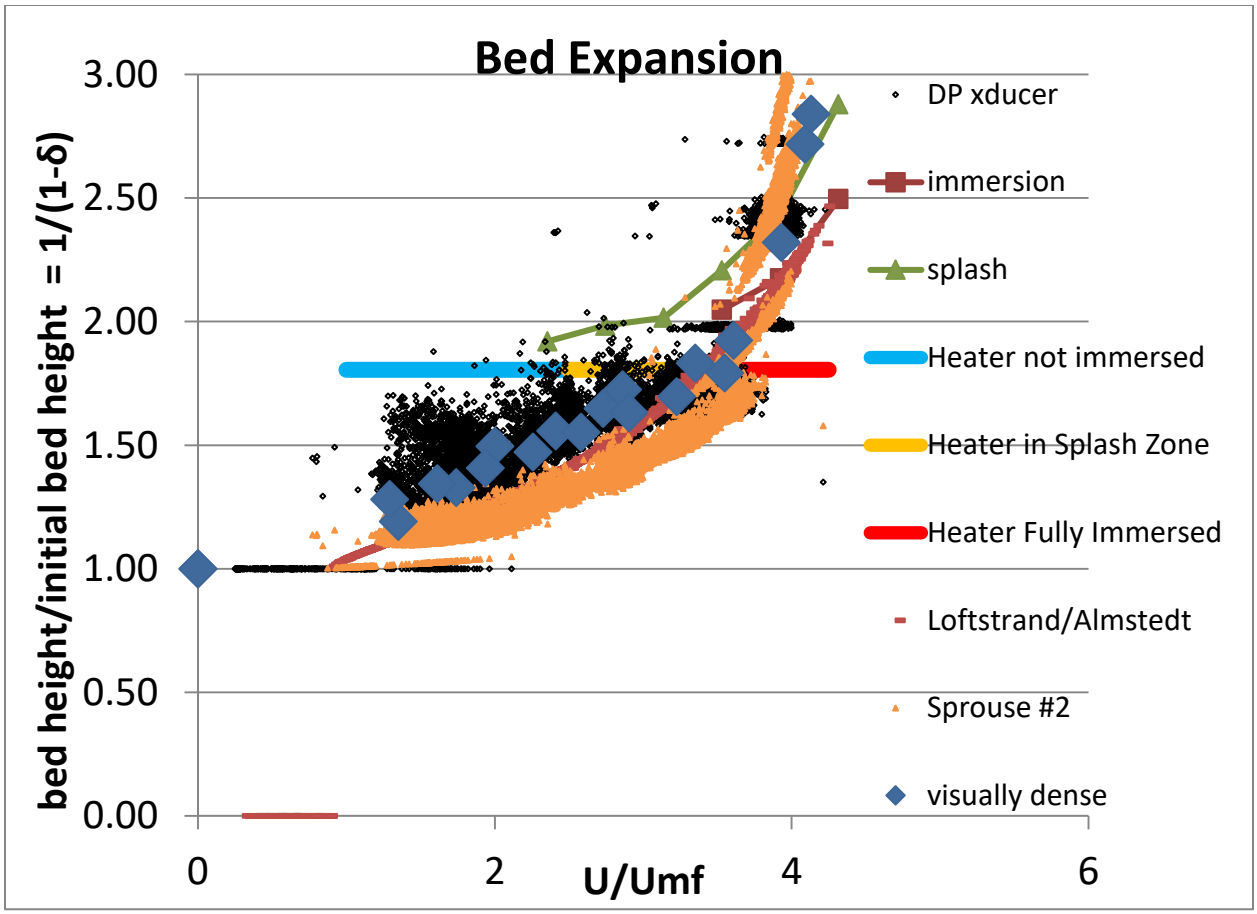

Figure 19: Bed Height Measurement Methods Plotted to Show Upper Heater Immersion, .32 PF

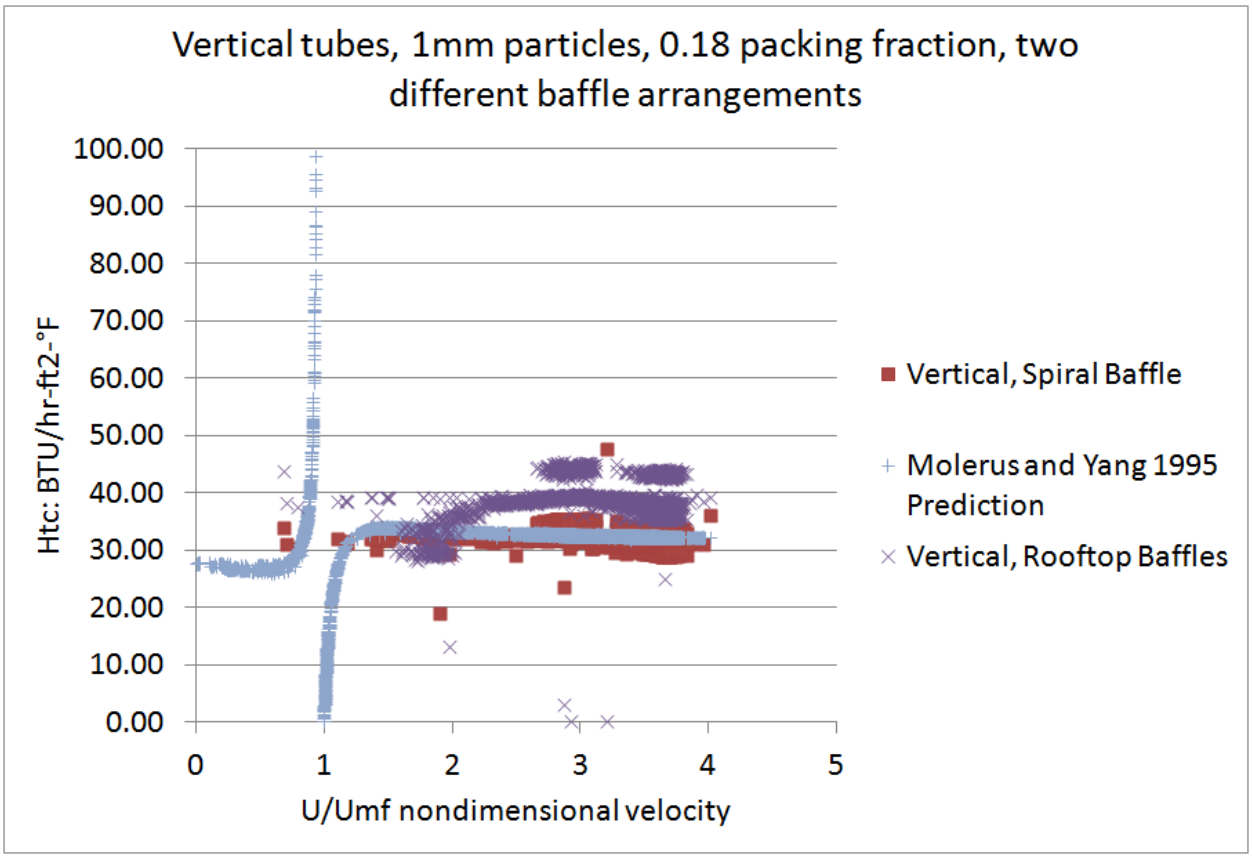

Figure 20: Vertical tubes produce high HTC with extensive baffles

The vertical tube arrangement was tested in order to establish the difference between two similar baffle designs. Although these were fairly simple designs, they were a lot harder to fabricate and install than the horizontal tube arrangements with no baffles. The purpose of the baffles is to control bubble growth and enforce particle/tube/bubble interactions and increase heat transfer coefficient. In many commercial CFB's, only vertical tubes are installed to improve tube life, however visual examination of the flow patterns in this bed does not indicate the tubes are going to be any less prone to erosion. In fact, it appears that zones in direct contact with baffles would be prone to faster erosion, and the baffles themselves would become a maintenance nightmare.

It can be clearly seen that the heat transfer coefficient with these baffles is very similar to measurements taken on horizontal tubes, therefore GTI sees no compelling reason to deviate from the practices which have been used with success in Vartan and Cottbus, which are demonstrating 15 year life on horizontal tube banks similar in design to these historical systems previously described.

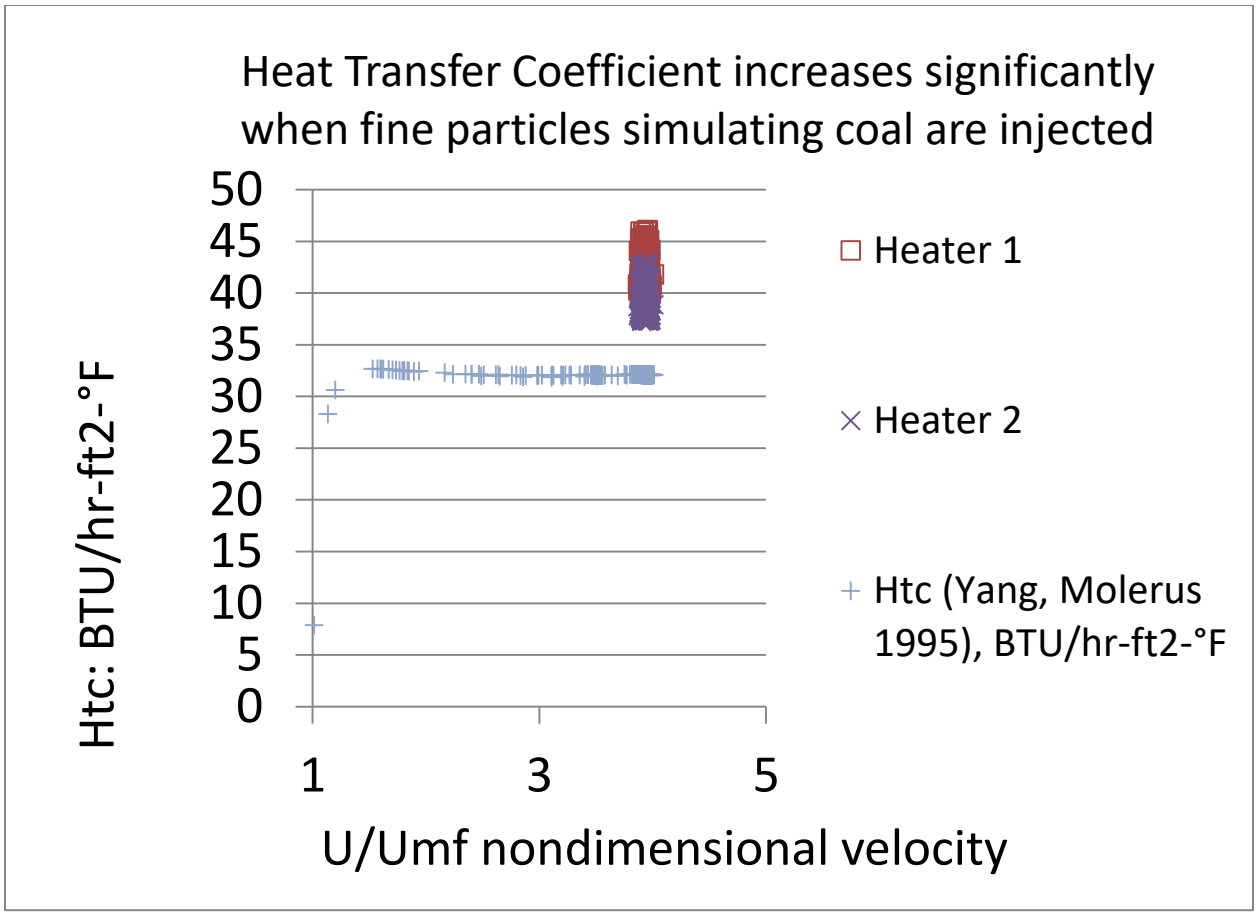

Particle Velocity Measurement

Two sets of tests were performed. The first test series was in December, 2012, using limestone particles, and the second set of tests was performed in May, 2014 using silicon carbide particles. The limestone particle data appeared to give reasonable solutions for particle residence time, however the finer particles tended to completely coat all internal parts, and the amount of data collected was insufficient to select a reasonable correlation from the literature. A less hygroscopic material was selected for the second set of tests.

Particle average velocity is inferred from measuring holdup (mass of fine particles held in the bed) with a known particle inlet flow. From the holdup mass and average bubbling bed height, and by measuring particle injection rate, the average velocity of particles can be determined. Four different particle sizes were prepared by sifting bags of fine limestone. Hubercarb Q40-200, which is 50-500 micron sized material, was separated into three different bins: 300-500, 150-300, and 75-150 microns. A fourth bin of 50-75 was prepared. Hubercarb W-4, which is 1-10 micron material, was used as the finest material tested, but these tests didn't yield any data because the material coated all surfaces and very little came out.

Another issue that was discovered during data analysis is that only using the bed mass at a single point in time was difficult to model analytically, due to insufficient information about whether or not the system had reached steady state. For the second set of tests, both the inlet flow and the outlet flow were measured every 30 seconds.

All the tests were conducted by following the procedure listed below.

- Turn on Data Acquisition and Control System (DACS) and verify instrumentation readings
- Run the air blower until left over limestone from previous tests are ejected out of the system
- Clean out catch drums and filters. Record initial weight of filter bags and catch drum.
- Measure out specified limestone weight and place into hopper
- Once the system is running wait until the air blow reaches 1100 SCFM to inject limestone
- Immediately stop air blower and close limestone injection valve when all the limestone is ejected out of the hopper
- Record final weight of filter bags and catch drum.

For test series two, these additional steps were performed:

- During flow, every 30 seconds the inlet supply hopper level and the cyclone outlet drum weight were measured and recorded.
- Instead of stopping the blower immediately, the system was operated until it seemed no more material was being elutriated from the bed.

The following Table 1 below summarizes the test data obtained from the 5 tests which were conducted with limestone. The first and fourth tests were ostensibly the same particle size, but visual examination showed that a significant quantity of the coarser material did not leave the bed even after a very long time. It seems likely that the largest particles, between 400 and 500 microns could not elutriate out of the bed, because the superficial velocity was at the terminal velocity of a 450-500 micron particle (this is actually the design condition of the cold flow bed). Three different correlations for terminal velocity were checked based on the references previously cited, and they all predict a slightly different "largest" elutriated particle in this situation. Therefore, the particle size of the fourth test should be adjusted down slightly, and the data will be more accurate for that test.

Table 1: Particle Hold-Up Data

Test #	Average Particle Size:	Bed Weight	Cyclone Initial Weight	Filter Initial Weight	Hopper Fill Weight	Cyclone Final Weight	Filter Final Weight	Hopper Final Weight	Stop Time
	[µm]	[lb]	[lb]	[lb]	[lb]	[lb]	[lb]	[lb]	[sec]
1	400	312.4	32.2	2.57	40	51.8	2.88	0	600
2	225	312.4	17.6	0.6	40	29.6	0.86	19.4	400
3	225	312.4	17.6	1.08	40	46.8	1.58	0	804
4	350	312.4	49.8	2.2	28	65.6	2.48	0	399
5	112.5	312.4	73	2.2	13	82.6	2.48	0	281

All tests were at 1100 SCFM and bed height of 48 inches. All the tests except for test #2 were run until all the limestone was ejected from the hopper. Test #2 was halted due to a mechanical issue which developed immediately before the test termination. The test data obtained was not corrupted due to this issue.

Table 1: Particle Hold-Up Data (continued)

Test #	Mass Flow Out	Mass Remaining In Bed	Mass Flow Rate In	Calculated Bulk Density of Limestone in Bed	Limestone Velocity Within Bed	Time In Bed
	[lb]	[lb]	[lb/sec]	[lb/ft3]	[ft/sec]	[sec]
1	19.9	20.1	0.07	2.94	0.01	301
2	12.3	8.3	0.05	1.22	0.02	162
3	29.7	10.3	0.05	1.51	0.02	207
4	16.1	11.9	0.07	1.74	0.02	170
5	9.9	3.1	0.05	0.46	0.06	67

The test data is analyzed as follows: particle elutriation rate E_i of a given particle size *i* from a fluidized bed has been demonstrated to be proportional to particle average

concentration X_i in the bed,[12] with a proportionality constant K_i. By measuring flow rate into the bed and flow of material coming out of the bed, the elutriation rate constant K_i may be found by using a finite difference incremental time procedure to match the data with the calculus with only one unknown:

$$E_i = K_{i\infty} X_i = K_{i\infty} \frac{W_i}{W}. \qquad (15)$$

This is depicted for the first data point in the following figure.

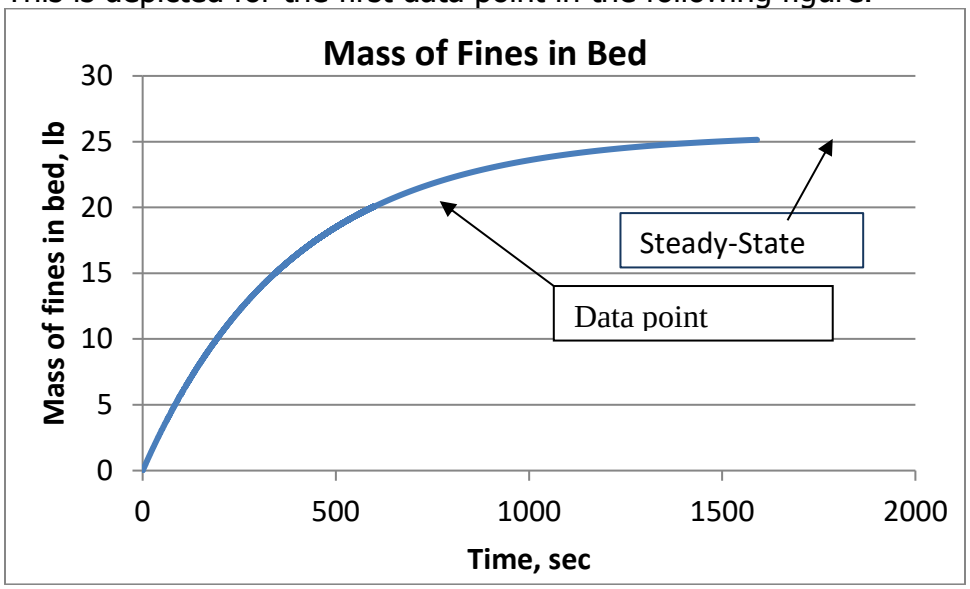

Figure 21: Experimental Determination of K_i

When K_i is determined experimentally by this procedure, the time analysis is run out to infinity to discover the steady state equilibrium particle residence time. The particle elutriation rate constants are then used to determine the steady state concentrations and hence the average particle velocity for a given mass flow rate.

From the results in Table 1 it can be seen that for all the particle sizes the residence time was greater than 1 minute. The testing residence time values provide confidence in the assumptions associated with the current chemical kinetics model.

The finest particle data points were problematic, since the finest limestone either had air moisture issues or static electricity issues. One test was attempted with particles of under ten microns, but the entire surface of the bed and elutriation tube and the cyclone was covered with material, making mass measurements impossible. The bed was full of well-grounded metal, so it is most likely a problem with moisture. A different surrogate material will have to be used in the future which is not hygroscopic.

Values for the correlation constants K_1 and K_2 (not to be confused with the Elutriation Rate, K_i) are given in the reference and were used here. The cold flow data was checked against this, giving a typical error of +/-20% when attempting to scale from one data point to another. This is not bad for the short amount of testing that was done.

When the data was compared to correlations to predict K as a function of particle size, however, the correlations were not in strong agreement with the data. The lack of a tighter correlation suggests that more careful data be taken, and in 2014, more tests were performed with a different material that was not as prone to clogging from humidity and static electricity. These tests also added weight measurements every 30 seconds on the exit flow stream as well, so the actual mass of material in the bed could be tracked, giving a somewhat clearer picture of the transient. In Figure 24, all of the data are presented. Of the various correlations discovered, the closest were Colakyan, Colakyan and Levenspiel, Geldart, and Zenz-Weil.

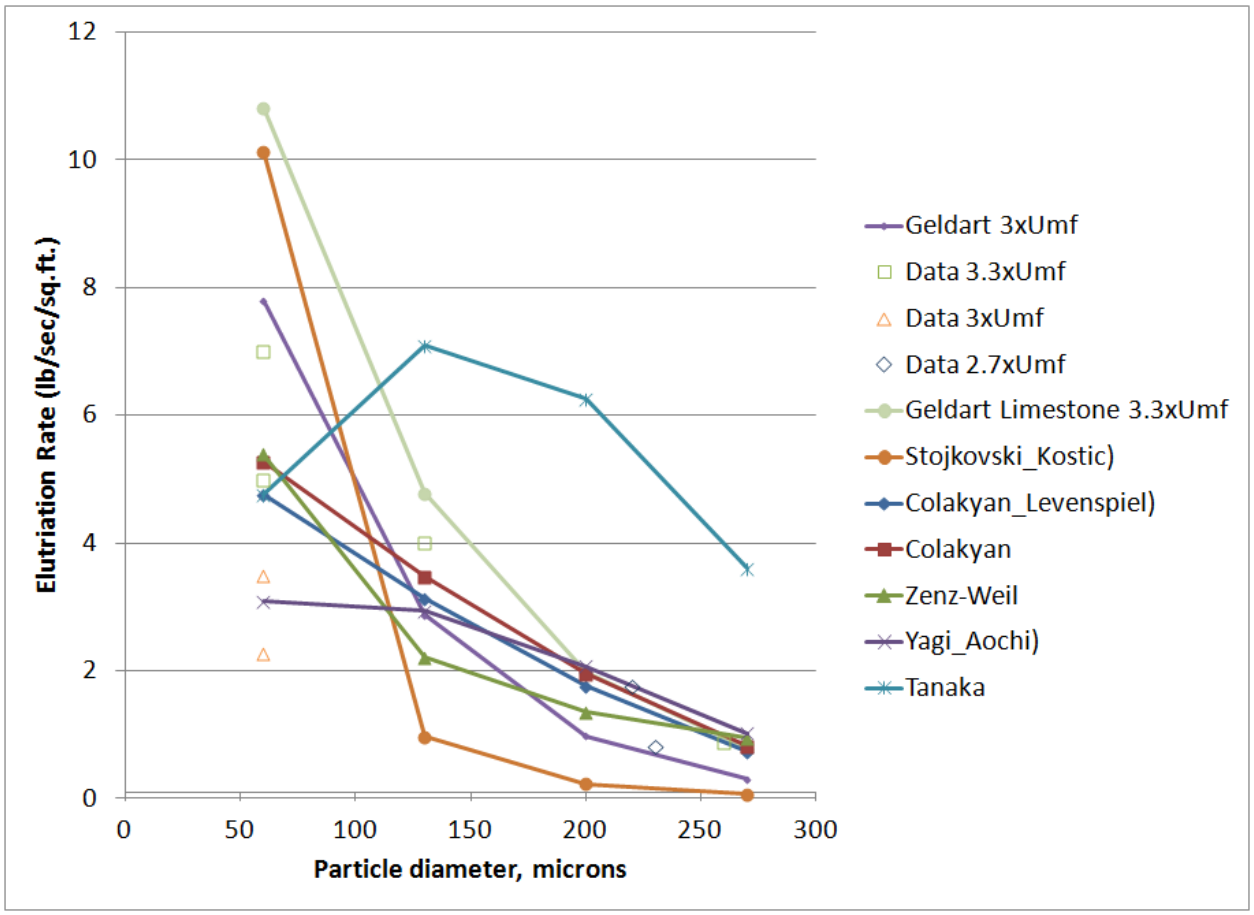

Figure 22: Experiments compared to correlations for K_i

The match is still not very good, and worse, when these correlations are tested at the conditions of the hot PFBC fluidized bed, they lose connection with physical reality, and return nonsensical answers. Of all these correlations, the only one which returns reasonable extrapolations to the hot PFBC conditions is the Stojkovski and Kostic equation (Equation 1 below). The residence time of the finest particles was therefore estimated based on this correlation [12], which shows that particle velocity is proportional to the relationship:

$$U_p \propto U_f \cdot \left\{1 - \left[K_1 \left(\frac{Fr^{1.125}}{\mathrm{Re}_p} \right)^{K^2} \cdot \rho_f U_f \cdot \right]^{-1.25} \right\} \qquad \text{(Equation 1)}$$

Consider Figure 23 below where some of these correlations are compared to a pair of common-sense models referred to as "Model 1" and "Model 2" are superimposed. Model 1 is currently used in the proprietary PFBC fluidized bed model owned by GTI and Model 2 is an adjustment to that same model decreasing the particle size at which residence time goes to infinity. Below 10 microns, the particle velocity approaches the gas superficial velocity, and the times become very short indeed, and it is a basic fact that above a certain size, larger particles will never leave the bed.

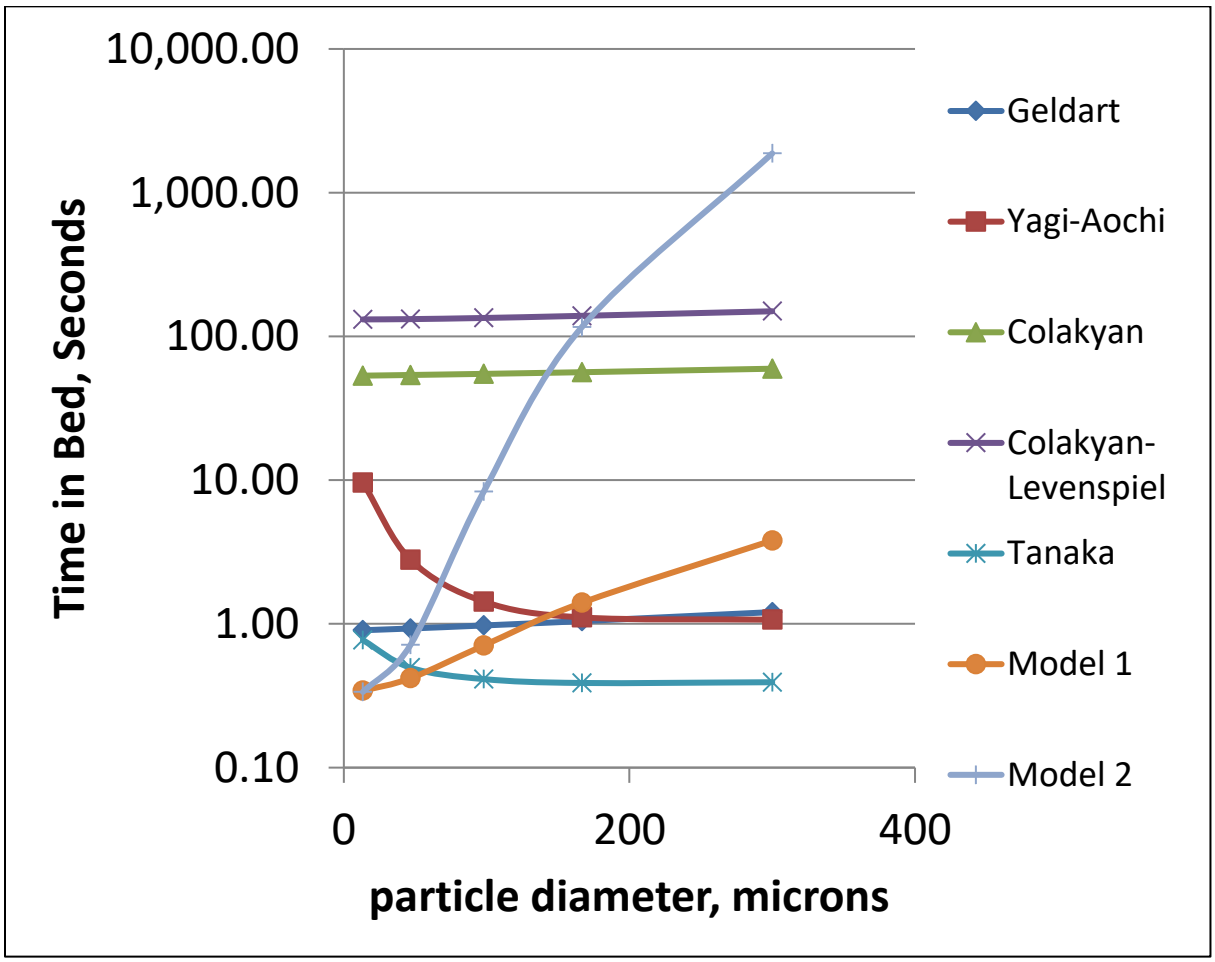

Figure 23: Comparison of correlations at high pressure.

The slope of the curve remains to be discovered. The Stojkovski and Kostic (S-K) model gives what appears to be a reasonable shape, but the slope is in question. Further testing will have to be done in this range to verify the extrapolation.

For this reason, during phase II, the University of Ottawa was chosen to perform high pressure elutriation tests in a similar fashion with an existing test rig which can come closer to the PFBC test conditions in pressure.

At high pressure, the same fluidization behavior will be exhibited at lower velocities, so the ideal injection flow rate will be at a lower velocity than an atmospheric bed. This increases residence time and it also decreases erosion of in-bed heat exchanger tubes.

As an example, the S-K equation (Equation 1) is used below to extrapolate residence time, and this compares favorably with the estimated particle burning rate from the literature as well. Some early experimental data shows that the elutriation curves may be flatter than shown here, which is good from a carbon utilization perspective. It means the coal will have more time to burn and achieve high carbon utilization.

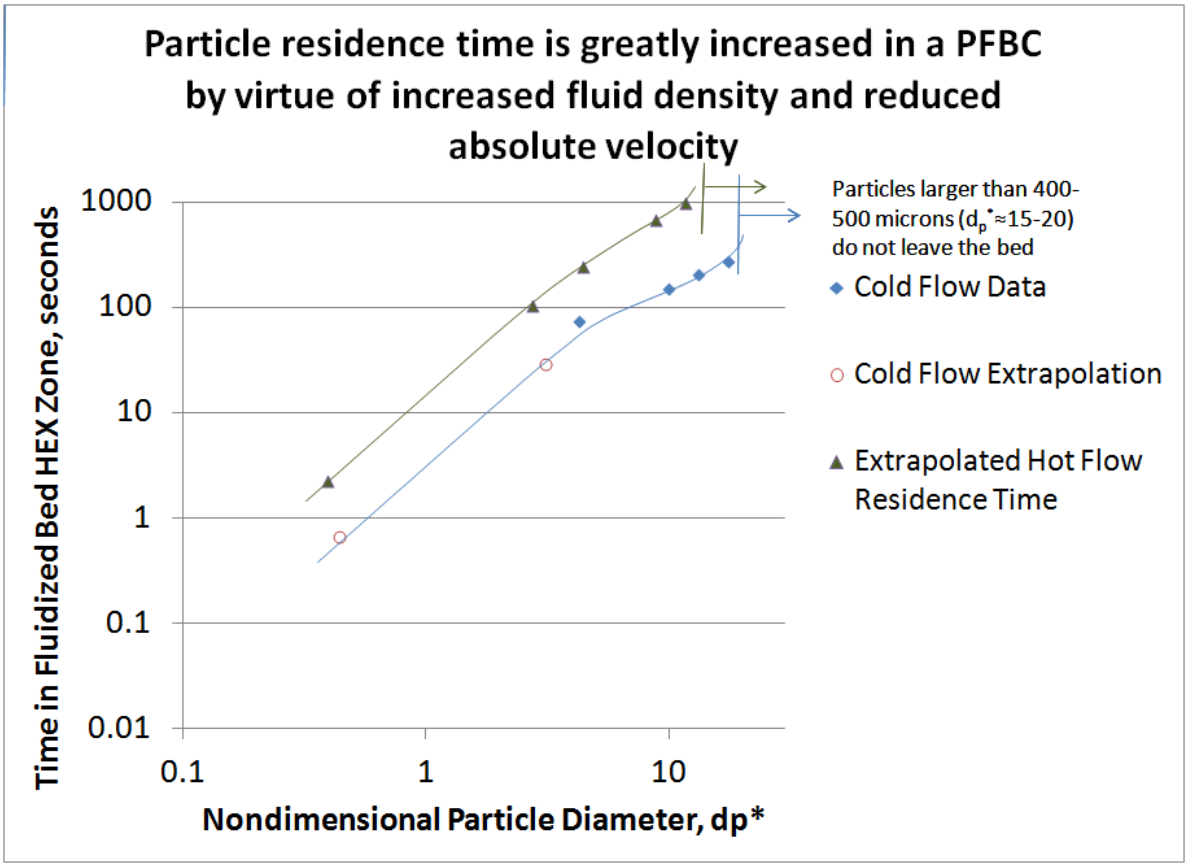

Figure 24: Extrapolated PFBC Residence Time

With appropriate models and experimentation, the goal will be to define the ideal particle size distribution for two feedstocks, coal and limestone, which will produce a healthy bed psd and reasonable reaction times. Coal will move quickly enough to combust within the in-bed heat exchanger, and limestone will ideally remain in the bed long enough (on the order of 20-30 minutes) to be completely spent in capturing sulfur. This will result in a resulting PSD which is not elutriated (projecting some measure of agglomeration) and the coarsest materials will settle to the bottom for dump system removal. (Figure 25).

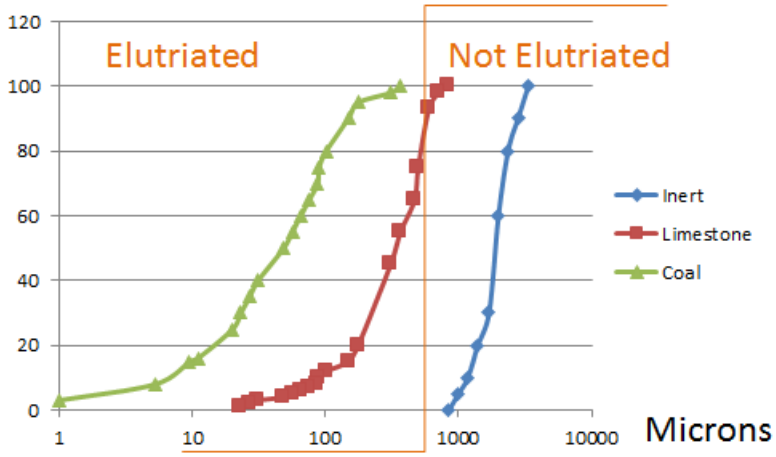

Micr

Figure 25: Particle size management conceptual diagram

Particle Pressure Measurement

Literature on fluidized bed pressure measurements indicates that two types of particle pressure are of interest to the bed design. One is the balance of forces on macro sized objects (heat exchanger surfaces) and the second is the localized particle impact pressure on a small surface, subtracting the gas pressure. The first is related to the vibrations and offset loads that must be supported by tube structures, and the second is related to tube erosion. Instruments capable of these types of measurements were investigated, and the measurement described in the first type was tested in cold flow (the second is of interest, and some materials were purchased to build a particle pressure sensor, however two considerations resulted in a decision not to continue the study: tube erosion is more easily managed by designing a bed to operate at velocities below 6 ft/s, and a choice of bed material that does not include silica. Also, this type of measurement is more difficult and doesn't actually provide correlations with erosion unless very long duration tests can be performed, and this was not part of the plan.

The cold flow program focused on the first type of measurement, because the bubble behavior of the atmospheric rig is likely to be similar to the combustor (similar Reynolds number and velocity regime), and visual examinations showed macroscopic forces were significant in the test rig. (Previously shown in Figure 12). The result of the measurements is shown below in Figure 26.

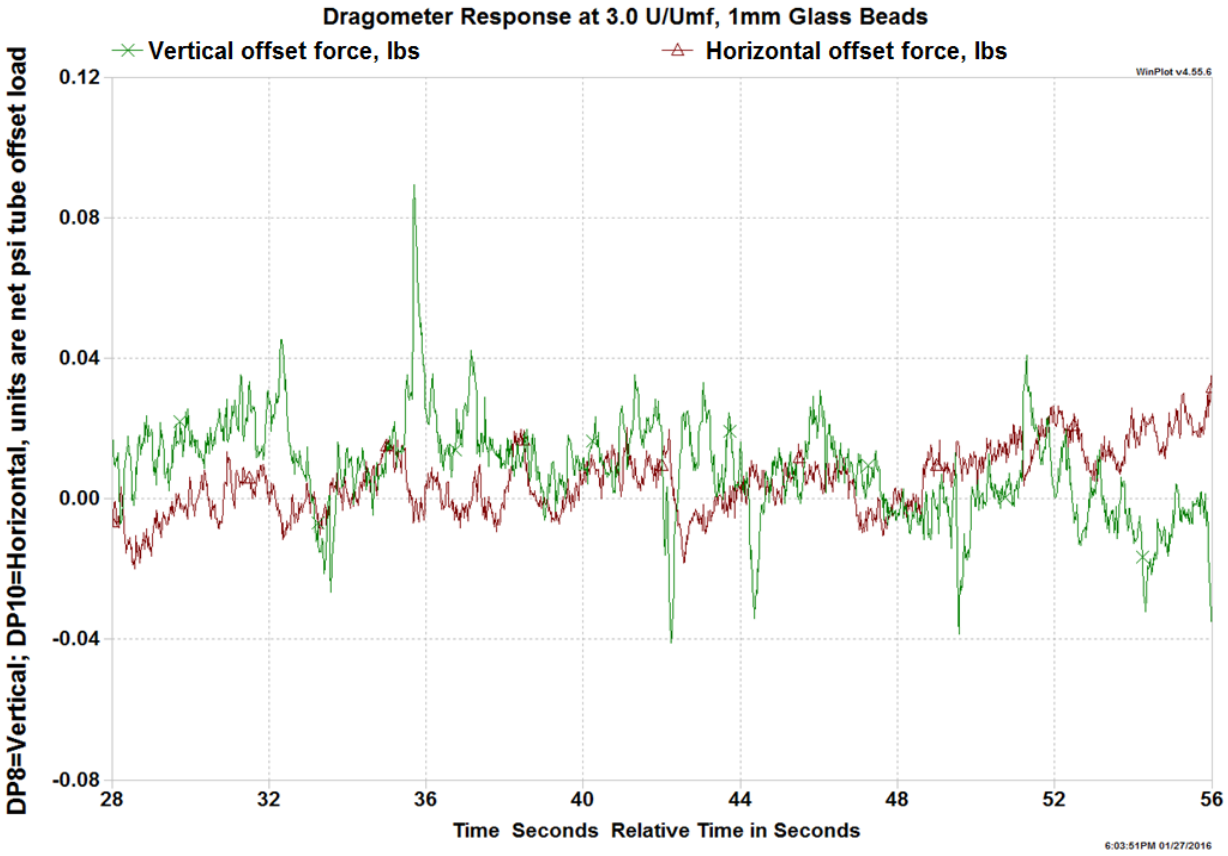

Figure 26: Dragometer output

The signal was analyzed for coherent oscillations. FFT analysis shows this is random noise with no dominant modes. Over a 1-2 second period, the .02-.04 ΔP magnitude oscillation equals an offset load of about

0.05-0.1 lb/sq.in. horizontal

0.15-0.2 lb/sq.in. vertical

These forces can be used to predict the distribution of load across a heat exchanger tube by multiplying by the average bubble size.

Conclusions

The cold flow test program for the Oxy-PFBC was a very successful effort, allowing improved predictability of bubbling behavior, pressure drops and standard deviation, heat transfer coefficient, and particle residence time. It also allowed the design team to develop detailed designs for the pilot plant, and gave a firm footing for directing future investigations at high pressure fluidized bed facilities. Since testing at high pressure will be more difficult, it is best to settle as many questions as possible with low pressure tests, and then focus on the more difficult unknowns at higher pressure. The test rig parts are still available at GTI if a future need arises, and most of the methods described here are valid approaches for high pressure cold flow tests, and the analytical methods can be used at high pressure as well. Many of the analytical methods will be used directly in the pilot testing. The instrumentation can all be adapted to high pressure hot testing in pilot, demonstration or commercial scales.

Bibliography

1. Wen-Ching Yang, editor, "Handbook of Fluidization and Fluid-Particle Systems", Marcel Dekker Inc., copyright 2003, Taylor & Francis Group LLC.
2. Prabir Basu, "Combustion and Gasification in Fluidized Beds", CRC Press, Taylor & Francis Group, copyright 2006.
3. T. W. Asegehegn et al, "Influence of Horizontal Tubes, Averaging Periods and Extraction Methods on the Hydrodynamics of Bubbling Gas-Solid Fluidized Beds", 7th International Conference on Multiphase Flow, Tampa, Florida USA, May 30-June 4, 2010.
4. S. W. Kim et al, "Heat transfer and bubble characteristics in a fluidized bed with immersed horizontal tube bundle", International Journal of Heat and Mass Transfer, 2003, Vol. 46, pp. 399-409.
5. O. Molerus and K.-E. Wirth, "Heat Transfer in Fluidized Beds", Chapman & Hall, copyright 1997.
6. J. C. Chen et al, "Heat transfer in fluidized beds: design methods", Powder Technology, Vol. 150, pp. 123-132, 2005.
7. J. Wiman and A. E. Almstedt, "Hydrodynamics, erosion and heat transfer in a pressurized fluidized bed: influence of pressure, fluidization velocity, particle size and tube bank geometry", Chemical Engineering Science, Vol. 52, No. 16, pp. 2677-2695, 1997.
8. Beeston and Essenhigh, "Kinetics Of Coal Combustion: The Influence Of Oxygen Concentration On The Burning-Out Times Of Single Particles"
9. Huang, X "Ignition And Devolatization Of Pulverized Coals In Lower Oxygen Content O2/CO2 Atmospheres", Cleaner Combustion and Sustainable World pp101-104, doubling of ignition and burnout times
10. Murphy and Shaddix, Sandia National Lab, "Combustion Kinetics Of Coal Chars In Oxygen-Enriched Environments", Combustion and Flame #144, 2006
11. Alliston, Rantee, Rautanen, Kvaerner Pulping, "Experience With FuelsFrom Biomass to Petroleum Coke and How Their Properties Affect Fluidized Bed Boiler Plant Design", 16th Int'l Conf. on Fluidized Bed Combustion, May 13 – 16, 2001
12. Stojkovski and Kostic, "Empirical Correlation for Prediction of the Elutriation Rate Constant," Thermal Science Volume 7, 2003, No. 2
13. Johnson and Flemmer, "Erosion of Heat Exchanger Tubes in Fluidized Beds", DOE contract DE-FC21-87MC24207, 1990
14. Rahman and Campbell, "Particle Pressures Generated Around Bubbles in Gas-fluidized Beds" J. Fluid Mechanics, 2002

Appendix B. Coal Reactivity Report

PENN STATE UNIVERSITY COAL REACTIVITY TESTS & ANALYSIS

Kenneth M. Sprouse; PE, Esq.
Chief Technologist -- Energy Systems
Aerojet Rocketdyne Inc.
Canoga Park, CA 91309

January 20, 2016

Note: This report was edited on Feb. 29, 2016 to remove proprietary information.

ABSTRACT

This report describes the model used for predicting the transient weight loss data from Illinois #6 bituminous coal in a Penn State University (PSU) laboratory scale oxy-fired pressurized fluidized bed combustor (PFBC). The PSU experimental apparatus was a small oxy-fired PFBC having a cross-sectional flow area of about 20-cm^2 contained within an electrically heated furnace. The PFBC operated at a pressure from atmospheric to approximately 7.89 atm. Furnace wall temperatures were set between 800 and 875ºC. The oxy-fluidization gas composition contained between 5.3 and 16.0 vol% oxygen (O_2) with the balance being carbon dioxide (CO_2) gas. The fluidization gas flow rate to the PFBC was 3.0 to 6.3 standard liters per minute (slpm) with superficial gas velocities on the order of 1.4 cm/s. The Illinois #6 bituminous particle sizes for the initial runs were nominally 74-microns but increased to approximately 177-microns for the later experiments. The amount of Illinois #6 bituminous coal mass delivered to the PFBC for each batch run -- after the oxy-fluidizing gas had achieved furnace temperature conditions – ranged between 3.2 to 5.0 grams. The GTI transient coal reactivity kinetic model used for PSU test data correlation assumes: (1) the gas flow through the PFBC is one-dimensional uniform plug flow (PF), and (2) the thin layer of coal or char mass within the fluidized bed recirculates under well-stirred-reactor (WSR) conditions. This PF/WSR kinetic model was shown to reasonably correlate the experimental test data by the adjustment of only one model parameter – i.e., the radiation heat transfer rate from the upper freeboard furnace section into the lower 0.25-cm thick fluidized bed layer. The radiation heat transfer rate into the bed was found to be on the order of 200 Watts. All other models parameters were taken from American Society for Testing and Materials (ASTM) ultimate/calorific analyses and historical kinetic parameters for bituminous coal devolatilization and heterogeneous char-O_2 oxidation as used by GTI since the 1980's whose origins are from the laboratory work conducted at the Massachusetts Institute of Technology (MIT) and West Virginia University WVU -- among other institutions.

INTRODUCTION & BACKGROUND

In order to update the Gas Technology Institute (GTI) 1-D Pressurized Fluidized Bed Combustor (PFBC) kinetic performance code with the coal reactivity test data generated by Penn State University (PSU) in their fluidized bed laboratory reactor, a numerical simulation code was written for the PSU reactor using the coal chemistry formulations found in the Gas Technology Institute (GTI) 1-D PFBC kinetic model. The GTI 1-D PFBC kinetic performance model was originally derived from the GTI 1-D entrained flow coal liquefaction, gasification, and combustion model originally developed under U.S. Department of Energy (DOE) funding in the 1970-80's by one of GTI's predecessor organizations – the Energy Systems Group of Aerojet Rocketdyne Inc. (AR – Canoga Park, CA).

It was found for elutriated fluidized bed reactor systems -- such as those advanced by Stewart and Mays (2012) for 1-step compact hydrogen generation reactors or Stewart et al. (2010) for PFBCs – that the GTI 1-D entrained flow coal reactor performance model could reasonably predict reactor performance in these more complex multi-dimensional fluidized recirculating flow reactors. The ability to predict performance with a simpler 1-D entrained flow analysis is due to the fact that the small reacting particles -- lime [CaO(s)] in the case of the compact hydrogen generator and coal in the case of the PFBC – are traveling with the fluidizing gas directly through the reactor without any appreciable recirculation. Hence, their residence time through the fluidized bed is measured on the order of seconds (similar to that of the reacting fluidization gas) rather than in minutes had their particle diameters been large enough to remain gravimetrically at all times within the bed. In the *Stewart Reactor's* elutriated fluidized bed concept, the small reacting particles (having diameters typically between 1 and 74-microns) are continuously injected into the bottom of the fluidized bed together with the bed's fluidizing gas. The reactor's large bed stabilization particles [having diameters typically in the 2-millimeter (mm) range] are generally made from a hard inert material such as alumina, Al_2O_3(s).

The relationship between the residence time of the small elutriation particles and the fluidizing gas during their short vertically upward journey through the fluidized bed is currently the subject of other on-going experimental studies under this program. The results of these studies will be provided in a subsequent report which is expected to give improved particle diameter-dependent hold-up relationships between the in-bed particle velocities and the in-bed gas velocity as a function of the bed stabilization particle size, the bed void fraction, the gas viscosity, and the particle densities (among other key variables).

The current GTI 1-D PFBC kinetic performance model currently assumes that the large inert bed stabilization particles do not move but are fixed in space within the fluidized bed. The result of this assumption is that the temperature of the inert bed stabilization particles at the bottom of the fluidized bed is substantially lower than the stabilization particle temperature at the top of the fluidized bed. This assumption can cause ignition problems within the 1-D PFBC kinetic performance code whenever the temperature and flow rate of the oxy-fluidization gas itself is insufficient for particle heating to ignition temperatures. To overcome this problem, a

well stirred reactor (WSR) formulation for the bed's stabilization particles near the bottom of the bed is currently being considered for development. The thermal energy flux into the bed's lower WSR due to recirculating bed stabilization particles will be determined by a diffusion/mixing analysis of gas sparged solid particle beds.

The WSR formulation will be used in the PSU coal reactivity model given below for describing the motion of the recirculating coal particles (as opposed to bed stabilization particles). Here, the PSU fluidized bed reactor is not designed to elutriate coal/char particles from the fluidized bed but continuously recirculates them within the bed. Since the fluidized bed height is extremely small at approximately 0.25-cm, only one WSR needs to be considered in the PSU model without requiring a diffusion/mixing analysis for particle mass and energy transfer between adjacent WSRs.

The main purpose of the PSU coal reactivity experiments is to measure the devolatilization and char-O_2 oxidation reaction rates from bituminous coal in a fluidized bed setting and determine whether these rates are consistent with those predicted from the coal chemistry formulations used by the GTI 1-D PFBC kinetic performance code described above. If the PSU reaction rates are not consistent with the GTI historical coal chemistry formulations found within the GTI 1-D PFBC kinetic performance code, then the PSU experiments will be used to subsequently modify the GTI coal chemistry kinetic parameters as required. It should be noted that the GTI coal chemistry kinetic parameters were originally used in high temperature (above 1,200ºC) entrained flow coal reactors [rather than 850ºC fluidized bed reactors] whereby: (1) the conversion residence times ranged from 10-milliseconds to 3-seconds [rather than tens of minutes], and (2) the mean coal particle sizes were under 30-microns (rather than 177-micron). However, as will be seen below, the historical GTI coal chemistry parameters for bituminous coal reasonably predict the coal conversion test data from the lower temperature, longer residence time, and larger coal particle PSU fluidized bed reactor.

In order to accommodate the larger bituminous coal particles having Sauter mean diameters, well in excess of 30 microns, a standard "shrinking core" representation for the char O2 oxidation reaction was added to the model's previous coal chemistry description.

PF/WSR MODEL FOR PSU PFBC COAL REACTIVITY EXPERIMENTS

The transient numerical simulation code -- for data correlation with the PSU pressurized fluidized bed combustor (PFBC) – is described in this section. The code uses a one-dimensional (1-D) plug flow (PF) representation for the gas flowing upward through the fluidized bed together with a well-stirred-reactor (WSR) representation for the granular coal particles within the fluidized bed. Initial coal particle sizes for these tests were to have had a nominal size distribution of 70 wt% passing through a 200 mesh screen (74-micron opening) similar to the distributions proposed for use in subsequent pilot plant and commercial PFBC "elutriated bed" combustors – see, e.g., Stewart et al. (2010). This type of "industrial grind" pulverized coal specification usually leads to Sauter mean diameters, D_{32}, of less than 30-microns from typical

pulverization mills. Although this particle size is desirable for the Stewart et al. (2010) "elutriated bed" PFBC (where it is required to have a superficial gas velocity higher than the terminal velocities of the coal particle), these smaller sizes present significant issues for a fluidized bed – such as the PSU PFBC – where elutriation of the particles from the reactor is not desired. Hence, to prevent particle elutriation from the bed during these experiments (as required for PSU's subsequent coal conversion data reduction methodologies), all tests with the PSU PFBC were conducted with near mono-sized particles at or above 74-microns in diameter. The total mass of coal charged to the PSU fluidized reactor for each test was on the order of 5 grams which produces a small coal layer (or fluidized bed height) of about 0.25-cm within the reactor.

Unlike the earlier PSU limestone sulfation tests that were also run in the same fluidized bed reactor, a transient model (as opposed to the steady state limestone sulfation model) is developed here for correlation with the coal combustion test data since the particle oxidation kinetics and heat release rates within an oxidizing coal particle can be substantial such that most of the particle weight loss is occurring under transient conditions. Hence, it is unlikely that the coal particle's temperature is the same as the surrounding furnace temperature walls while substantial particle reactions (both endothermic and exothermic) are taking place within the particle. Without the use of a calibrated optical pyrometer system to measure particle temperatures within the solids bed, the transient model will be the primary tool used to determine this important parameter.

The transient numerical simulation code was developed for correlating with the twelve PSU pressurized fluidized bed experiments. All model constants in the code above were taken from three sources. The data first source was from standardized American Society for Testing and Materials (ASTM) data as shown in Table 2 below. The primary data constants from this source are the ultimate and calorific heating parameters provided there. The second source of model constants was the historical model properties for bituminous coal which GTI (and its predecessor entity – Rocketydne) compiled over the years and correlated with its own test data in short residence time (SRT) entrained flow gasification, liquefaction, and combustion. The basis of the constants reported in Table 3 below is primarily from the work performed by Prof. Jack Howard and his associates at the Massachusetts Institute of Technology (MIT) in the 1970-80's. Much of this research is captured in the seminal reference work by Elliot (1981). The third source of data for such standard parameters as the specific heats and enthalpy-of-formations for standard gases and liquids (e.g., oxygen, carbon dioxide, steam, water) were taken from the National Institute of Standards and Technology (NIST) reference source by Chase et al. (1985). The gas thermal conductivity and viscosity parameters were alternatively obtained from the NIST reference source by Friend (1992).

Finally, it should be noted that the constant, V^{**}_{maf}, found in Table 3 is significantly higher than the ASTM Proximate Analysis value for maf volatile matter found in Table 2 (i.e., 0.645 versus 0.464). This is due to the fact that Prof. Howard and associates found that dilute phase bituminous coal pyrolysis at temperatures higher than the limiting furnace temperatures

specified in ASTM D5142 (i.e., 950ºC) will produce substantially more volatile matter than found from ASTM D5142 testing procedures (here nearly 40% higher). The modeling of mass devolatilization rate of organic volatiles within a coal particle, follows the multi-parallel reaction scheme developed at the Massachusetts Institute of Technology (MIT) by Prof. Jack Howard and co-workers in the 1970's – see Elliot (1981). However, at temperatures below 950ºC , there should not be a significant difference using Howard's model to predict the coal particle devolatilization rate from lower temperature fluidized beds and other simpler pyrolysis models found in the literature which use just the ASTM Proximate Analysis volatile matter result.

Table 2. ASTM Properties for the Illinois #6 Bituminous Coal Tested at PSU

Moisture Ash Free (maf) Proximate Analysis (ASTM D5142)	
Mass Fraction Volatile Matter	0.464
Mass Fraction Fixed Carbon	0.536
As Received Ultimate Analysis Model Parameters (ASTM D3176)	
Mass Fraction of Water, η^{o}_{wat} (i.e., $N_p W^{o}_{wat} / W^{o}_{coal}$)	0.0901
Mass Fraction of Carbon, η^{o}_{car} (i.e., $N_p W^{o}_{car} / W^{o}_{coal}$)	0.6140
Mass Fraction of Hydrogen, η^{o}_{hyd} (i.e., $N_p W^{o}_{hyd} / W^{o}_{coal}$)	0.0439
Mass Fraction of Nitrogen, η^{o}_{nit} (i.e., $N_p W^{o}_{nit} / W^{o}_{coal}$)	0.0139
Mass Fraction of Sulfur, η^{o}_{sul} (i.e., $N_p W^{o}_{sul} / W^{o}_{coal}$)	0.0412
Mass Fraction of Oxygen, η^{o}_{ox} (i.e., $N_p W^{o}_{ox} / W^{o}_{coal}$)	0.0782
Mass Fraction of Ash, η^{o}_{ash} (i.e., $N_p W^{o}_{ash} / W^{o}_{coal}$)	0.1187
As Received Heat of Combustion (ASTM D5865)	
Higher Heating Value, $\Delta_c H^{o}_{coal}$ (kJ/g)	26.4

Table 3. GTI Historical Model Properties for Bituminous Coal

Maximum Mass Fraction of maf Volatile Material, V^{**}_{maf}	0.645
Devolatilization Pre-Exponential Rate Constant, k_o (s^{-1})	1.67×10^{13}
Mean Devolatilization Activation Energy, E_o (J/mol)	2.29×10^{5}
Standard Deviation of the Activation Energy Distribution, σ (J/mol)	7.20×10^{4}
Specific Internal Surface Area of Coal/Char Particle, S (cm^2/g)	2.81×10^{6}
Initial Coal Particle Density, ρ_p (g/cm^3)	1.27
Initial Coal Particle Internal Porosity, ε_p (vol%)	10.0
Final Ash Porosity Under Non-Slagging Conditions, $\varepsilon_{p,ash}$ (vol%)	70.0
Gaseous Volatiles Standard Enthalpy of Formation, $\Delta_f H^o_{vol}$ (kJ/g)	-0.135
Gaseous Volatiles Specific Heat, $c_{p_{vol}}$ (J/g·K)	1.39
Coal Particle Specific Heat, c_{pp} (J/g·K)	1.30
First Order Heterogeneous Specific Reaction Rate Constants	
Char-O_2 Reaction, k_{ox}	
Pre-Exponential Velocity Constant, A_{ox} (m/s)	8.22×10^{4}
Activation Energy, E_{ox} (J/mol)	1.298×10^{5}
Char-CO_2 Reaction, k_{CO2}	
Pre-Exponential Velocity Constant, A_{CO2} (m/s)	6.78×10^{2}
Activation Energy, E_{CO2} (J/mol)	2.481×10^{5}

PF/WSR MODEL CORRELATION WITH PSU EXPERIMENTS

PSU ran a total of twelve bituminous coal reactivity experiments in their PFBC reactor that has a nominal 20-cm^2 cross-sectional freeboard gas flow area. Since all of the PF/WSR model parameter constants are known (except the radiation heat transfer rate from the upper furnace walls and upper freeboard combustion zone into the lower coal particle layer, $\dot{Q}_{rad,in}$); the model correlation activity here will be to fit the transient coal weight loss data by adjusting the radiation heat transfer rate, $\dot{Q}_{rad,in}$, into the bed. For these tests, nominal values for $\dot{Q}_{rad,in}$ between 180 and 400-Watts gave reasonable correlation for all twelve experiments. The general trend for $\dot{Q}_{rad,in}$ is that higher furnace temperatures produce higher values for the radiation heat transferred into the particle bed.

Table 4 provides the tests summary for the PSU coal reactivity tests. Twelve tests were conducted and identified as Run Numbers 1 through 12 by PSU in which they also provided to GTI the moisture-ash-free (maf) conversion results. The reactor pressure for most tests was 8 bar with the last three tests conducted near atmospheric pressure of 0.3 to 0.4 bar-gauge. Two coal particle sizes were used: the first three tests with nominal 74-micron particles, and the later nine tests with nominal 125 to 177-micron particles. Similar to the PSU limestone sulfation experiments, three furnace temperature settings were used: 800ºC (instead of 825ºC in the calcination tests), 850ºC, and 875ºC. The carbon dioxide (CO_2) fluidizing reactant gas is internally heated within the furnace so that its injection temperature into the reactor is nominally the furnace temperature itself. The fluidizing gas flow rates for these experiments ranged from 3.0 to 6.3 SLPM (standard liters per minute) while the inlet oxygen (O_2) concentration of the reactor's fluidizing gas ranged from 5.3 to 16 vol%. Finally, the amount of bituminous coal used for each test ranged from 3.2 to 5.0 grams.

The type of data collected from each test is shown in Figure 1. The exiting concentrations of oxygen and carbon dioxide gas (in vol%) is continually measured along with the exiting carbon monoxide and sulfur oxide gas (in parts per million, ppm). These concentrations are subsequently used together with the measured fluidizing gas flow rate to determine the coal's moisture-ash-free (maf) weight loss history from a PSU data reduction analysis. These maf weight loss histories are then divided by the initial maf mass of bituminous coal placed into the reactor to provide the coal's maf mass conversion history as reported in Figures 2 through 5. For the last three experiments shown in Figures 5a, 5b, and 5c; the experimental maf mass conversion time histories were only reported by PSU after the conversion reached the ASTM D5142 Proximate volatile matter analysis of 46.4 wt%.

As seen in Figures 2 through 5, the coal particle's 9.01 wt% moisture is vaporized within approximately 30 seconds after introduction into the furnace's fluidized bed. However, it takes the particles approximately another 2-minutes before their temperature increases to the point that organic devolatilization is initiated near 260ºC. This devolatilization period last for approximately another 4 to 8 minutes before the particle has essentially completed the pyrolysis process and reached the ASTM D5142 proximate analysis' 46.4 wt% maf conversion value. The PF/WSR reactor model indicates that during pyrolysis the oxygen gas concentration at the coal particle surface is reduced by the outward flow of pyrolysis gases -- such that the exothermic char-O_2 reaction is very low during this period. Following the pyrolysis period, Figure 2 through 5 show that it takes another 10 to 20 minutes (or even longer in some cases) to complete the char-O_2 oxidation process.

The temperature plots in Figures 2 through 5 (from the PF/WSR model) also show that it can take 10 minutes or longer for the coal particles to reach temperatures near the set furnace temperature reported in Table 4 for each test. This is due to the fact that the sensible heat delivered to the fluidized bed by the fluidizing/oxidizing gas is very low compared to the overall heat capacity of the coal particles within the bed. Indeed, it was found that the furnace's

radiation heat transfer rate into the bed, $\dot{Q}_{rad,in}$, was the most influential and sensitive parameter in matching the experimental and model prediction maf conversion profiles. For example, if $\dot{Q}_{rad,in}$ was dropped below 100 Watts; it was found that the particles would never heat up to cause appreciable maf conversion of the coal particle within the time period of the experimental run. Likewise, increasing the $\dot{Q}_{rad,in}$ term much above 500 Watts would produce a run-away coal particle temperature profile well into the ash slagging regime that was also unrealistic. It was also seen with the smaller coal particles from the first three runs (Figure 2), that the coal particle temperature never effectively reached a plateau – but continued increasing substantially through the final char-O_2 oxidation period. Particle temperature plateauing with the larger 177-micron particles was primarily a result of the "shrinking core" model whereby the larger particles produce more diffusion resistant for the oxygen gas trying to reach the particle's unreacted carbon within its receding core region.

Although the fluidizing/oxidizing gas entering the bottom of the reactor's fluidized bed was already pre-heated to the furnace temperature, the gas was quickly cooled by the lower temperature coal particles so that this gas actually exited the bed at the coal particle temperature. Even as the coal particles heated up to the furnace temperature (and in some case even higher due to the char-O_2 exothermic reactions, the fluidizing/oxidizing gas flow rate was so low that the gas always exited the fluidized bed within a few degrees of the particle's temperature. As mentioned earlier, the fluidizing/oxidizing gas flow rate through the fluidized bed was required to be very low due to the small size of the coal particles (which had very low terminal velocities thus requiring very low gas superficial velocities) when compared to a usual fluidized bed coal particle size at a few millimeters in diameter.

Although the gas temperature exiting the fluidized bed was shown to be within a few degrees of the bed's particle temperature, it is expected that combustion of the any unburned volatiles during the initial low temperature stages of pyrolysis are subsequently being burned to carbon-dioxide and steam in the furnace's upper freeboard section of the reactor. Here the hot furnace walls continue to heat the fluidized bed's slow moving exiting gases via radiation and natural convection until volatile burning is initiated.

Table 4. PSU Coal Reactivity Test Summary

Run Number	Particle Size (microns)	Furnace Temperature (ºC)	Reaction Pressure (bar-g)	Coal Charge (g)	Gas Flow Rate (SLPM)	Inlet Oxygen Concentration (vol%)
1	74	800	8.0	4.46	5.20	7.6
2	74	850	8.0	5.00	5.50	6.8
3	74	875	8.0	5.00	5.60	7.2
4	125-177	800	8.0	5.00	6.30	7.2
5	125-177	850	8.0	4.21	6.30	7.5
6	125-177	875	8.0	3.93	5.50	7.0
7	125-177	800	8.0	4.13	3.00	16.0
8	125-177	850	8.0	4.60	3.00	16.0
9	125-177	875	8.0	4.13	3.00	16.0
10	125-177	800	0.3	3.28	3.00	5.3
11	125-177	850	0.3	4.82	3.00	5.9
12	125-178	850	0.4	3.19	3.00	6.5

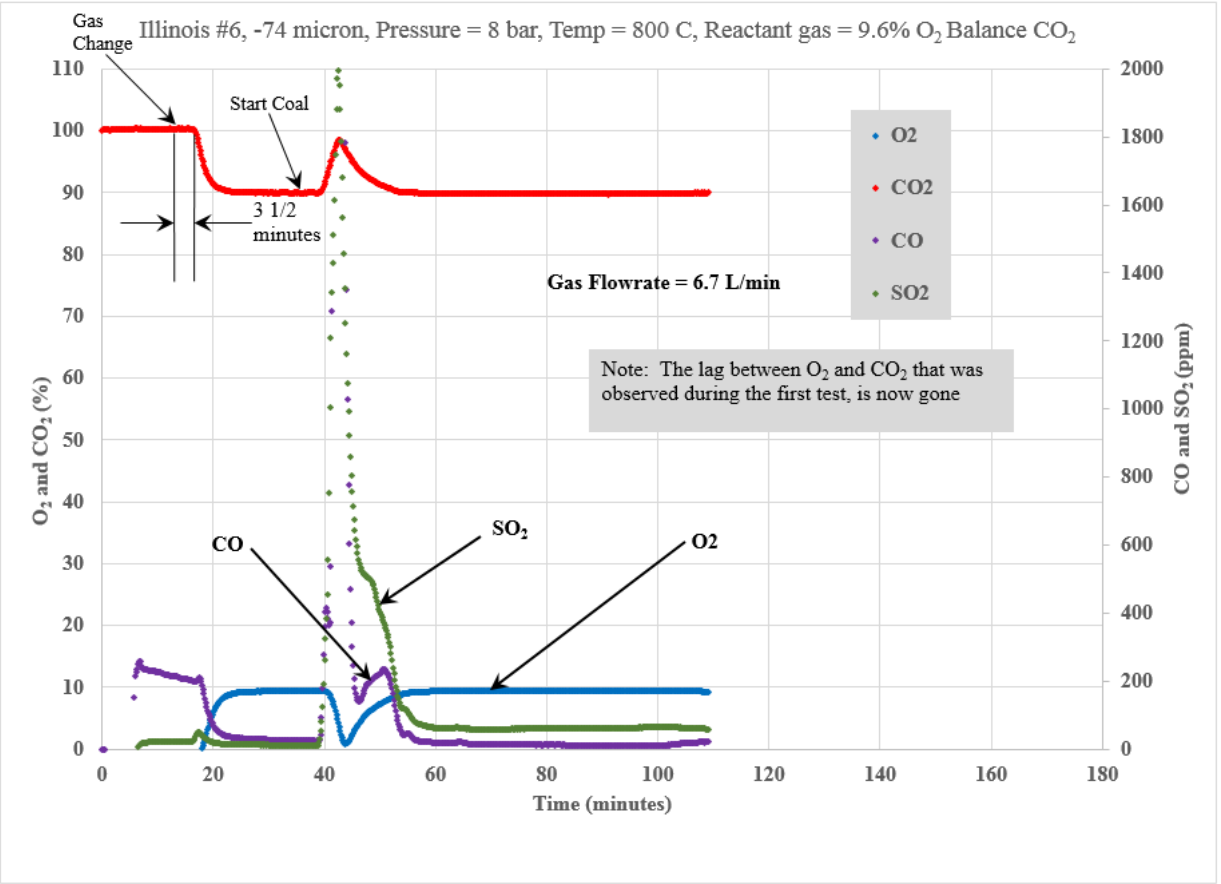

Figure 1. Typical Raw Data from a PSU Coal Reactivity Test (Jan 26, 2015 Checkout Run).

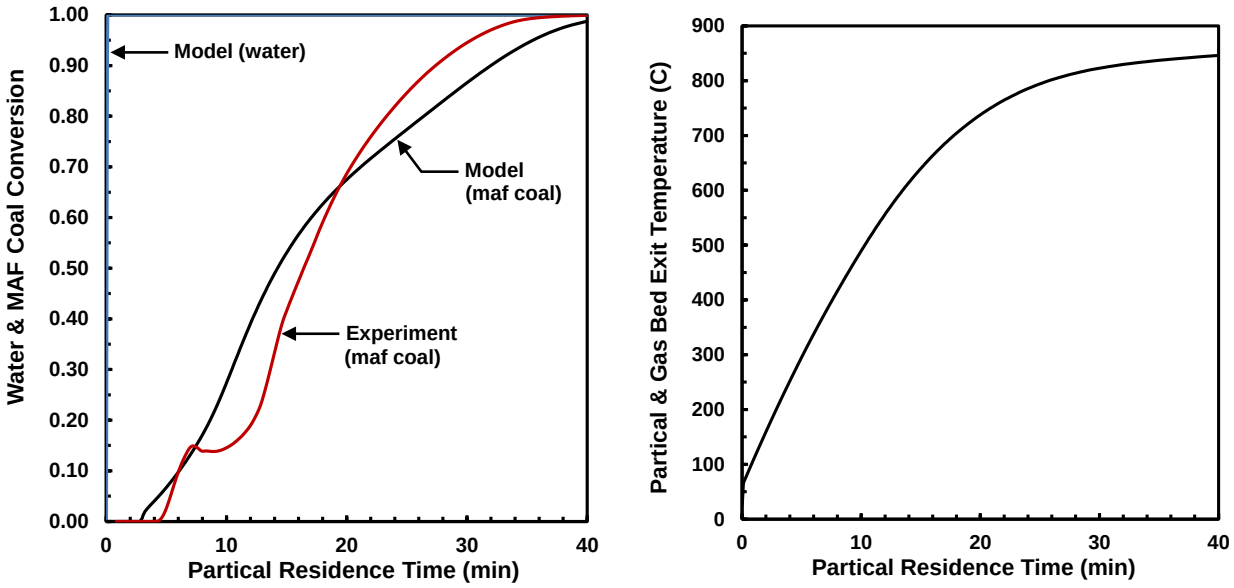

Figure 2a. PSU Coal Reactivity Test – Run No. 1
(Furnace Temp = 800ºC; Pressure = 8 barg; Particle Size = 74 µm; Inlet Oxygen = 7.6 vol%)
($\dot{Q}_{rad,in}$ = 200 Watts)

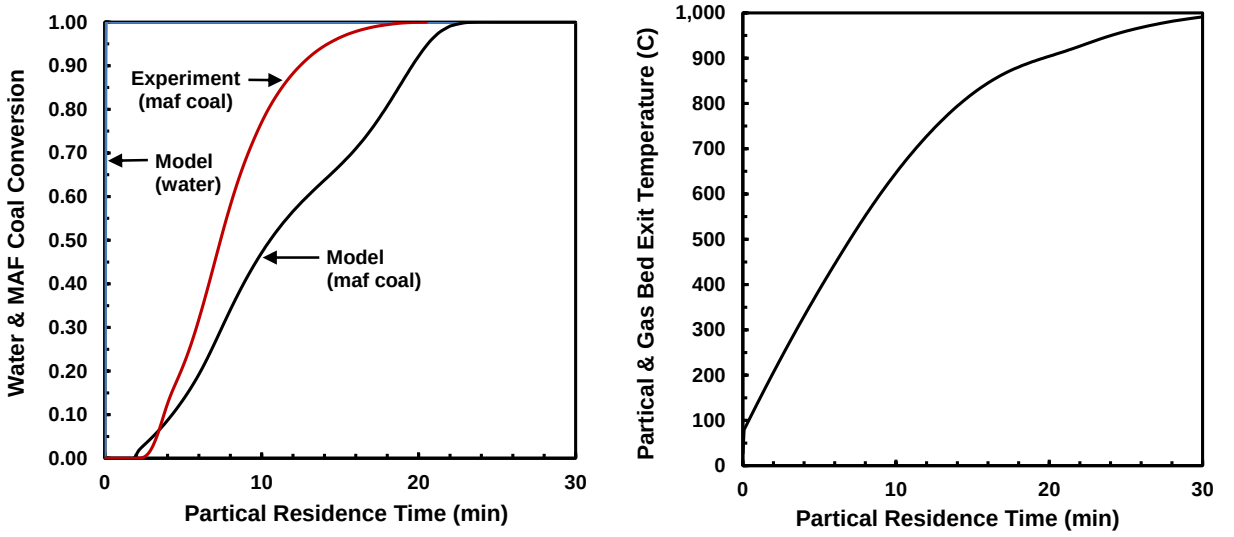

Figure 2b. PSU Coal Reactivity Test – Run No. 2
(Furnace Temp = 850ºC; Pressure = 8 barg; Particle Size = 74 µm; Inlet Oxygen = 6.8 vol%)
($\dot{Q}_{rad,in}$ = 350 Watts)

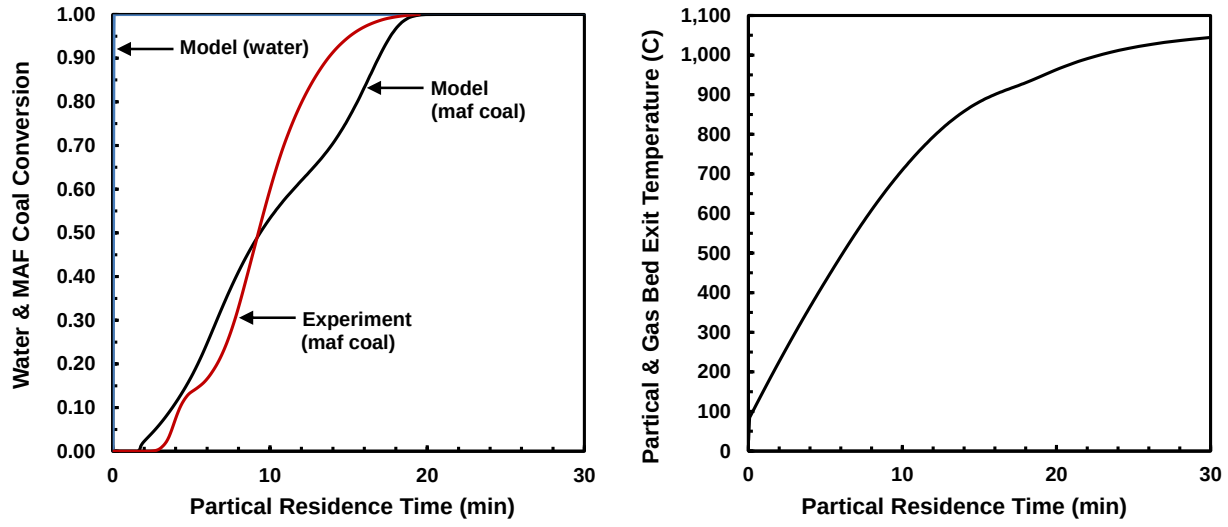

Figure 2c. PSU Coal Reactivity Test – Run No. 3
(Furnace Temp = 875ºC; Pressure = 8 barg; Particle Size = 74 µm; Inlet Oxygen = 7.2 vol%)
($\dot{Q}_{rad,in}$ = 400 Watts)

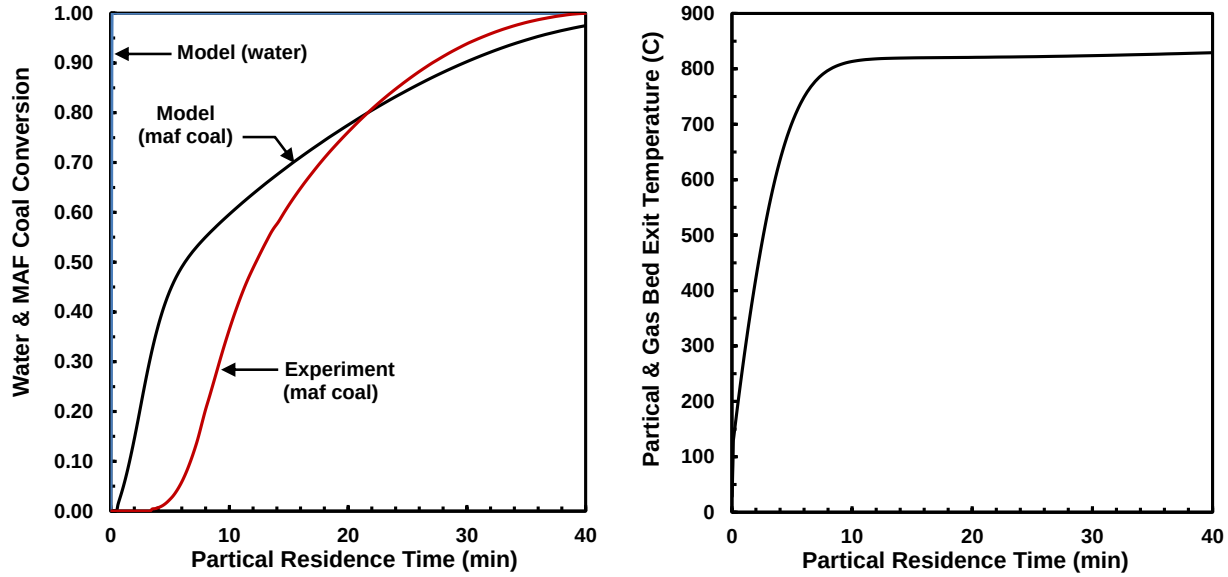

Figure 3a. PSU Coal Reactivity Test – Run No. 4
(Furnace Temp = 800ºC; Pressure = 8 barg; Particle Size = 177 µm; Inlet Oxygen = 7.2 vol%)
($\dot{Q}_{rad,in}$ = 180 Watts)

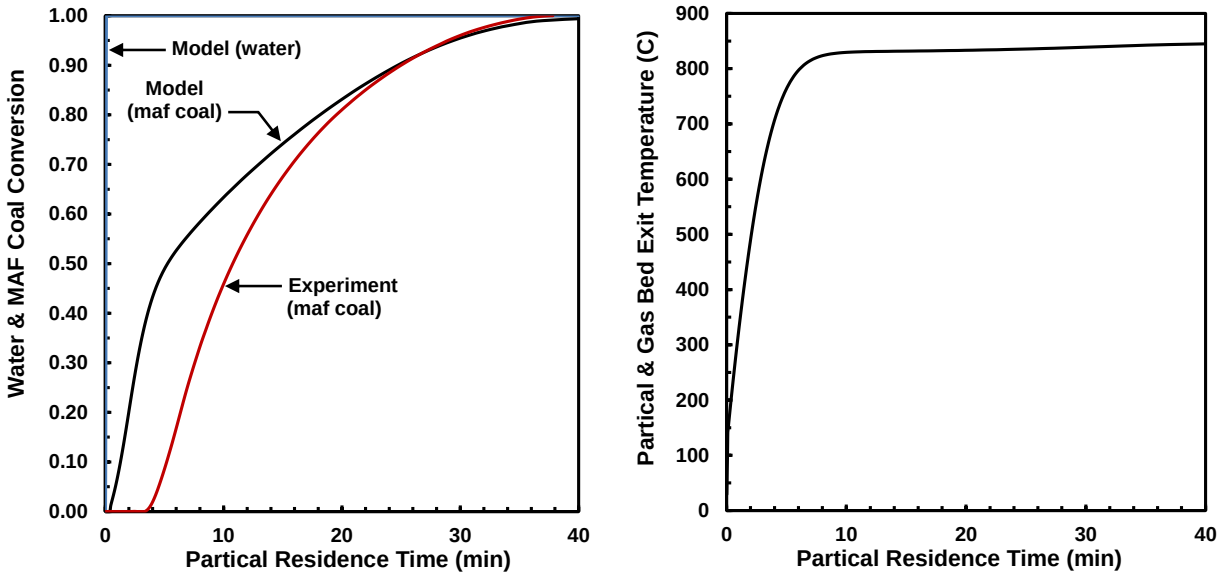

Figure 3b. PSU Coal Reactivity Test – Run No. 5
(Furnace Temp = 850ºC; Pressure = 8 barg; Particle Size = 177 µm; Inlet Oxygen = 7.5 vol%)
($\dot{Q}_{rad,in}$ = 180 Watts)

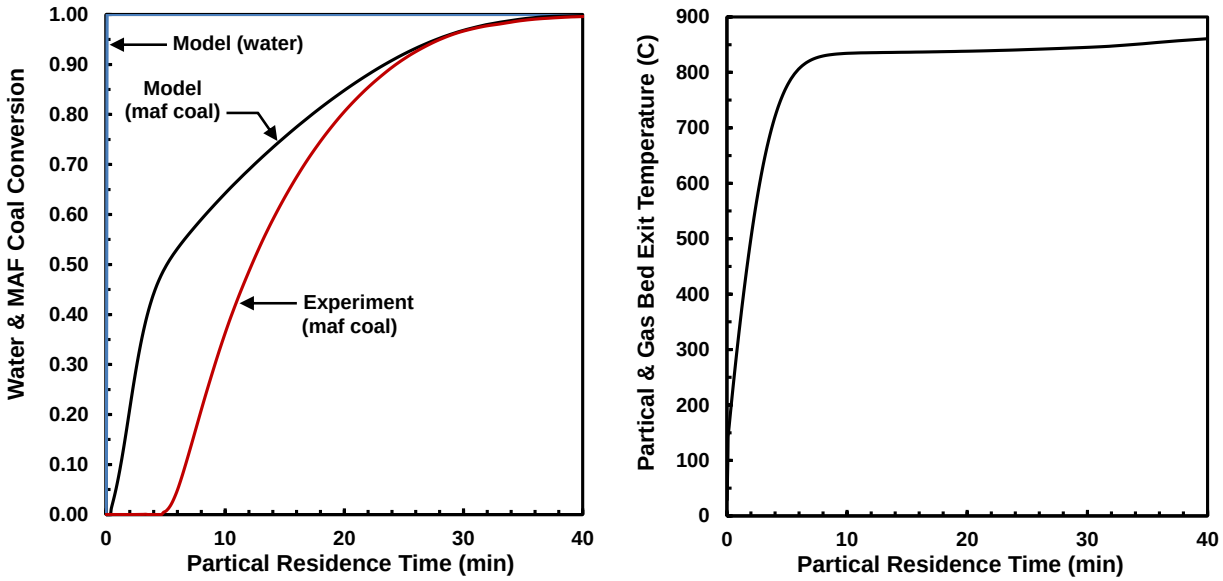

Figure 3c. PSU Coal Reactivity Test – Run No. 6
(Furnace Temp = 875ºC; Pressure = 8 barg; Particle Size = 177 µm; Inlet Oxygen = 7.0 vol%)
($\dot{Q}_{rad,in}$ = 180 Watts)

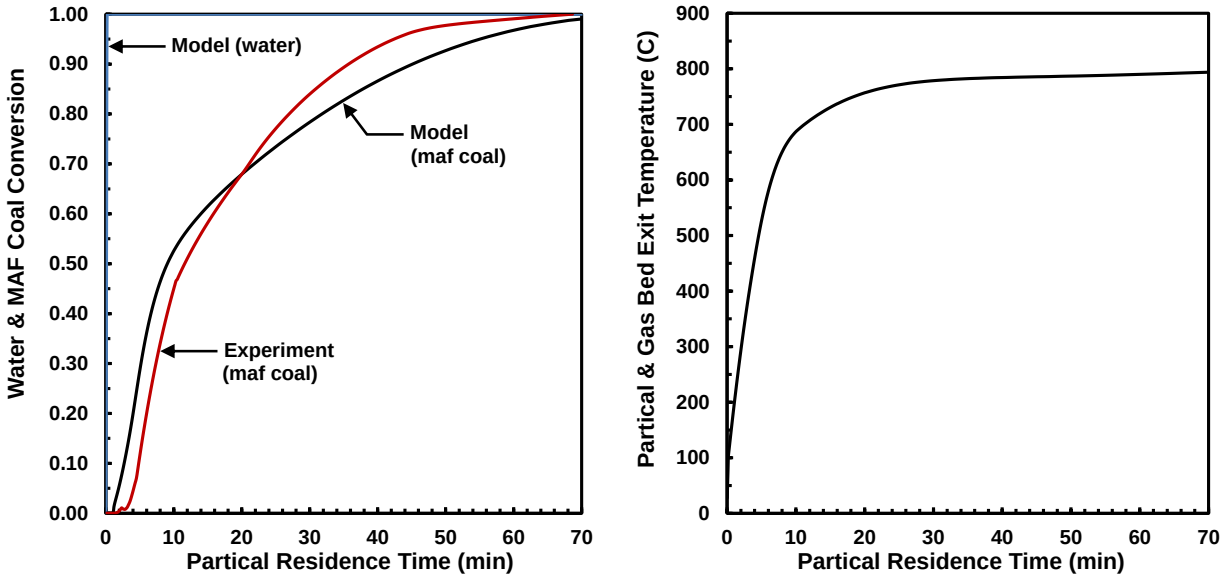

Figure 4a. PSU Coal Reactivity Test – Run No. 7
(Furnace Temp = 800ºC; Pressure = 8 barg; Particle Size = 177 µm; Inlet Oxygen = 16 vol%)
($\dot{Q}_{rad,in}$ = 100 Watts)

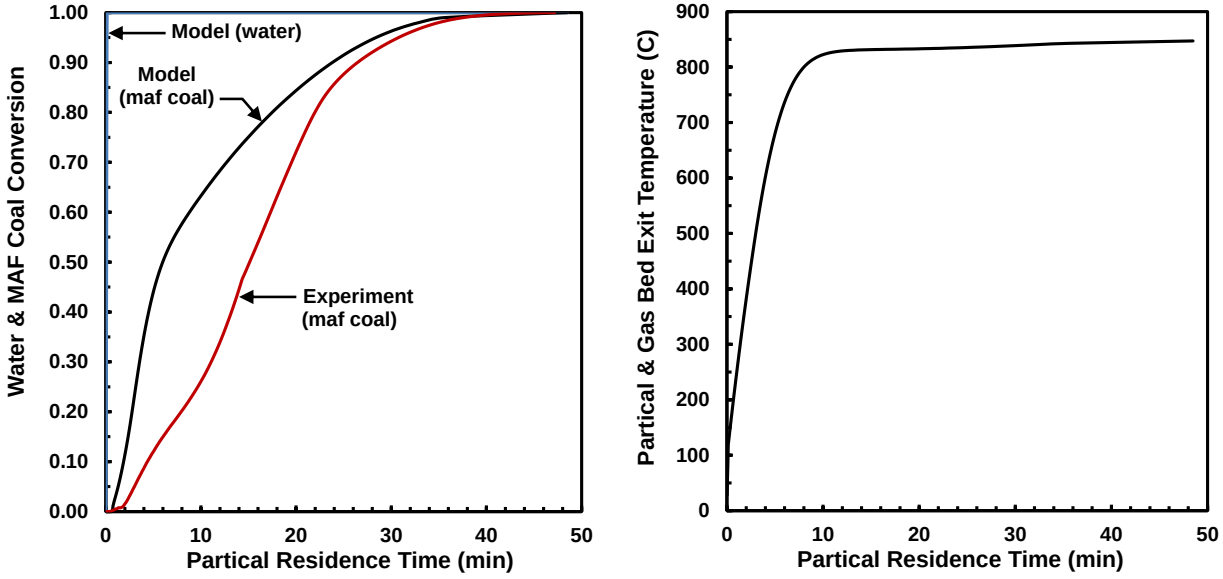

Figure 4b. PSU Coal Reactivity Test – Run No. 8
(Furnace Temp = 850ºC; Pressure = 8 barg; Particle Size = 177 µm; Inlet Oxygen = 16 vol%)
($\dot{Q}_{rad,in}$ = 180 Watts)

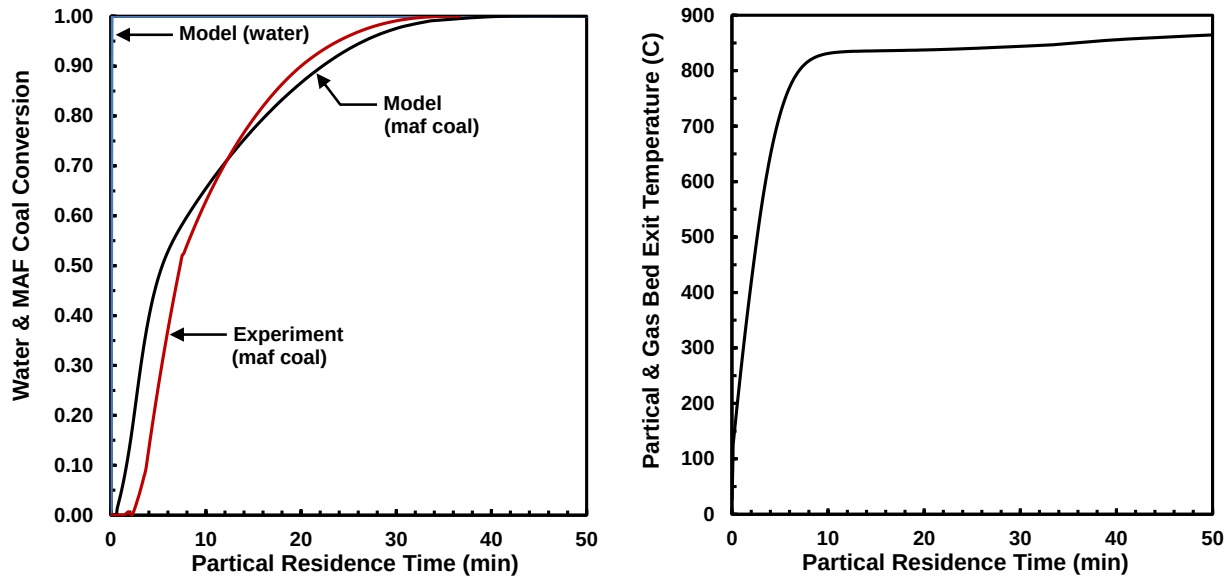

Figure 4c. PSU Coal Reactivity Test – Run No. 9
(Furnace Temp = 875ºC; Pressure = 8 barg; Particle Size = 177 µm; Inlet Oxygen = 16 vol%)
($\dot{Q}_{rad,in}$ = 180 Watts)

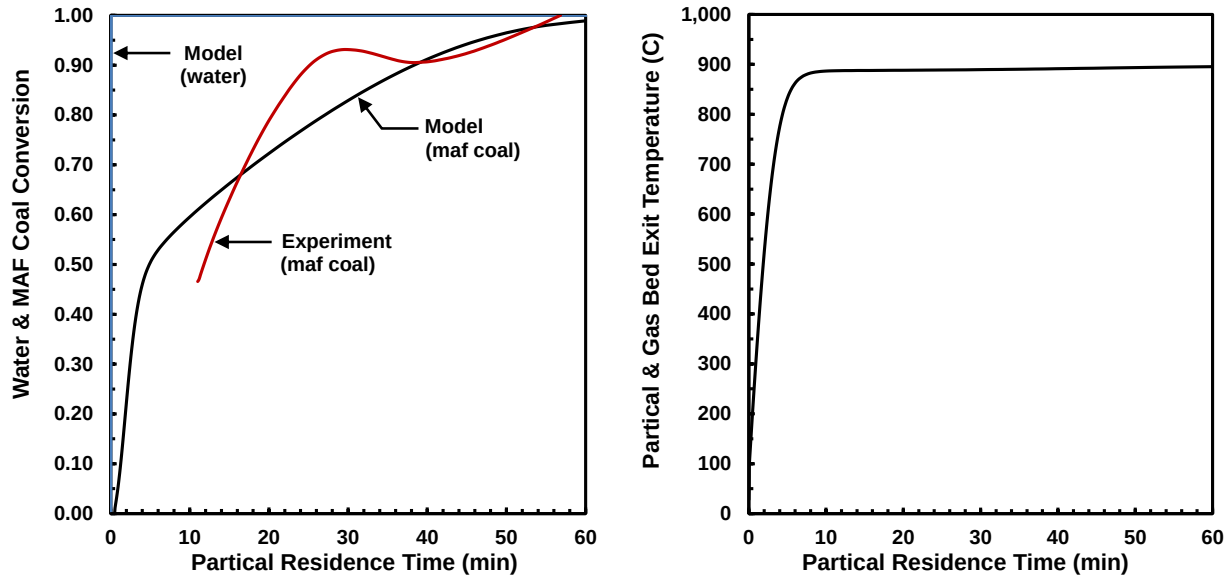

Figure 5a. PSU Coal Reactivity Test – Run No. 10
(Furnace Temp = 800ºC; Pressure = 0.3 barg; Particle Size = 177 µm; Inlet Oxygen = 5.3 vol%)
($\dot{Q}_{rad,in}$ = 225 Watts)

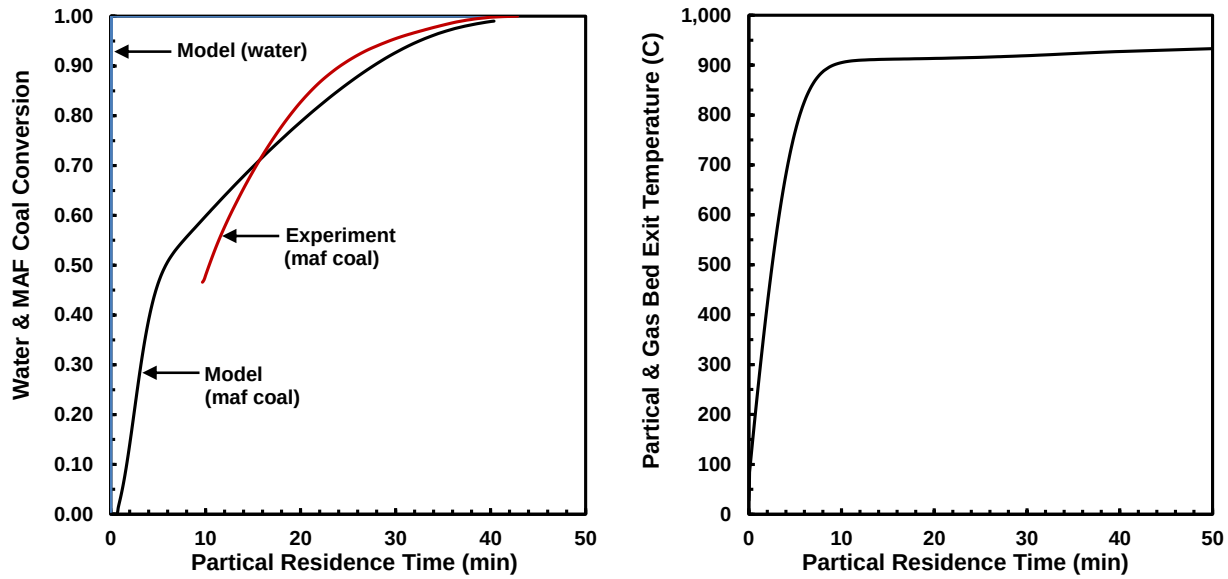

Figure 5b. PSU Coal Reactivity Test – Run No. 11
(Furnace Temp = 850ºC; Pressure = 0.3 barg; Particle Size = 177 µm; Inlet Oxygen = 5.9 vol%)
($\dot{Q}_{rad,in}$ = 250 Watts)

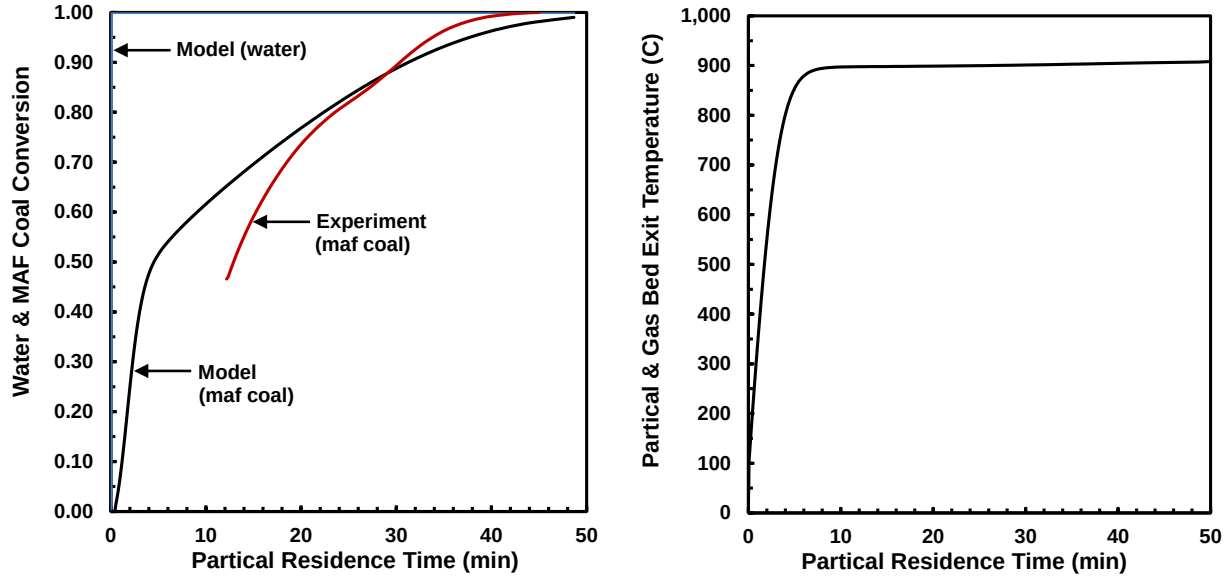

Figure 5c. PSU Coal Reactivity Test – Run No. 12
(Furnace Temp = 850ºC; Pressure = 0.4 barg; Particle Size = 177 µm; Inlet Oxygen = 6.5 vol%)
($\dot{Q}_{rad,in}$ = 230 Watts)

CONCLUSIONS

The PF/WSR model developed above for simulating the experimental PSU PFBC reactor, showed reasonable data correlation for the twelve bituminous coal reactivity tests conducted. For the most part, the PF/WSR simulation model used historical kinetic data developed at the Massachusetts Institute of Technology (MIT – Cambridge, MA) in the 1980's and other laboratories – as reported by Elliott (1981). For the PF/WSR model simulation used in this report, the only adjustable parameter used to obtain correlation was the furnace radiation heat transfer rate, $\dot{Q}_{rad,in}$. Due to the importance this term has on determining the particle temperature and hence the particle's time dependent maf mass conversion weight loss profiles, it is recommended that PSU consider adding and calibrating an optical pyrometer to the experimental test set-up when testing granular material that is subject to substantial particle heat-release rates as encountered in char-O_2 oxidation.

The fact that the GTI historical kinetic constants for bituminous coal devolatilization and char oxidization (being use to predict the short residence CANMET oxy-PFBC pilot plant combustor performance) are reasonably able to correlate the longer coal burn-out times found within the PSU PFBC reactor is quite encouraging.

The "shrinking core" char-O_2 model was found to be very effective in providing this correlation with the historical GTI kinetic data. The shrinking core representation provides relatively fast burn-out rates for particles at or below the distribution's Sauter, D_{32}, mean diameter of approximately 24-microns [typical from a standard entrained-flow industrial grind specification of 70 wt% passing through a 200-mesh (or 74-micron opening) screen]. The "shrinking core" model significantly increases the burn-out resistance for large particles since the oxidizing gas must move through a growing diffusion resistant ash shell that scales to the square of the particle diameter.

Finally, the longer burn-out times produced by the PSU PFBC were also attributed to the high carbonaceous solids loading within the PSU fluidized bed when compared to the fluidizing/oxidizing gas flow rate. As mentioned above, the particle heat up times to reach pyrolyzing temperatures were quite long due to the significant cooling of the fluidizing/oxidizing gas by the particles themselves. Not only did the low fluidizing/oxidizing gas flow rates (required for coal blow-out prevention) drastically slow down the coal particle heating rates, there also wasn't enough oxygen gas in this stream to maintain rapid combustion once the char particles reached temperatures above 650ºC. Here it was found that the oxygen concentration within the fluidizing gas would drop to zero, terminating maf coal conversion at the top of the fluidized bed even though the bed still contained significant unburned carbon. This condition also led to increased conversion times within the PSU PFBC test apparatus. In the CANMET pilot plant PFBC, there will be significantly more fluidizing gas surrounding each coal/char

particle during its flight through the fluidized bed to provide faster particle heat up rates and higher oxygen concentrations at the char's surface during the particle combustion period.

REFERENCES

Chase, M.W., et al., *JANAF Thermochemical Tables*, 3d Ed., Parts I and II -- *J. Phys. Chem. Ref. Data, 14* (Suppl. No. 1) – American Chemical Society, New York, NY (1985).

Elliott, M.A. (Ed.), *Chemistry of Coal Utilization* (Second Supplementary Volume), Wiley, New York, NY (1981).

Friend, D.G., *NIST Thermophysical Properties of Pure Fluids (Version 3.0)*, NIST Stan. Ref. Database 12, National Institute of Standards and Technology, Gaithersburg, MD (1992).

Stewart, A.E., G. Subbaraman, J.A. Mays, and J.A. Hartung; "Reactor System and Solid Fuel Composite Therefor;" *U.S. Patent Application No. 12/794,218* (2010).

Stewart, A.E., and J.A. Mays; "Reactor System and Method Therefore," *U.S. Patent No. 8,105,541* (2012).

ACKNOWLEGDMENTS

The following individuals made important contributions in providing the materials, facilities and test data discussed within this report. Prof. Sarma V. Pisupati (Chair, Energy Engineering Program -- Penn State University), Mr. David K. Johnson (Research Assistant, Penn State University), and Ms. Aditi Khadilkar (Research Assistant, Penn State University).

Appendix C. Limestone Reactivity Report

PENN STATE SULFATION TESTS & KINETIC ANALYSIS

Kenneth M. Sprouse; PE, Esq.
Chief Technologist -- Energy Systems
Aerojet Rocketdyne Inc.
Canoga Park, CA 91309

January 8, 2015

Note: This report was edited on Feb. 29, 2016 to remove proprietary information.

ABSTRACT

This report describes the Gas Technology Institute (GTI) sulfation kinetic model used to correlate a series of Penn State University (PSU) experiments on various limestone feedstocks. The experimental apparatus was a small pressurized fluidized bed reactor (PFBR) contained within a constant temperature electrically heated furnace. The PFBR operated at a pressure of approximately 7.89 atm and at temperatures between 825 and 875ºC. The fluidization gas composition was nominally 92 vol% carbon dioxide (CO_2), 7 vol% oxygen (O_2) and 2,400 parts per million dry (ppm-dry) or 0.24 vol% sulfur dioxide (SO_2). The fluidization gas flow rate to the PFBR was approximately 5 standard liters per minute (slm) and its superficial gas velocity within the PFBR was on the order of 1.4 cm/s. Four granular limestones were tested – identified as Graymont, Michigan, Dolomite-A, and Dolomite-B – which had been pulverized to a particle size of minus 200 mesh (or minus 74-micron). The limestone mass charge into the PFBR was approximately 5 grams. The GTI sulfation kinetic model used for test data correlation assumes: (1) the gas flow through the PFBR is one-dimensional uniform plug flow (PF), and (2) the thin layer of limestone mass within the fluidized bed recirculates under well-stirred-reactor (WSR) conditions. This PF/WSR kinetic model was shown to reasonably correlate the experimental test data. The activation energy of the sulfation's rate limiting reaction step was found to be 24.1 kcal/mol with pre-exponential velocities ranging from 4.6 cm/s (for Dolomite-B) to 746 cm/s (for Dolomite-A). It is envisioned that these kinetic parameters will be subsequently used in the GTI generalized pressurized fluidized bed combustor (PFBC) performance model.

It should be noted that this report is a revision of an earlier report dated July 24, 2015. It was discovered that the Michigan limestone was incorrectly identified during subsequent post-test physical property measurements. The labeled Michigan limestone originally tested was in fact another Dolomite containing only 55.1 wt% calcium carbonate, $CaCO_3$(s). Kinetic model correlation on this material, now identified as Dolomite-B, was re-run using the updated physical parameters. To complete the PSU work statement, another set of three experiments using the correct Michigan limestone was performed in the PSU PFBR reactor. Kinetic model correlation with these last three limestone experiments is also included in this revised report.

INTRODUCTION & BACKGROUND

Removal of gaseous sulfur oxides (sulfur dioxide, SO_2, and sulfur trioxide, SO_3, or SOx) from air fired coal combustors has been generally accomplished over the years with the use of calcined limestone (i.e., lime, CaO). Usually, this lime is hydrated to calcium hydroxide [$Ca(OH)_2$] by the addition of water (within a pre-injection slaking process) for subsequent post combustion injection into the combustor's flue gas. The use of pressurized fluidized bed combustors (PFBCs) for the coal combustion reactor has the potential of eliminating the limestone's calcination and slaking pre-processes by injecting the limestone ($CaCO_3$) directly into the combustor for direct SOx removal. The GTI oxy-fired PFBC (for economical post combustion carbon dioxide, CO_2, capture and sequestration) is expected to use direct injection of limestone into the combustor as the combustor system's primary SOx removal process.

Penn State completed twelve tests on four limestones in order to provide sulfation data to GTI on its oxy-fired PFBC design which injects micron size (minus 74-mircons) coal particles into a pressurized fluidized bed that is stabilized by inert millimeter sized oxide particles (e.g., aluminum oxide). In such a bed, the coal particle residence times are on the same order as the gas (i.e., seconds) rather than minutes (as is the case with conventional fluidized bed designs). The Penn State testing was designed to help determine whether elutriated micron sized limestone particles can be injected into the bed (similar to the micron size coal particles) or whether they need to be introduced as millimeter sized bed stabilization particles. The results below indicate that the limestone will need to be injected into the bed as millimeter sized particles.

PF/WSR MODEL FOR PENN STATE PFBR DATA CORRELATION

Chemistry

The main chemical reaction for the capture of gaseous SOx (SO_2 and SO_3) by solid limestone and the subsequent production of solid gypsum ($CaSO_4$) is:

$$CaCO_3(s) + SO_3(g) \underset{\leftarrow}{\overset{k_{sox}}{\rightarrow}} CaSO_4(s) + CO_2(g) \qquad \text{(R1)}$$

where k_{sox} is the elementary first-order forward reaction rate constant for the equilibrium reaction, Reaction R1. This reaction liberates gaseous CO2 and requires gaseous sulfur tri-oxide, SO_3, as the reactant. Since the coal's fuel bound sulfur is usually produced as sulfur dioxide, SO_2, during high temperature particle combustion, any captured sulfur dioxide must first be converted to sulfur tri-oxide at the lower sulfation temperatures. For excess oxygen, O_2, environments; this conversion can be described by the equilibrium reaction:

$$SO_2(g) + \frac{1}{2}O_2(g) \rightleftharpoons SO_3(g) \qquad \text{(R2)}$$

Reactions R1 and R2 represents a system of four elementary kinetic reactions – two forward reactions and two backward reactions. Here, the forward reaction of equilibrium Reaction R1 will be considered the rate determining step (RDS) for the SOx capture kinetics. For the GTI PF/WSR model, the equilibrium constants for Reactions R1 and R2 (i.e., $K_{p,r1}$ and $K_{p,r2}$) are expressed in the Clausius-Clapeyron format whose constants are determined from the National Institute of Standards and Technology (NIST) reference, Chase et al. (1985). Here,

$$K_{p,r1} = A_{p,r1} \exp\left(\frac{B_{p,r1}}{R\,T_p}\right) \qquad (1)$$

and:

$$K_{p,r2} = A_{p,r2} \exp\left(\frac{B_{p,r2}}{R\,T_p}\right) \qquad (2)$$

where R is the universal gas constant (1.986 cal/mol-K), T_p is the limestone particle temperature, and values for the constants $A_{p,r1}$, $B_{p,r1}$, $A_{p,r2}$, and $B_{p,r2}$ are found in Table 1 below. It should be noted that the constant $A_{p,r1}$ is dimensionless while the constant $A_{p,r2}$ has units of $atm^{-1/2}$.

The first-order forward RDS kinetic rate constant, k_{sox}, from Reaction R1 is given by the equation:

$$k_{sox} = A_{sox} \exp\left(\frac{-E_{sox}}{R\,T_p}\right) \qquad (3)$$

where A_{sox} is the pre-exponential first order heterogeneous rate constant with units of velocity (e.g., cm/s), and E_{sox} is the RDS activation energy. Both constants A_{sox} and E_{sox} are determined from the Penn State PFBR experiments as further discussed below.

As noted in the abstract, the Penn State PFBR sulfation tests were run at a pressure of 7.89 atm and at temperatures below 900ºC. These conditions are below the limestone's calcination temperature -- whereby limestone is converted to lime via the following reaction:

$$CaCO_3(s) \rightleftharpoons CaO(s) + CO_2(g) \qquad \text{(R3)}$$

At 7.89 atm, the NIST chemical equilibrium data base shows that the limestone calcination decomposition temperature is approximately 1,050ºC. Hence, the current model does not account for the reactions of SO_3 with calcium oxide, CaO(s).

Table 1. Clausius-Clapeyron Sulfation Equilibrium Constants

Pre-exponential Constants, A_p	
Reaction R1, $A_{p,r1}$	4.452×10^{-2}
Reaction R2, $A_{p,r2}$	1.433×10^{-5} atm$^{-1/2}$
Exponential Constants, B_p	
Reaction R1, $B_{p,r1}$	52.83 kcal/mol
Reaction R2, $B_{p,r2}$	23.33 kcal/mol

Penn State PFBR Hydrodynamics

As stated in the abstract above, the hydrodynamic analysis of the Penn State PFBR assumes: (1) the gas flow through the bed is one-dimensional uniform plug flow (PF), and (2) the thin layer of limestone mass within the fluidized bed recirculates under well-stirred-reactor (WSR) conditions. When this is the case, the fraction of calcium within the limestone particles that is calcium carbonate, f_{sox}, is the same for all particles within the bed and is determined by the following mass balance equation:

$$f_{sox} = 1 - \frac{\hat{M}_{CaCO_3}}{\hat{M}_g \, W^o_{LS} \, Y^o_{CaCO_3}} \int_{t=0}^{t} \dot{m}_g \left(\chi^o_{sox} - \chi_{sox,out} \right) dt \qquad (11)$$

where $\hat{M}_{CaCO_3}$ is the molecular weight of calcium carbonate (100.1 g/mol), W^o_{LS} is the initial mass of limestone loaded into the PFBR at the start of a test, $Y^o_{CaCO_3}$ is the initial mass fraction of calcium carbonate within the limestone loaded into the PFBR, $\dot{m}_g$ is the mass flow

rate of fluidizing gas into the PFBR, χ^{o}_{sox} is the initial mole fraction of SOx (SO_2 plus SO_3) within the fluidizing gas fed to the PFBR, and $\chi_{sox,out}$ is the mole fraction of SOx (SO_2 plus SO_3) within the gas exiting the PFBR.

For a single limestone particle surrounded by a gaseous medium (containing carbon dioxide, oxygen, and oxides of sulfur); the instantaneous molar flow rate of SOx (SO_2 plus SO_3) into the particle, $\dot{n}_{sox}$, using the chemistry scheme described above can be shown to be:

$$\dot{n}_{sox} = \frac{4\,\pi\,r_s^{2}\,P\,k^{*}_{sox}\,f_{sox}\left\{\chi_{sox} - \left[1 + \frac{1}{K_{p,r2}\left(P\,\chi_{O_2}\right)^{1/2}}\right]\frac{(1-f_{sox})\,\chi_{CO_2}}{f_{sox}\,K_{p,r1}}\right\}}{R\,T_p\left[1 + \frac{2\,r_s\,\rho_g\,c_p\,k^{*}_{sox}\,f_{sox}}{\lambda\;Nu} + \frac{1}{K_{p,r2}\left(P\,\chi_{O_2}\right)^{1/2}}\right]} \quad (4)$$

where r_s is the limestone particle radius, P is the gas pressure, k^{*}_{sox} is the effective heterogeneous RDS forward reaction rate constant for a porous particle, f_{sox} is the fraction of calcium within the particle that is calcium carbonate, χ_{sox} is the mole fraction of SOx (i.e., SO_2 plus SO_3) within the gas stream, χ_{CO_2} is the mole fraction of carbon dioxide (CO_2) within the gas stream, χ_{O_2} is the mole fraction of oxygen (O_2) within the gas stream, ρ_g is the gas density, c_p is the gas specific heat, λ is the gas thermal conductivity, and Nu is the Nusselt number for gas flow past a particle.

Completing a continuity mass balance on the fluidizing gas passing through the PFBR and using Equation 4 for the determination of the SOx consumption rate within a given control volume inside the bed will show that the effective heterogeneous RDS forward reaction rate constant for the porous particles, k^{*}_{sox}, is given by:

$$k^{*}_{sox} = \frac{\left[1 + \frac{1}{K_{p,r2}\left(P\,\chi_{O_2}\right)^{1/2}}\right]}{\rho_g\, f_{sox}\left\{\frac{3\,W^{o}_{LS}}{\rho_p\, r_s\, \dot{m}_g\, \ln\left[\frac{\left(\chi^{o}_{sox} - \beta\right)}{\left(\chi_{sox,out} - \beta\right)}\right]} - \frac{2\, r_s\, c_p}{\lambda\, Nu}\right\}} \qquad (12)$$

where the parameter β is given by:

$$\beta = \left[1 + \frac{1}{K_{p,r2}\left(P\,\chi_{O_2}\right)^{1/2}}\right]\frac{\left(1 - f_{sox}\right)\,\chi_{CO_2}}{K_{p,r1}\, f_{sox}} \qquad (13)$$

In the derivation of Equation 12; it is required that gypsum, $CaSO_4(s)$, is not liberating $SO_3(g)$ anywhere within the bed. From Equation 4, this condition implies that the parameter β is less than the exiting SOx mole fraction (i.e., $\beta < \chi_{sox,out}$).

Equations 12 and 13 also require that the gaseous mole fractions of carbon dioxide, χ_{CO_2} , and oxygen, χ_{O_2} , do not change across the bed, but remain nearly constant at their PFBR injection values. The first principal derivation of Equation 12 is subsequently provided in Appendix B of this report.

It should be noted that using granular limestone at minus 200-mesh (or minus 74-micron) particle sizes requires a relatively tight band on the PFBR's superficial gas velocity. The velocity must be fast enough to fluidized the particles with good bed recirculation in order to invoke the well-stirred reactor (WSR) assumption while not exceeding a particle's gravitational terminal velocity and causing the loss of granular bed material through elutriation.

The minimum superficial fluidization velocity, $u_{s,m}$, can be determined from the Ergun equation [see, e.g., Bird et al. (1960)] and is given by:

$$\frac{K'_{pq}\,\rho_g}{\varepsilon_o^{\,3}\,D_{pq}}\,u_{s,m}^{\,2} \;+\; \frac{K''_{pq}\,(1-\varepsilon_o)\,\mu}{\varepsilon_o^{\,3}\,D_{pq}^{\,2}}\,u_{s,m} \;=\; \rho_s\,g \qquad (14)$$

where K'_{pq} is the Burke-Plummer constant (equals 1.75 for mono-size spherical particles), K''_{pq} is the Blake-Kozeny constant (equals 150 for mono-size spherical particles), ε_o is the static unconsolidated bed void fraction, D_{pq} is the mean diameter of the particle size distribution, μ is the gas dynamic viscosity, ρ_s is the true solids density with no voids, and g is the gravitational acceleration constant (equals 9.81 m/s^2).

The mean particle diameter of a given particle size distribution, D_{pq}, is calculated from the following formula:

$$D_{pq} \;=\; \left[\frac{\int_o^{\infty} D_p^{\,p}\; f_n\; d\,D_p}{\int_o^{\infty} D_p^{\,q}\; f_n\; d\,D_p}\right]^{1/(p-q)} \qquad (15)$$

where D_p is a particle diameter within the particle size distribution (PSD), f_n is the particle size number distribution of the PSD (in units of particles/μm), and the integer constants p and q are the constants defining a particular mean diameter of the PSD. This definition of diameter means was first developed by Mugele and Evans (1951). When the PSD is mono-spherical (i.e., all particles are perfect spheres with only one diameter), all particle means calculated from Equation 15 will exactly equal the mono-diameter. When p equals 3 and q equals 2, the mean particle diameter D_{32} is the well-known Sauter mean diameter (also called the volume-surface mean diameter).

It should be noted that Penn State did not determine the particle size number distribution function, f_n, for the minus 200 mesh (minus 74-micron) PSDs used in these experiments. Hence, effective mean diameters cannot be determined from Equation 15 for use in Equation 14. However, an upper limit on the minimum fluidization velocity can still be estimated from Equation 14 using 74-microns as the mean particle diameter, D_{pq}, for the granular limestones. Also, the static unconsolidated bed void fraction, ε_o, was not determined. However, it is known that ε_o is approximately 0.52 for many granular materials.

If it is assumed that the Burke-Plummer and Blake-Kozeny constants (K'_{pq} and K''_{pq}) are essentially the same values (1.75 and 150 respectively) for the various mean diameters, the minimum superficial gas velocities for the carbon dioxide gases used in these experiments at 7.89 atm pressure and 800ºC temperature will be found from Equation 14 to be approximately 0.73 cm/s. This value is about one-half of the actual superficial gas velocities tested – as provided in the abstract above. Hence, this should ensure that the limestone particles' well-stirred-reactor (WSR) assumption -- as used in the derivation of Equation 12 above -- is valid over the PFBR's nominal 0.25 cm bed height.

The limestone particle terminal velocities must also be greater than the gas superficial velocity to ensure that no limestone is elutriated from the fluidized bed and lost from the PFBR. Each particle's terminal velocity, $v_{p,t}$, can be determined from the following equation:

$$v_{p,t} = \frac{D_p^2 \rho_p g}{18 \mu \left[1 + 0.1104 \sqrt{Re} \right]^2} \qquad (16)$$

Setting the particle terminal velocity, $v_{p,t}$, from Equation 16 equal to the Penn State's PFBR superficial gas velocity, u_s, of nominally 1.4 cm/s, will show that the limestone's cut-off particle size, $D_{p,cut}$, for these experiments is about 20-microns. Without knowing the actual particle size number distribution, f_n, for the minus 200 mesh (minus 74-micron) PSDs used in these experiments; it is difficult to determine what percentage of limestone particles have diameters below this value. From previous AR/GTI work on entrained flow coal gasifiers, this could be as high as 30 wt% of the total granular solids' mass.

Based upon this result and the uncertainty in the f_n distribution, Penn State continually monitored the PFBR's downstream filters to determine whether they were picking up any limestone or gypsum. For the twelve experiments conducted whose results are reported below, no limestone particles were found on the downstream filters.

PENN STATE PFBR TEST DATA

As mentioned above, Penn State conducted twelve experiments with four different limestones at three discrete temperatures. For each experiment, a constant flow rate of gas was delivered to the PFBR. The inlet gaseous mole fractions of carbon dioxide, CO_2, oxygen, O_2, and sulfur dioxide/trioxide, SOx, were kept constant over the course of each individual experiment. After establishing a hot gas flow through the PFBR at constant temperature, a fixed charge of minus 200-mesh (minus 74-micron) granular limestone was added to the reactor

whereby it was uniformly fluidized at the bottom of the PFBR – just above the gas distribution frit. During the run, the instantaneous exit SOx mole fraction, $\chi_{sox,out}$, was continuously measured for use in determining f_{sox} from Equation 11 above. From the calculated values of f_{sox}, an effective instantaneous reaction rate, k_{eff}, time history was reported as shown in Figure 1 using the following definition for k_{eff}:

$$k_{eff} \equiv - \frac{1}{P \chi^{o}_{sox}} \frac{\partial f_{sox}}{\partial t} \tag{17}$$

This figure shows all effective reaction rates are zero at time zero (t = 0.0) and begin increasing to a maximum value before slowly decreasing as time increases. The initial increase in k_{eff} is most likely due to the initial particle heat-up period whereby the particle temperature, T_p, has yet to reach the reactor temperature after being introduced into the hot PFBR. The subsequent decrease in k_{eff} is due to the limestone's conversion of calcium carbonate (CaCO3) to gypsum (CaSO4) within the particles over time -- so that there is less calcium carbonate surfaces for reaction.

Figure 1, reports the measured PFBR furnace temperatures (in degrees Celsius) for each test conducted. The name of the limestone used for each test (Graymont, Michigan, Dolomite-A, or Dolomite-B) is also provided. Penn State University also provided values for the internal Brunauer–Emmett–Teller (BET) surface area, porosity, particle density, and limestone [$CaCO_3$(s)] mass fraction for each of the three limestones. The results for these important physical properties (which are used in the correlation model below) are shown in Table 2. The true solids density, ρ_s, is related to the particle density by the following equation:

$$\rho_s = \frac{\rho_p}{\left(1 - \varepsilon_p\right)} \tag{18}$$

Using Equation 18 and the constant values reported in Table 2 below show that the true solids density for the nearly pure limestones (Graymont and Michigan) is about 2.85 g/cm^3. This result is well within the range of standard crystalline densities reported for calcite (2.71 g/cm^3) and aragonite (2.93 g/cm^3) – see, e.g., Lide (1996).

Table 2. Limestone Physical Properties

	BET Internal Surface Area, S (m^2/g)	Particle Porosity, ε_p (void fraction)	Particle Density, ρ_p (g/cm^3)	$CaCO_3$ Fraction, $Y^o_{CaCO_3}$ (weight fraction)
Graymont	3.10	0.04	2.74	0.982
Michigan	1.70	0.02	2.79	0.888
Dolomite-A	0.89	0.01	2.88	0.523
Dolomite-B	15.77	0.16	2.78	0.551

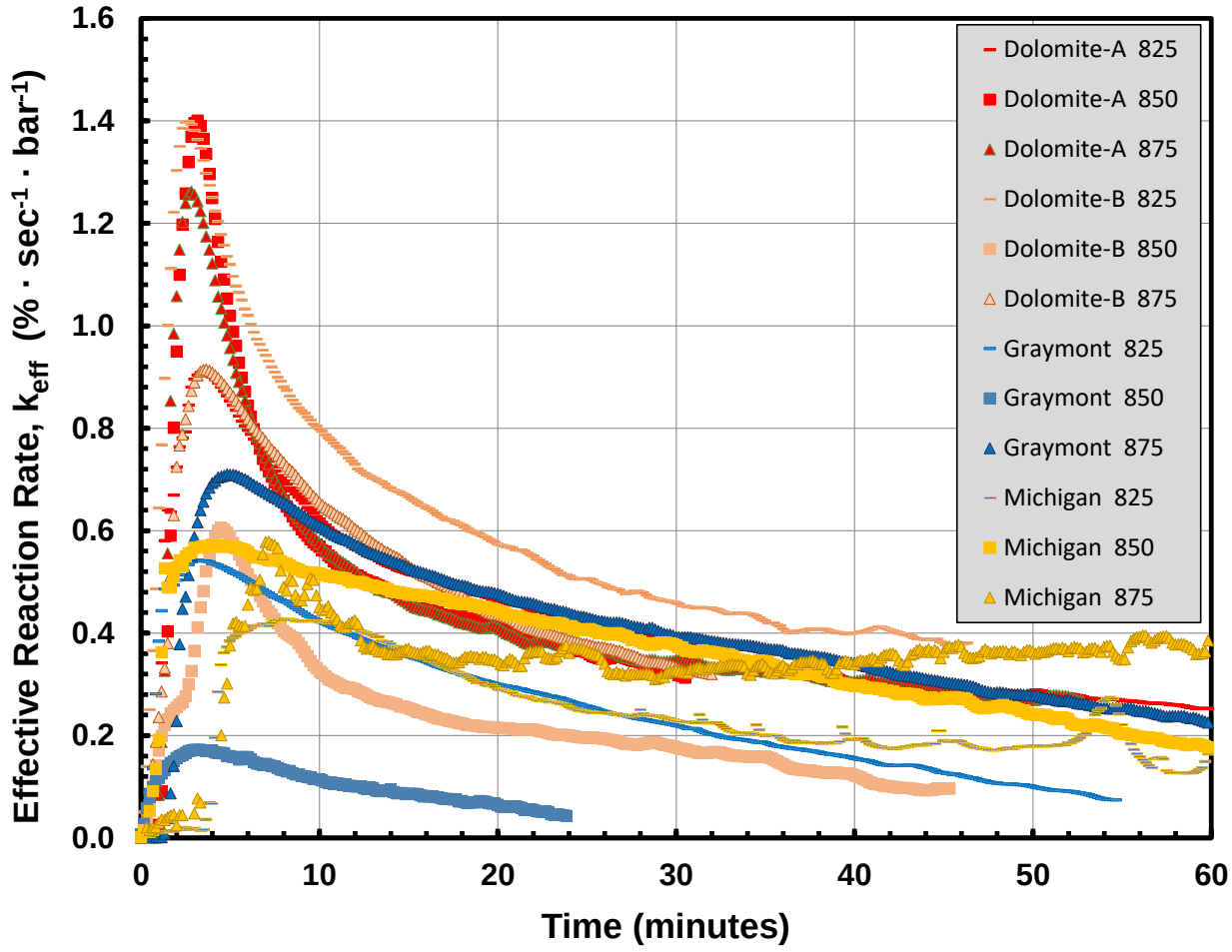

Figure 1. Limestone Sulfation Reaction Rate Histories

From the Penn State data shown in Figure 1 and Table 2 above, the kinetic rate constant parameters A_{sox} and E_{sox} for the forward reaction rate constant, k_{sox} (see, Equation 3), were subsequently determined as detailed in the next section.

PF/WSR MODEL CORRELATION

From the experimental test data provided in Figure 1 above, it was determined that the following two non-dimensional parameters contained within Equations 12 and 13 were significantly less than 1.0. These parameters are:

$$\frac{2\, r_s\, \rho_g\, c_p\, k^*_{sox}}{\lambda\, Nu} \quad << \quad 1.0 \qquad (19)$$

and:

$$\frac{\left(1 - f_{sox}\right) \chi_{CO_2}}{f_{sox} \; K_{p,r1} \; \chi^{o}_{sox}} \quad << \quad 1.0 \tag{20}$$

When Equations 19 and 20 are valid, Equations 11, 12, 13, and 17 can be combined to show the direct relationship between the effective heterogeneous RDS forward reaction rate constant, k^{*}_{sox}, and the effective instantaneous reaction rate, k_{eff}, at any instant in time. This combination produces the important result:

$$k^{*}_{sox} = \frac{r_s \, \rho_p \, Y^{o}_{CaCO3} \, R \, T_p}{3 \, \hat{M}_{CaCO_3}} \left[1 + \frac{1}{K_{p,r2} \left(P \, \chi_{O_2} \right)^{1/2}} \right] \left[\frac{\chi^{o}_{sox} \; \ln\left(\frac{\chi^{o}_{sox}}{\chi_{sox,out}} \right)}{\left(\chi^{o}_{sox} \; - \; \chi_{sox,out} \right)} \right] \frac{k_{eff}}{f_{sox}} \tag{21}$$

As shown in Equation 11 and Figure 1, both f_{sox} and k_{eff} are functions of time. However, these parameters coupled with the time history of $\chi_{sox,out}$ effectively render the parameter, k^{*}_{sox}, a constant over the course of an experiment -- as expected.

Once the effective heterogeneous RDS forward reaction rate constant, k^{*}_{sox}, is determined for each test using Equation 21; the elementary first-order forward RDS kinetic rate constant, k_{sox}, is determined for each experiment from Equations 6 through 9 -- which also require the use of the parameters found in Table 2 above. For each limestone, Arrhenius plots of the k_{sox} data were prepared from the three discrete temperatures tested according to Equation 3 above. The RDS activation energies, E_{sox}, and the pre-exponential constants, A_{sox}, found for each limestone are reported in Table 3 below.

The Table 3 RDS kinetic constants are the key limestone sulfation kinetic input parameters to be used in the GTI PFBC 1-D performance code for sizing the pilot plant combustor at CANMET along with the physical limestone properties reported in Table 2. The Graymont, Michigan, and Dolomite-B limestones were found to react mostly from internal surface area reactions. For these limestones, the parameter $\left\lfloor r_s \, S \, \rho_p \, \eta^{*} / \, 3 \right\rfloor$ from Equation 6

was found to be significantly greater than 1.0. For the Dolomite-A limestone, this parameter was approximately 2.5 – indicting appreciable exterior surface reactions during the experiment due to its high pre-exponential constant, A_{sox}, of 746 cm/s.

Dolomite-B was found to have the lowest kinetic rate constant (A_{sox} = 4.6 cm/sec) of all the limestones tested at PSU. Although Figure 1 shows the effective reaction rates, k_{eff}, for Dolomite-B to be similar to the other limestones; it only achieves these comparable rates due to the order of magnitude increase in its specific internal surface area and porosity when compared to the other limestones. Further investigation should be made as to why the Dolomite-B pre-exponental constant for the calcium carbonate reaction is so low compared to the other limestones. For example, crystallography tests may show that there is more annealed calcium carbonate crystals in Dolomite-B than in the other PSU limestones tested -- which could possibly produce the slower surface reaction rate.

Table 3. Limestone RDS Kinetic Parameters

	Pre-exponental Constant, A_{sox} (cm/s)	Activation Energy, E_{sox} (kcal/mol)
Graymont	55.4	24.1
Michigan	248	24.1
Dolomite-A	746	24.1
Dolomite-B	4.6	24.1

CONCLUSIONS

These Penn State sulfation tests coupled with GTI's kinetic analysis indicate that millimeter size particles are likely necessary to achieve the residence time and sulfur capture desired. Injecting micron size limestone particles into a PFBC will cause limestone residence times within the reactor to be on the same order as the fluidizing gas -- i.e., only a few seconds. Due to the relatively slow sulfation kinetics of the limestones tested, these residence times need to be on the order of minutes in order to achieve reasonable limestone conversion and utilization within the reactor. Fortunately, this can be accomplished by the use of millimeter sized

limestone particles as found in conventional fluidized bed combustors. For larger limestone particles, Equation 4 shows how the physical and kinetic limestone parameters in Tables 2 and 3 can be used to scale to larger limestone particle diameters.

As noted in the model's chemistry section, the limestone calcination temperature within a 7.89 atm PFBC is increased from 825ºC (for atmospheric pressure combustors) to approximately 1,050ºC. This means there is less likelihood of converting the limestone into more porous and more reactive lime (CaO) particles during the fluidized bed combustion process. This observation also suggests that limestone residence times on the order of minutes will be required for the GTI PFBC.

REFERENCES

Bird, R.B., Stewart, W.E., and Lightfoot, E.N., *Transport Phenomena*, Wiley, New York, NY (1960).

Chase, M.W., et al., *JANAF Thermochemical Tables*, 3d Ed., Parts I & II, *J. Phys. Chem. Ref. Data*, *14* (Suppl. No. 1), American Chemical Society, New York, NY (1985).

Lide, D.R. (Ed.), *Handbook of Chemistry and Physics*, 77th Ed., Chemical Rubber Company (CRC) Press, Boca Raton, FL (1996).

Mugele, R.A. and Evans, H.D., *Ind. Eng. Chem.*, *43*, 1317 (1951).

ACKNOWLEGDMENTS

The following individuals made important contributions in providing the materials, facilities and test data discussed within this report. Prof. Sarma V. Pisupati (Chair, Energy Engineering Program -- Penn State University), Mr. David K. Johnson (Research Assistant, Penn State University), and Ms. Aditi Khadilkar (Research Assistant, Penn State University).

APPENDIX A

Derivation of Single Limestone Particle SOx Capture Rate Equation

The derviation of the SOx capture rate equation (Equation 4) begins with the following heterogeneous reaction rate for a single particle when using the chemistry of Reactions R1 and R2:

$$\dot{n}_{sox} = \frac{4 \pi r_s^2 \rho_g}{\hat{M}_g} \left[f_{sox} \, k^*_{sox} \, \chi_{s,SO_3} - (1 - f_{sox}) k^*_{CO_2} \, \chi_{CO_2} \right] \quad \text{(A1)}$$

where χ_{s,SO_3} is the mole fraction of sulfur trioxide in the gas at the exterior particle surface, and $k^*_{CO_2}$ is the effective heterogeneous reaction rate constant for the reverse Reaction R1. All other variables have the same definitions as the report's main body.

The molar flow rate of SOx into the particle, $\dot{n}_{sox}$, is also given by the simple continuity equation:

$$\dot{n}_{sox} = \dot{n}_{SO_2} + \dot{n}_{SO_3} \quad \text{(A2)}$$

where $\dot{n}_{SO_2}$ is the molar flow rate of sulfur dioxide into the limestone particle from the surrounding gas, and $\dot{n}_{SO_3}$ is the molar flow rate of sulfur trioxide into the limestone particle from the surrounding gas.

From equilibrium it is assumed that the ratio of the effective forward and backward rate constants for Reaction R1 is equal to the equilibrium constant, $K_{p,r1}$:

$$K_{p,r1} = \frac{k^*_{sox}}{k^*_{CO_2}} \quad \text{(A3)}$$

Now the molar flow rate of sulfur dioxide to the particle's surface through the particle's boundary layer is given by:

$$\dot{n}_{SO_3} = \frac{2 \, Nu \, \pi \, r_s \, \lambda}{c_p \, \hat{M}_g} \left(\chi_{SO_3} - \chi_{s,SO_3} \right) \quad \text{(A4)}$$

where χ_{SO_3} is the mole fraction of sulfur trioxide in the particle's surrounding freestream gas. Similarly the same equation can be written for sulfur dioxide, namely:

$$\dot{n}_{SO_2} = \frac{2\,Nu\,\pi\,r_s\,\lambda}{c_p\,\hat{M}_g}\left(\chi_{SO_2} - \chi_{s,SO_2}\right) \tag{A5}$$

where χ_{SO_2} is the mole fraction of sulfur dioxide in the particle's surrounding freestream gas, and χ_{s,SO_2} is the mole fraction of sulfur dioxide at the particle's surface.

For Reaction R2 with the assumption that both of its forward and backward reaction rates are much faster than k^*_{sox}, equilibrium shows that the mole fraction ratio between sulfur trioxide and sulfur dioxide at the particle surface can be determined from:

$$K_{p,r2} = \frac{\chi_{s,SO_3}}{\chi_{s,SO_2}\;\chi_{O_2}{}^{1/2}\;P^{1/2}} \tag{A6}$$

Finally, the mole fraction of SOx contained within the gas freestream, χ_{sox}, is simply:

$$\chi_{sox} = \chi_{SO_2} + \chi_{SO_3} \tag{A7}$$

To produce Equation 4, one can combine Equations A1 through A7 and eliminate the following seven variables: $\dot{n}_{SO_2}$, $\dot{n}_{SO_3}$, $k^*_{CO_2}$, χ_{s,SO_2}, χ_{s,SO_3}, χ_{SO_2}, and χ_{SO_3}.

APPENDIX B

Derivation of Forward Kinetic Rate Constant From PFBR Experimental Parameters

The derviation of the effective heterogeneous RDS forward reaction rate constant for porous particles, k^{*}_{sox} (Equation 12) from the PFBR's experimental parameters, begins with the SOx species continuity equation through the fluidized granular bed. This equation is written here as:

$$\frac{\dot{m}_g}{\hat{M}_g}\,\frac{\partial \chi_{sox}}{\partial z} \;=\; -\,N_p\,\dot{n}_{sox}\,A \qquad \text{(B1)}$$

where z is the axial position within the fluidized bed, A is the fluidized bed cross-sectional area, and N_p is the particle number density within the fluidized bed. All other variables have the same definition as given above. The particle number density, N_p, is in turn given by:

$$N_p \;=\; \frac{3\left(1-\varepsilon\right)}{4\,\pi\,r_s^{\,3}} \qquad \text{(B2)}$$

where ε is the fluidized bed's void fraction. Furthermore, the total mass of limestone initially placed into the fluidized bed, W^{o}_{LS}, is related to the bed's void fraction, ε, by:

$$W^{o}_{LS} \;=\; \left(1-\varepsilon\right)\,V\,\rho_p \qquad \text{(B3)}$$

where V is the volume of the fluidized bed given as:

$$V \;=\; \int_{z=0}^{L} A\,\partial z \qquad \text{(B4)}$$

Combining Equations B1 through B3 provides the following first order differential equation:

$$\frac{\partial \chi_{sox}}{\partial z} \;=\; -\,\frac{3\,A\,W^{o}_{LS}\,\hat{M}_g\,\dot{n}_{sox}}{4\,V\,\pi\,r_s^{\,3}\,\rho_p\,\dot{m}_g} \qquad \text{(B5)}$$

Substituting Equation 4 above into Equation B5 and integrating over z -- from z equals 0 (where χ_{sox} equals χ^{o}_{sox}) to z equals L (where χ_{sox} equals $\chi_{sox,out}$) – will produce the result given by Equations 12 and 13 where use is also made of Equation B4.

Appendix D. CFD Analysis Task Report

the Energy to Lead

REPORT

Payment Milestone

Project: Advanced Oxy-Combustion Technology Development and Scale Up for New and Existing Coal-Fired Power Plants (Phase II)

Milestone: CFD Analysis Task Complete

November, 2016

GTI Contact:
William W. Follett
Program Manager
818-405-9546
Bill.Follett@gastechnology.org

Gas Technology Institute
1700 S. Mount Prospect Rd.
Des Plaines, Illinois 60018
www.gastechnology.org

Table of Contents

List of Figures

List of Tables

Project Overview:

Gas Technology Institute (GTI) has a Phase II program that is a US$19.061M Cooperative Agreement Cost Share, with US$11.924M of Department of Energy (DOE) funding, to advance the oxygen-fired pressurized fluidized bed combustion (Oxy-PFBC) technology from technology readiness level (TRL) 3 to TRL 6 through pilot scale testing. The period of performance is July 1, 2014 through March 31, 2017. This Phase II effort is preceded by a US$1.267M Phase I program with US$1.0M of DOE funding. This program was originally awarded to Aerojet Rocketdyne, but was novated to GTI on Dec. 18, 2015. Alberta Innovates is contributing CDN$1,595,602 of cost share to the program.

The goal of the Oxy-PFBC program is to capture greater than 90% of CO_2 emissions while increasing the levelized cost of electricity (LCOE) by less than 35% compared to a case without CO_2 capture. The GTI system is currently projected to exceed these goals. The captured CO_2 may be sequestered at dedicated sites or at oilfields for enhanced oil recovery.

The program Phase II objectives include:

1. Test the system at pilot scale to achieve TRL 6 while evaluating system performance and operability
2. Continue to improve performance and cost models to predict commercial scale cost of electricity and validate these models with pilot scale results
3. Assess system components designed in Phase I to confirm scalability, performance and cost
4. Develop a Phase III project plan for building and operating a demonstration scale plant, including risk mitigation, and identification of partners and host sites.

Milestone Overview

Milestone Description:

Task 4: Analysis will develop and utilize a CFD model of the Oxy-PFBC (Oxygen-fired Pressurized Fluidized Bed Combustor), including development of physics models and anchoring by testing for coal reactivity, limestone sulfation and agglomeration.

Milestone Objective

The objective of the milestone is to develop an initial CFD capability that can support analysis of the pilot scale geometry while supporting scale up to the demo and commercial scales. The initial CFD capability is expected to lay the groundwork for further tool development in future programs.

Milestone Approach Overview

The approach, as originally envisioned, would develop and validate physics models for coal kinetics, limestone kinetics and agglomeration, and add these models to a 3-D CFD code. Investigations into the CFD capabilities showed that our requirements were beyond current CFD and computing capabilities in terms of practical support for the reactor development due to the complexity of the Oxy-PFBC reactor geometry and physics, which include multiple particle types and sizes, multiple gas species, complex chemistry, gas-particle-wall heat transfer, and heat exchanger tube banks.

As a result, the approach was modified to develop two hybrid approaches that combine CFD with tools that are less computationally intense. This also enables fast turnaround analysis that supports design and optimization efforts. The first approach enhanced the GTI 1-D PFBC Performance Code to combine coal kinetics and fluidized bed thermal transport models. The thermal transport model can utilize input from CFD analysis or test data to calibrate the code for a given configuration. The second approach utilizes an agglomeration model that includes coal, limestone and ash thermochemistry models, and input from CFD for bed hydrodynamics. These approaches provide the appropriate physics modeling with quick turnaround time to support analysis and design activities necessary for scaling up to demo and commercial scales.

The agglomeration model and the 1-D PFBC Performance Code were validated with test data and the results are provided in this report. The coal reactivity and limestone sulfation physics models were previously validated against test data as documented in payment milestone reports submitted to Alberta Innovates on March 1, 2016 (References 1 and 2). Presented in this report is a fluidized-bed thermal transport model for the 1-D PFBC Performance Code that was developed and validated with test data from the Grimethorpe PFBC Plant in England.

The CFPD Barracuda® CFD code has been applied to the full reactor configuration and the initial results are presented. These results have provided insight into the three-dimensional flow fields that dominate the injection-end of the reactor. This work also provides a foundation to add additional physics to future computations.

Also covered in this report, an agglomeration modelling approach is described, where CFD is run to determine the collision velocity and frequency between fluidized bed particles. These results are used as input to the agglomeration model, which then computes the probability of particle agglomeration at a particular bed temperature. As the solution is marched in time, it predicts when – or if – the bed will de-fluidize. This hybrid approach has been validated with test data. The results show a very low probability of agglomeration in the GTI Pilot Plant.

1-D PFBC Performance Code Enhancement

Heritage Code

The GTI 1-D PFBC Performance Code was originally derived from the GTI 1-D entrained flow coal liquefaction, gasification, and combustion code developed beginning in the 1970's. The code uses a quasi-one-dimensional plug flow representation for the gas flowing upward through the fluidized bed together with a well-stirred-reactor representation for the granular coal particles within the fluidized bed. Finite-rate chemical kinetics, particle-layer diffusion, and heat transfer processes are modeled at the particle level. In the mathematical sense, a system of steady-state parabolic ordinary differential equations is solved in a single "space marching" sweep from the reactor entrance to the exit. The code's coal combustion kinetics accuracy was recently validated by the Penn State reactivity tests documented in Reference 1.

The heritage GTI 1-D PFBC Performance Code modelled the fluidized bed particles based on void fraction, i.e. their blockage of the gas flow along with the coal particles and the resultant effect on gas-to-wall heat transfer. Due to the space-marching nature of the solution, the fluidized bed particles were effectively fixed in space within the fluidized bed. The result of this modelling approach was that the bed particles were unable to transport heat axially, which caused difficulties in the coal particle ignition process as well as exaggerated axial temperature profiles. Accurate prediction of the axial temperature profile, including the peak temperature, is important to successful Oxy-PFBC reactor design. The temperature must be high enough to fully engage the coal chemical kinetics, but low enough to avoid the formation of slag and undesirable products such as CO and NO_X.

Axial Diffusion Model Concept

An Axial Diffusion Model (ADM) was developed to provide bi-directional axial thermal diffusion/transport capability. The ADM is based on two key concepts. The first concept is that particles of a fluidized bed operating in the bubbling and turbulent regimes move, on average, at their local terminal velocities relative to the gas. This concept was demonstrated in the seminal work of Richardson and Zaki (Reference 3) where they showed – via experiment – that spherical particle sedimentation (terminal) velocities for finite void fractions were equivalent to average velocities in a fluidized bed.

The second concept is based on the experimental observations that, while these bubbling- and turbulent-regime fluidized bed particles move at an average velocity that keeps them fluidized in the reactor, they tend to "dart" around for significant distances in every direction. This motion allows the particles to transport significant amounts of heat around the reactor.

Axial Diffusion Model Development

The Axial Diffusion Model (ADM) solves a second-order elliptic, steady-state, inhomogeneous ordinary linear differential equation. A finite-volume formulation with sub-models for particle drag and particle-gas heat transfer is used. The ADM is comparable in complexity to the heritage 1-D PFBC Performance Code – herein referred to as the "Combustion Solver" – and was designed and tested as a separate code, then integrated with the Combustion Solver.

The Combustion Solver and the ADM are coupled together to provide an effectively full-elliptic simulation of the fluidized bed that allows heat to flow through the bed particles in both the upstream and downstream directions. Since both the combustion solver and the ADM are distinct steady-state

models, their coupling requires iterative solution, referred to as "global iterations". Figure 1 illustrates this process. The global iterations are not temporal per se, but they do add a second dimension to the solution, with the associated complexity ramifications.

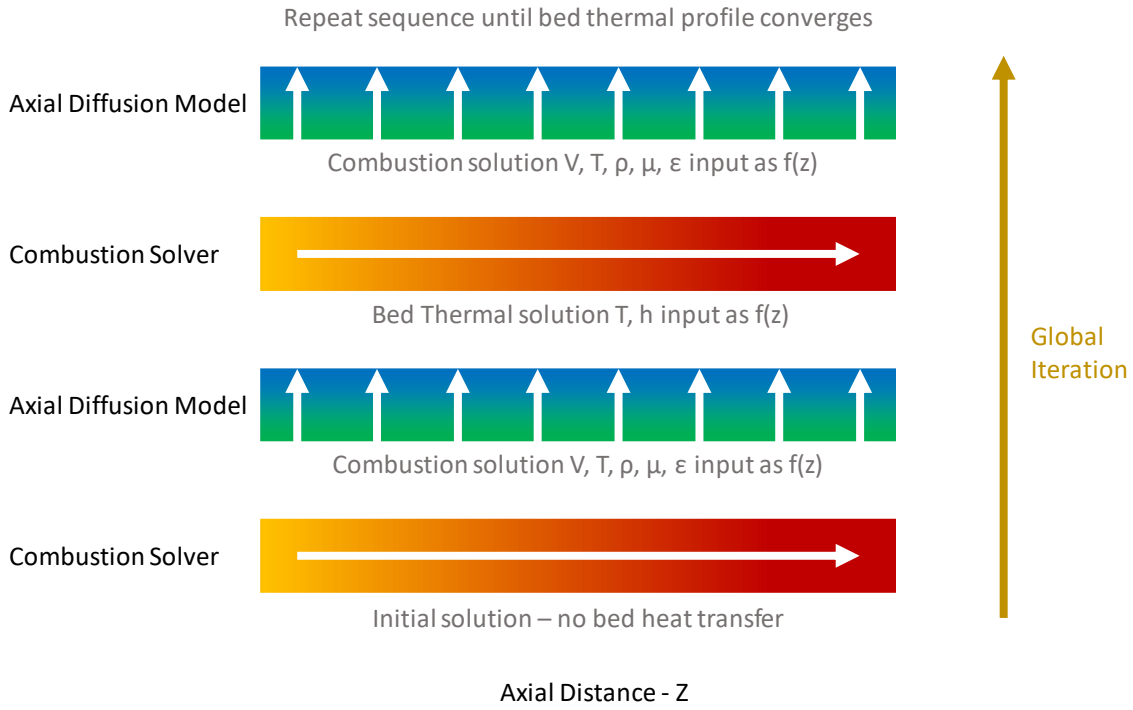

Figure 1 – Combustion Solver/ADM Coupling

The ADM was designed to utilize the AVX vector instructions in modern CPU's and runs a case in several minutes. This performance is fast enough to support the automation and optimization goals of the PFBC analysis strategy.

Axial Diffusion Model Calibration/Validation

The ADM employs one primary non-dimensional parameter for mathematical closure. This parameter requires calibration using axial temperature profile data from experiment, or CFD. The closure parameter is physics-based, i.e. it is not a "universal knob" that can always be dialed to match data. Issues such as incorrect reactor thermal balance, or coal reaction rate, can result in a match being impossible to obtain for any value of the closure parameter. Since the parameter is physics-based, it is hoped that it will show similarity characteristics over a wide range of reactor configurations and operating conditions.

Data from the "Grimethorpe" PFBC tests (Reference 4) was used to validate, and establish a baseline value for, the ADM closure parameter. The Grimethorpe reactor was geometrically similar to the GTI Pilot Plant reactor, albeit at larger (50 MWth) scale and reacted coal with air. Grimethorpe used fluidized bed particles of similar size, and composition, to the GTI Pilot Plant reactor. Axial temperature profile data from two Grimethorpe configurations was available: "A2" and "C". C had a smaller heat exchanger than A2.

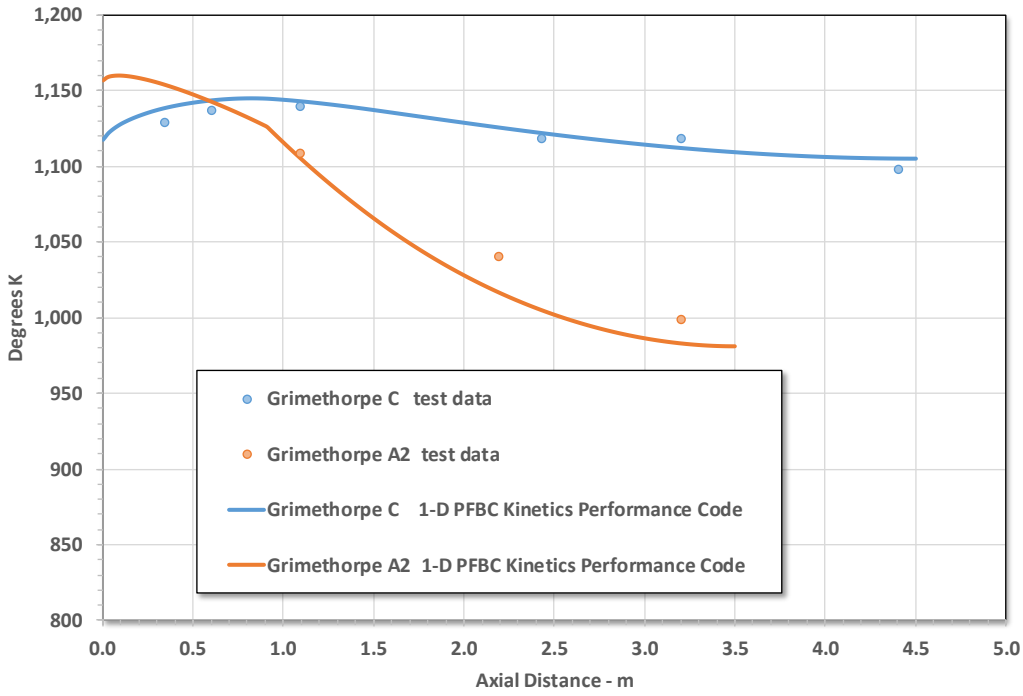

Figure 2 – Grimethorpe A2 and C Best-Match Temperature Profiles

Figure 2 shows 1-D PFBC Performance Code cases that best matched each Grimethorpe case. Temperature is plotted against axial length through the reactor. A slightly different closure parameter value was used for each, but using the same value for each would shift the peak temperature by only about 25°K. As a point of reference, the peak temperature of these Grimethorpe cases run without the ADM, i.e. without the thermal diffusion of the fluidized bed, is about 1900°K versus ~1150°K with the ADM model. This large temperature difference demonstrates the significant heat transport capability of the fluidized bed, and the importance of modelling this effect accurately.

The upcoming GTI Pilot Plant testing and future Barracuda CFD analysis can provide more detailed, calibration/validation data for the 1-D PFBC Performance Code that is more traceable to the GTI Oxy-PFBC configuration.

Pilot Plant Reactor Full-Configuration CFD Analysis

Introduction

Consistent with the revised Oxy-PFBC analysis strategy, CFD analysis of the full reactor configuration can provide important information not available from the other levels of analysis. The complex reactor internal geometry may produce similarly complex flow fields. Test data will reflect the impact of such flows, but not necessarily provide the diagnostic information required to understand the flow fields.

A study was performed to evaluate candidate CFD codes and select one for full-configuration analysis use. The following set of criteria was established:

1. Productively model the complex Oxy-PFBC reactor geometry including the numerous heat exchanger tubes
2. Model multiple particle groups in a dense fluidized bed, since the bed and coal particle groups exhibit fundamentally different behavior in the reactor
3. Model multiple gas species in addition to the multiple particle groups
4. Model gas-particle-wall heat transfer
5. Solution turnaround times rapid enough to support program goals

The following CFD codes/code suites were evaluated against the criteria: ANSYS® Fluent, CPFD Barracuda®, and NETL MFiX. CPFD Barracuda® was selected for the full-configuration reactor CFD analysis. The other two codes have certain advantages and may be used in the future for other applications.

Barracuda CFD Model

The CPFD Barracuda code computes the fluid phase in an Eulerian frame of reference (i.e. on the computational grid) and allows an essentially unlimited number of compressible gas species in the model. The solids phase is computed as discrete (Lagrangian, gridless) and allows an essentially unlimited number of particles, and particle species with a particle size distribution for each species. This capability meets the simulation criteria established above for the Oxy-PFBC reactor. The bidirectional coupling of the phases (aerodynamic drag, sub-grid solids displacement of gas) treats the dense fluidized bed physics.

A computational grid was generated based on GTI CAD reactor geometry. The resulting numerical model included:

- An 800,000 cell mesh included all flow-specific geometric details
- 297,520 computational cells (for scalar quantities)
- 1.03 million computational faces (for vector quantities)
- 3.66 million computational particles (at startup)

All gas flows were modeled. These included the main combustible gas mixture, the fuel feed gas, and purge gas flows. All solid particles were modeled. These included the large fluidized bed particles, the smaller fluidized bed fuel-feed particles, and the coal fuel particles with a particle size distribution applied. A boundary condition was set such that any particle reaching the reactor upper

surface would be removed from the computation, i.e. elutriated. Two solutions were run. Both used an isothermal bed condition of 1000°K. The first solution used only the large fluidized bed particles, while the second solution added the fuel feed with the smaller elutriated limestone particles and the elutriated coal particles.

Barracuda CFD Results

The fluidized bed physics are, by nature, three-dimensional, and time dependent – or unsteady. The Barracuda solutions capture this behavior and, as such, there is no converged, or steady, solution. A fixed bed of particles is impulsively fluidized by the gas flow. The solution is then progressed in time until a cyclical, or periodic behavior is obtained. The solution is then run further in time and data is collected for flow visualization, and engineering parameters of interest. Figure 3 shows a reactor cross section view from the first solution as a snapshot in time. The color contour show particle volume fraction. The fluidized bed is operating as desired in the bubbling regime, and at the desired bed height which submerges the entire heat exchanger.

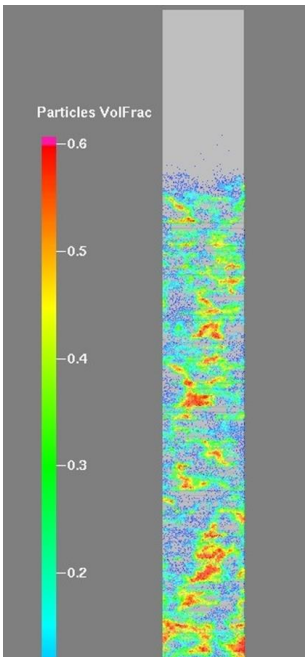

Figure 3 – Barracuda Solution Fluidized Bed Particle Volume Fraction

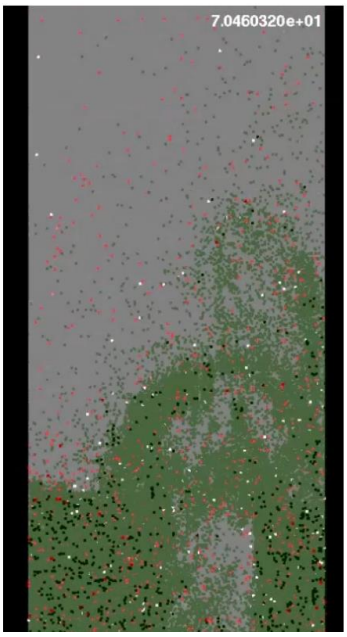

Figure 4 – Barracuda Solution Fluidized Bed Particle Freeboard Ejection

Figure 4 shows a reactor cross section view from the second solution as a snapshot in time. This view is a detail at the top of the bed showing the freeboard region. The large fluidized bed particles are colored green, the smaller elutriated limestone particles are colored white, and the elutriated coal fuel particles are colored red. Both Figure 3 and 4 are actually still views from animations that show the dynamic nature of the particles. Some of the green particles are ejected up into to the freeboard area, but – as desired – only a negligible number are elutriated out of the top of the computational domain. Many of the smaller white and red particles are elutriated, as intended.

The Barracuda model was designed to extract engineering parameters at spatial locations matching instrumentation ports in the GTI Pilot Plant reactor. Figure 5 shows pressures as a function of time. Following from the discussion above, the solution was judged to have attained a periodic behavior at 20 seconds. The pressure data from that point onward are of interest. The pressure oscillations are relatively benign, consistent with a stable bubbling bed.

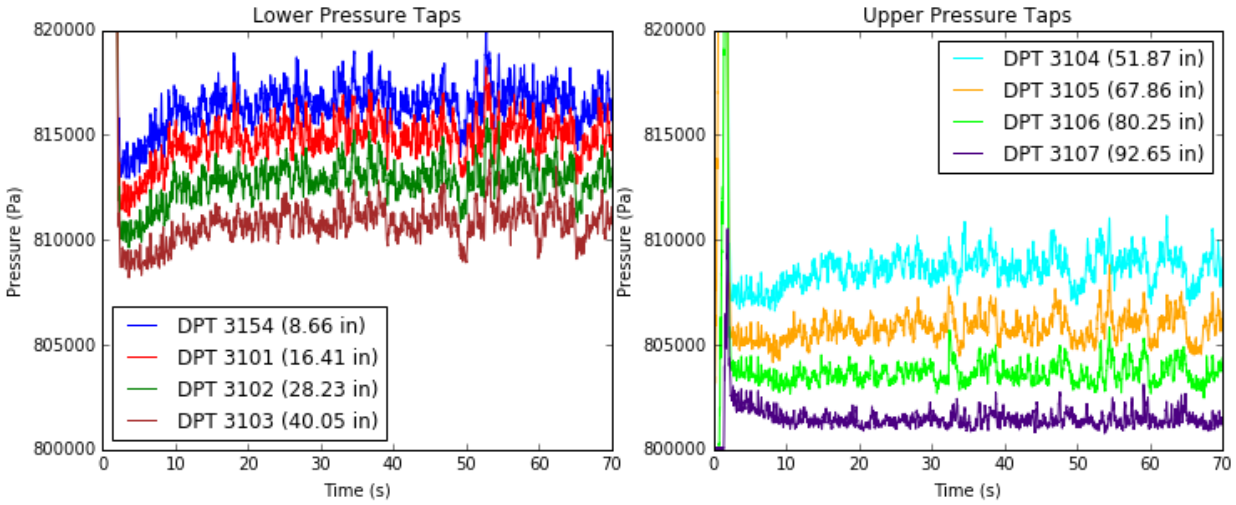

Figure 5 – Barracuda Solution Pressure-Time History

Barracuda CFD Future Work

The analysis performed thus far has demonstrated the ability of Barracuda to model the complex PFBC physics and geometry in a timely manner. These results also support a number of reactor design decisions and predictions as summarized below.

Future work could include steps to enhance the level of physics in the analysis by adding surface heat transfer through the heat exchangers. This modeling can provide unique calibration/validation data for the 1-D PFBC Performance Code. Coal combustion combined with heat exchanger operation can then be added to compute a fully-three-dimensional temperature field. These results will also benefit the 1-D PFBC Performance Code and provide insights to potential problem areas such as combustion hot spots and surface erosion. Additional parametric cases to fine tune the various reactor gas flows may be added at the current (isothermal) or enhanced levels of physics and deemed advantageous for the reactor design.

Barracuda CFD Conclusions

- Barracuda has the capability to simulate the Oxy-PFBC geometry, including multiple particle sizes and types with reasonable computational resource and time requirements. Combustion kinetics is expected to increase computational time by a factor of 4-10X, which is still reasonable.
- Initial full-configuration reactor CFD simulations successfully completed. All flow-specific geometric details were modeled.
- Stable fluidized bed, with vigorous bubbling but no slugging behavior, observed throughout the reactor
- Fluidized bed density supports reactor design predictions
- Elutriation of the large bed particles from the reactor was negligible, as desired

Fluidized Bed Ash Agglomeration

Introduction

An agglomeration model was developed that uses Stokes' criterion to compute particle agglomeration and bed de-fluidization by using the FactSage™ computational thermodynamics package to compute the amount of slag and its viscosity, and the MFiX computational fluid dynamics (CFD) code to compute particle collision frequency and velocity. The agglomeration model calculates changes in particle size with time and can provide predictions of when or if agglomeration will begin and how long until the particles are large enough to de-fluidize (i.e. fall out of suspension). The overall model architecture is shown in Figure 6.

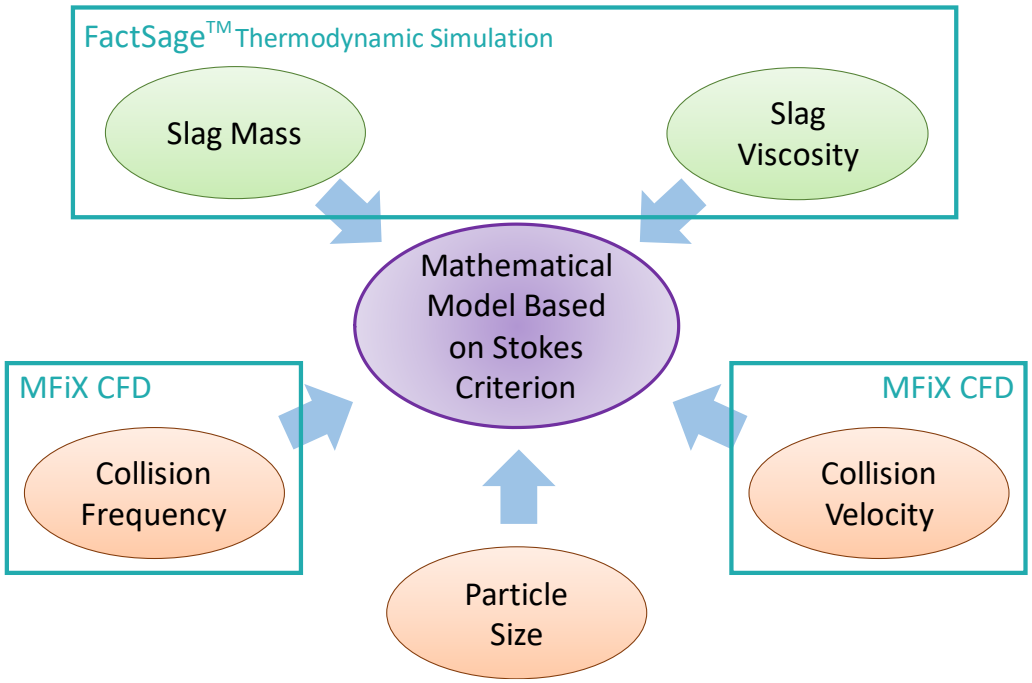

Figure 6 – Agglomeration Model Overall Architecture

The model was validated using experimental data in the open literature and provided reasonable predictions of de-fluidization times (within 11%) for these experiments. The validated code predicted that there is a low likelihood of agglomeration in the GTI Oxy-PFBC combustor.

Model Development Methodology

The following sections discuss the various aspects of the agglomeration model development. The model was developed based on testing two-particle collisions for sticking. The chemistry of the formation and rheology of the viscous liquid that can bind particles on collision is studied using computational thermodynamics, while the physical properties that define particle motion are studied using CFD. The agglomeration model is comprised of a mathematical code that uses these inputs on the binder's chemical properties and particle physics to track changes in particle sizes over time. This includes consideration of the binder dispersion on the solid particle surface and also the differences in collision dynamics that relate to particle size. The model is developed to aid in the utilization of parameters at the particle level.

Quantification of Particle Growth

The initial particle size distribution (PSD) is divided into narrow size intervals. Each particle increment has a top size and a bottom size and the mean of these values is used to represent the average diameter of particles in that interval. The particles are assumed to be spherical. The initial bed mass is distributed amongst the size intervals, and the number of particles in each bin is calculated. When an agglomerate is produced by a collision of a particle from one size interval with that from another, the mass of the resultant particle is calculated to be the sum of the individual masses of the colliding particles. If two colliding particles stick, the resultant agglomerate diameter is calculated, based on the resultant mass and assuming the particle density to be remaining constant. The agglomerate may then move into a higher sized interval, before the next time step. The changes in the number of particles are tracked and the model can trace the temporal evolution of ash particle size distribution in the system.

Stokes' Criterion for Particle Adhesion

The Stokes' criterion has been previously used to determine if colliding particles remain stuck together, in the process of granulation for pellet production (Reference 5). The Stokes' number is given as

$$S_t = \frac{4\rho_i U_c d_i}{9\mu_i}$$

Where U_c is the velocity associated with a collision, and μ_i is the viscosity of a liquid layer on the surface of the particle.

The use of this criterion assumes that for collision of particles with a liquid bridge separating them, the forces of viscous dissipation dominate while the surface tension and capillary forces are negligible. This assumption is suitable for the high viscosity slag-liquid that acts as the binding liquid in the fluidized bed combustion and gasification industry.

The Stokes' number is a ratio of the kinetic energy to the viscous dissipative forces. If the viscous dissipation on collision of the particles exceeds their kinetic energy then the particles remain stuck, otherwise they rebound. This criterion helps to combine the effects of both chemistry and physics based parameters into the model. The viscous liquid in the gasification and combustion industry is the slag-liquid formed from ash at high temperatures. Thus, the ash material properties and chemistry as well as operating temperature are used in the determination of the viscous dissipation. The kinetic energy depends on the particle physics such as the collision velocity. Since this test is applied to two-particle collisions in the system, the collision frequency is used to calculate the number of collisions that occur.

Hence, for particles to agglomerate they should

1. Be wetted by a viscous liquid
2. Undergo a collision in the liquid wetted region
3. Pass the Stokes' test.

Particle wetness is dictated by the ash chemistry, while the tendency to collide with another particle is determined by the physics and bed hydrodynamics. The Stokes' test includes both chemistry, in terms of slag rheological properties, and also physics, in terms of particle velocities.

Collision Frequency Distribution

In order to correctly incorporate the agglomerate growth kinetics for the entire particle size distribution, the determination of collision frequency distribution is required. The number density – number of particles per unit volume – of a given mass of smaller particles will be higher and hence the particles are likely to undergo more collisions in a given time. Instead of an arbitrary correlation of collision frequency to the number of particles, in this study the collision frequency is calculated based on the kinetic theory of granular flow. Hence, the particle granular temperature and the number density of particles in the intervals are used in the Rahaman formula (Reference 6) to compute the distribution of collision frequencies between particles of different sizes. The Rahaman formula was chosen since this was developed utilizing a granular mixture of particles consisting of different sizes with unequal granular temperatures, unlike prior models that considered only mono-sized particles.

The granular temperature required for the above calculation of the collision frequency is obtained using the MFiX (Multiphase Flows with Interphase eXchanges) CFD code (Reference 7). MFiX is open-source software which has been validated for multiphase simulations in gasifiers and combustors. The mass and momentum balance equations as well as the Schaeffer frictional model are solved to obtain the particle velocities and granular energy using the Eulerian-Eulerian method.

Slag-Liquid Mass, Viscosity and Particle Wetness

In addition to the physics-based parameters described above, the methods for the incorporation of the chemistry-based parameters into the agglomeration model have been discussed in this section. The mass of slag-liquid is determined by the ash chemistry and operating conditions such as the temperature and gaseous atmosphere. The viscosity of the slag-liquid formed helps to determine if the viscous dissipation of the particles' kinetic energy would be sufficient to result in sticking. The viscosity of the slag-liquid is dependent on the chemical composition of the liquid. The extent of particle wetness depends on the amount of liquid, the contact angle and the particle size. A brief description of the methods used for these calculations is described below.

Thermodynamic simulations based on quasi-chemical computations with the FactSage computational thermodynamics package were used to obtain the amount of slag-liquid formed at equilibrium under a given temperature condition. The phases formed were studied under both oxidizing and reducing environments. These slag formation tendencies have also been analyzed experimentally using high temperature X-ray diffraction and thermo-mechanical analysis (References 8,9).

Chemical composition of the slag obtained from the FactSage calculations was used to calculate the slag viscosity with the modified Urbain model (Reference 10). This empirical model was chosen, based on the review of viscosity models by Vargas et al. (Reference 11). The study found the Botinga-Well and Urbain models to closely match experimentally measured viscosity values. However, the Botinga-Well model does not perform adequately for coals rich in iron-containing phases. Vargas concluded that Urbain model made reasonable predictions for these high rank coals. Since the modified Urbain model is empirical, and was developed for completely molten slag-liquid, the slag-liquid oxide composition obtained from FactSage was used as an input for the calculation. Thus the viscosity of the clear slag-liquid at the desired temperature was calculated. The equation for partial wetting adopted by Thielmann, et al. (Reference 12) was used to obtain the radius of the area wetted by the slag-liquid. Based on the ratio of the wetted area and the particle surface area, the probability of a wet collision is estimated.

Agglomeration Model Validation

The Penn State Ash Agglomeration was validated using experimental test data from the literature. Additionally, the mechanism of agglomerate growth was validated by studying agglomerates that were formed in the CANMET small scale reactor.

A case study of biomass combustion in a fluidized bed reactor, in which experiments had been performed at various operating conditions (Reference 13), was chosen for validation of the agglomeration model. Initially, all 11 cases from Reference 13 were simulated using the model. Based on these results, the model was refined. First, the model was modified to simulate a semi-continuous process. For application to a semi-continuous system, the ash feed rate (ashrate) was used as an input and the slag amount increased with time.

$$\text{amt}_i = w_{sl} \times \varphi_{mold} \times M_{bed} \times \text{ashrate} \times \Delta t$$

The ash alone contributed to the slag formation and its contribution to increase in particle size is considered negligible – it being a very small percentage of bed material. Additional data on the initial void fraction and bed mass was obtained by contacting the authors of Reference 13 and the values were corrected from previous attempts. Additionally, it was recognized that ash particles are likely to be at higher temperature than the measured average bed temperature due to char burning. Hence the simulations were performed with ash particles at higher temperatures, instead of the bulk bed temperature. Since presence of phases such as potassium silicates indicated that particle temperatures of about 50 % particles may have reached above 1200˚C. With these modifications, the de-fluidization time was obtained for the following cases. De-fluidization time was defined as the time required for 95% of the bed material to de-fluidize in these simulations. Table 1 shows that the simulation results obtained and are comparable to the experimental results reported in Reference 13, when ash particle temperatures are higher than the bed temperature.

Bed temperature (°C)	Superficial gas velocity (m/s)	Particle diameter (µm)	De-fluidization time (h)	De-fluidization time obtained from model (h)
800	0.25	425–500	15.36	13.9
850	0.25	425–500	7.23	8.0
900	0.25	330–355	7.22	6.9

Table 1 – Comparison of De-fluidization Time from Model Simulations and Experiments

Proposed Agglomeration Process Mechanism Validation

A unified model was developed to study the effect of particle-level variations in slag-liquid amounts, collision frequency, and granular temperature on agglomerate growth in poly-disperse systems. The effect of chemical composition, temperature, and gaseous atmosphere on slag-liquid formation was studied. Also, the effect of superficial gas velocity, bed mass, particle size and density on collision frequency and granular temperature were studied. The resultant effect of these parameters on agglomeration was understood using the model developed. Based on this, it was suggested that agglomeration begins at the particle-level around low-melting particles at a relatively lower temperature and subsequently propagates in the bed (References 8, 9). The propagation may be due

to higher temperatures that result from bed instabilities and dead zones arising from the initiation of agglomeration. This is believed to be due to higher temperatures experienced by included mineral particles embedded in hot char particles or local variations in the gaseous atmosphere causing reducing conditions which lower the melting point of some minerals.

In order to validate this phenomenological mechanism, agglomerate samples obtained from a CANMET full-scale combustion facility were analyzed. The agglomerate samples were cut and polished then observed under a scanning electron microscope and the elements present in them were mapped across a cross section of the agglomerate. The results presented in the following section showed the presence of regions that formed slag-liquid at low temperatures initiating agglomeration and also the other highly molten regions that are likely to cause propagation at higher temperatures, thereby supporting the mechanism.

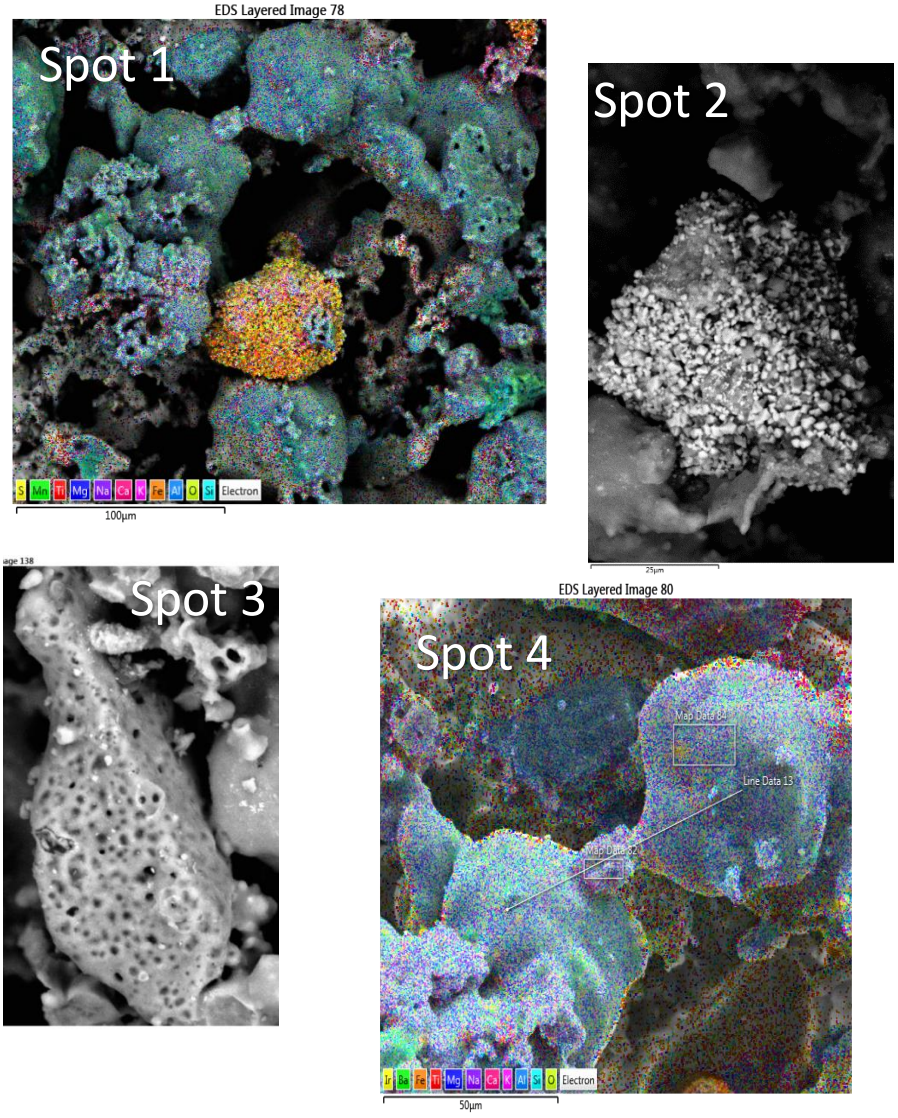

Figure 7 – Stages of Agglomerate Growth Observed Through SEM-EDX of CANMET System Samples

Different stages of agglomeration were identified based on the Scanning Electron Microscopy-Energy-dispersive X-ray Spectroscopy (SEM-EDX) study of these agglomerates. Different regions of the agglomerates were studied and several instances of the four stages as shown in Figure 7 were found throughout the sample. Compositional analysis was performed on 8 to 10 spots of Stages 1 and 4. The average composition obtained was analyzed using FactSage simulations to predict the initiation temperature of slag formation in these regions.

Stage 1 shows small iron particles sticking together to form a larger sphere. These particles begin slag formation at a lower temperature of 820˚C as shown in Figure 8. The amount of slag formed from this composition is less than 20 % even at higher temperatures. Hence this is just enough to initiate agglomeration and lead to the formation of bigger agglomerates that are rich in iron. Stage 2 shows that slag formed at higher temperatures begins to engulf these iron spheres. Stage 3 shows one such completely coated iron agglomerate. Finally, the coated agglomerates begin to stick to one another as shown in Stage 4 wherein bridging is clearly seen between two slag-coated agglomerates.

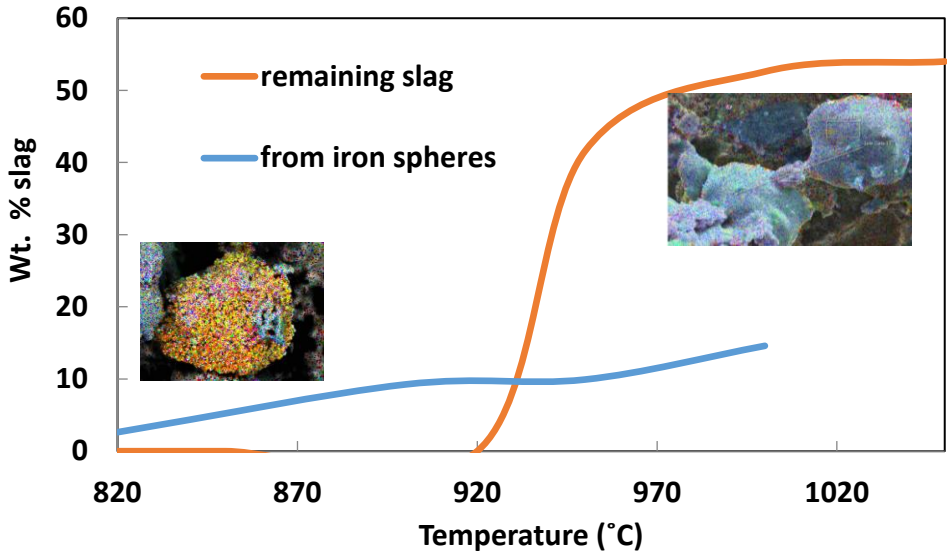

Figure 8 – Slag Formation Tendency of Components in Spot 1 and Spot 4

Prediction of agglomerate growth using GTI operating conditions

Simulations using ash chemistry, limestone composition, and operating conditions such as particle size and superficial gas velocity provided by GTI were performed to predict agglomeration growth rate under the specified conditions. Predictions indicate a low probability of agglomeration. Agglomeration model results also indicate the importance of bed material for ash agglomeration behavior.

Simulations to predict the agglomeration tendency using GTI-specified operating conditions were performed. Three cases were run. The first case represents expected conditions in the GTI Oxy-PFBC, while the other cases are deviations from these conditions. The first case represents the GTI Oxy-PFBC operating environment at 8 bar pressure and using limestone bed material. The second case uses the same Oxy-PFBC gas composition and limestone bed, but reduces the pressure to atmospheric levels. Finally, the third case uses the same Oxy-PFBC operating environment at 8 bar

pressure and the appropriate gas composition, but removes the limestone bed and replaces it with an ash bed.

For the first and second cases, the slag formation tendency of Illinois-6 coal with limestone under oxy-fuel combustion environment was obtained using FactSage thermodynamic simulations, as shown in Figure 9. The bed solids in equilibrium with the gas consisted of 90 % limestone and 10 % ash. It is seen from Figure 9 that slag formation was significant only at temperatures higher than 1,200˚C, both at atmospheric pressure and 8 bar. This bed composition is similar to what is expected for the Oxy-PFBC pilot plant. Since slag formation occurs at 1200˚C, which is well above the planned bed temperature of 800-900˚C, the risk of slag formation during normal operation is low.

The third case, which removes the limestone bed and replaces it with an ash bed, was allowed to equilibrate with the same gaseous atmosphere. As shown in Figure 9, a higher amount of slag was seen and there was significant slag formation above 900˚C.

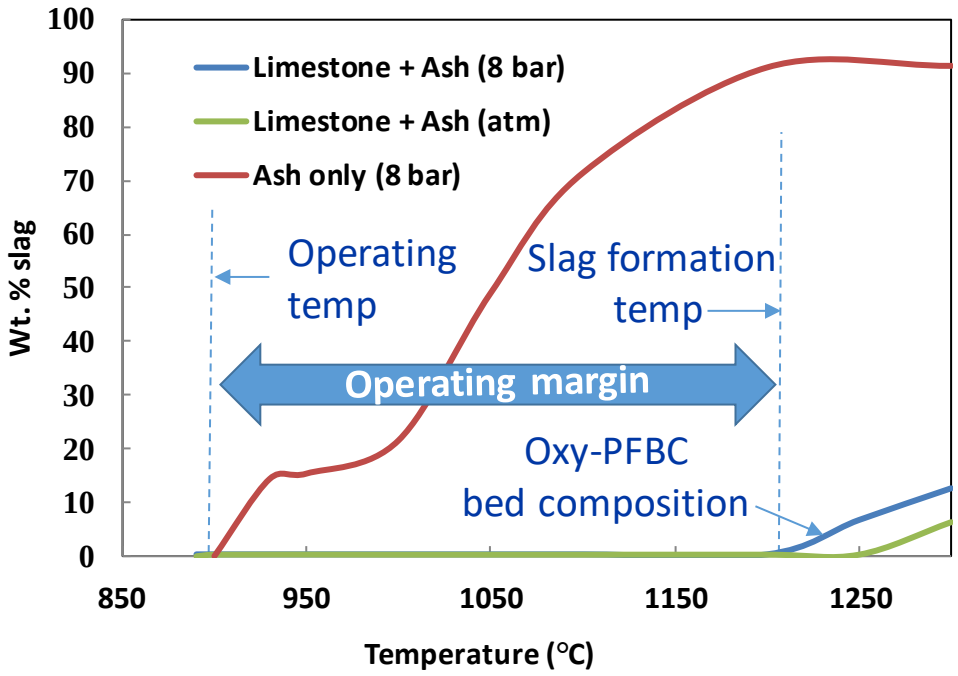

Figure 9 – Slag Formation Tendencies of Bed Material at Atmospheric and 8 Bar Pressure

Fluidized Bed Ash Agglomeration Conclusions

An agglomeration model was developed that combines thermochemistry with CFD-computed hydrodynamics to model agglomeration in a fluidized bed. The model was validated and provides reasonable agreement with experimental data, including matching the time for bed de-fluidization due to agglomeration within 11%.

The agglomeration model predicts that the probability of agglomerate growth at conditions in the GTI pilot Oxy-PFBC is low in the specified bed temperature range of 800-900°C, since in the presence of a bed with 90% sulfated dolomite, slag formation begins only at temperatures above 1,200°C.

A bed with ash alone begins to form slag at lower temperatures of 900°C, while a bed with 90% dolomite and 10% ash forms slag above 1200°C. Hence, the proportion of ash and sorbent in the bed is likely to significantly impact the probability of agglomerate growth.

Overall Conclusions

The ability to model the GTI Oxy-PFBC combustor configuration with 3-D CFD capability was demonstrated with the code, Barracuda. It was demonstrated that Barracuda was able to simulate the complex geometry and particle physics, including multiple particle types and sizes. Chemistry will be demonstrated at a future time, but there are no known limitations of the code in this respect.

Two additional models were developed that work synergistically with CFD to provide complex physics analysis capabilities with computational times that can support design activities. These models are the 1-D PFBC Performance Code developed by GTI and the Agglomeration Model developed by Penn State University.

The 1-D PFBC Performance Code was enhanced by adding an Axial Diffusion Model to better capture the thermal energy transport provided by the fluidized bed. CFD can be used to provide an input parameter that calibrates the bed thermal energy transport for a given bed geometry. The 1-D PFBC Performance Code was successfully validated with data from the Grimethorpe pressurized fluidized bed combustor testing, while the coal kinetics physics model within the code was validated with test data from Penn State University.

The agglomeration model was validated and shown to predict defluidization time within 11%. CFD is used to provide input parameters of particle collision frequency and velocity for a given bed operating condition. The validated code predicts a low probability of agglomeration for the GTI pilot Oxy-PFBC since the bed is expected to operate at 300°C below the slag formation temperature of 1,200°C. The slag formation temperature was influenced significantly by the presence of dolomite bed material.

References

1. Sprouse, K.M. “Penn State University Coal Reactivity Tests & Analysis.” Gas Technology Institute AI-EES 2228 Payment Milestone (2016).
2. Sprouse, K.M. “Penn State Sulfation Tests and Kinetic Analysis.” Gas Technology Institute AI-EES 2228 Payment Milestone (2016).
3. Richardson, J.F., and W.N. Zaki. “Sedimentation and Fluidization: Part I.” Trans. Inst. Chem. Eng 32 (1954): 35ff.
4. NCB (IEA Grimethorpe) Ltd. “IEA Grimethorpe Pressurized Fluidized-Bed Test Facility Tube Bank ‘C’ Design, Installation, and Commissioning.” Grimethorpe, Barnsley, South Yorkshire. S72 76AB, DOE-METC—83-56 (1982).
5. Cryer, S.A. “Modeling Agglomeration Processes in Fluid-Bed Granulation.” AIChE J. 45 (1999): 2069–2078.
6. Rahaman, M.F., J. Nasera, and P.J. Witta. “An Unequal Granular Temperature Kinetic Theory: Description of Granular Flow with Multiple Particle Classes.” Powder Technology 138.2-3 (2003): 82-92.
7. Syamlal, M., W. Rogers, and T.J. O'Brein. “MFiX Documentation Theory Guide.” Morgantown: NETL, Dept. of Energy 1993.
8. Khadilkar, A.B., P.L. Rozelle, and S.V. Pisupati. “A Study on Initiation of Ash Agglomeration in Fluidized Bed Gasification Systems.” Fuel 152 (2015): 48–57.
9. Khadilkar, A.B., P.L. Rozelle, and S.V. Pisupati. “Effect of Heterogeneity in Coal Ash Chemical Composition on the Onset of Conditions Favorable for Agglomeration in Fluid Beds.” Energies, 8 (11) (2015): 12530–12545.
10. Van Dyk, J.C., F.B. Waanders, S.A. Benson, M.L. Laumb, and K. Hack. “Viscosity Predictions of the Slag Composition of Gasified Coal Utilizing FactSage Equilibrium Modelling.” Fuel, 88.1 (2009): 67-74.
11. Vargas, S., F.J. Frandsen, and K. Dam-Johansen. “Rheological Properties of High-Temperature Melts of Coal Ashes and Other Silicates.” Progress in Energy and Combustion Science 27 (2001): 237-429.
12. Thielmann, F., et al. “The Effect of Primary Particle Surface Energy on Agglomeration Rate in Fluidised Bed Wet Granulation.” Powder Technology 181.2 (2008): 160-168.
13. Chaivatamaset, Pawin, Panchan Sricharoon, and Suvit Tia. “Bed Agglomeration Characteristics of Palm Shell and Corncob Combustion in a Fluidized Bed.” Applied Thermal Engineering 31 (2011): 2916-2927.

Appendix E. PSU Agglomeration Model Report

Unified Model for Prediction of Agglomeration in Fluidized Beds and Validation Attempts of Proposed Particle-level Growth Mechanism of Ash Agglomerates

Report- Draft

Prepared for
Gas Technology Institute

by
Aditi Khadilkar and Sarma V. Pisupati

EMS Energy Institute and
Energy and Mineral Engineering Department
The Pennsylvania State University

11/28/2016

Table of Contents

1. Introduction

Prediction of agglomeration is challenging since the heterogeneity in ash chemical composition, gaseous atmosphere and distributive granular physics properties affect the process simultaneously. A model to predict agglomeration for applications such as combustion and gasification would require incorporation of chemical composition of the fuel along with particle level differences in the same, inclusion of the effects of variations in temperature, slag amount and viscosity across the bed and also the variations in hydrodynamics.) Attempts have been reported in the literature[1-4] to include variations in collision velocities of particles. Terrazas-Velarde et al.[5] address non-uniformities in collision frequency, which is another parameter affecting particle dynamics. However, these models do not include the effects of particle chemistry. On the other hand, some models[6, 7] take into account bulk chemical composition of the fuel but do not address the differences due to hydrodynamics. A modeling methodology for agglomeration prediction, that considers both the particle chemical composition and particle hydrodynamics was developed at Penn State.

Mineral matter in fuel ash is distributive and the bulk chemical composition is not representative. Based on mineral processing operations used, such as grinding, the mineral content is distributed amongst particle classes and therefore each particle class differs in chemical composition. Thus, the bulk fuel contains classes of particles that may be rich in specific minerals such as a class that contains heavy, iron-based minerals or calcium-based minerals. The particles of such a class can be assumed to be reasonably homogeneous in composition, while each particle class would have a composition distinct from another. The term “particle-level” refers to the differences that exist at the level of these ash particle classes. The term “bulk” composition refers to the overall composition of the whole coal that contains these specific mineral-rich particle classes. The particle-level differences in size and composition have been ignored in using only the composite fuel for analysis and prediction. A consideration of particle-level non-uniformities in the prediction of ash behavior and agglomeration is warranted. Khadilkar et al.[8, 9] showed that the bulk ash chemical composition did not

indicate slag formation at low temperatures, while the study of particle-level heterogeneities revealed that it can begin at lower temperatures than the FBC operating temperatures of 850 °C.

2. Objective

To develop a mechanistic understanding of agglomerate growth in fluidized bed combustors, based on the modeling results and to discuss attempts to validate the proposition.

3. Materials and Methods

3.1. Model Development Methodology

The following sections discuss the various aspects of model development. The model is developed based on testing two-particle collisions for sticking. The chemistry of the formation and rheology of the viscous liquid that can bind particles on collision is studied using computational thermodynamics, while the physical properties that define particle motion are studied using computational fluid dynamics. The agglomeration model developed comprises of a mathematical code that uses these inputs on the binder's chemical properties and particle physics to track changes in particle sizes over time. This includes consideration of the dispersion of the binder on the solid particle surface as also the differences in collision dynamics that relate to particle size. The model is developed to aid utilization of parameters at the particle-level.

3.1.1. Quantification of particle growth

The initial particle size distribution (PSD) is divided into narrow size intervals. Each particle increment has a top size and a bottom size and the mean of these values is used to represent the average diameter of particles in that interval. The particles are assumed to be spherical. The initial bed mass is distributed amongst the size intervals. The number of particles in each bin is calculated. When an agglomerate is produced by a collision of a particle from one size interval with that from another, the mass of the resultant particle is calculated to be the sum of the individual masses of the colliding

particles. If two colliding particles stick, the resultant agglomerate diameter is calculated, based on the resultant mass and assuming the particle density to be remaining constant. The agglomerate may then move into a higher sized interval, before the next time step. The changes in the number of particles are tracked and the model can trace the temporal evolution of ash particle size distribution in the system.

3.1.2. Stokes' criterion to determine sticking of colliding particles

The Stokes' criterion has been previously used to determine if colliding particles remain stuck together, in the process of granulation for pellet production[4]. The Stokes' number is given as

$$S_t = \frac{4\rho_i U_c d_i}{9\mu_i}$$

U_c is the velocity associated with a collision

μ_i is the viscosity of a liquid layer on the surface of the particle.

The use of this criterion assumes that on collision of particles with a liquid bridge separating them, the forces of viscous dissipation dominate while the surface tension and capillary forces are negligible. This assumption is suitable for the high viscosity slag-liquid that acts as the binding liquid in the fluidized bed combustion and gasification industry.

The Stokes' number is a ratio of the kinetic energy to the viscous dissipative forces. If the viscous dissipation on collision of the particles exceeds their kinetic energy then the particles remain stuck, otherwise they rebound. This criterion helps to combine the effects of both chemistry and physics based parameters into the model. The viscous liquid in the gasification and combustion industry is the slag- liquid formed from ash at high temperatures. Thus, the ash material properties and chemistry as well as operating temperature are used in the determination of the viscous dissipation. The kinetic energy depends on the particle physics such as the collision velocity. Since this test is applied to two-particle collisions in the system, the collision frequency is used to calculate the number of collisions that occur.

Hence, for particles to agglomerate- 1) They should be wetted by a viscous liquid, 2) they should undergo a collision in the liquid wetted region and 3) they should pass the Stokes' test.

Particle wetness is dictated by the ash chemistry, while the tendency to collide with another particle is determined by the physics and bed hydrodynamics. The Stokes' test includes both chemistry, in terms of slag rheological properties, and also physics, in terms of particle velocities.

3.1.3. Calculation of collision frequency distribution

In order to correctly incorporate the agglomerate growth kinetics for the entire particle size distribution, the determination of a distribution of collision frequencies is required. The number density (number of particles per unit volume) of a given mass of smaller particles will be higher and hence they are likely to undergo more collisions in a given time. In stead of an arbitrary correlation of collision frequency to the number of particles, in this study the collision frequency is calculated based on the kinetic theory of granular flow. Hence, the particle granular temperature and the number density of particles in the intervals are used in the Rahaman formula[10] to compute the distribution of collision frequencies between particles of different sizes. The Rahaman formula was chosen since this was developed utilizing a granular mixture of particles consisting of different sizes with unequal granular temperatures, unlike prior models that considered only mono-sized particles.

The granular temperature required for the above calculation of the collision frequency is obtained using CFD with the software – MFIX (Multiphase Flows with Interphase eXchanges) based on finite volume method[11]. This is an open-source software which has been validated for multiphase simulations in gasifiers and combustors. The mass and momentum balance equations as well as the Schaeffer frictional model are solved to obtain the particle velocities and granular energy using the Eulerian-Eulerian method.

3.1.4. Calculation of slag-liquid amount, viscosity and particle wetness

In addition to the physics-based parameters described above, the methods for the incorporation of the chemistry-based parameters into the agglomeration model have been discussed in the following sections. The amount of slag-liquid is determined by the ash chemistry and operating conditions such as the temperature and gaseous atmosphere. The viscosity of the slag-liquid formed helps to determine if the viscous dissipation of the particles' kinetic energy would be sufficient to result in sticking. The viscosity of the slag-liquid is dependent on the chemical composition of the liquid. The extent of particle wetness depends on the amount of liquid, the contact angle and the particle size. A brief description of the methods used for these calculations have been described below.

3.1.4.1. FactSage™ thermodynamic equilibrium simulations (Computational thermodynamics)

Thermodynamic simulations based on quasi-chemical computations are used to obtain the amount of slag-liquid formed at equilibrium under a given temperature condition. The phases formed were studied under both oxidizing and reducing environments and the methodology has been discussed in detail in previous studies. These slag formation tendencies have also been analyzed experimentally using high temperature X-ray diffraction and thermo-mechanical analysis[8,9].

3.1.4. 2. Calculation of slag-liquid viscosity

The chemical composition of the slag obtained from FactSage™ calculations was used to calculate the slag viscosity with the modified Urbain model[12]. This empirical model was chosen, based on the review of viscosity models by Vargas et al.[13]. The study found the Botinga-Well and Urbain model to closely match experimentally measured viscosity values. However, the Botinga –Well model does not perform adequately well for coals rich in iron containing phases. Vargas concluded that Urbain model made reasonable predictions for high rank coals. Since the modified Urbain model is an empirical model that has been developed for completely molten slag-liquid, the slag-liquid oxide composition obtained from FactSage™ was used as an input for the

calculation. Thus the viscosity of the clear slag-liquid at the desired temperature is calculated.

3.1.4.3. Calculation of probability of particle collision in a slag-liquid wetted region (wet collision)

The equation for partial wetting adopted by Thielmann et al.[14] was used to obtain the radius of the area wetted by the slag-liquid. Based on the ratio of the wetted area and the particle surface area, the probability of a wet collision is estimated.

3.2. Experimental methods

Agglomerate samples obtained from a laboratory-scale combustion facility in Canada were analyzed. Agglomerate samples were also generated in a laboratory-scale fluidized bed combustor at Penn State as described below using Pittsburgh No. 8 coal rejects for analysis. The chemical composition of the Bailey rejects is shown in Table 1. The agglomerate samples were polished and observed under a scanning electron microscope and the elements present in them were mapped across a cross section of the agglomerate.

Table 1: ICP-AES and sulfur analysis of Pittsburgh No.8 coal rejects

Species	SiO_2	Al_2O_3	Fe_2O_3	CaO	TiO_2	K_2O	MgO	Na_2O	BaO + SrO	MnO	S
Wt. %	62.57	24.82	5.74	2.17	1.26	2.5	0.83	0	0.09	0.02	1.61

3.2.1. Laboratory scale fluidized bed reactor

A laboratory-scale fluidized bed was used to produce agglomerates from a fraction of Pittsburgh No. 8 seam coal. The rejects of this coal were used for this purpose as the rejects have a high ash content of 81.6 % and so would reduce effects of the presence of carbon, as that is not accounted for in the model. The reactor was operated as a combustor by using 3% oxygen, 15% carbon dioxide, 10% water and 72% nitrogen as the fluidizing gas. The particle size distribution used consisted of about 48 % in the size range of 250-355 μm and 52% between 149-250 μm. The size and velocity distribution

were chosen such that the superficial gas velocity would be greater than the minimum fluidization velocity and less than the terminal velocity of majority of the particles, taking into consideration the limitation of gas flow rate permissible in the laboratory setup. A 200 g sample was used and the experiment was run for 2 h 15 min, using a gas flow rate of about 10 L/min.

3.2.2. Scanning electron microscopy coupled with energy dispersive x-ray spectroscopy (SEM-EDX)

The samples were tested in a FEI Quant 200 SEM coupled with a 10 mm^2 EDX detector (Oxford Instruments, Concord, MA). This technique was used to conduct post mortem analysis of agglomerate samples. They were given a conducting iridium coating to avoid excessive charging of the sample surface with electrons during the experiments. This helped to identify the elements in the regions that formed slag bridges as compared to the solid particles. The elemental analysis was performed using the software Aztec version 2.4.

4. Results and Discussion

The following results show the effect of prominent chemistry-based and physics-based parameters on agglomeration. They also demonstrate that the rate of agglomerate growth can be modeled at the particle-level, as a combined effect of the chemical and physical properties of the particle and binder system.

4.1. Results from the incorporation of the collision frequency distribution

The initial particle size distribution used in this study was divided into 4 size intervals and consisted of a larger number of fine particles. The PSD was divided into size intervals and they have been labeled with numbers from 1 to 4, wherein particles in interval 1 have the largest size. The size progressively decreases from interval 1 to 4. As agglomeration progresses, the number of smaller particles decreases along with an increase in size of larger particles. Thus, the collision frequency of smaller particles goes on decreasing with time. The initial distribution of collision frequencies amongst all

possible binary collisions depends upon the number of particles in the size intervals undergoing collision. This is dictated by the initial particle size distribution and the average particle diameter of particles in each size interval.

Figure 1 illustrates the decrease in collision frequency of smaller particles with time as agglomeration progresses. Initially, the collision frequency is higher for binary collisions among the smaller sized particles since they are greater in number. Binary collisions of particles in interval 3 and 4 with other particles within the same size class are seen to occur at higher frequencies. Similarly, frequency of collisions between particles of classes 3 and 4 with each other (Represented as 3-4 or 4-3) is also high. At the same time, the collision frequency of collisions 1-1, i.e. the particles in the largest size interval with other particles within the same interval is low. As time progresses, the frequency of 1-1 collisions begins to increase while that of 4-4, 4-3 collisions decreases. After 3 hours, all collisions of particles in size interval 1 with other particles (1-1, 1-2, 1-3, 1-4) are higher than the collisions of the smaller sized particles with one another (2-2, 2-3, 2-4, 3-3, 3-4, 4-4). Further decrease in the frequency of all binary collisions is seen after 10 hours as the particles begin to defluidze. Utilization of the unequal kinetic theory of granular flow thus helps to obtain the entire distribution of collision frequencies that can be utilized in the prediction of agglomerate growth.

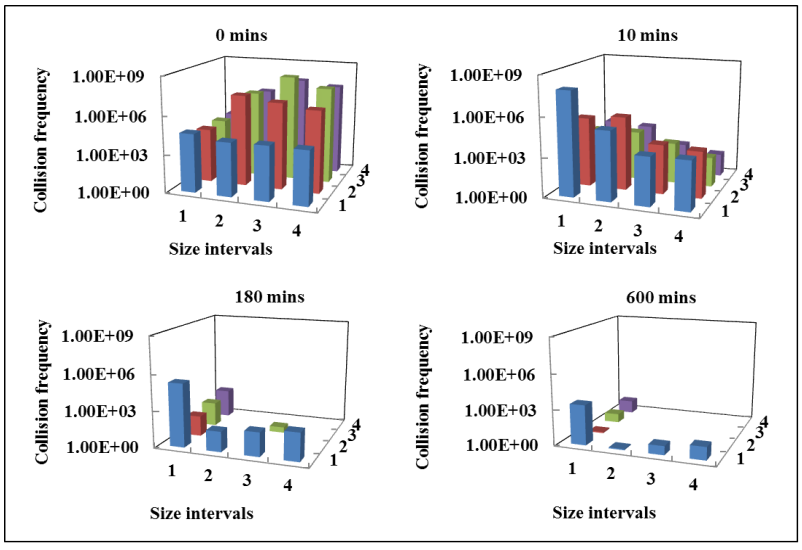

Figure 1. Evolution of the distribution of particle collision frequencies with time during agglomeration

Accordingly, the above distribution of collision frequencies that evolves as agglomeration progresses was utilized in prediction of agglomerate growth kinetics in the Penn State ash agglomeration model.

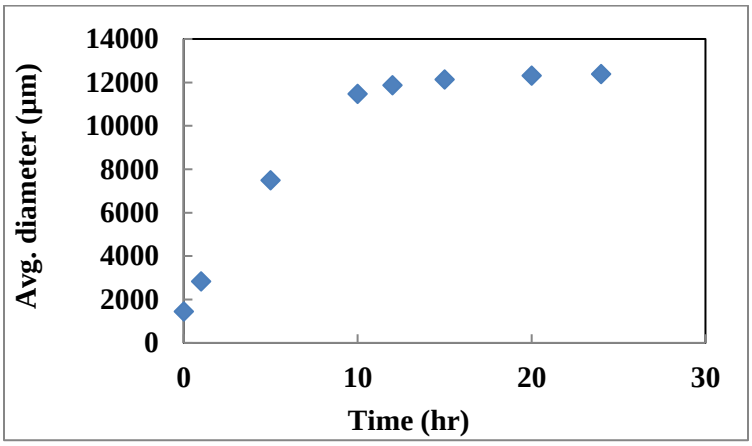

Figure 2: Agglomerate growth rate predicted using the ash agglomeration model

Figure 2 shows the rate of growth of agglomerates obtained using this model. It is seen that initially, the size of the agglomerates increases rapidly and then begins to stabilize as the frequency of collisions begin to decrease. This modeling methodology is proposed as a more realistic method to obtain particle growth kinetics than assumption of a constant collision frequency or an arbitrary dependence on the number of particles in the system.

In addition to the effects of physics-based parameters, the effects of chemistry-based parameters were also incorporated into the ash agglomeration model.

4.2. Results from the incorporation of amount of slag (binder) on agglomerate growth rate

The amount of slag depends on the chemistry of the ash particles. The effect of ash chemistry on the slag formation tendencies has been studied in detail in previous work[8, 9]. In this study, the amount of slag obtained using the ash chemistry has been incorporated into the Penn State ash agglomeration model as a probability of a given particle being wet.

Figure 3 shows the predictions made using the model with this incorporation of the amount of slag. It is seen that as the amount of slag increases, the probability of wet

collisions increases and hence the rate of agglomeration increases. At the end of 10 hours, the particles begin to defluidize if 15 % slag is present in the system, while their average diameter is only about 4000 µm if 5 % slag is available.

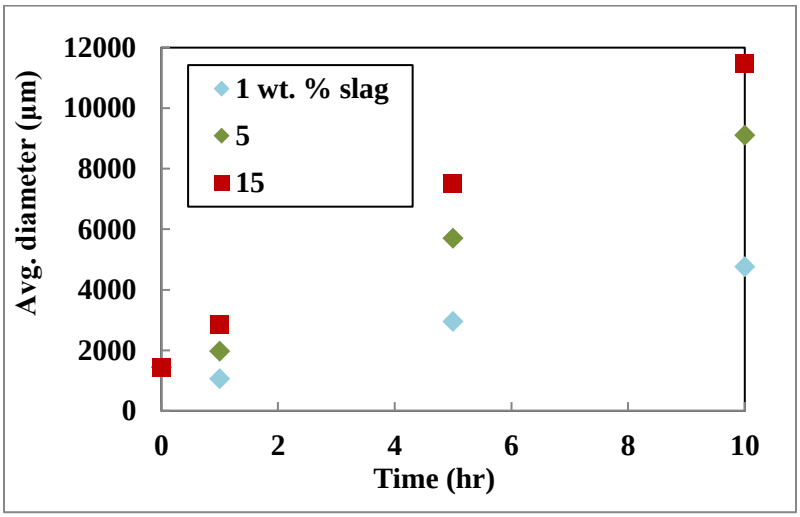

Figure 3: Effect of amount of slag on agglomerate growth

4.3. Resultant agglomerate growth obtained through a combination of chemistry-based and physics-based parameters

Figure 4 shows that the model can also be used to predict the evolution of the entire particle size distribution with time. It is seen that the finer particles from size interval 4 get converted to larger particles over time. After 3 hours most of the particles are in the largest size interval and significant defluidization occurs after 10 hours.

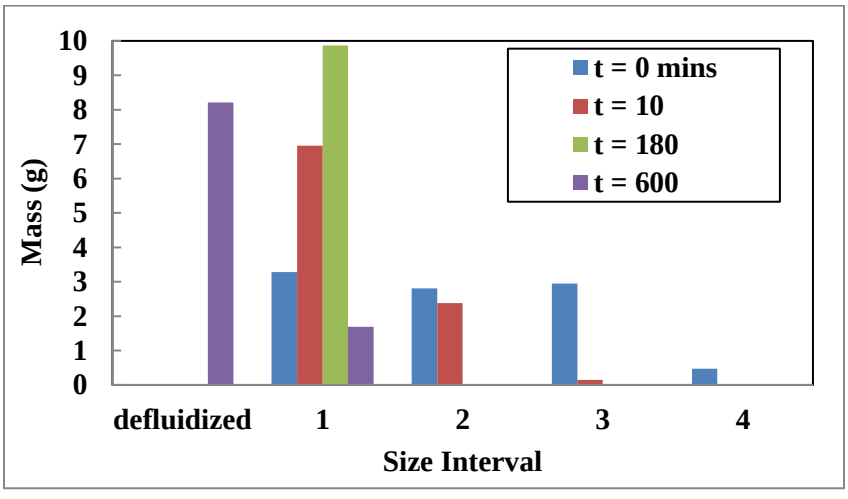

Figure 4: Evolution of particle size distribution with time

Slag formation onset temperature was as low as 850 ˚C for density fractions of Pittsburgh No.8 and Illinois No. 6 coals and Skidmore anthracite. The amount of slag formed at initiation was less than 10 %. In order to determine the extent of growth at low slag amounts, a sensitivity analysis to the amount of slag was performed using the agglomeration modeling methodology. Particle agglomerate growth was limited by slag-liquid amounts up to 20 wt. % slag after which it plateaus as shown in Figure 5. When the slag is less than 15 wt. %, the diameter does not increase significantly since the slag viscosity is too high and amount too low. As the slag-liquid amount increases further, although the extent of particle wetness increases, the number of solid particles decreases as they melt to form the slag-liquid. So, it is believed that the collision frequency of particles decreases although the wetness of particles increases. However, the amount of slag that can undergo solidification into a larger agglomerate is higher, as explained in regime 3 described below.

Three regimes of agglomerate growth are proposed as follows-

Regime 1: Slag-liquid amount less than 10%- In this regime, the agglomerate growth is limited by the amount of slag-liquid available for sticking, although a large number of particles are present in the system. Thus, the probability that the particles undergo a wet collision is low. The rate of growth is slow and the time required for the particles to reach the defluidization size would be very long.

Regime 2: Slag-liquid amount between 10-30 %- In this regime, the agglomerate growth rate is maximum. An adequate number of particles are available in the system and there is enough slag-liquid for particle sticking on collision. The particles in this regime are likely to be completely coated with slag-liquid layers and the probability of wet collisions will be high. The particle growth rate is high and significant defluidization would occur.

Regime 3: Slag-liquid amount greater than 50%- In this regime although a large amount of slag is available for wetting ash particles, since this slag is formed by the melting of solid particles, the number of particles in the system is low. The collision frequency of particles is likely to be low and although there is adequate amount of slag-liquid, the particle-particle interaction is limited. In order to demonstrate the effect of the large slag

amounts present in regime 3, the average agglomerate diameter was calculated assuming the extreme case that all the slag coalesces and deposits into a large solid agglomerate. Thus, Figure 1 shows an increase in average diameter with increasing slag amount. In the case of bituminous coals and anthracite, at the low operating temperatures in fluidized bed combustors, regime 1 and 2 are more likely to occur in the bed. Additionally, regime 1 and 2 are of interest in understanding the initiation of agglomerate growth and are the focus of the modeling study.

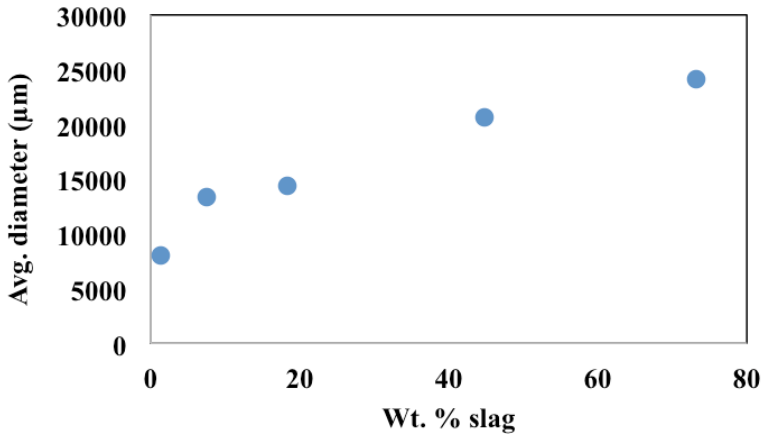

Figure 5: Effect of slag-liquid amount on agglomerate growth with solidification of slag formed

4.4. Proposed mechanism of the process of agglomeration in fluidized beds

The heterogeneous behavior of bed ash helps to explain the occurrence of agglomeration at temperatures lower than operating temperatures in fluidized bed combustors and gasifiers. The amount of slag depends on the particle temperature and chemistry. At low temperatures, certain low-melting components such as those in particle classes with high iron- and calcium-based components studied, can initiate the slag formation. However, the slag-liquid amounts are generally low at these temperatures. Hence, agglomeration would be initiated due to the particle-level chemistry in Regime 1. The agglomerate growth is likely to propagate in Regime 2.

Experimental studies by Atakül et al.[15] showed that agglomeration occurs at 125-200 ˚C lower than characteristic IDT and about 300-400 ˚C lower than the flow temperature (FT) in a laboratory-scale fluidized bed combustor. They identified the

temperature at which agglomeration was initiated based on the detection of bed temperature fluctuations and pressure drop measurements, as well as pictures of the active bed surface. Since the iron- and calcium-based mineral rich SG4 fraction has been identified as the initiator of agglomeration, in the present study, a comparison of IDT of bulk coal with the slag-liquid formation onset temperature obtained for the SG4 density fraction of Pittsburgh No. 8 coal and Illinois No. 6 coal is shown in Table 2. This comparison shows that the initiation of slag formation could occur at temperatures around 400-600 °C lower than the measured IDT temperature. This indicates that agglomerate growth is likely to be initiated around particles of certain compositions such as of the SG4 particle class, at temperatures significantly lower than AFT predictions that are based on bulk coal properties.

Table 2: Initial deformation temperatures of Bituminous coals from AFT measurements under reducing conditions[16]

	Pittsburgh No. 8	Illinois No.6
Initial deformation temperature (IDT) using whole coal (°C)	1,237	1,201
Particle-level Slag Formation Onset Temperature (°C)	840	650

The proposition that agglomeration is initiated around a few particles and then propagates throughout the fluidized bed reactor is supported by the study of agglomerates presented in a report by the U.S. Department of Energy (DOE)[17]. In this study undertaken by the U.S. DOE, agglomerates formed in thirteen fluidized bed combustion units were observed using SEM, which showed the presence of dark cores with rims. The agglomerates were also found to have a high calcium sulfate and iron oxide content. These observations further support the onset of conditions favorable for agglomeration by sticking of particles with composition similar to the SG4 fraction, which could have a dark iron core at locations of initiation of agglomerate formation with rims of alumino-silicate rich slag. Below 850 °C, the SG4 fraction in all the three coals studied begin to form slag under reducing conditions[18]. The amount of slag is less than 10 weight % near the onset temperature. Agglomerate growth is likely to be initiated around these particles but as shown by the modeling results in Figure 5, it is not likely to lead to defluidization

at these low slag-liquid amounts. At higher temperatures that can occur in bed, the SG4 fraction can form up to 90 % slag. Once initiated, agglomerate growth is likely to propagate in the bed due to one or more of the following reasons:

1) Temperature excursions due to changes in system hydrodynamics- Once particle size increases, and defluidization begins, degree of mixing will be reduced and temperature fluctuations increase. Local hot spots can form in a poorly mixed bed[19]. An empirical equation to obtain the critical velocity needed to avoid dead zone formation for particles of a certain size in fluidized beds was developed by Wen et al.[20]. As per their work, an increase in dead zone formation occurs with an increase in particle size. Similarly, a decrease in mixing at the onset of defluidization, resulted in temperature fluctuations and differences in temperatures measured by thermocouples at different heights in a fluidized bed combustor, in the study by Scala et al.[21]. A discussion of the effect of hydrodynamics on heat transfer in fluidized beds by Bock et al.[22] showed that heat transfer decreases with an increase in particle size and subsequent changes in bubble motion. Hence, with an increase in particle size with agglomerate growth and also dead zone formation at the onset of defluidization, heat transfer is likely to decrease causing an increase in particle temperatures. Bottom ash particles that are agglomerating are primarily of Geldart type A or B and as they grow in size, they will eventually move into type D. For BFBs, an increase in size of type A and B particles causes a decrease in the heat transfer co-efficient. As the particle size increases from 100 to 1,000 μm, the heat transfer co-efficient of heat transfer to heat exchanger surfaces decreases by about 4.5 times, mainly due to decrease in particle convection that causes decreased renewal of particles from heat transfer surfaces[23]. Additionally, after agglomeration is initiated, as particle size increases, the ratio of the particle velocity to the minimum fluidization velocity of the larger particles can decrease. This will increase the possibility of particle segregation. Hence it is possible that once agglomeration is initiated by particles melting at low temperatures, such as those rich in iron- and calcium-based minerals, the change in bed hydrodynamics would lead to further agglomeration due to decreasing particle velocities and decreasing bed voidage. As agglomeration proceeds, the volume of the expanded bed decreases due to the lesser fluidization of the heavier particles formed. Thus, with decreasing voidage and subsequent increasing collision frequency, agglomeration rate

may increase initially. As it progresses, decrease in granular temperature and particle number density and the resulting collision frequency decrease would also decrease agglomeration rate. Thus particles grow quickly once the process of agglomeration is initiated until a stable size is reached as the agglomeration rate begins to decrease.

2) Temperature rise due to deposition on heat-transfer surfaces- One more plausible mechanism of the propagation of agglomeration in the system is due to decrease in heat transfer efficiency after initiation of agglomeration. Once particles of larger sizes form by sticking of mineral matter with low slag-formation temperatures, the particle velocity decreases and they can deposit on to heat transfer surfaces, thereby decreasing the efficiency of heat transfer. The decrease in heat transfer can cause a rise in bed temperature leading to melting of alumino-silicate rich components, which have higher slag-formation temperatures as shown from the analysis of density fractions. The increase in slag amount would then cause an increased agglomeration rate. This mechanism is prone to occur when there are in bed heat exchanges, which are generally restricted to bubbling fluidized bed systems.

3) Presence of local pockets of reducing conditions in the bed- Besides a local increase in particle temperatures, agglomeration is also likely to occur due to changes in the local gaseous atmospheric conditions. The temperature required for the formation of a certain amount of slag-liquid is lower in a reducing gaseous environment than an oxidizing gaseous environment[9]. Local reducing conditions can exist in a fluidized bed reactor around regions in which char particles are concentrated. The literature shows that mineral matter within a carbonaceous particle experiences a high temperature and a reducing atmosphere[24]. Once a few particles such as those from the SG4 density fraction, rich in iron- and calcium-based minerals become sticky at low temperatures, char particles can stick to their sticky surface as illustrated in Figure 11. This photograph shows an agglomerate that was formed in an industrial fluidized bed combustor unit with black carbonaceous particles within the mineral matter. The concentration of char particles within mineral matter and slag can create these local reducing conditions. The included minerals in these char particles are also then subjected to the reducing environment and begin to form slag at lower temperatures.

In order to support the mechanism of agglomerate growth in fluidized bed reactors, microscopic analyses of agglomerate samples was performed as follows-

4.5. SEM-EDX analysis of agglomerates obtained from a laboratory scale FB combustion facility at Canada

Agglomerates that formed within two hours during combustion in a laboratory-scale combustion facility in Canada were used as samples to conduct a post-mortem study to understand the agglomerate growth mechanism. In order to avoid a biased analysis, microscopic imaging was performed in randomly selected regions across the entire sample surface. In this way, the entire sample surface was scanned to identify particles with different morphologies. Also, EDX of the whole sample cross section was done at a low magnification (50x to 200x) to identify regions with higher concentration of a particular type of element. Regions distinct in elemental composition were then magnified for detailed study with microscopic images and elemental maps, so as to account for all different types of particle behaviors. Primarily two distinct morphologies were observed across the sample surface as shown in Figure 6- small particles adhering to form a larger sphere and slag-coated particles with bridges. The latter showed that greater slag amounts were formed and coated the particles. Morphologies showing discrete adhered particles indicated lower slag amounts. The formation of higher amount of slag was believed to have occurred at higher temperatures. Hence, the slag-coated particles were likely to be a later stage (causing propagation at higher temperatures) in the agglomeration process, after initiation by the smaller adhered particles. In order to test this implication of the two distinct morphologies observed, the elemental composition of each of them was studied using EDX. EDX was performed on 8 to 10 spots of the two morphologies identified in Figure 6.

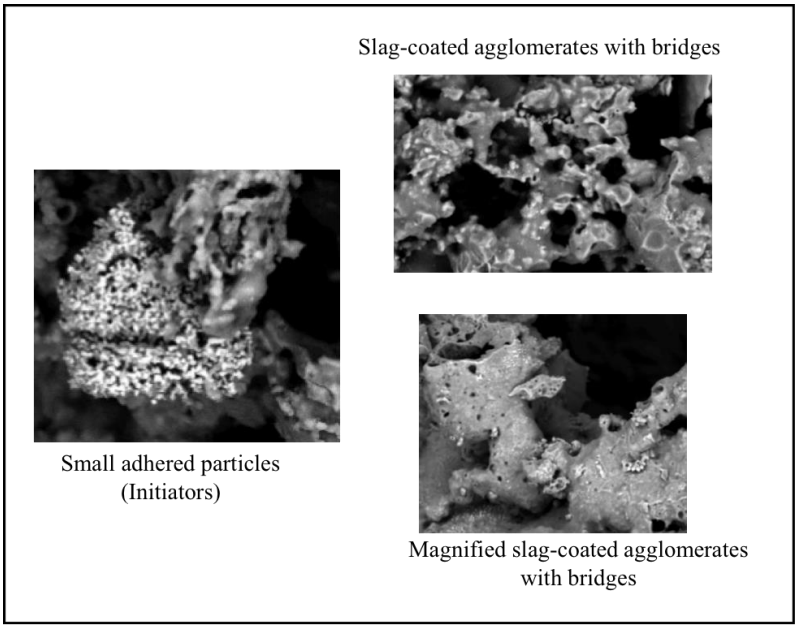

Figure 6: Morphologies of initiators and slag-coated particles observed by SEM of agglomerates

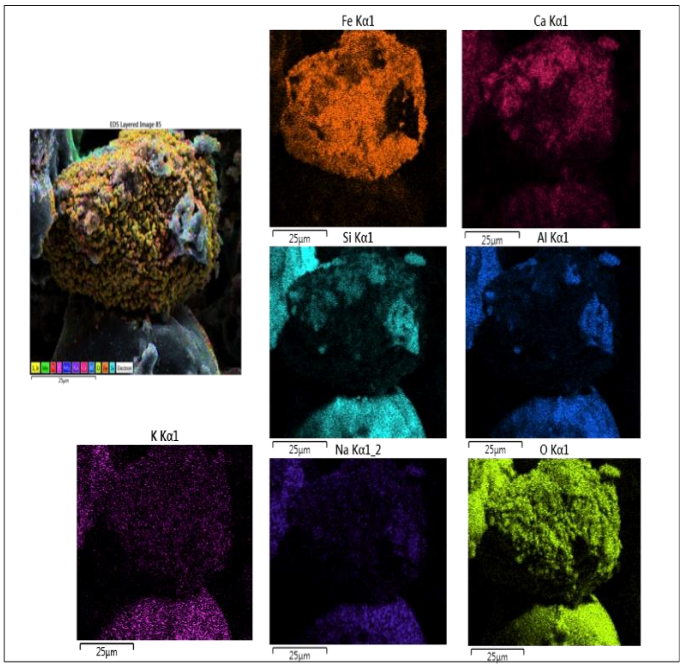

Figure 7: SEM-EDX of initiator and alumino-silicate slag coating

The EDX results are shown in Figure 7. The orange sphere in the figure is mapped to high concentrations of iron- and calcium-containing phases. Previous work using FactSage, TMA and XRD also indicated that density fractions rich in calcium- and

iron-based minerals showed slag formation onset temperature less than 850 °C. The amount of slag obtained at initiation for these density fractions was less than 10 %. When the slag amount is less than 15%, the modeling results in Figure 5 showed that the agglomerate growth was restricted and particles did not reach their defluidization size in 10 hours. These density classes rich in calcium- and iron-based minerals were thus believed to initiate agglomerate growth at the particle-level, which would then be followed by propagation. Further, molten slag (blue) seen to adhere to these initiators, is rich in silicon and aluminium with some sodium and potassium content as seen in Figure 3. In order to obtain a semi-quantitative estimate of the composition of the initiators and slag-coated particles, EDX was used and the average composition of the studied spots is reported in Table 3.

In order to verify that the initiators begin to form slag at lower temperatures than fluidized bed operating temperatures and propagation occurs with the coating of these initiators after formation of higher slag amounts, the EDX composition shown in Table 2 was used to perform FactSage simulations under oxidizing conditions. FactSage thermodynamic simulations were performed to predict the initiation temperature of slag formation in these regions. It was found that the initiators, which are rich in iron phases, began slag formation at 820 °C as shown in Figure 8, while the alumino-silicate rich slag was formed at a higher temperature of 920 °C. Slag-coated agglomerates began to form bridges with this higher slag amount. The amount of slag formed from the components in the initiators was also less than 10% up to 950 °C. Since the particles do not melt completely, the SEM images show small discrete particles of these initiators adhering to form larger spheres.

Table 3: EDX compositional analysis of stage 1 and stage 4

	Small adhered particles (Initiators/Stage 1)		Slag melting at higher temperature (Slag on slag-coated agglomerates/stage 4)	
Element	Wt.%		Wt.%	
	Mean	Standard deviation	Mean	Standard deviation
O	36.9	8.4	57.5	4.4
Na	0.2	0.2	1.8	0.3
Mg	1.1	0.6	1.5	0.5
Al	1.9	0.5	10.7	1.5
Si	4.4	2.1	21.5	2.7
K	0	0.1	1.8	0.5
Ca	3.1	1.9	1.8	1.4
Mn	2.2	1.1	0	-
Fe	50.3	8.2	3.1	0.8

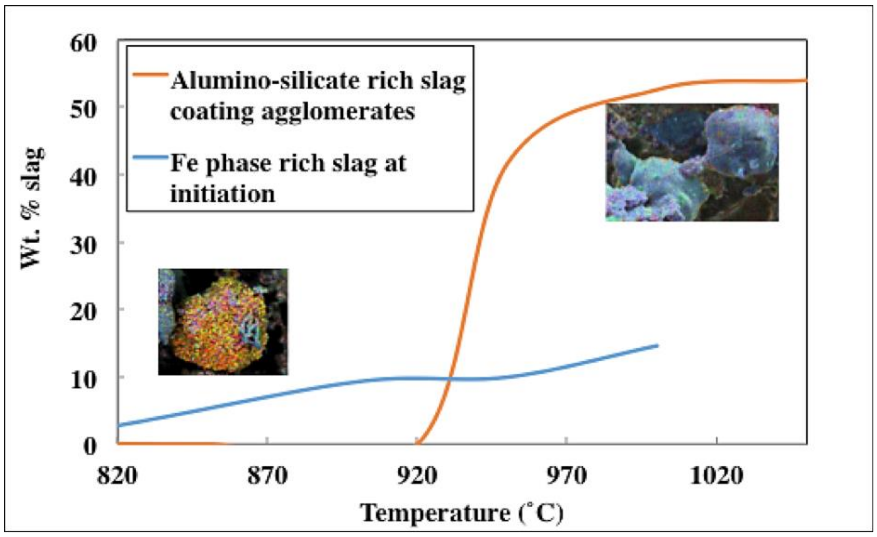

Figure 9: Slag formation tendency of components in stage 1 and stage 4 using FactSage simulations

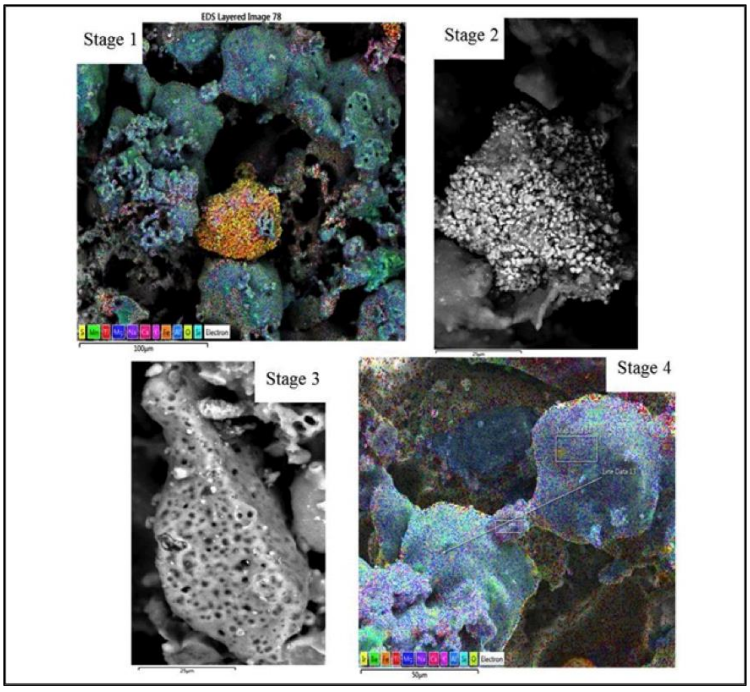

Figure 9: Stages of agglomerate growth observed through SEM-EDX of agglomerates

Through this SEM-EDX study of agglomerates, four different stages of agglomeration were identified as shown in Figure 9. Stage 1 shows small particles rich in iron–based minerals adhered together to form a larger sphere. These particles begin to form slag at a lower temperature of 820 ˚C, as shown in Figure 8. The amount of slag formed from this composition is less than 20 % at temperatures up to 1,000 ˚C. Hence, this is adequate to initate agglomeration and lead to the formation of bigger spheres that are rich in iron, but not sufficient to make the particles grow up to their defluidization size. Stage 2 shows that slag formed at the higher temperatures, begins to coat these iron spheres. Stage 3 shows a completely coated agglomerate from stage 1. Finally, with the formation of up to 40 % slag at higher temperatures of above 920 °C, the coated agglomerates begin to stick to one another as shown in stage 4, wherein bridging is clearly seen between two slag-coated agglomerates.

Figure 10: Agglomerates of Pittsburgh No. 8 coal rejects produced in PSU reactor

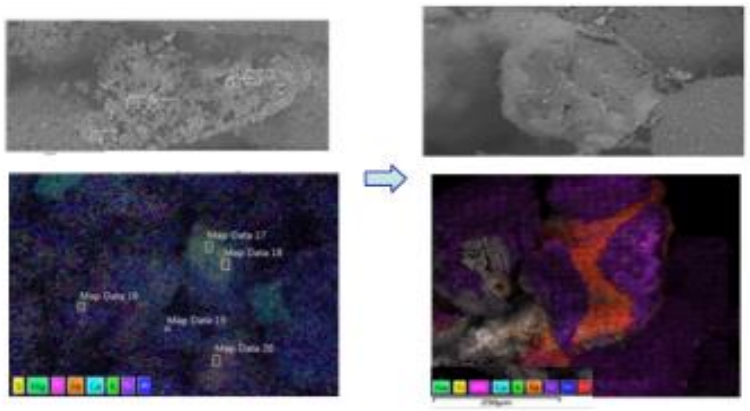

Figure 11: SEM-EDX images of agglomerate of Pittsburgh No. 8 coal rejects

4.6. SEM-EDX analysis of agglomerates produced in laboratory fluidized bed reactor at Penn State

Agglomerates of Pittsburgh No. 8 seam coal rejects were produced in the laboratory-scale reactor at Penn State. These are shown in Figure 10. The composition of this material is shown in Table 1.

The SEM-EDX analysis of the agglomerates in Figure 8 shows two particles rich in siliceous minerals (violet) adhered by a slag bridge (orange) rich in iron and calcium containing minerals. SEM-EDX analysis of these agglomerates also showed regions with smaller, discrete particles adhering together as shown in Figure 11. Across the entire cross section of the sample, 25 regions including those with bridging and with smaller particles adhering were observed. 9 spots in regions with initiators (small, discrete particles adhering) were studied using EDX and found to be rich in calcium-containing compounds with the composition as shown in Table 4. Similarly, 15 spots in the regions that formed slag bridges as shown in Figure 11 were also analyzed for their elemental composition. The composition of the highly molten slag is shown in Table 4.

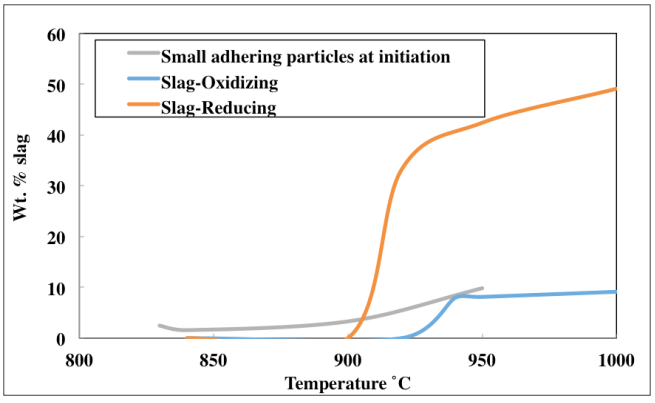

Figure 12: Slag formation tendency of components in small adhering particles and alumino-silicate slag-forming components using FactSage

FactSage simulations under oxidizing conditions were performed with the ash compositions in Table 3 to identify the temperature at which slag formation begins for the initiators rich in calcium-based minerals. The results shown in Figure 12 indicate that the agglomeration was initiated at 830 ˚C by the calcium-rich particles. The temperature of particles in bed is then likely to rise by one of the plausible mechanisms discussed further in the manuscript, causing propagation of agglomeration with the formation of liquid bridges above 930 ˚C. This onset temperature of slag-formation from the alumino-silicate components that lead to bridging was calculated using FactSage simulations under oxidizing conditions.

Table 4: EDX of initiators and alumino-silicate, high temperature melting slag

Element	Initiator		Alumino-silicate Slag	
Wt.%	Mean	Standard Deviation	Mean	Standard deviation
C	2.1	0.94	1.3	0.39
O	40	0.64	40	9.5
Na	0.3	0.12	0.4	0.21
Mg	0.4	0.02	0.4	0.16
Al	4.4	0.88	9	1.8
Si	6.7	1.11	12.3	2.2
S	0.9	0.19	0.1	0.07
K	0.5	0.41	1.6	0.62
Ca	5.1	0.17	0.7	0.43
Ti	0.3	0.86	0.5	0.08
Fe	40	1.7	34	14

The slag formation onset temperature of the alumino-silicate components that have relatively higher melting temperatures was also computed under a reducing environment. Under this condition, the temperature of onset of slag formation was lowered to 910 ˚C and the amount of slag was 30-50 %, which was higher than under oxidizing conditions. Hence, in the presence of pockets of reducing gaseous conditions in

the reactor, these components could cause propagation of agglomeration. FactSage analysis showed that the amount of slag-liquid formed from the alumino-silicate components was lower in case of Pittsburgh No. 8 coal rejects than the agglomerates obtained from Canada. Hence, the intermediate stage of the formation of a slag-coating on agglomerates, before bridging, which was seen for the agglomerates from Canada, was not seen in the Pittsburgh No. 8 rejects. Partially slag-covered agglomerates formed bridges in case of agglomerates from Pittsburgh No. 8 coal rejects.

5. Conclusions

In this work, a mechanism for agglomerate growth based on initiation at the particle-level followed by propagation in bed is proposed. SEM-EDX study of agglomerates from fluidized bed combustors substantiated this mechanism. It showed that iron-based minerals such as pyrite and also eutectics involving iron- and calcium-based minerals were identified as low-temperature initiators (≤ 850 °C) of agglomeration. The amount of slag formed at initiation is less than 10 %. As shown by the modeling work, this is enough only for sticking together of few smaller particles thereby initiating an increase in particle size. At that stage, the particles do not exceed the defluidization size. The alumino-silicates, which are present in larger amounts in bituminous coals, begin to form slag at higher temperatures (850 °C to 950 ˚C) and help propagation of the agglomeration process. Similarly, formation of a local reducing environment around char particles entrapped in agglomerates is likely to lead to larger amounts of slag at lower temperatures.

References:

1. Ennis, B.J., Tardos, R. Pfeffer, A microlevel-based characterization of granulation phenomena, *Powder Technology* **1991**, 65, 257–272.
2. Moseley, J.L., O'Brein, T.J., A model for agglomeration in a fluidized bed, *Chemical Engineering Science* **1993**, 48, 3043–3050.
3. Tan, H. S., Goldschmidt, M. J. V., Boerefijn, R., Hounslow, M. J., Salman, A. D., Kuipers, J. A. M., Building population balance model for fluidized bed melt

granulation: lessons from kinetic theory of granular flow, *Powder Technology* **2004**, *142* (2-3), 103–109.

4. Cryer, S.A., Modeling agglomeration processes in fluid-bed granulation, *AIChE J.* **1999**, 45, 2069–2078.
5. Terrazas-Velarde, K., Peglow, M., Tsotsas, E., Kinetics of fluidized bed spray agglomeration for compact and porous particles, *Chemical Engineering Science* **2011**, 66, 1866–1878.
6. Kang, S.W., Sarofim, A.F., Beér, J.M., Agglomerate formation during coal combustion: a mechanistic model, *Combustion and Flame* **1991**, 86, 258–268.
7. Li, S., Shang, L.,Teng, H., Lu, Q., A model for agglomeration in bio-fuel fired fluidized bed, *Journal of Thermal Science* **2010,** 19, 451–458.
8. Khadilkar, A. B.; Rozelle, P. L.; Pisupati, S. V., A study on initiation of ash agglomeration in fluidized bed gasification systems, *Fuel*, **2015**, 152, 48–57.
9. Khadilkar, A.B., Rozelle, P., Pisupati, S., Effect of heterogeneity in coal ash chemical composition on the onset of conditions favorable for agglomeration in fluid beds, *Energies* **2015**, *8* (11), 12530–12545.
10. Rahaman, M.F., Nasera, J., Witta, P.J. An unequal granular temperature kinetic theory: description of granular flow with multiple particle classes. *Powder Technology*, (2003) 138 (2-3), 82-92.
11. Syamlal, M., Rogers, W., O'Brein, T.J. MFIX Documentation Theory Guide, NETL, Dept. of. Energy. 1993: Morgantown.
12. Van Dyk, J.C., Waanders, F. B., Benson, S. A., Laumb, M. L., Hack, K., Viscosity predictions of the slag composition of gasified coal, utilizing FactSage equilibrium modelling. *Fuel* (2009) 88(1): p. 67-74.
13. Vargas, S., Frandsen, F. J., Dam-Johansen, K., Rheological properties of high-temperature melts of coal ashes and other silicates, *Progress in Energy and Combustion Science* (2001) 27, 237-429.
14. Thielmann, F. et al., The effect of primary particle surface energy on agglomeration rate in fluidised bed wet granulation. *Powder Technology* **2008**, 181, 2, 160-168.

15. Atakül, H., Hilmioğlu, B., Ekinci, E., The relationship between the tendency of lignites to agglomerate and their fusion characteristics in a fluidized bed combustor, *Fuel Processing Technology*, **2005,** 86**,** 12–13, 1369–1383.
16. Matuszewski, M, Detailed coal specifications, Final Report- DOE/NETL-401/012111, **2012**.
17. Brown, R.C.; Dawson, R.; Smeek, J. L. Bed material agglomeration during fluidized bed combustion, Final report for U. S. Department of Energy, No. DE-FG22-92PC92530, 1996.
18. Khadilkar, A., Rozelle, P. and Pisupati, S., Comparative study of fluidized bed agglomeration of high rank coal ash with consideration to particle-level heterogeneities, *Proceedings of the International Conference of Coal Science and Technology*, **2015,** Melbourne, Australia.
19. Visser, H. J. M., van Lith, S. C., Kiel, J. H. A., *Journal of Energy Resources Technology* **2008**, *130* (1), 011801-1- 011801-6.
20. Wen., C. Y., Krishnan, R., Kalyanaraman, R., Particle mixing near the grid region of fluidized beds, *Proceedings of the International Fluidization Conference* **1980**, 405.
21. Scala, F., Chirone, R., Characterization and Early Detection of Bed Agglomeration during the Fluidized Bed Combustion of Olive Husk, *Energy & Fuels* **2006**, 20, 120-132.
22. Bock, H.-J., Molerus, O., Influence of hydrodynamics on heat transfer in fluidized beds, *Proceedings of the International Fluidization Conference*, New Hampshire, U. S. A., **1980**, 217.
23. Basu, P., Combustion and Gasification in Fluidized beds, CRC Press, Florida, **2006.**
24. Scott, D. H., Ash behaviour during combustion and gasification, IEA Coal Research Report, **1999.**